UNIVERSITÄT
DUISBURG
ESSEN

Open-Minded

A RATIONAL SYNTHESIS AND ANTI-TUBERCULAR EVALUATION OF THE CALLYAERINS, A MARINE CYCLIC PEPTIDE CLASS BEARING A RARE (*Z*)-2,3-DIAMINOACRYLAMIDE MOIETY

DISSERTATION

zur Erlangung des

Doktorgrades der Naturwissenschaften

– Dr. rer. nat. –

vorgelegt von

Florian Schulz

geboren in Gelsenkirchen

Fakultät für Chemie

der

Universität Duisburg-Essen

2019

Die vorliegende Arbeit wurde im Zeitraum von Oktober 2014 bis Dezember 2018 im Arbeitskreis von Prof. Dr. Markus Kaiser am Zentrum für medizinische Biotechnologie der Universität Duisburg-Essen durchgeführt.

Tag der Disputation: 06.12.2019

Gutachter: Prof. Dr. Markus Kaiser

Prof. Dr. Michael Ehrmann

Vorsitzender: Prof. Dr. Malte Behrens

für meinen Vater und Marie

DOI: 10.17185/duepublico/70841
URN: urn:nbn:de:hbz:465-20231030-140139-4

Table of Contents

1 Introduction

1.1 Tuberculosis disease

For most people in the Western countries, tuberculosis (TB) no longer poses a health threat – even though 1.7 billion people corresponding to 23 % of the world's population are estimated to carry a latent TB infection and are thus at the risk of developing active TB disease during their lifetime. Fortunately, the disease initiation occurs merely in a small fraction of cases. While the disease is currently still well treatable in developed countries, in world regions without proper medical facilities, TB is much more fatal and the prevailing conditions in these areas even promote the dissemination, onset and formation of TB infections resistant to available chemotherapies. Therefore, tuberculosis continues to pose a serious health threat which demands further research and development of new drug substances[1].

Similar to other bacterial diseases, tuberculosis infections are treated with antibiotics. The discovery and initial administration of this class of drugs remains as a milestone in the history of medicine. For the first time, a previously death-causing bacterial infection became curable within days. However, today it is well-known that every application of an antibiotic also unavoidable promotes the generation of drug-resistant bacterial strains. Hence, each antibiotic substance has a 'programmed termination date' and the progress in drug development maintains a Sisyphean task for mankind.

To date, two categories of drug-resistant tuberculosis strains are distinguished: Multi-drug-resistant tuberculosis (MDR-TB) are TB infections that are resistant to both rifampicin and isoniazid treatment, the two most powerful anti-TB drugs developed so far; these infections therefore require treatment with a second-line regimen. In addition, extensively drug-resistant TB (XDR-TB) infections are nowadays known that are defined as MDR-TB plus resistance to at least one drug in both of the two most important classes of medicines in an MDR-TB regimen, i. e. fluoroquinolones and second-line injectable agents (amikacin, capreomycin or kanamycin), which in general are less effective, more toxic and much more expensive than first-line drugs[1,2].

Drug-resistant TB continues to be a public health crisis. For example, in 2017, 558 000 people worldwide developed TB resistant to rifampicin (RR-TB) treatment, the most

effective first-line drug; of these, 82 % had even MDR-TB. Three countries thereby accounted for almost half of the world's cases of MDR/RR-TB: India (24 %), China (13 %) and the Russian Federation (10 %). However, the highest proportions are found in Eastern Europe and Central Asia, with around 20 % of new cases and 50 % of previously treated cases having MDR-TB. The highest proportions (>50 % in previously treated cases) are found in countries of the former Soviet Union. Among the reported MDR-TB cases in 2017, 8.5 % were even estimated to have extensively drug-resistant TB (XDR-TB). Altogether, these findings illustrate that in particular many countries in Eastern Europe have become hotspots for MDR-TB infections. Besides the personal disaster for infected people in these countries, intensified immigration and travel from these regions have led to concerns that these TB infections may also manifest in the more densely populated Western countries[1,3].

Tuberculosis is caused by infection with the bacterium *Mycobacterium tuberculosis*. For some strains, the long-feared post-antibiotic era has already been reached as they are virtually fully resistant to all currently available anti-TB drugs[4]. This frightening news have led after decades of passivity in development of antitubercular drugs, to renewed interest in the discovery of alternative chemotherapies, first in the academic sector and now also in the pharmaceutical industry.

1.2 Approved antibiotics for TB treatment

1.2.1 First-line anti-TB drugs

More than 20 anti-tuberculosis drugs have so far been developed for the treatment of TB. Most of them were developed in the years between 1940 and 1960. These anti tubercular drugs are nowadays used in several combinations depending on the individual circumstances. First-line TB drugs are thereby usually employed in the treatment of new patients; these persons are very unlikely to show resistance to any TB drug. Such first-line TB drugs are Rifampicin, Isoniazid, Ethambutol, Pyrazinamide and Streptomycin. Accordingly, second-line drugs are reserved for the treatment of drug-resistant TB. Currently, several new TB drugs are in the development phase and hopefully some of them will manage to achieve drug approval.

Rifampicin

Rifampicin is a distinct derivative from the antibiotic rifamycin natural product family that are biosynthesized by the bacterium *Amycolatopsis rifamycinica.* It was introduced in 1972 as an antitubercular agent. It is one of the most effective anti-TB antibiotics known so far and constitutes together with isoniazid the basis of the TB multidrug treatment regimen. On a molecular level, rifampicin targets the β-subunit of mycobacterial RNA polymerase, thereby inhibiting the generation of full-length messenger RNA[5]. Accordingly, most *M. tuberculosis* rifampicin-resistant isolates carry mutations in a 'hot-spot region' spanning codons 507-533 of the *rpoB* gene[6,7]. Almost all rifampicin-resistant strains also show resistance to other chemotherapeutic drugs, especially isoniazid. Therefore, rifampicin resistance is often used as a surrogate marker for the occurrence of MDR-TB infections[8].

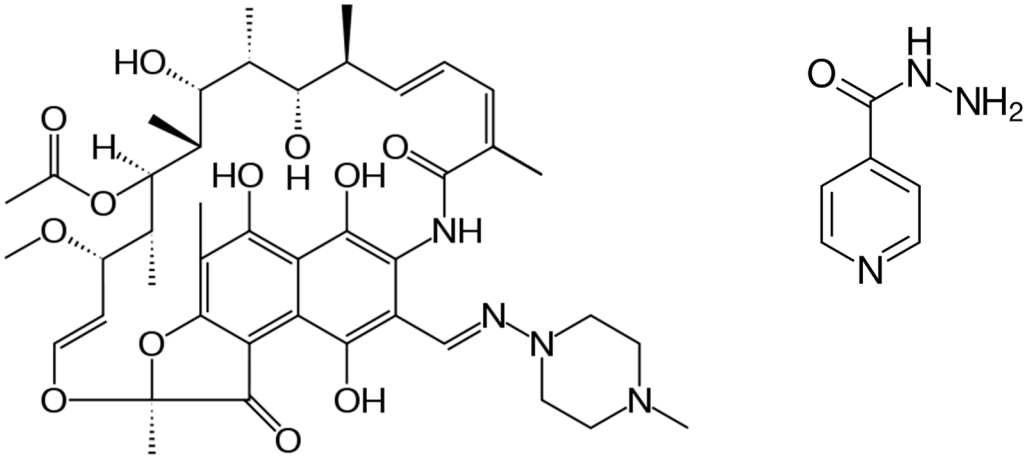

Figure 1: Chemical structures of rifampicin (left) and isoniazid (right).

Isoniazid

Isoniazid is used as an anti-TB agent since 1952 and constitutes together with rifampicin the standard basis for TB treatment. Isoniazid is a pro-drug that requires activation by the bacterial catalase-peroxidase enzyme KatG and is therefore, in contrast to rifampicin, only active against metabolically-active replicating bacilli[9]. Isoniazid inhibits the synthesis of fatty acids by binding to the NADH-dependent enoyl-acyl carrier protein (ACP)-reductase InhA[10]. The molecular mechanisms of isoniazid resistance are associated with mutations in a couple of genes, predominantly *katG* and *inhA*, but also *ahpC*, *kasA* and *ndh*[11,12].

Ethambutol

Ethambutol is part of the first-line regimen in the treatment of TB and was first introduced in 1966. Ethambutol is bacteriostatic against actively growing TB bacilli and impairs the biosynthesis of cell wall arabinogalactan by inhibition of arabinosyl transferase[13]. Resistance to ethambutol treatment is triggered by mutations in the gene *embB*[14]. The predominant mutations at position *embB*306 thereby lead to variable levels of ethambutol resistance. As only 68 % ethambutol resistant strains however carry mutations directly in the *embB* gene, alternative resistance mechanism have to be present that are so far only marginally characterized[15].

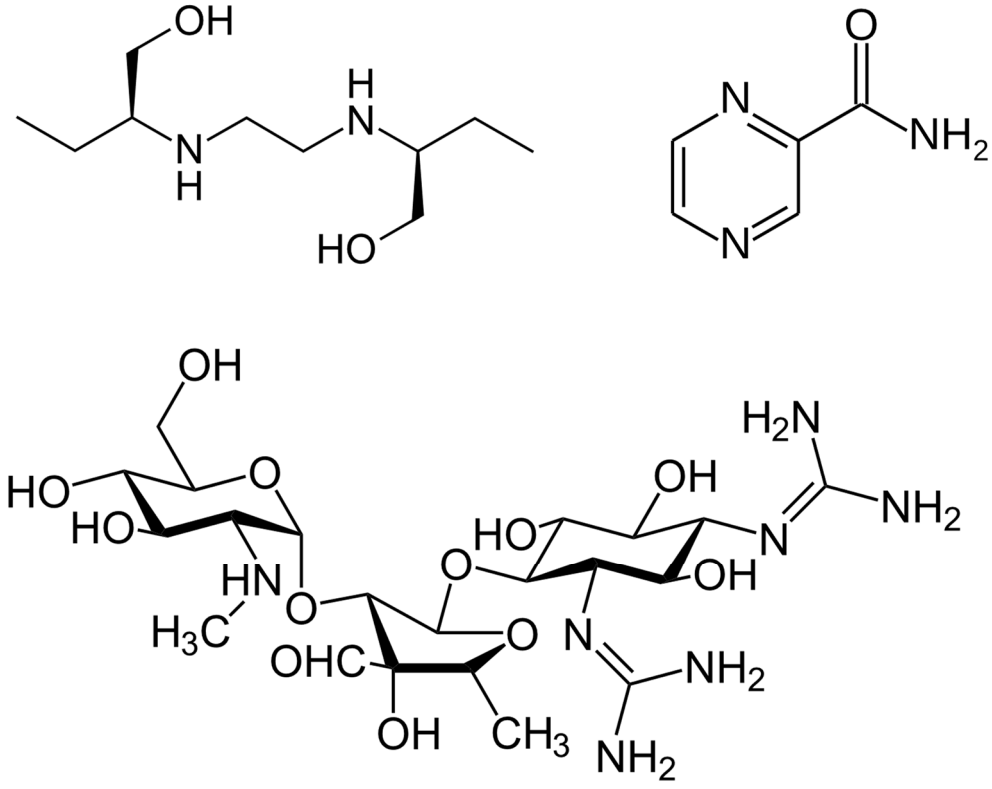

Figure 2: Chemical structures of Ethambutol (left), Streptomycin (bottom) and Pyrazinamide (right).

Streptomycin

Streptomycin was the first successful antibiotic against TB and was isolated from the soil bacterium *Streptomyces griseus*. Streptomycin is an aminocyclitol glycoside and inhibits the initiation step in ribosomal protein biosynthesis by binding to 30S subunit at the ribosomal protein S12 and the 16S rRNA, which are coded by the genes *rpsL* and *rrs,* respectively[16,17].

Pyrazinamide

Pyrazinamide was introduced in the early 1950s and is part of the first-line regimen for TB treatment. Pyrazinamide is an analog of nicotinamide and acts as a prodrug. Mutations in the *pncA* gene of *M. tuberculosis*, which encodes a pyrazinamidase and converts pyrazinamide to its active form pyrazinoic acid, are responsible for the majority of occurring pyrazinamide resistances. Pyrazinoic acid impairs the bacterial membrane energetics by inhibiting membrane transport[18]. However, a recent study also identified the ribosomal protein 1 derived from the *rpsA* gene as a target of pyrazinoic acid, leading to protein translation impairment in *M. tuberculosis*[19].

1.2.2 Second-line anti-TB drugs

Second-line anti-TB drugs can be classified into the following structural groups: Fluoroquinolones (Levofloxacin, Moxifloxacin, Gatifloxacin, Ofloxacin), Thioamides (Ethionamide, Prothionamide), Oxazolidinones (Cycloserine, Terizidone, Linezolid, Clofazimine), *para*-Aminosalicylic acid, Thioacetazone, Macrolides (Clarithromycin), Aminoglycosides (Kanamycin, Amikacin), cyclic peptides (Capreomycin, Viomycin), Nitroimidazole (Delamanid, Pretomanid), Diarylchinoline (Bedaquilin).

Table 1 provides an overview of the currently used first- and second-line anti-tuberculosis drugs and their target of action[20].

Table 1: First- and second-line TB drugs, genes involved in their activation and mechanisms involved.

Drug	**Gene**	**Mechanism Involved**	**Ref.**
Rifampicin	*rpoB*	RNA polymerase	6,7,21
Isoniazid	*katG*, *inhA*	Catalase/peroxidase; enoyl reductase	12
Ethambutol	*embB*	Arabinosyl transferase	13,14
Pyrazinamide	*pncA*, *rpsA*	Pyrazinamidase; ribosomal protein 1	22–24
Streptomycin	*rpsL*, *rrs*, *gidB*	S12 ribosomal protein, 16A rRNA, 7-methylguanosine methyltransferase	16,17,25
Quinolones	*gyrA*, *gyrB*	DNA gyrase	26,27
Capreomycin/ Viomycin	*rrs*, *tlyA*	16S rRNA, rRNA methyltransferase	28,29
Kanamycin/ Amikacin	*rrs*	16S rRNA	30
Ethionamide	*ethA*	Enoyl-ACP reductase	31,32
Para-aminosalicylic acid	*thyA*, *folC*	Thymidylate synthase A	33–35
Bedaquiline	*atpE*	ATP synthase	36–38
Delamanid	*ddn, fgd, fbiA, fbiB, fbiC*	Deazaflavin-dependent nitroreductase, F_{420}-dependent glucose-6-phosphate dehydrogenase	39,40

1.2.3 Anti-TB drugs currently in clinical developoment

Besides the established TB drugs, several other compounds including also alternative substance classes are currently in clinical trials (Figure 3).

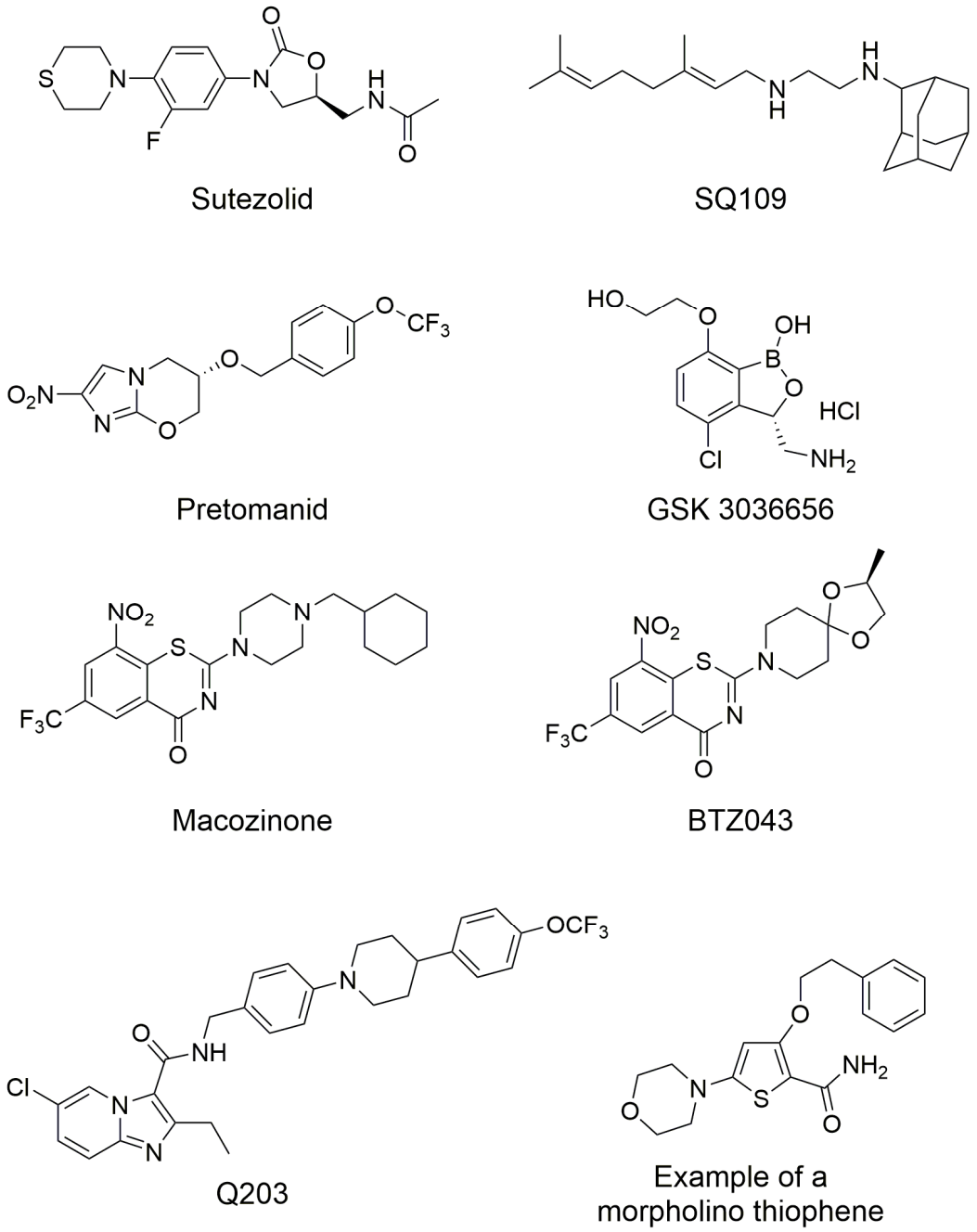

Figure 3: Chemical structures of new anti-TB drugs currently in clinical development.

Sutezolid (PNU-100480, PF-02341272) is an oxazolidinone antibiotic currently in development as a treatment for extensively drug-resistant tuberculosis. It differs from the established drug linezolid by replacement of the morpholine oxygen with a sulfur moiety[41,42].

SQ109 (an ethylene diamine analogue) targets MmpL3, a membrane transporter of trehalose monomycolate involved in mycolic acid donation to the cell wall core of *M. tuberculosis*[43].

Pretomanid (PA-824) is a nitroimidazole derivative and is supposed to act on the mycolic acid biosynthetic pathway through cellular depletion of ketoymycolates and the accumulation of hydroxymycolates[44]. In a newer study Pretomanid displayed a different metabolic pattern compared to other antibiotics, suggesting that its mode of action may however be different[45].

GSK 3036656, an oxaborole, targets and inhibits Leucyl-tRNA Synthetase (LeuRS), thereby shutting down mycobacterial protein biosynthesis[46].

Macozinone (PBTZ-169) and BTZ043 are 1,3-benzothiazin-4-ones (benzothiazones), that inhibit Decaprenylphosphoryl-β-D-ribose 2′-epimerase 1 (DprE1), which catalyzes the epimerization of decaprenylphosphoryl-β-D-ribose to decaprenylphosphoryl-β-D-arabinose, thereby providing a precursor to the cell wall arabinogalactan polysaccharide[47,48].

Q203 is an imidazopyridine antitubercular compound that acts on the respiratory chain; it just entered Phase I clinical trials. Q203 targets the cytochrome *b* subunit (QcrB) of the cytochrome bc_1 complex. This complex is an essential component of the respiratory electron transport chain of ATP synthesis[49].

A similar mode-of-action is found for morpholino thiophenes that also target QcrB[50].

Despite these advances, in order to overcome the imminent threat of MDR/XDR-TB, there is still an urgent need to develop new drugs with novel modes of action that do not evolve rapid resistance. A source for structurally new potential anti-TB drugs are small naturally occuring peptides that are presented in the following section.

1.3 Small natural peptides with anti-mycobacterial activity

Apart from the small molecule anti-TB drugs in clinical development, a row of naturally occurring peptides with anti-mycobacterial activity were recently isolated from different species. Some of these anti-mycobacterial peptides are classified as anti-microbial peptides (AMPs).

Generally, anti-microbial peptides are a diverse group of molecules found in most living organisms and recognized for their relevant role in the immune response[51]. They are usually short in length (between 12 and 50 amino acids), cationic and amphiphilic, enabling them to interact in both aqueous and lipid-rich environments[52]. Among those, some AMPs show particular interest in mycobacterial treatment, either for monotherapy or combined with other drugs[53].

Anti-mycobacterial peptides have a few advantages, such as low immunogenicity, selective affinity to prokaryotic negatively charged cell envelopes, and diverse modes of action[54]. Most of them are derived either from bacterial extraction, host immune cells, or mycobacteriophages. Some of the challenges faced by anti-mycobacterial peptides include the difficulty in permeating the mycobacterial cell wall to the target sites, stability of the peptides at physiological conditions and degradation by cytoplasmic proteases[55]. Nonetheless, the multiple functions of anti-mycobacterial peptides, especially direct killing of pathogens and immune modulators in infectious and inflammatory conditions, indicate that they are promising candidates for future drug development[54].

In the following enumeration the focus is set on small (< 20 amino acids) and mainly cyclic peptides that exhibit activity against *M. tuberculosis* in particular, highlighting the sources, effectiveness and bactericidal mechanisms of these anti-mycobacterial peptides. Hereby, the selection outlines the scope of anti-tubercular peptides that are accessible for chemical synthesis whereas for several substances, no total synthesis was reported so far.

Viomycin and Capreomycin

Viomycin and Capreomycin are approved second-line anti-TB drugs and share a similar structure and mode of action. Both are cyclic peptides and catch special interest for this work due to their 2,3-diaminoacrylic acid (DAA) moiety (see Figure 4), which is also found as a ring forming element in all Callyaerins.

Viomycin belongs to the tuberactinomycin antibiotics natural product class and possesses several nonproteinogenic amino acids. It is an effective agent in the treatment of multidrug resistant tuberculosis. As the first member of the tuberactinomycin family, it was isolated and described in the 1960s and was used as an anti-TB drug until it was substituted by the less toxic, but structurally related natural product capreomycin[56]. Viomycin inhibits bacterial protein synthesis by blocking elongation factor G-catalyzed translocation of messenger RNA, thereby causing misreading of the genetic code[57].

Capreomycin is not a single compound but a mixture of two cyclic pentapeptides isolated in 1960 from *Streptomyces capreolus*. It is applied *via* injection, mostly in combination with other antibiotics. Capreomycin also inhibits protein synthesis by binding at the interface between ribosomal proteins L12 and L10[58] and mutations in the gene *tlyA* cause capreomycin resistance. TlyA is an rRNA methyltransferase specific for 2'-O-methylation of ribose in rRNA. The occurring *tlyA* mutations thereby impair its methylation activity[29].

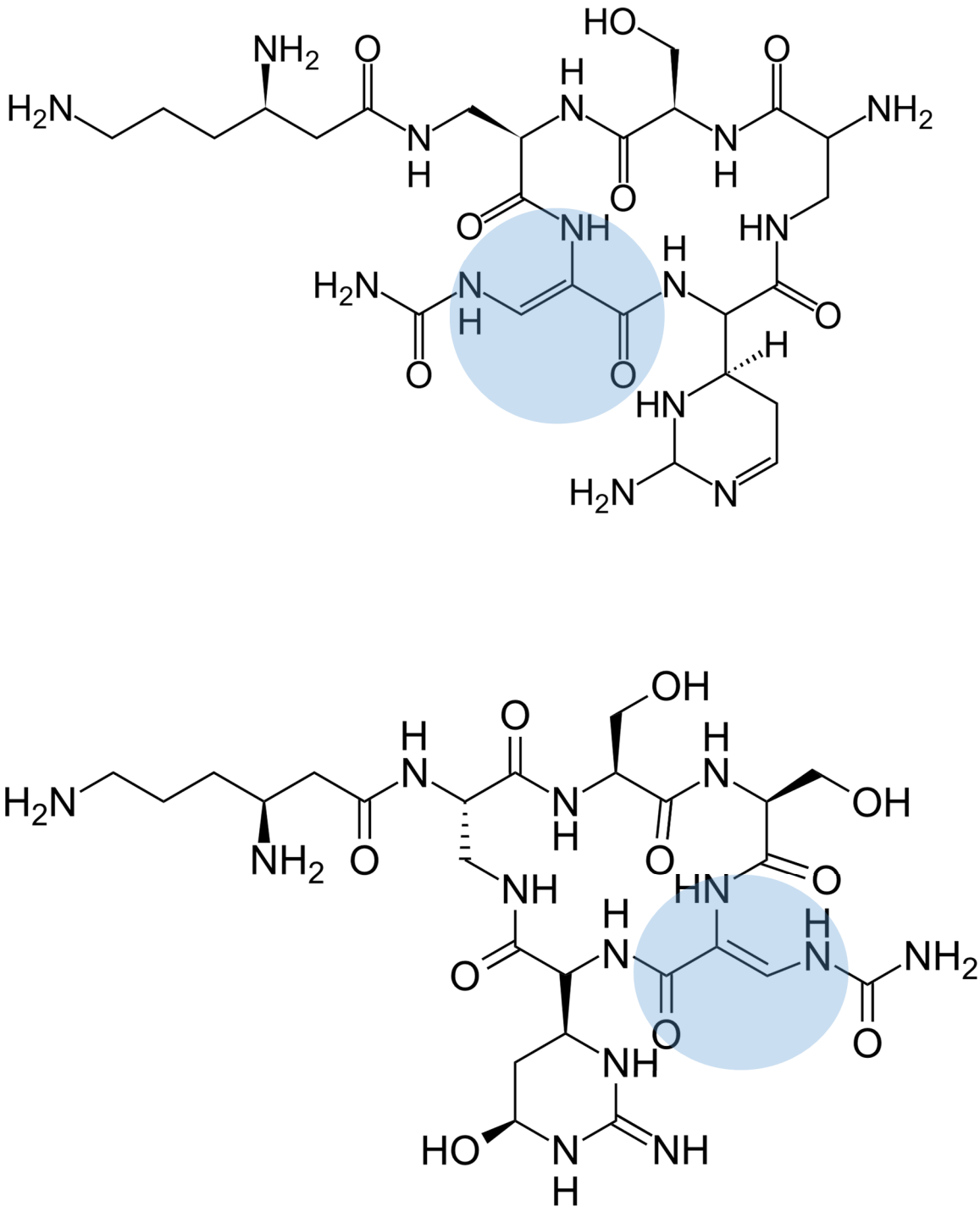

Figure 4: Chemical structures of the antitubercular cyclic peptides Capreomycin IA (top) and Viomycin (bottom). Both carry a 2,3-diaminoacrylic acid (DAA) moiety (highlighted in blue).

Teixobactin

Teixobactin is a cyclic nonribosomal depsipeptide and was originally isolated from the gram-negative bacterium *Eleftheria terrae*. It displays potent growth inhibitory activities against *S. aureus* and *M. tuberculosis* H37Rv. So far and promisingly, no Teixobactin-resistant strains could be obtained. In a new mode of action, Teixobactin inhibits cell wall synthesis by binding to the precursor metabolites of the peptidoglycans and teichoic acid, lipid II + III, respectively[59]. Somehow surprisingly, the analysis of synthetic Teixobactin obtained from total synthesis also revealed an inhibitory activity against *M. tuberculosis* H37Rv; however, this activity was lower than the reported values for the isolated compound Teixobactin[60].

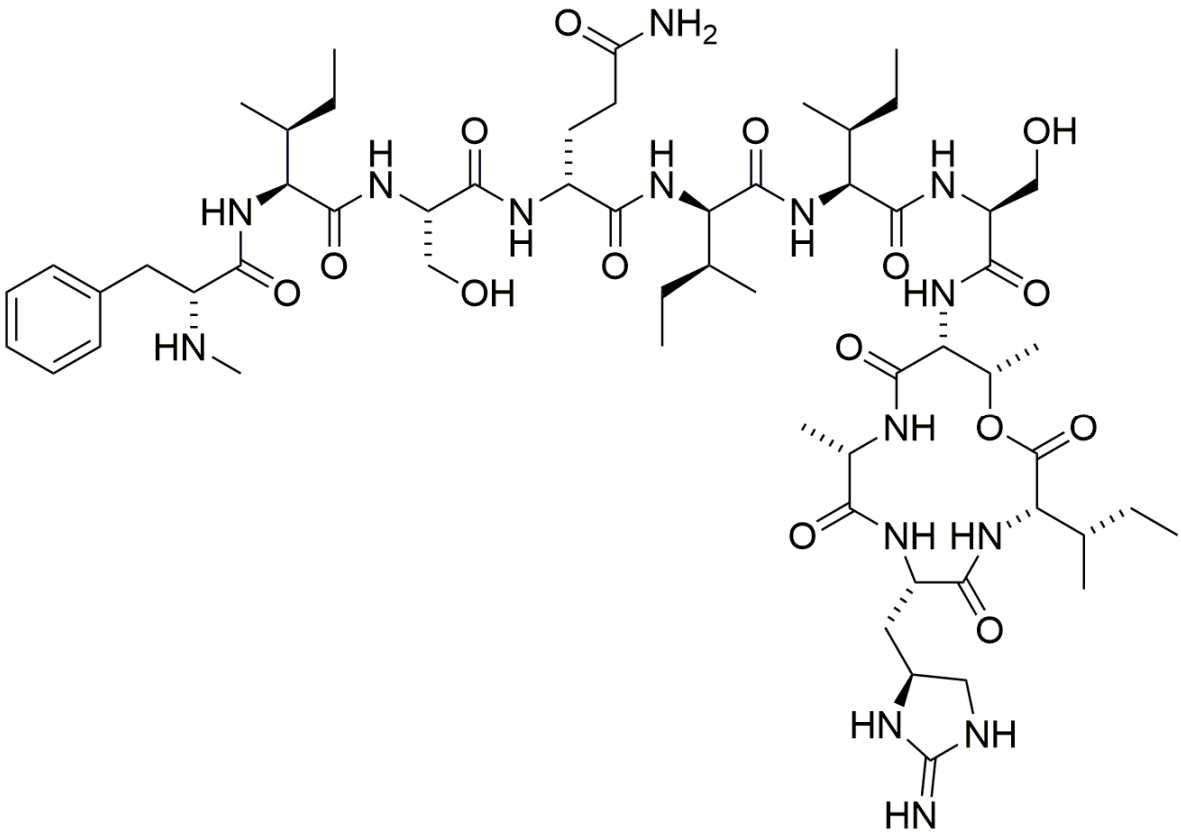

Figure 5: Chemical structure of Teixobactin.

Wollamide A + B

The cyclic hexapeptides Wollamide A and B were isolated from *Streptomyces nov.* sp. from an Australian soil sample[61]. Wollamide B and analogues demonstrated high extracellular antimycobacterial potency and drug-relevant attributes such as water solubility and blood plasma stability. Their poor membrane permeability however was proposed to potentially hamper their ability to traverse from blood vessels into target cells[62]. Importantly, the antimicrobial activities of Wollamides A and B do not result from a disruption of the bacterial membrane, warranting further investigation into their mechanism of action[63]. A recent structure-activity relationship study of Wollamide B found two derivatives with slightly improved pharmacokinetic properties that could be used as new lead structures for further development[64].

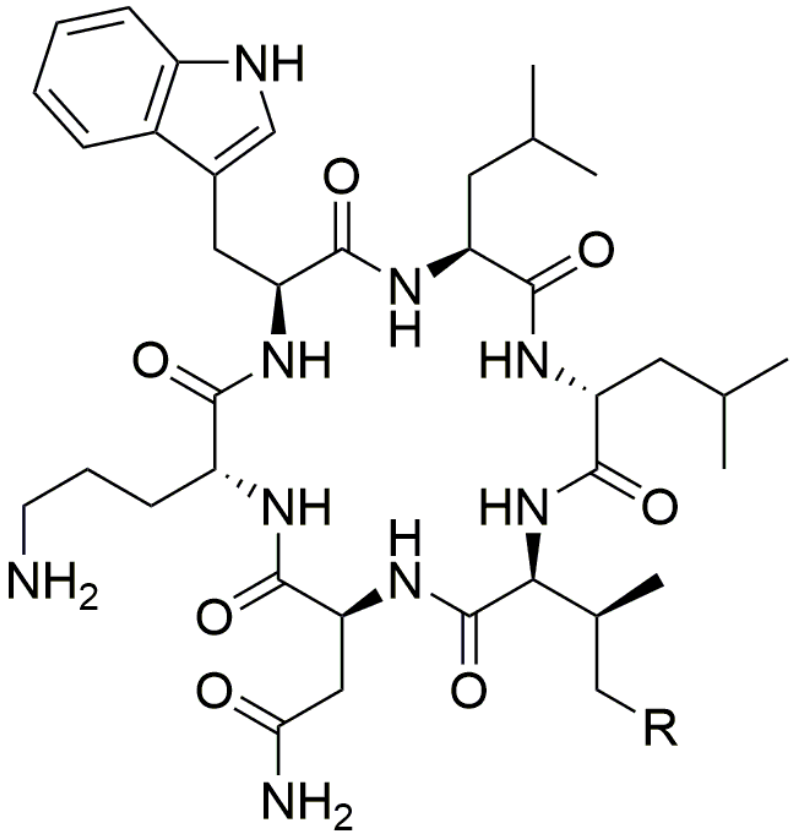

Wollamide A, R = CH_3
Wollamide B, R = H

Figure 6: Chemical structures of Wollamides A and B.

Cyclomarin A

Cyclomarin A is a cyclic heptapeptide from marine *Streptomyces* sp. and is active against *M. tuberculosis* including a panel of multidrug-resistant clinical isolates[65]. The target is caseinolytic protease C1 (ClpC1), which is essential for mycobacterial survival[66]. Total synthesis of Cyclomarin A resulted in derivatives with activity against *M. tuberculosis* and also against *Plasmodium falciparum*, highlighting a broad-spectrum activity of this natural product[67].

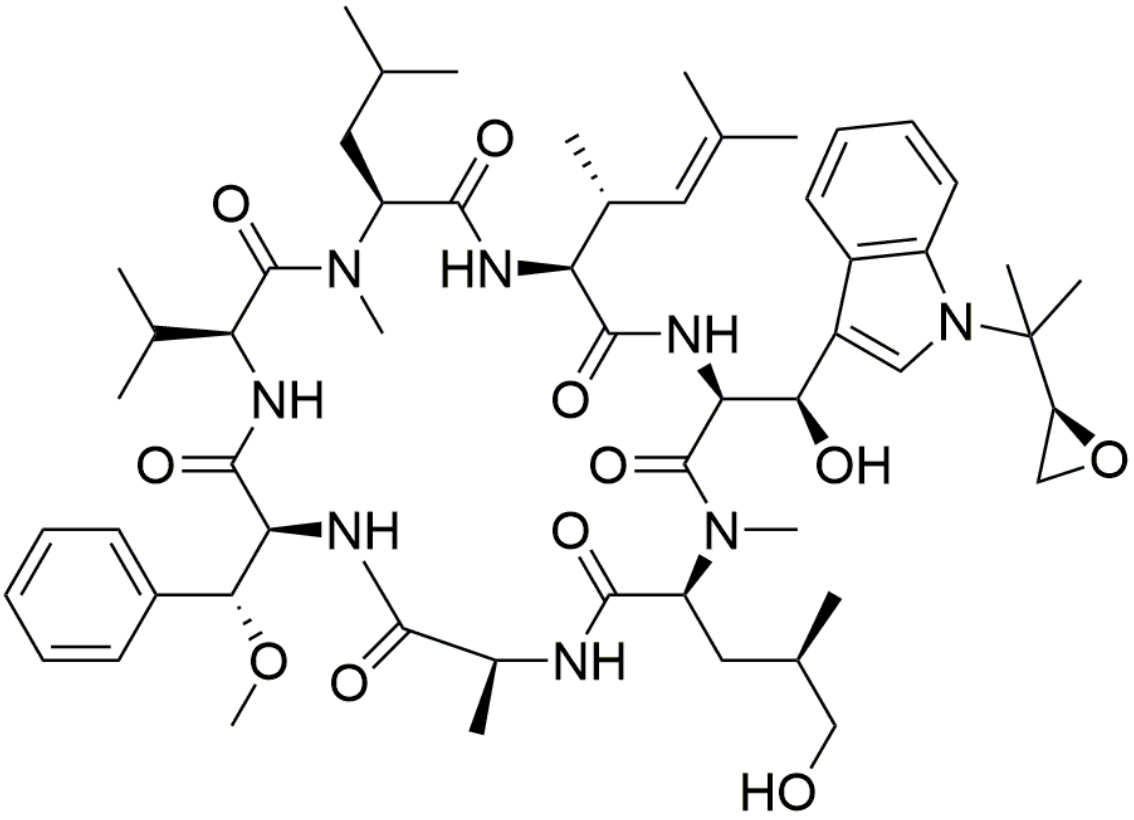

Figure 7: Chemical structure of Cyclomarin A.

Lariatins

Lariatins are a group of novel anti-mycobacterial peptides isolated from the Gram-positive bacterium *Rhodococcus jostii*. The spatial structure was described as a threaded loop resembling a ‘lasso’, in which the C-terminal tail of the peptide passes through the ring structure formed by the N-terminal segment[68]. Lariatin A is currently in early-stage development with good *in vitro* activity against *M. tuberculosis*. A recent mutational study of Lariatin A found that amino acids Tyr6, Gly11, and Asn14 were essential for anti-mycobacterial activity, while mutation of Val15, Ile16 and Pro18 enhanced activity[69]. Total synthesis or target elucidation in *M. tuberculosis* were not reported so far. A proteomic study with a biotinylated Lariatin A probe in *M. smegmatis* identified the protein MSMEG1878 with unknown function as binding partner, which seems to interact with a single-stranded DNA binding protein, coded by the gene *ssb*, suggesting that the protein is involved in DNA replication[70].

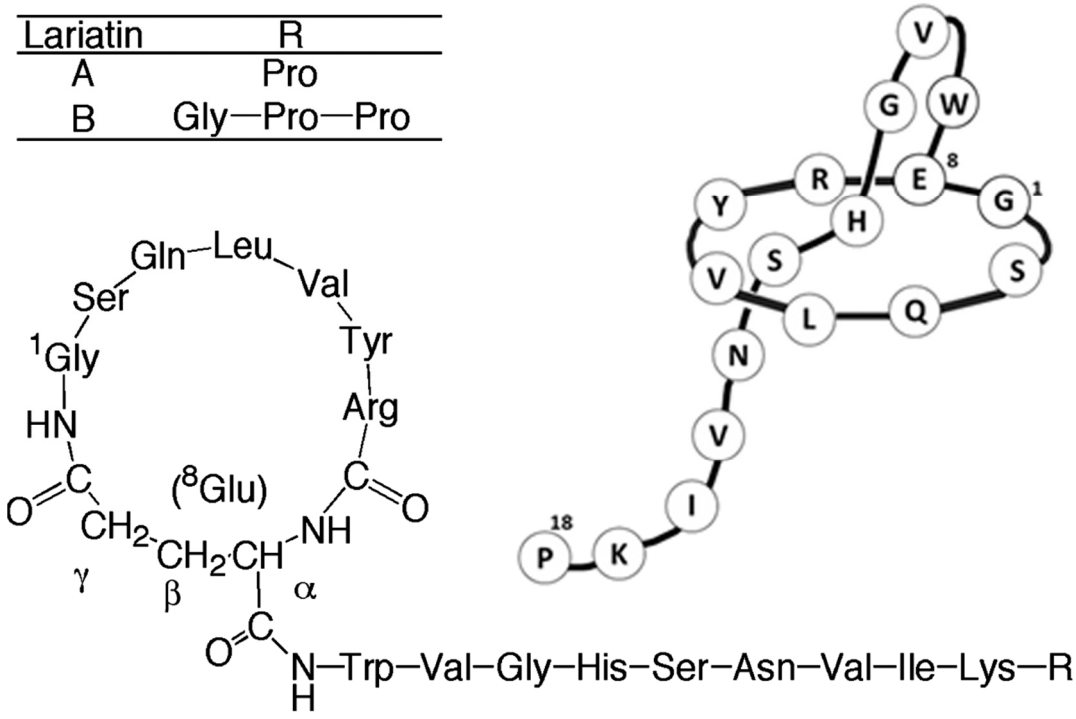

Figure 8: Chemical structures of Lariatins A + B and the topologic structure of Lariatin A.

Lassomycin

Lassomycin is a highly basic, ribosomally encoded cyclic peptide purified from an extract of the soil bacterium *Lentzea kentuckyensis* sp. and displays growth inhibitory activity against MDR- and XDR-TB strains. Generation of a lassomycin resistant strain of *M. tuberculosis* led to the discovery of its target ClpC1. Lassomycin binds to a highly acidic region of the ClpC1 ATPase complex and stimulates its ATPase activity without stimulating ClpP1P2-catalyzed protein breakdown, which is responsible for protein degradation and maintaining cellular homeostasis[71]. Recent attempts to synthesize Lassomycin resulted in derivatives that however were found to be inactive against *M. tuberculosis*; this unexpected finding was explained by a potential incorrect three-dimensional structure in which the naturally occurring threaded 'lasso' structure was not formed[72,73].

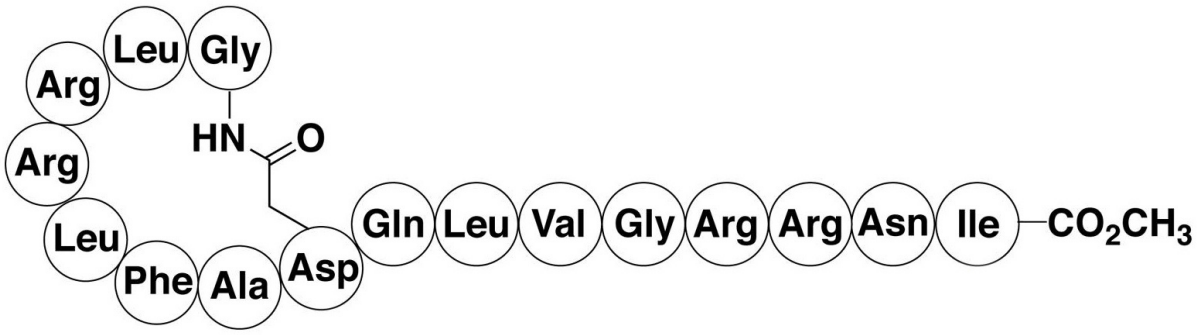

Figure 9: Chemical structure of Lassomycin. Also, this compound is proposed to form a 'lasso' three-dimensional structure.

Ecumicin

Similar to Lassomycin, Ecumicin also targets ClpC1 and increases the activity of this ATPase[74]. Ecumicin was isolated from an Actinomycete strain and displays promising activity against drug-susceptible, MDR and XDR *M. tuberculosis* strains. When delivered in polymeric micelle formulation, Ecumicin led to reduced *M. tuberculosis* bacterial load in the lungs of infected mice. However, Ecumicin was not as effective as rifampicin *in vivo*, requiring the improvement of its pharmacokinetic properties[75]. Total Synthesis of Ecumicin was recently reported[76].

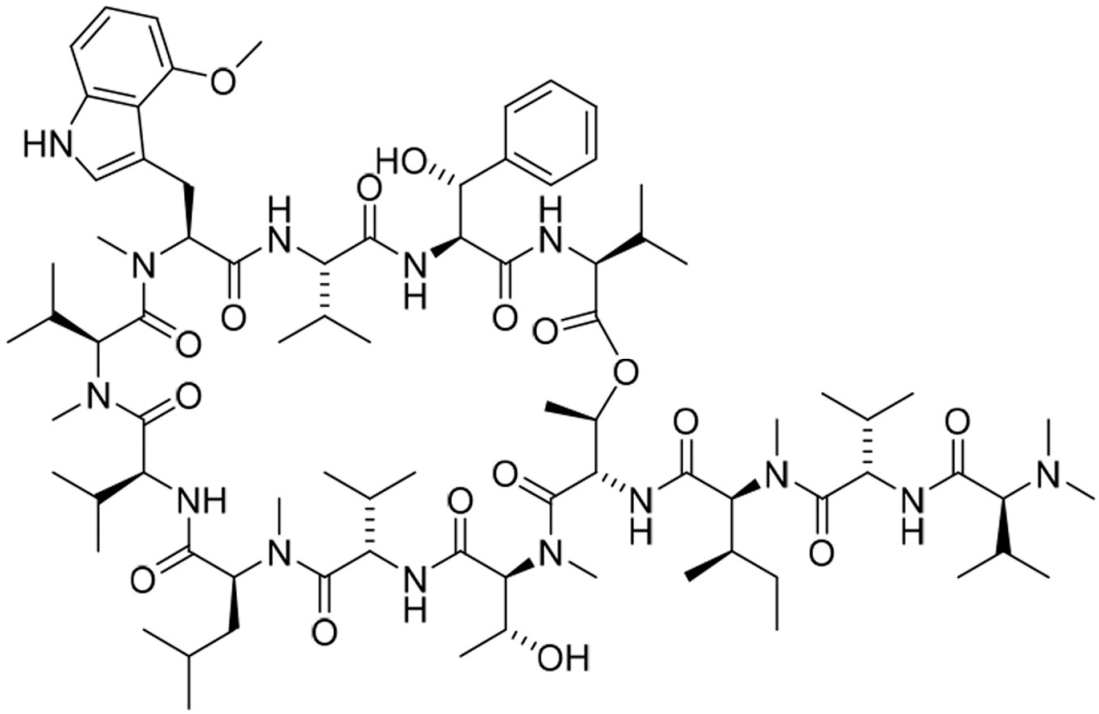

Figure 10: Chemical structure of Ecumicin.

Griselimycins

Griselimycin is a natural cyclic peptide isolated from a *Streptomyces* species in the 1960s. Recent lead optimization of Griselimycin resulted in identification of a novel synthetic analog derivative Cyclohexylgriselimycin (CGM) with activity against intracellular *M. tuberculosis* including drug-resistant strains. In acute as well as chronic mouse model of TB, treatment with CGM significantly reduced bacterial loads compared to untreated mice. Griselimycin binds to the DNA β-sliding clamp, coded by *DnaN* gene, that anchors the DNA to DNA polymerase, hence inhibiting DNA polymerase III and preventing DNA replication[77].

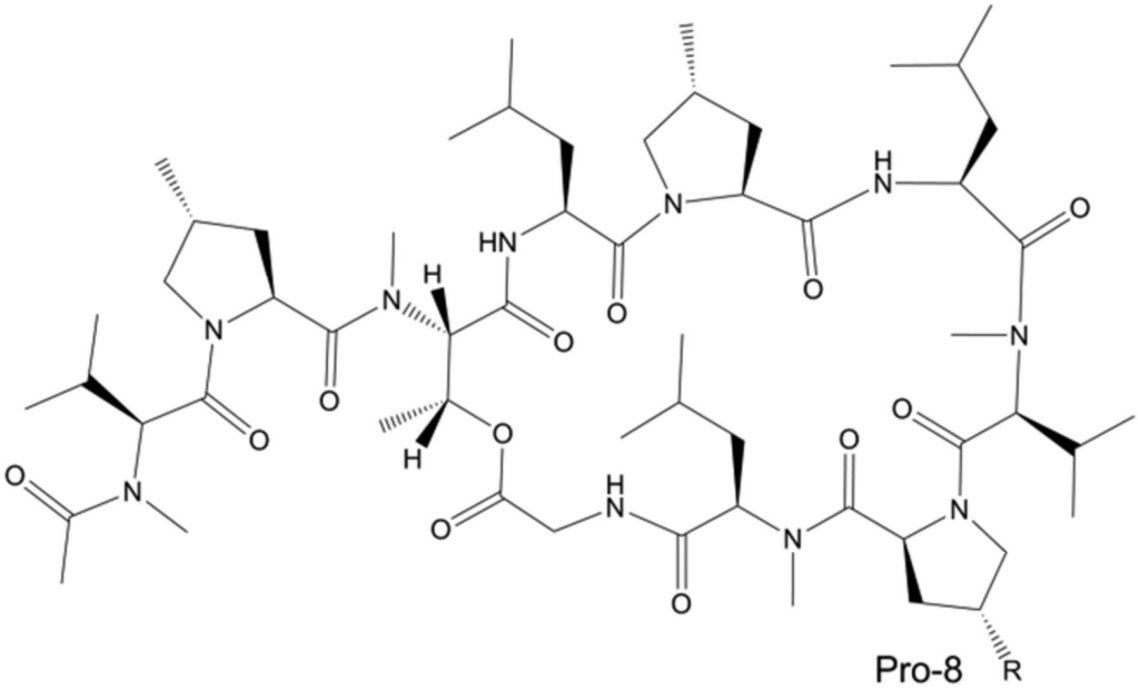

Figure 11: Chemical structures of Griselimycins.

Trichoderins

Trichoderins are a new class of aminolipopeptides and were isolated from a culture of marine sponge-derived fungus of *Trichoderma* sp. They exhibit activity against *M. tuberculosis in vitro* under standard aerobic growth conditions as well as dormancy-inducing hypoxic conditions, with Trichoderin A being most promising candidate[78]. The activity of Trichoderins appears to be attributed to the inhibition of ATP synthesis in the mycobacteria, although further studies are required to confirm this hypothesis[79]. Recently, a first total synthesis of Trichoderin A was reported[80].

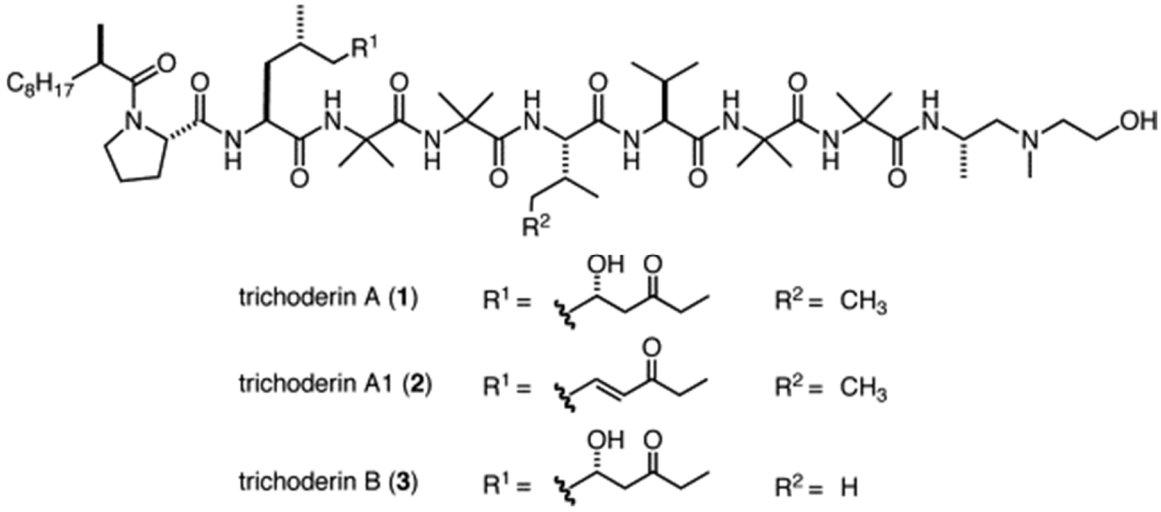

Figure 12: Chemical structures of Trichoderins.

Sansanmycins

Sansanmycins are members of the uridylpeptide family and were isolated from *Streptomyces* sp[81]. Sansanmycin A and B showed activity against drug susceptible and MDR strains of *M. tuberculosis*[82]. Likewise, semi-synthetic and biosynthetic modifications to the Sansanmycin natural product has resulted in derivatives with greater activity[83,84]. Uridylpeptide antibiotics prevent cell wall biosynthesis by inhibiting translocase I, which is coded in the gene *MraY* and involved in peptidoglycan synthesis. In *M. tuberculosis*, the Sansanmycins seem to target the same enzyme[85].

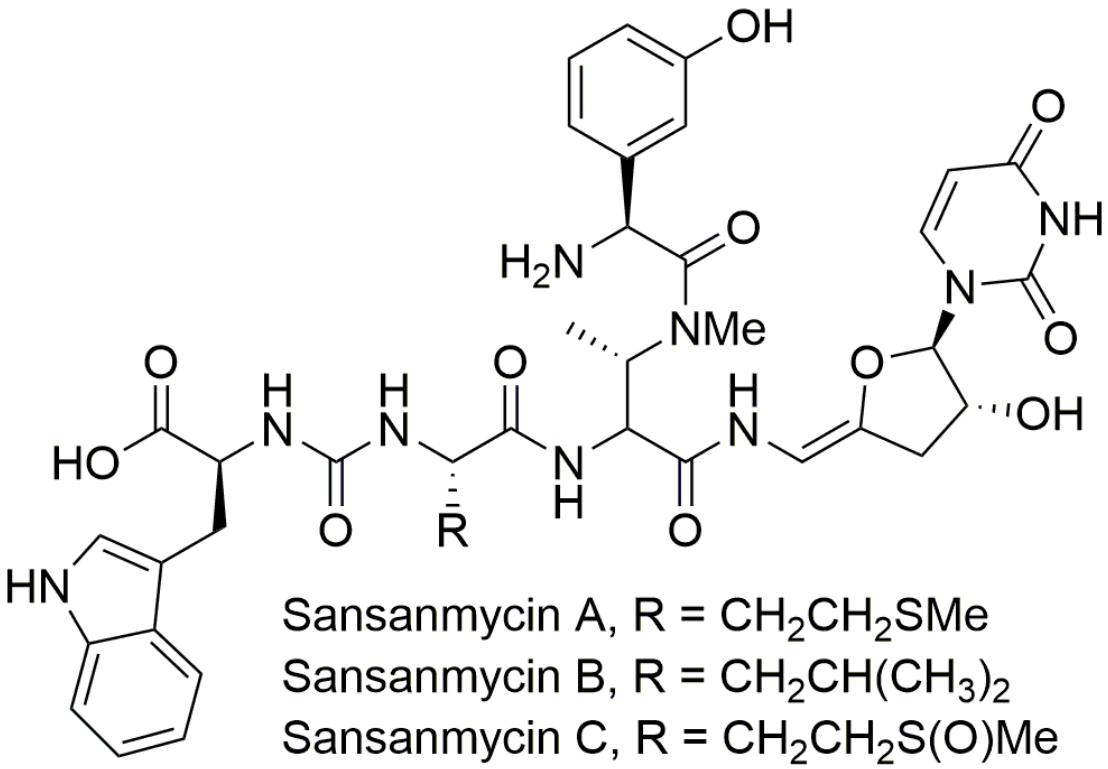

Figure 13: Chemical structures of Sansanmycins A-C.

1.4 Callyaerins

1.4.1 Marine sponges

Marine sponges are invertebrate animals that settle the sea bottom and exhibit a large variety of fascinating shapes and colors[86]. Currently, there are around 8.700 species of sponges (phylum *Porifera*) inhabiting different marine and freshwater habitats around the world[87,88]. Most of them are sessile and soft-bodied lacking a hard outer shell, which makes them vulnerable to potential predators, and therefore must rely on chemical defenses to repel predators, to keep competitors away or to paralyze prey[89]. It is therefore not surprising that throughout millions of years marine sponges evolved bioactive metabolites against pathogenic fungi, bacteria and algae; many of them display fascinating chemical structures or bioactivities. Indeed, even today, marine sponges are still considered as a 'gold mine' for natural products that show high bioactivity with antimicrobial, antiviral, antitumor, and general cytotoxic properties[90,91]. The chemical diversity of secondary metabolites isolated from sponges includes cyclic peptides, alkaloids[92], terpenes or terpenoids, nucleotides, sterols and many others[93,94]. Here, we will focus only on the Callyaerins due to their potent antitubercular activity.

1.4.2 The cyclic peptide family of the Callyaerins

Callyspongia aerizusa is a marine tube sponge found in shallow water offshore in Indonesia[95] but also occurs in the Coral Sea between the Great Barrier Reef and New Caledonia[96]. The Callyaerins, a family of cyclic peptides, were first isolated from this species in 2010 by the Proksch group[95]. Biological studies on the Callyaerins revealed that several Callyaerins, especially Callyaerin A and B, exhibit potent inhibitory activity against *M. tuberculosis* while showing only low cytotoxicity against human cell lines[97]. However, due to the limited amount of the natural product isolates of these Callyaerins, further biological assays could not be performed with these compounds. In addition, the mechanism of action in *M. tuberculosis* also remains to be elucidated.

To date, the structures of thirteen natural Callyaerins (corresponding to Callyaerins A - M) were reported (see Figure 14)[97]. All these cyclic peptides are proline-rich, hydrophobic and contain 9-13 amino acid residues, from which 3-4 are prolines or proline analogues. The rest are predominantly hydrophobic amino acids such as Ile, Leu, Val, and Phe, with all amino acids present in the L-configuration. The core of their

structure is an unusual, non-proteinogenic *(Z)*-2,3-diaminoacrylic acid (DAA) residue, which constitutes the template for ring closure (5-8 residues) and supports the linkage to the peptide side chain (3-5 residues)[95]. The endiamino group of the DAA moiety supports the rigid structure of the cyclic peptides[98]. Also the high number of proline residues (or γ-hydroxyprolines) in Callyaerins may provide additional rigidity to the peptide backbone due to their restricted dihedral angles and may lead to higher affinity and selectivity for protein binding[99,100].

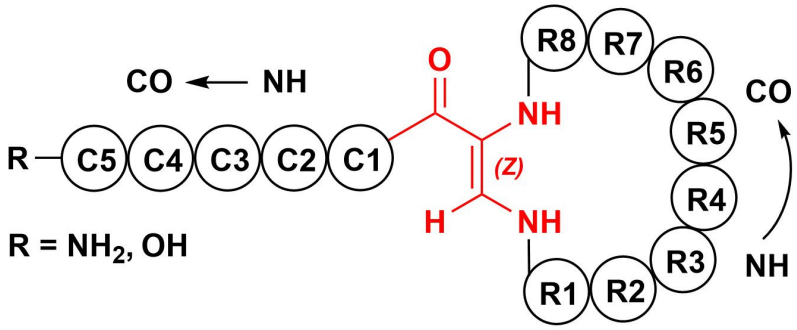

#	Callyaerin	R1	R2	R3	R4	R5	R6	R7	R8		C1	C2	C3	C4	C5	R
1	A	Ile	Hyp	Val	Ile	Leu	Pro	Pro	Leu		Pro	Ile	Phe	Gly		NH_2
2	B	Ile	Hyp	Ile	Ile	Leu	Pro	Pro	Leu		Pro	Ile	Phe	Gly		NH_2
3	C	His	Hyp	Leu	Leu	Pro	Pro	Val			Pro	Leu	Phe	Gly		NH_2
4	D	Ile	Hyp	Ile	Phe	Pro	Pro	Leu			Pro	Ile	Asn	Ala	Ile	NH_2
5	E	Leu	Pro	Phe	Phe	Pro	Pro	Val			Pro	Ile	Ile	Gly		NH_2
6	F	Val	Pro	Val	Phe	Pro	Pro	Leu			Phe	Ile				NH_2
7	G	Leu	Pro	Phe	Phe	Pro	Pro	Leu			Pro	Pro	Phe	Gly		NH_2
8	H	Val	Pro	Val	Phe	Pro	Pro	Leu			Pro	Ile				NH_2
9	I	Leu	Pro	Phe	Phe	Pro	Pro	Val			Pro	Leu	Phe	Gly		NH_2
10	J	Phe	Pro	Leu	Phe	Pro	Pro	Val			Pro	Ile	ile	Gly		NH_2
11	K	Phe	Pro	Phe	Gly	Leu	Pro	Pro	Phe		Pro	Phe	Ile	Asp		OH
12	L	Ile	Hyp	Glu	Ile	Val	Pro	Pro	Leu		Pro	Leu	Phe			NH_2
13	M	AMOIPA	Hyp	Leu	Leu	Pro	Pro	Val			Pro	Leu	Phe	Gly		NH_2
14	Callynormine A	Ile	Hyp	Val	Leu	Pro	Pro	Leu			Pro	Phe	Leu			OH

Figure 14: General structure and amino acid sequences of all natural Callyaerins (based on [45])

1.4.3 The ring forming unit *(Z)*-2,3-diaminoacrylic acid (DAA) in Callyaerins

The structural rare *(Z)*-2,3-diaminoacrylic acid (DAA) unit is the ring forming element in all Callyaerins and is essential for the antimycobacterial activity of Callyaerin A. This was shown by chemical synthesis of an all-amide analogue, which was inactive against *Mtb*, highlighting the important role of the rare DAA moiety for bioactivity[101].

The suspected biosynthesis of the DAA moiety may proceed by oxidation of a serine or cysteine residue to generate a formyl glycine which will undergo Schiff base formation with the free amino group of the last amino acid in the linear sequence, followed by double bond migration[98]. Formylglycine (FGly) has been found in both eukaryotic and prokaryotic sulfatases. FGly-hydrate is located within the catalytic center of the enzyme, where it is covalently sulfated or phosphorylated during catalysis[102–104].

The first chemical synthesis of Callyaerin A was recently reported. It is based on a solid phase approach in which a linear precursor for Callyaerin A is synthesized. To incorporate the ‘serine aldehyde moiety’, an Fmoc-protected formylglycine-diethylacetal as a masked form of formylglycine is used (see Figure 15). The intramolecular cyclization between the formylglycine and the N-terminal amine of the linear peptide precursor forms the DAA unit[101].

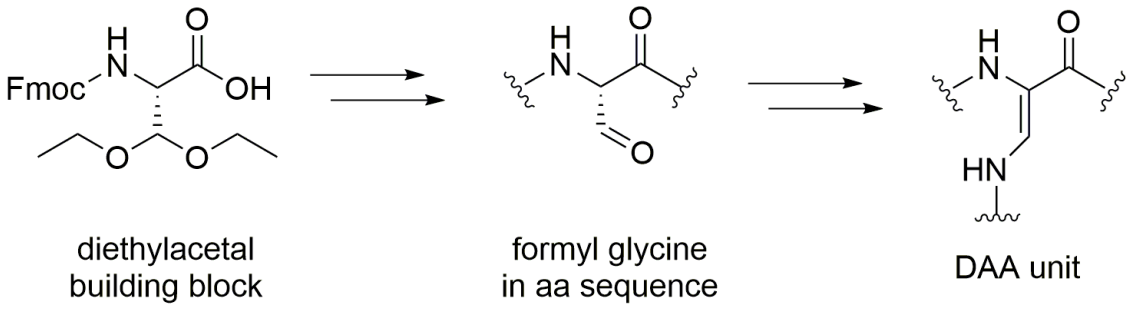

Figure 15: Reported synthetic approach for the DAA unit in Callyaerins. An Fmoc-protected formylglycine-diethylacetal building block is used in SPPS. After acidic peptide cleavage and deprotection the unstable aldehyde is formed and reacts with the free N-terminus to the DAA unit.

For this synthetic approach the Fmoc-protected formylglycine-diethylacetal building block has to be prepared in a 6-step synthesis from the commercially available D-serine-methylester[105]. By contrast, the oxidation of serine-containing peptides to the

corresponding peptidyl tosyl enolates[106,107], which could further react with the N-terminal amine to furnish a cyclic peptide with a DAA moiety, was reported as unsuccessful[101]. Further alternative syntheses, although highly desirable, have not been reported so far.

Another example for DAA-containing cyclic peptides is Callynormine A, which previously had been isolated from the Kenyan sponge *Callyspongia abnormis*[98]. So far, the occurrence of this peptide class is limited to the sponge genus Callyspongia. The bioactivity of Callynormine A is still unknown, but a new synthetic access to sufficient amount of substance from this work will enable further biological studies.

Generally, the DAA group is of special interest for the synthesis of biomimetic cyclic peptides, as it is expected to introduce additional rigidity into their structure.

2 Objectives

The aim of this study was the synthesis and the derivatization of a new class of antitubercular agents, the Callyaerins, as well as the evaluation of their biological properties and pharmaceutical potential, *via* a concerted chemical biology approach. To this end, three different sub-objectives were defined:

The first sub-objective was to establish a chemical synthesis of Callyaerins, thereby allowing to confirm the proposed chemical structures of the isolated natural products and to generate sufficient material for further biological investigations. Therefore, emphasis was put into the development of an easily accessible synthesis route that enables parallel synthesis of a whole series of derivatives for gaining insights into the underlying structure-activity relationships. Fortunately, Callyaerins are mostly built up from standard amino acids that can be synthesized with reasonable efforts *via* solid phase peptide synthesis (SPPS). Therefore, the challenging part in the total synthesis of Callyaerins is the ring formation taking place between the amino group of the N-terminal amino acid and a reactive group within the peptide sequence (e. g. a formyl glycine moiety). Such a reactive moiety must either be directly compatible with the harsh SPPS conditions (e. g. by masking it with a suitable protecting group) or has to be selectively generated after SPPS. The first-mentioned strategy, equivalent to the synthesis of a protected building block for SPPS, was used for the first total synthesis of Callyaerin A published in 2018 by the Brimble group[101]. Their approach required a 6-step synthesis of a suitably acetal-protected formyl glycine building block for SPPS. In this thesis however, an alternative approach was envisaged in which the aldehyde function was generated *a posteriori* of the peptide synthesis from a linear precursor peptide harbouring a ‘standard’ serine moiety at this position during SPPS (see 3.1).

With a straightforward synthesis route established, the second sub-objective of this thesis was to elucidate the structure-activity relationships underlying Callyaerins’ bioactivity. Accordingly, many different derivatives in which alanine substitutions or other modifications were incorporated, were synthesized and their corresponding MIC_{90} values for distinct *M. tuberculosis* strains were determined. These structure-activity relationships were also used to potentially identify more potent Callyaerin derivatives than the isolated natural products.

Finally, besides determination of the bioactivity in various virulent or attenuated mycobacterial strains, also growth inhibition vs. human cell lines were planned to gain insights into the mycobacterial vs. human selectivity and thus pharmaceutical potential of Callyaerins.

As a last third sub-objective, a target identification of Callyaerins in *M. tuberculosis via* a proteomic approach was envisaged. For this purpose, the synthesis of an affinity probe was required, e. g. a biotin-tagged Callyaerin derivative, which should then have been used to enrich target proteins from a cell lysate to an avidin-coated resin. Protein identification should then have been performed by mass spectrometry (MS)-based proteomics, thereby gaining insights into the molecular mode-of-action of Callyaerins' bioactivity.

In the next chapters, a description is given on how these different aims were achieved.

3 Results and discussion

3.1 Synthesis of Callyaerins

3.1.1 Retrosynthesis of Callyaerin A

The retrosynthetic approach conducted in this thesis is shown in Figure 16 for Callyaerin A as an example.

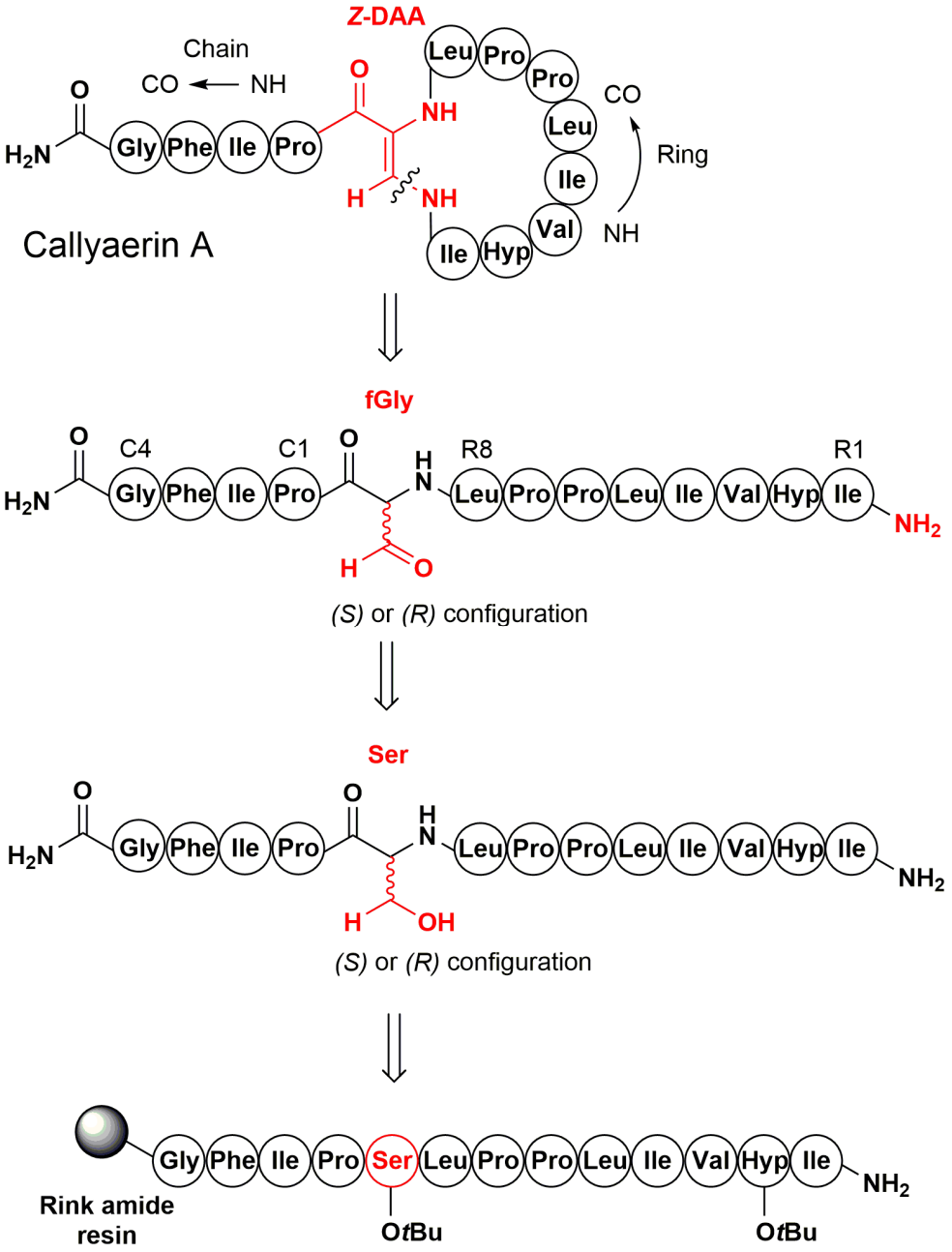

Figure 16: Envisaged retrosynthesis scheme for Callyaerin A. A combined solid phase peptide synthesis (SPPS) approach with a solution phase oxidation reaction was put forward as a feasible strategy.

All members of the Callyaerin's class of natural products share the structurally rare *Z*-diamino acrylic acid (*Z*-DAA) group as a cyclization element of an otherwise linear amino acid sequence. Therefore, a rational retrosynthesis must focus on the ring forming reaction leading to the *Z*-DAA group.

The following considerations were thereby essential to guide the development of a suitable synthesis route: Obviously, the Z-DAA group is an amino acid derivative which strongly favors on generating this moiety from an amino acid analogue. The other side-chain nitrogen atom represents the N-terminus of the first ring amino acid on position R1 (Ile for Callyaerin A) and is therefore predestinated for a retrosynthetic disconnection. The *Z*-enamine substructure can be generated by an intramolecular condensation reaction with a formyl glycine residue, followed by a subsequent double bond migration to the more stable conjugated position. Interestingly, the stereochemical information at the α-chiral center gets lost in this cyclisation reaction due to the nature of the double bond. Hence, either the *R*- or *S*-configuration of the α-formylglycine is applicable in this synthesis.

Furthermore, the aldehyde function can be generated from an alcohol group by selective oxidation. In the present retrosynthesis route, the reactive residue for ring formation is thus reduced to a simple serine moiety which is easily implementable into a peptide by standard Fmoc-SPPS with a side-chain protected Fmoc-serine residue.

In the synthesis of the linear peptide, a Rink amide resin was furthermore chosen as the solid support due to the C-terminal amide function in most of the Callyaerins. In case of a desired free carboxylic C-terminus (e. g. for Callyaerin K), a 2-chlorotrityl resin may be used.

3.1.2 Solid phase peptide synthesis of linear precursors for Callyaerins and derivatives

3.1.2.1 General Fmoc based SPPS

The envisaged strategy for the synthesis of Callyaerins and derivatives was the assembly of a linear amino acid sequence *via* Fmoc-based solid phase peptide synthesis with subsequent cyclisation reaction between an oxidized serine residue within the linear peptide sequence and its free N-terminus.

Almost all members of the Callyaerin family possess an amide group at their C-terminus. Therefore, a Rink amide resin was used as the solid support in the solid phase peptide synthesis to provide the amide group after cleaving the C-terminus from the resin under acidic conditions. For the linear synthesis of Callyaerin K and Callynormine A, the two natural products with a free carboxylic acid at their C-terminus, a 2-chlorotrityl chloride resin was however employed instead.

All building blocks for the linear peptide synthesis were protected with a Fmoc group at their N-terminus; the amino acid side chain functionalities were orthogonally protected (e. g. *t*Bu or Boc) according to standard Fmoc solid phase peptide synthesis protocols. All used amino acids were in the L-configuration. The liquid handling during synthesis was assisted by an automated solid phase peptide synthesizer.

A synthesis scheme of the linear peptide assembly is depicted in Figure 17. The synthesis started with the coupling of a Fmoc-protected amino acid to the resin. Subsequently, cycles of Fmoc deprotection *via* piperidine and coupling of the next amino acid were repeated to assemble the total linear peptide sequence. Piperidine-mediated Fmoc deprotection of the last amino acid then led to an exposed unprotected N-terminus. The final cleavage of the linear peptide from the resin resulted in an amide group at the C-terminus if Rink amide resins or a carboxylic acid group if 2-chlorotrityl chloride resins were used, respectively.

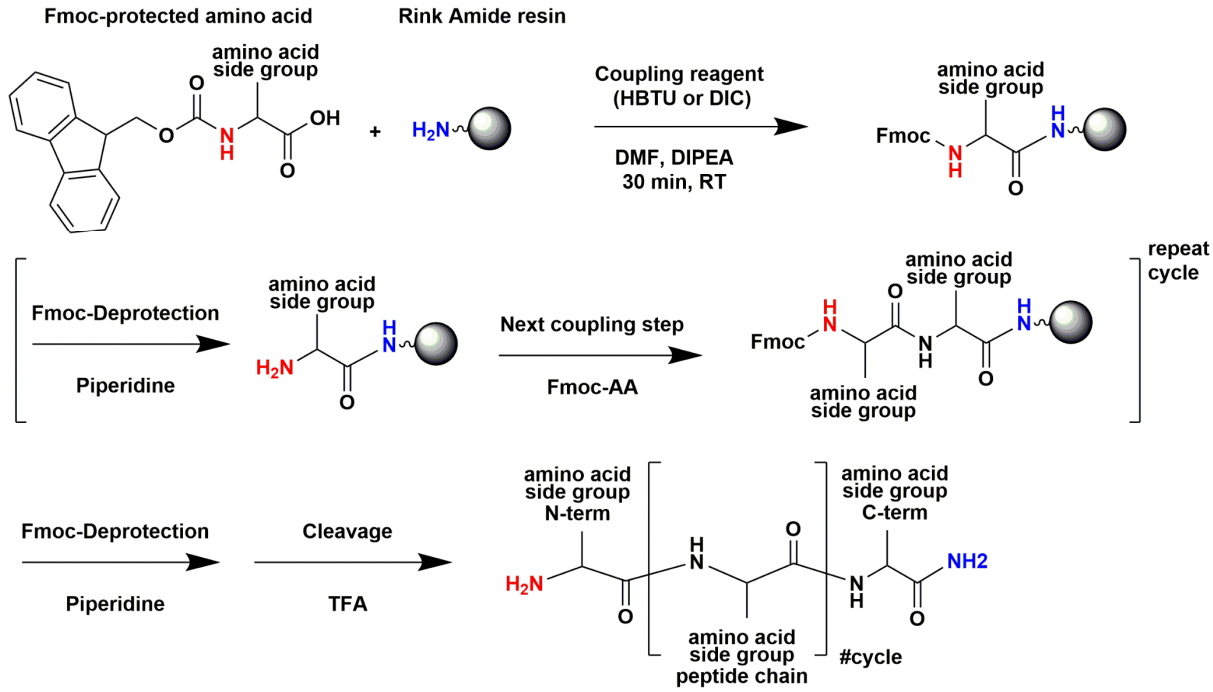

Figure 17: Scheme of the solid phase peptide synthesis *via* Fmoc chemistry on a Rink amide resin.

To ensure efficient amino acid couplings during peptide synthesis, double couplings, either with HBTU (Hexafluorophosphate Benzotriazole Tetramethyl Uronium) or DIC (*N,N'*-Diisopropylcarbodiimide) as coupling reagents and DIPEA (*N,N*-Diisopropylethylamine) as a base were used. For all coupling steps, HOBt (Hydroxybenzotriazole) was added to lower racemization during coupling. In all coupling, deprotection and washing steps, DMF (Dimethylformamide) was employed as the solvent. Piperidine was used for the deprotection of the Fmoc group. The final cleavage of the linear peptide from the resin was conducted with a cleavage cocktail consisting of 95 % TFA (Trifluoroacetic acid), 2.5 % TIPS (Triisopropyl silane) and 2.5 % water.

The cleavage solution was added to cold diethylether to induce precipitation of the linear, fully deprotected peptide. The residue was separated from the liquid phase and redissolved in an acetonitrile/water solution and purified by preparative HPLC (also acetonitrile/water). After lyophilization, the linear peptide was received as a 'fluffy' light powder.

3.1.2.2 Serine as building block for ring closing reaction to form the (Z)-2,3-diaminoacrylamide moiety

All Callyaerins share a (*Z*)-2,3-diaminoacrylamide moiety as the 'linking unit' between the macrocycle and the extracyclic linear chain. In the present synthesis route, a serine

residue was incorporated as a (*Z*)-2,3-diaminoacrylamide precursor into the linear peptide. By a subsequent oxidation of the serine hydroxyl group to a reactive aldehyde moiety, the serine residue was suitable to form the desired (*Z*)-2,3-diaminoacrylamide moiety in a ring closing reaction with the free N-terminus (also see 3.1.3). Even in presence of other hydroxyl groups, e. g. from hydroxyl proline (Hyp), oxidation primarily occurred at the serine moiety.

The use of the standard amino acid serine as building block for forming a ring closing joint is thus very convenient, because serine is commercially available as a *tBu*-protected amino acid (Fmoc-L-Ser(*t*Bu)-OH) and very cheap (< 1 € per gram). Another advantage is the stability of the deprotected residue (-OH group) in the linear precursor peptide, which can be worked up under acidic and aqueous conditions and dried in the rotary evaporator at water bath temperatures of 40 °C for hours. This synthesis methodology is thus for more practical and straight-forward than the previously reported approach that relied on a lengthy synthesis of a suitable-protected Fmoc-serine aldehyde building block.

3.1.2.3 Hydroxyproline

Many Callyaerins, including the bioactive Callyaerins A and B, share a *L*-4-hydroxyproline residue in the R2 position. The corresponding building block that was used during the synthesis, i. e. Fmoc-L-Hyp(*t*Bu)-OH, is the most expensive protected amino acid (30 € per gram) of the whole synthesis route. For this reason, a couple of Callyaerin derivatives were synthesized in which the hydroxyproline was replaced by the cheaper and structurally related amino acid proline. Accordingly, if later assays turn out that these proline derivatives are as active as the parent hydroxyproline compounds (see 3.2.2), the amino acid exchange Hyp → Pro represents an economic way to generate bioactive Callyaerin derivatives in higher amounts, e. g. for more extensive biological assays, at reasonable costs.

Hydroxyproline bears a secondary alcohol group which is deprotected under resin peptide cleavage conditions together with the primary alcohol group of the serine residue in the same sequence. Accordingly, the oxidation of the primary alcohol group of the serine residue may also result in an oxidation of the secondary alcohol group of the hydroxyproline residue. Importantly, the developed synthesis of Callyaerins

however did not significantly result in secondary alcohol oxidation, even if an excess of the oxidation reagent was used. Only upon longer oxidation reaction times, the formation of an oxidized byproduct with the corresponding mass of the oxidized secondary alcohol was observed in test reactions in small quantities (less than 3 %). These side-products however were easily separated from the desired Callyaerin product with the established HPLC method.

3.1.3 Cyclisation reaction and formation of the (*Z*)-2,3-diaminoacrylamide unit

Having the linear fully deprotected peptide in hand, the oxidation of the primary alcohol group of the serine residue to an aldehyde was achieved by selective oxidation with Dess-Martin periodinane.

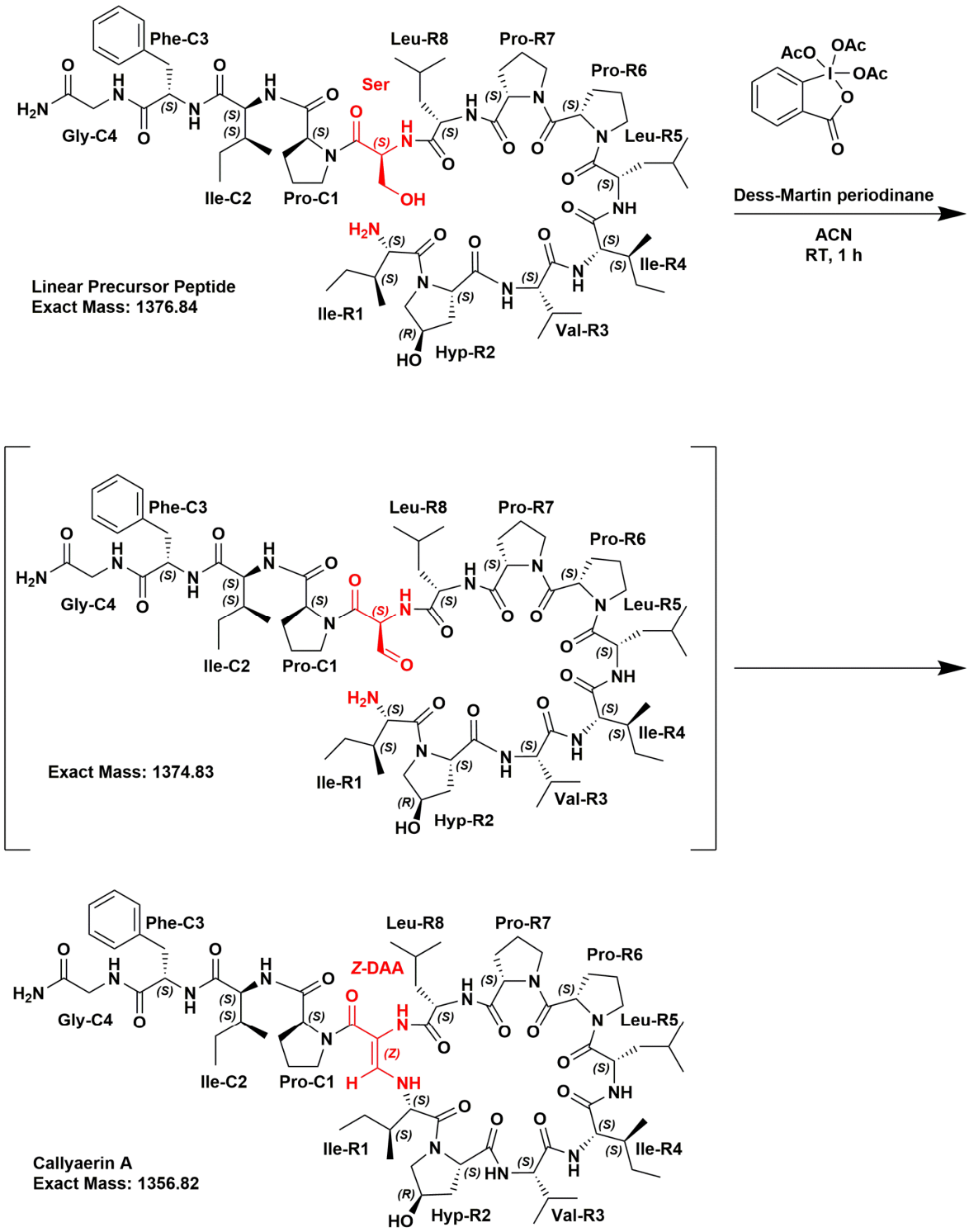

Figure 18: Scheme of the intramolecular cyclisation reaction of the linear precursor peptide for Callyaerin A.

In the corresponding oxidation reaction, acetic acid is formed as a side product from the Dess-Martin periodinane reagent. Generally, an acidic environment catalyzes the reaction of an amine with an aldehyde to form an enamine functionality[108]. Therefore, no additional acid was needed to perform the cyclization reaction.

Acetonitrile was chosen as the reaction solvent for the following reasons. First, it turned out to be a suitable solvent for the overall very hydrophobic cyclic peptides of the Callyaerin family. Second, it is aprotic and thus does not interfere with the Dess-Martin oxidation. Third, it is miscible with water in any proportion and can be used as directly as a solvent in analytical and preparative HPLC runs. Fourth, it is, in comparison to for example DMF and DMSO, easy to evaporate due to its high vapor pressure.

Dess-Martin periodinane is however only moderately soluble in acetonitrile, while the linear precursor peptide as well as the cyclic Callyaerin products are highly soluble in acetonitrile. The difference in solubility was utilized in the work-up procedure of the reaction solution. In a centrifuge tube, four equivalents of DMP were suspended in acetonitrile, containing the dissolved linear precursor peptide. The excess of DMP was then removed by centrifugation and the supernatant was directly injected into HPLC for purification of the product.

The analysis of the reaction mixtures by LC-MS revealed the following Dess-Martin-periodinane-derived reaction products as shown in Figure 19. These hydrophilic substances elute early and can be easily separated by RP-HPLC from all Callyaerin derivatives. The desired cyclic Callyaerin products were the most hydrophobic compounds and thus eluted as the latest products in the RP-HPLC purification runs.

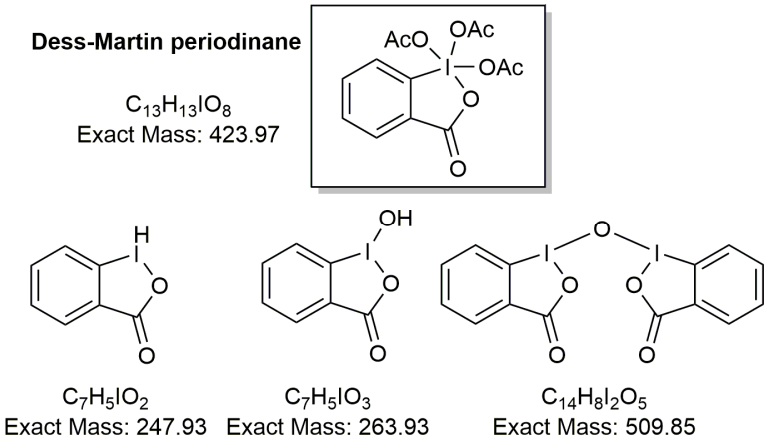

Figure 19: Structures of the oxidation reagent Dess-Martin periodinane and of three reaction products observed in reaction control LC-MS runs.

3.1.4 Synthesis of Callyaerins A and B derived affinity and fluorescence probes

In order to synthesize affinity and fluorescent Callyaerin probes, e. g. for proteomic and microscopic experiments, ‘clickable’ derivatives of Callyaerin A and B were prepared. These derivatives contained an alkine or azide group, which was integrated into the sequence by exchange of the glycine residue in chain position C4 vs. either a Propargyl glycine (Pra) or Azidohomoalanine (Aha) residue, respectively. The corresponding compounds *CalA_C4Pra, CalA_C4Aha* and *CalB_C4Pra* were also active against the *M. tuberculosis* H37Rv strain (see 3.2.1) and should therefore be suitable for click reactions *in vitro* or even *in vivo*.

For proteomic experiments, the availability of an affinity probe is essential (i. e. a bioactive compound that can be used to enrich target proteins *via* affinity purification prior to the MS analysis). A widely applied system for such target enrichments is the use of the highly stable Avidin-Biotin interaction (also see 3.3). Accordingly, an Azide-PEG3-Biotin conjugate was chosen as a partner in the click reaction with *CalA_C4Pra*. The corresponding synthesis of *Biotin-CalA* and *Biotin-CalB* is shown in Figure 20. Both probes were used in 3.3.2 for a proteomic affinity enrichment experiment in *M. tuberculosis*.

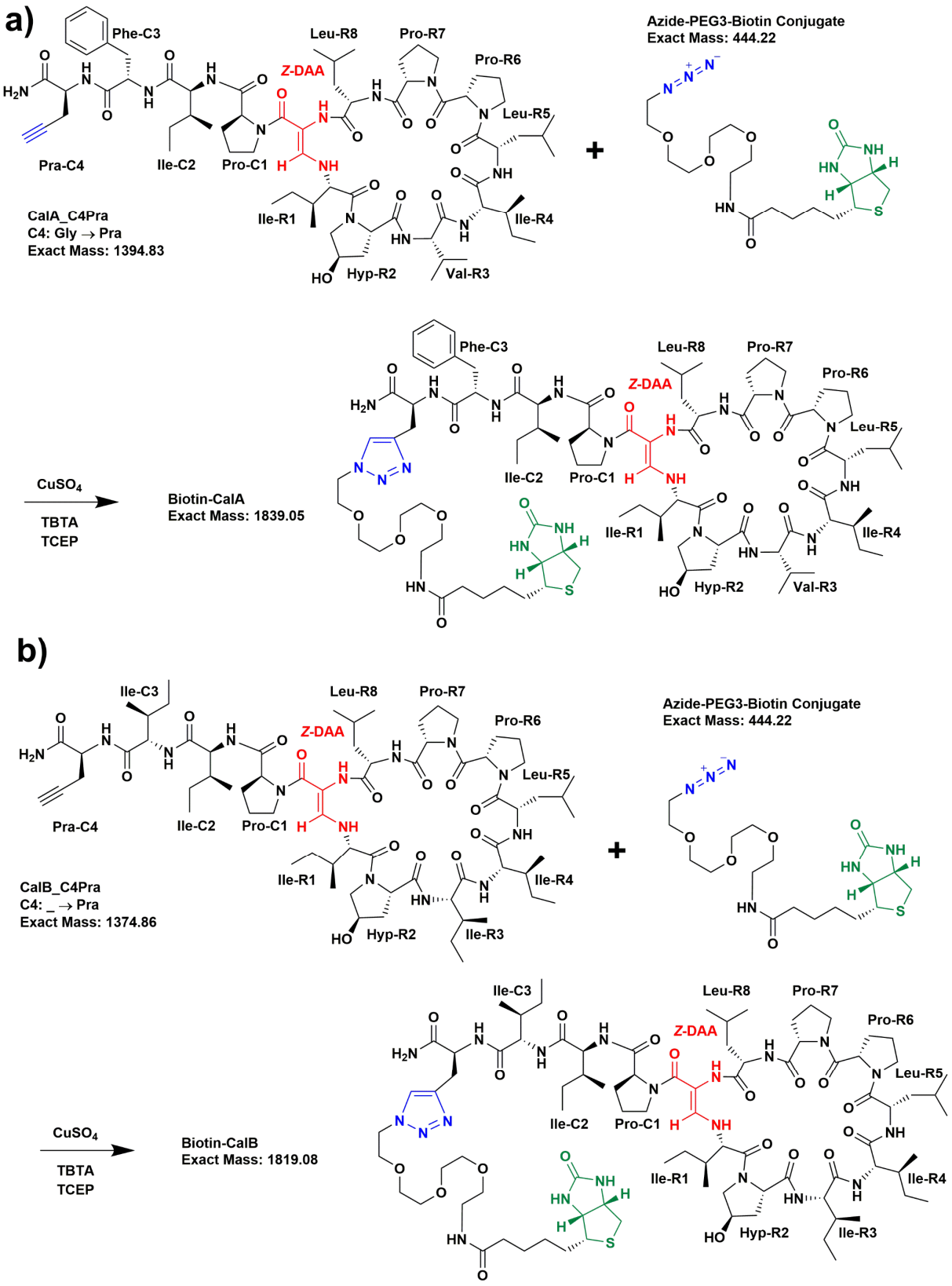

Figure 20: Scheme of the click reaction between the alkyne tagged derivatives of Callyaerin A and B and an Azide-PEG3-Biotin conjugate to form the respective Biotin probes. a) Click reaction of *CalA_C4Pra* to *Biotin-CalA*. b) Click reaction of *CalB_C4Pra* to *Biotin-CalB*.

According to the synthesis of the biotin-tagged probe, an additional chemical probe with a fluorescent dye was synthesized in an analogous manner as described in Figure 21).

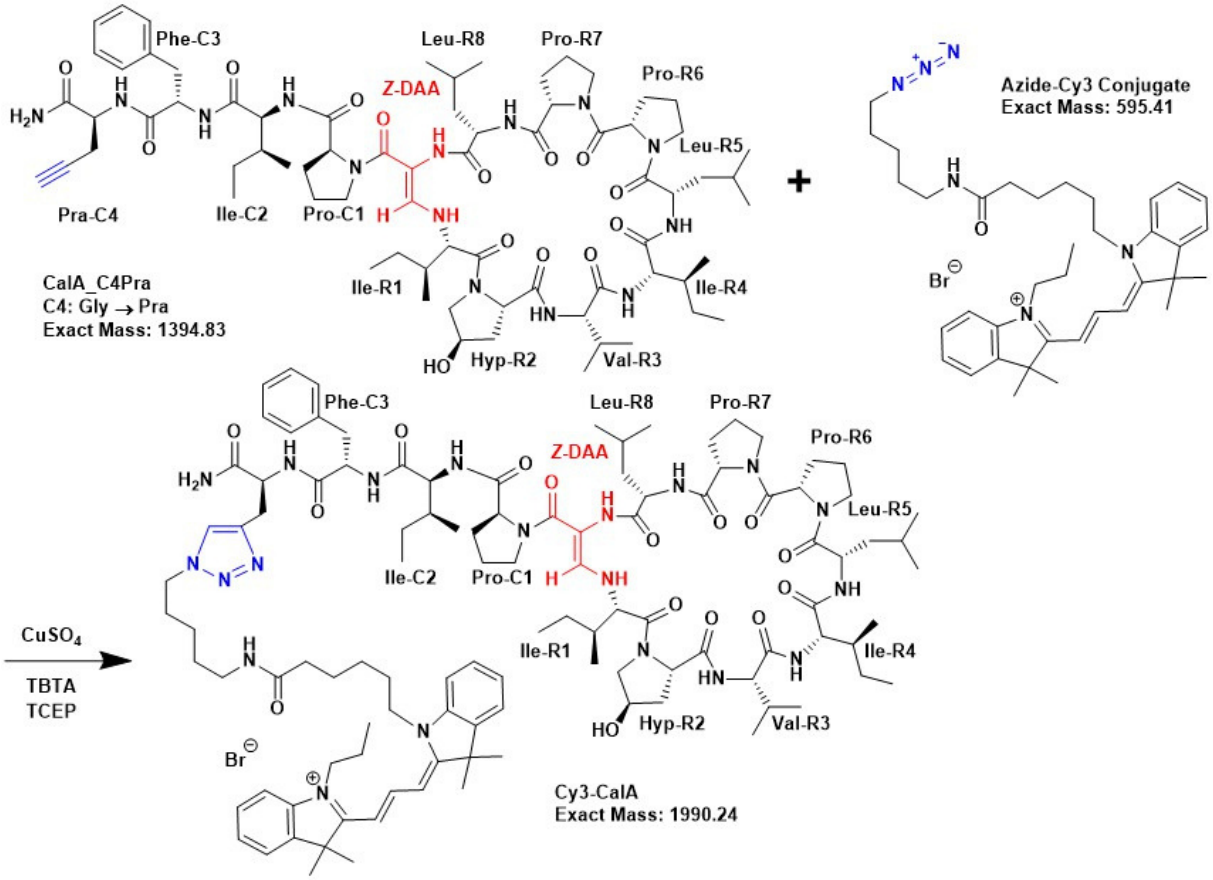

Figure 21: Scheme of the click reaction between the alkyne-tagged derivative of Callyaerin A *CalA_C4Pra* and an Azide-PEG3-Cy3 conjugate to generate the respective Cy3-CalA probe.

Here, an Azide-Cy3 conjugate was linked in a click reaction with the alkyne-tagged Callyaerin A derivate *CalA_C4Pra*. The resulting *Cy3-CalA* probe is a prospective marker for microscopic or photometric experiments, e.g. for studying the mode of action of Callyaerins. Initial microscopic experiments on living human HeLa cells indicated a suitable permeability of the cytoplasmic membrane for the *Cy3-CalA* probe (data not shown). Furthermore, this chemical probe may find applications in life cell fluorescence imaging on *M. tuberculosis*.

3.1.5 List of all synthetic Callyaerins and derivatives

In the present work, the developed synthesis route was used for the generation of most members of the Callyaerin natural product family. More specifically, these were the natural compounds Callyaerin A – L and Callynormine A. Callyaerin M, whose structure was also described in the initial research article[97], was not synthesized as its generation requires the prior synthesis of the uncommon amino acid 2-amino-3-(5-methoxy-2-oxoimidazolidin-4-ylidene)propanoic acid (AMOIPA).

Additionally, a set of Callyaerin A derivatives was synthesized for subsequent structure-activity relationship studies. Table 2 lists all during the thesis synthesized Callyaerins and derivatives with the sequences of the linear precursors containing a serine residue for cyclisation with the free N-terminus. The general structure of all natural Callyaerins is depicted in Figure 22.

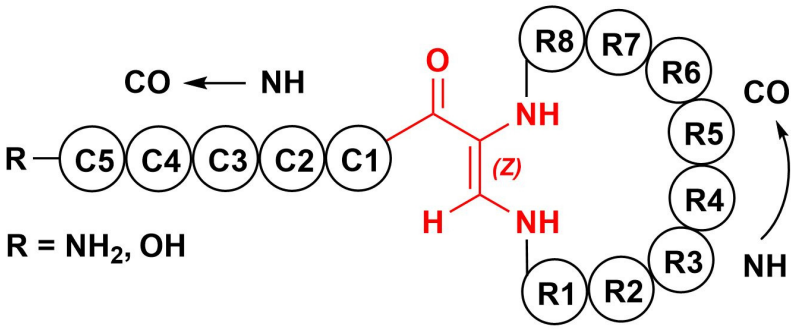

#	Callyaerin	R1	R2	R3	R4	R5	R6	R7	R8		C1	C2	C3	C4	C5	R
1	A	Ile	Hyp	Val	Ile	Leu	Pro	Pro	Leu		Pro	Ile	Phe	Gly		NH_2
2	B	Ile	Hyp	Ile	Ile	Leu	Pro	Pro	Leu		Pro	Ile	Phe	Gly		NH_2
3	C	His	Hyp	Leu	Leu	Pro	Pro	Val			Pro	Leu	Phe	Gly		NH_2
4	D	Ile	Hyp	Ile	Phe	Pro	Pro	Leu			Pro	Ile	Asn	Ala	Ile	NH_2
5	E	Leu	Pro	Phe	Phe	Pro	Pro	Val			Pro	Ile	Ile	Gly		NH_2
6	F	Val	Pro	Val	Phe	Pro	Pro	Leu			Phe	Ile				NH_2
7	G	Leu	Pro	Phe	Phe	Pro	Pro	Leu			Pro	Pro	Phe	Gly		NH_2
8	H	Val	Pro	Val	Phe	Pro	Pro	Leu			Pro	Ile				NH_2
9	I	Leu	Pro	Phe	Phe	Pro	Pro	Val			Pro	Leu	Phe	Gly		NH_2
10	J	Phe	Pro	Leu	Phe	Pro	Pro	Val			Pro	Ile	ile	Gly		NH_2
11	K	Phe	Pro	Phe	Gly	Leu	Pro	Pro	Phe		Pro	Phe	Ile	Asp		OH
12	L	Ile	Hyp	Glu	Ile	Val	Pro	Pro	Leu		Pro	Leu	Phe			NH_2
13	M	AMOIPA	Hyp	Leu	Leu	Pro	Pro	Val			Pro	Leu	Phe	Gly		NH_2
14	Callynormine A	Ile	Hyp	Val	Leu	Pro	Pro	Leu			Pro	Phe	Leu			OH

Figure 22: General structure and amino acid sequences of all natural Callyaerins (based on [45])

In this thesis, a special nomenclature is used to denote changes in their sequence that were incorporated for structure-activity relationships. In this nomenclature, first the parent Callyaerin is noted, following by a short code describing the specific position in the sequence of the Callyaerin that has been substituted and finally the one-letter-code for the amino acid that has been placed into this position. For example, *CalA_R1A* is a Callyaerin A derivative with an alanine on ring position R1, *CalA_C3W* has a tryptophan on chain position C3 and *CalA_C4X* has no amino acid on chain position C4 (X for deletion). A combination of exchanges is denoted with a plus sign (e. g. *CalA_R2P+C3I+C4X*).

Table 2: List of all during this thesis synthesized Callyaerins and derivatives with their corresponding linear sequence (i.e. prior to oxidation and ring formation), final yield and method of characterization.

#	substance	exact mass calc. [Da]	linear sequence 1=Hyp,2=Pra,3=Aha	SPPS # (reactor)	yield [mg]	NMR
1	Callyaerin A	1356.82	I1VILPPLSPIFG	R58	7.50	$^{1}H,^{13}C$
2	Callyaerin B	1279.83	I1IILPPLSPII	R56	33.33	^{1}H
3	Callyaerin C	1267.71	H1LLPPVSPLFG	R82	8.70	^{1}H
4	Callyaerin D	1385.81	I1IFPPLSPINAI	R76	5.73	^{1}H
5	Callyaerin E	1261.72	LPFFPPVSPIIG	R69	60.10	$^{1}H,^{13}C$
6	Callyaerin F	1093.63	VPVFPPLSFI	R70	14.07	^{1}H
7	Callyaerin G	1293.69	LPFFPPLSPPFG	R71	35.00	^{1}H
8	Callyaerin H	1043.62	VPVFPPLSPI	R72	4.73	^{1}H
9	Callyaerin I	1295.71	LPFFPPVSPLFG	R73	47.74	^{1}H
10	Callyaerin J	1261.72	FPLFPPVSPIIG	R78	29.00	^{1}H
11	Callyaerin K	1459.72	FPFGLPPFSPFID	R105	1.36	-
12	Callyaerin L	1315.75	I1EIVPPLSPLF	R77	2.30	-
13	Callynormine A	1187.70	I1VLPPLSPFL	R104	1.64	-
14	CalA_R1A	1314.77	A1VILPPLSPIFG	R67	7.97	^{1}H
15	CalA_R2A	1314.81	IAVILPPLSPIFG	R106	3.16	-
16	CalA_R2P	1340.82	IPVILPPLSPIFG	R52	36.50	^{1}H
17	CalA_R3A	1328.79	I1AILPPLSPIFG	R35	8.27	^{1}H
18	CalA_R3F	1404.82	I1FILPPLSPIFG	R126	7.22	^{1}H
19	CalA_R3I	1370.83	I1IILPPLSPIFG	R90	5.61	^{1}H
20	CalA_R3L	1370.83	I1LILPPLSPIFG	R98	23.70	^{1}H
21	CalA_R4A	1314.77	I1VALPPLSPIFG	R51	21.50	^{1}H
22	CalA_R5A	1314.77	I1VIAPPLSPIFG	R45	34.40	^{1}H
23	CalA_R5D	1358.76	I1VIDPPLSPIFG	R100	4.74	-
24	CalA_R6A	1330.80	I1VILAPLSPIFG	R121	12.83	-
25	CalA_R7A	1330.80	I1VILPALSPIFG	R125	8.06	^{1}H
26	CalA_R8A	1314.77	I1VILPPASPIFG	R46	10.95	^{1}H
27	CalA_R8W	1415.80	I1VILPPWSPIFG	R61	6.17	-
28	CalA_R8V	1342.80	I1VILPPVSPIFG	R99	9.17	^{1}H
29	CalA_C1A	1330.80	I1VILPPLSAIFG	R68	2.37	-
30	CalA_C2A	1314.77	I1VILPPLSPAFG	R33	3.44	^{1}H
31	CalA_C3A	1280.79	I1VILPPLSPIAG	R38	1.40	-
32	CalA_C3L	1322.83	I1VILPPLSPILG	R59	6.30	^{1}H
33	CalA_C3I	1322.83	I1VILPPLSPIIG	R64	0.84	-
34	CalA_C3W	1381.81	I1VILPPLSPIWG	R60	4.70	^{1}H
35	CalA_C4A	1370.83	I1VILPPLSPIFA	R39	2.60	^{1}H
36	CalA_C4X	1299.80	I1VILPPLSPIF	R62	1.90	^{1}H
37	CalA_C4Pra	1394.83	I1VILPPLSPIF2	R55	14.40	^{1}H
38	CalA_C4Aha	1425.85	I1VILPPLSPIF3	R84	8.20	^{1}H
39	CalA_C5A	1441.87	I1VILPPLSPIFGA	R63	3.00	^{1}H
40	CalA_C3X+C4X	1152.73	I1VILPPLSPI	R95	8.78	^{1}H
41	CalA_C3I+C4X	1265.81	I1VILPPLSPII	R96	4.59	-
42	CalA_R2P+C3I+C4X	1249.82	IPVILPPLSPII	R97	8.91	^{1}H

#	substance	exact mass calc. [Da]	linear sequence 1=Hyp,2=Pra,3=Aha	SPPS # (reactor)	yield [mg]	NMR
43	CalA_R3I+R2P	1354.84	IPIILPPLSPIFG	R119	6.67	-
44	CalB_C4Pra	1374.86	I1IILPPLSPII2	R79	10.24	-
45	Biotin_CalA probe	1839.05	from CalA_C4Pra		5.25	-
46	Biotin_CalB probe	1819.08	from CalB_C4Pra		1.11	-
47	Cy3-CalA probe	1990.24	from CalA_C4Pra		0.80	-

3.1.6 HRMS data of all synthetic Callyaerins and derivatives

HR-MS measurements of all synthetic Callyaerins and derivatives were performed on an Ultra High Resolution-TOF mass spectrometer with an ESI source. The results are listed in Table 3. All measured values fit to the calculated ion masses $[M+H]^+$ with an average delta of 1.58 ppm.

Table 3: HRMS data of all synthetic Callyaerins and derivatives.

#	synthetic substance	exact mass calculated	$[M+H]^+$ calculated	$[M+H]^+$ measured	delta [ppm]	sum formula cyclic peptide
1	Callyaerin A	1356.8169	1357.8242	1357.8276	2.52	$C_{69}H_{108}N_{14}O_{14}$
2	Callyaerin B	1279.8268	1280.8341	1280.8369	2.20	$C_{65}H_{109}N_{13}O_{13}$
3	Callyaerin C	1267.7077	1268.7150	1268.7175	1.99	$C_{63}H_{93}N_{15}O_{13}$
4	Callyaerin D	1385.8071	1386.8144	1386.8167	1.68	$C_{69}H_{107}N_{15}O_{15}$
5	Callyaerin E	1261.7223	1262.7296	1262.7328	2.55	$C_{66}H_{95}N_{13}O_{12}$
6	Callyaerin F	1093.6324	1094.6397	1094.6411	1.30	$C_{58}H_{83}N_{11}O_{10}$
7	Callyaerin G	1293.6910	1294.6983	1294.7013	2.34	$C_{69}H_{91}N_{13}O_{12}$
8	Callyaerin H	1043.6168	1044.6241	1044.6250	0.88	$C_{54}H_{81}N_{11}O_{10}$
9	Callyaerin I	1295.7067	1296.7140	1296.7167	2.10	$C_{69}H_{93}N_{13}O_{12}$
10	Callyaerin J	1261.7223	1262.7296	1262.7323	2.16	$C_{66}H_{95}N_{13}O_{12}$
11	Callyaerin K	1459.7176	1460.7249	1460.7258	0.63	$C_{77}H_{97}N_{13}O_{16}$
12	Callyaerin L	1315.7540	1316.7613	1316.7626	1.01	$C_{66}H_{101}N_{13}O_{15}$
13	Callynormine A	1187.6954	1188.7027	1188.7045	1.53	$C_{61}H_{93}N_{11}O_{13}$
14	CalA_R1A	1314.7700	1315.7773	1315.7800	2.07	$C_{66}H_{102}N_{14}O_{14}$
15	CalA_R2A	1314.8064	1315.8137	1315.8152	1.16	$C_{67}H_{106}N_{14}O_{13}$
16	CalA_R2P	1340.8220	1341.8293	1341.8324	2.33	$C_{69}H_{108}N_{14}O_{13}$
17	CalA_R3A	1328.7856	1329.7929	1329.7937	0.62	$C_{67}H_{104}N_{14}O_{14}$
18	CalA_R3F	1404.8169	1405.8242	1405.8268	1.87	$C_{73}H_{108}N_{14}O_{14}$
19	CalA_R3I	1370.8326	1371.8399	1371.8419	1.48	$C_{70}H_{110}N_{14}O_{14}$
20	CalA_R3L	1370.8326	1371.8399	1371.8424	1.84	$C_{70}H_{110}N_{14}O_{14}$
21	CalA_R4A	1314.7700	1315.7773	1315.7795	1.69	$C_{66}H_{102}N_{14}O_{14}$
22	CalA_R5A	1314.7700	1315.7773	1315.7804	2.37	$C_{66}H_{102}N_{14}O_{14}$
23	CalA_R5D	1358.7598	1359.7671	1359.7702	2.30	$C_{67}H_{102}N_{14}O_{16}$

#	synthetic substance	exact mass calculated	$[M+H]^+$ calculated	$[M+H]^+$ measured	delta [ppm]	sum formula cyclic peptide
24	CalA_R6A	1330.8013	1331.8086	1331.8087	0.09	$C_{67}H_{106}N_{14}O_{14}$
25	CalA_R7A	1330.8013	1331.8086	1331.8108	1.67	$C_{67}H_{106}N_{14}O_{14}$
26	CalA_R8A	1314.7700	1315.7773	1315.7783	0.78	$C_{66}H_{102}N_{14}O_{14}$
27	CalA_R8W	1429.8122	1430.8195	1430.8212	1.20	$C_{74}H_{107}N_{15}O_{14}$
28	CalA_R8V	1342.8013	1343.8086	1343.8112	1.95	$C_{68}H_{106}N_{14}O_{14}$
29	CalA_C1A	1330.8000	1331.8073	1331.8103	2.27	$C_{67}H_{106}N_{14}O_{14}$
30	CalA_C2A	1314.7700	1315.7773	1315.7793	1.54	$C_{66}H_{102}N_{14}O_{14}$
31	CalA_C3A	1280.7856	1281.7929	1281.7929	0.02	$C_{63}H_{104}N_{14}O_{14}$
32	CalA_C3L	1322.8326	1323.8399	1323.8417	1.38	$C_{66}H_{110}N_{14}O_{14}$
33	CalA_C3I	1322.8326	1323.8399	1323.8424	1.91	$C_{66}H_{110}N_{14}O_{14}$
34	CalA_C3W	1395.8278	1396.8351	1396.8365	1.02	$C_{71}H_{109}N_{15}O_{14}$
35	CalA_C4A	1370.8326	1371.8399	1371.8424	1.84	$C_{70}H_{110}N_{14}O_{14}$
36	CalA_C4X	1299.7955	1300.8028	1300.8055	2.09	$C_{67}H_{105}N_{13}O_{13}$
37	CalA_C4Pra	1394.8326	1395.8399	1395.8426	1.95	$C_{72}H_{110}N_{14}O_{14}$
38	CalA_C4Aha	1425.8500	1426.8573	1426.8591	1.28	$C_{71}H_{111}N_{17}O_{14}$
39	CalA_C5A	1427.8541	1428.8614	1428.8635	1.49	$C_{72}H_{113}N_{15}O_{15}$
40	CalA_C3X+C4X	1152.7271	1153.7344	1153.7360	1.41	$C_{58}H_{96}N_{12}O_{12}$
41	CalA_C3I+C4X	1265.8111	1266.8184	1266.8205	1.68	$C_{64}H_{107}N_{13}O_{13}$
42	CalA_R2P+C3I+C4X	1249.8162	1250.8235	1250.8257	1.78	$C_{64}H_{107}N_{13}O_{12}$
43	CalA_R3I+R2P	1354.8377	1355.8450	1355.8477	2.01	$C_{70}H_{110}N_{14}O_{13}$
44	CalB_C4Pra	1374.8639	1375.8712	1375.8728	1.18	$C_{70}H_{114}N_{14}O_{14}$
45	Biotin_CalA probe	1839.0481	1840.0554	1840.0559	0.28	$C_{90}H_{142}N_{20}O_{19}S$
46	Biotin_CalB probe	1819.0794	1820.0867	1820.0910	2.38	$C_{88}H_{146}N_{20}O_{19}S$
47	Cy3-CalA probe	1990.2445	1991.2518	1991.2486	-1.59	$C_{109}H_{161}N_{20}O_{15}^+$

3.1.7 Comparison of synthetic Callyaerin A with the natural compound

Three different methods were used to confirm that synthetic Callyaerin A matched to natural Callyaerin A which was donated by the Kalscheuer lab from the HHU Düsseldorf, Germany.

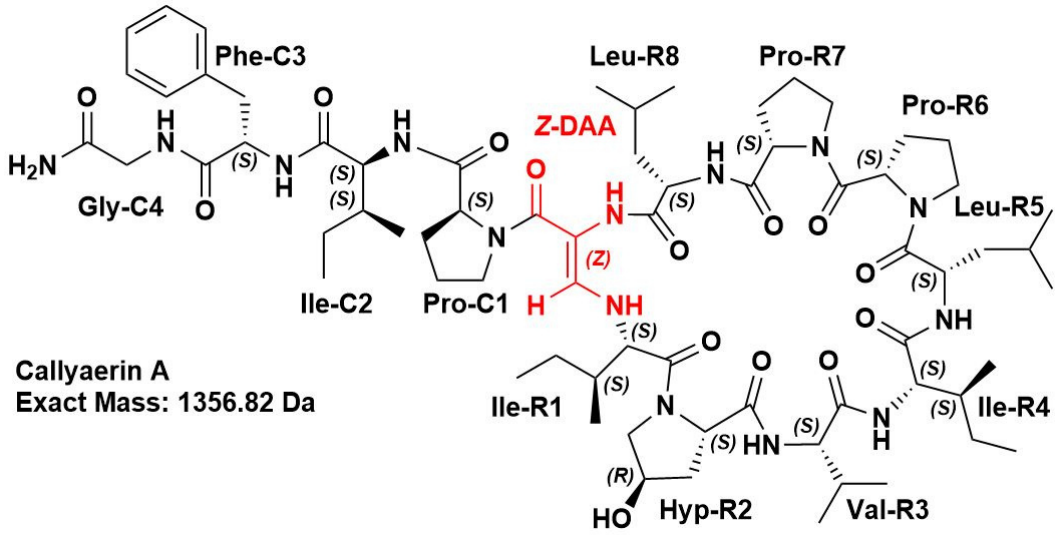

Figure 23: Chemical structure of Callyaerin A.

First, an LC-MS coelution experiment was performed. In Figure 24, the obtained total ion chromatograms of the individual compounds, i. e. natural and synthetic Callyaerin A, and a mixture of both compounds are depicted. These measurements demonstrate the synthetic and natural Callyaerin displayed the same low-resolution mass (*m/z* = 1357) and retention time (38.2 min).

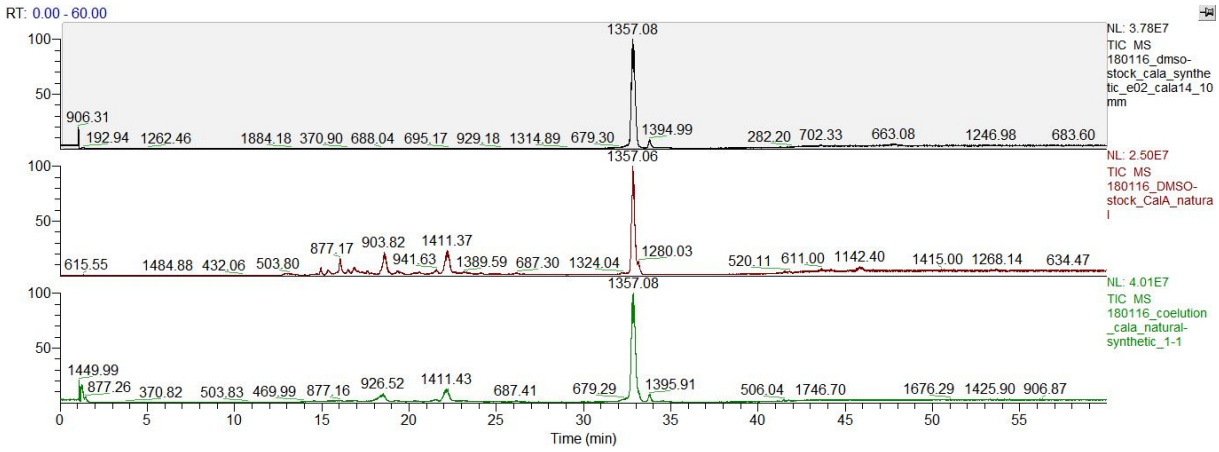

Figure 24: LC-MS coelution experiment with synthetic and natural Callyaerin A. Top: synthetic Callyaerin A, middle: natural Callyaerin A, bottom: 1:1 mixture of synthetic and natural Callyaerin A. Stock solution concentration was 10 mM in DMSO for each compound. A linear gradient from 10% to 100% acetonitrile within 60 min was used.

Second, a high-resolution ^{1}H-NMR spectrum of the synthetic Callyaerin A in DMSO-d_6 was acquired and compared to a corresponding published spectrum of natural Callyaerin A[109]. Both spectra displayed very high similarities as shown in Figure 25. A detailed analysis and comparison of all ^{1}H and ^{13}C signals of Callyaerin A is given in Table 4.

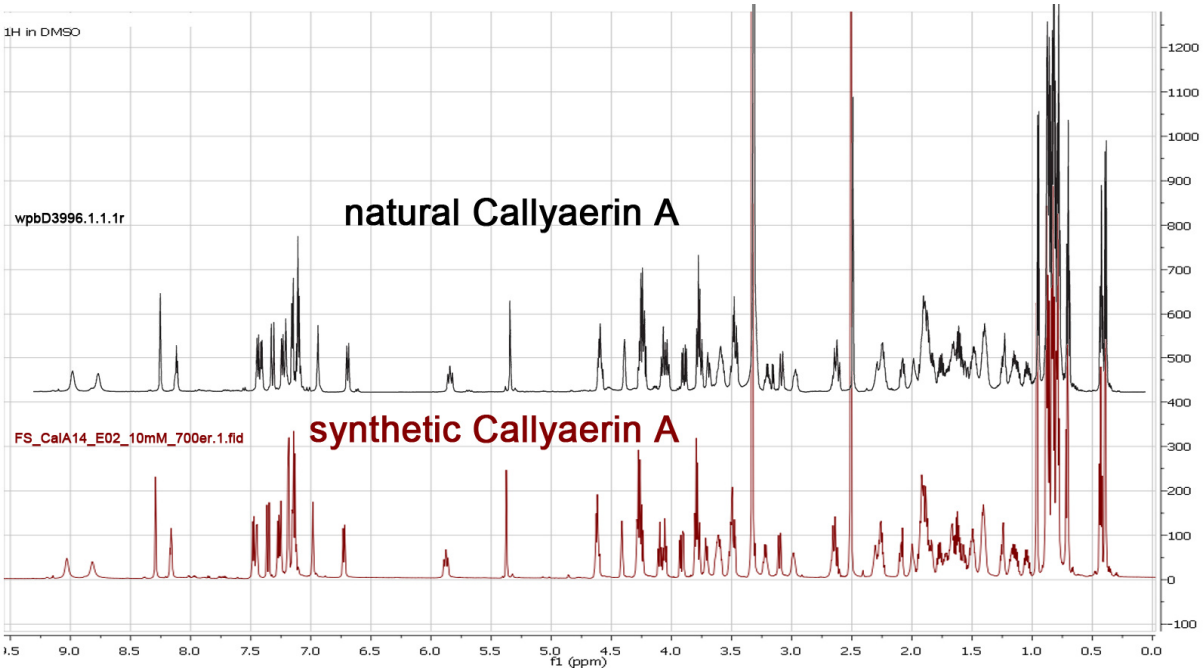

Figure 25: ^{1}H-NMR spectra comparison of natural Callyaerin A[56] (600 MHz, DMSO-d_6) and synthetic Callyaerin A (700 MHz, DMSO-d_6). The ^{1}H-NMR spectrum of the natural Callyaerin A was extracted from the dissertation of Georgios Daletos, HHU Düsseldorf, Germany.

Table 4: ^{1}H and ^{13}C NMR data of synthetic Callyaerin A (700 MHz, DMSO-d_6) and their comparison to the published values of natural Callyaerin A[95] (600 MHz, DMSO-d_6).

unit	position	synthetic δ_C	synthetic δ_H (*J* in Hz)	natural δ_C	natural δ_H (*J* in Hz)
DAA	N*H*		8.29 s		8.29 s
	CO	167.7		167.7	
	α	98.2		98.2	
	β	143.4	7.36 d (13.3)	143.4	7.35 d (13.2)
R1 Ile	N*H*		5.86 dd (12.8, 10.8)		5.87 dd (13.1, 10.2)
	CO	172.0		172.0	
	α	64.4	4.08 m	64.4	4.08 m
	β	37.8	1.41 m	37.8	1.41 m
	γ	24.0	1.41 m, 0.79 m	24.0	1.41 m, 0.79 m
	γ′δ	14.2, 10.5	0.79 m, 0.43 t (7.3)	14.2, 10.5	0.79 m, 0.42 t (7.3)
R2 Hyp	CO	173.3		173.3	
	α	55.6	4.26 m	55.6	4.26 m
	β	37.7	2.09 m, 1.89 m	37.7	2.08 m, 1.89 m
	γ	68.7	4.41 m	68.7	4.41 m
	δ	56.7	3.79 m, 3.71 dd (11.4, 3.7)	56.7	3.77 br d, 3.70 dd (11.4, 3.7)
	OH		5.37 d (3.1)		5.36 d (3.1)
R3 Val	N*H*		9.03 br s		9.03 br s
	CO	172.0		172.0	
	α	66.1	2.99 m	66.1	2.98 dd (10.7, 7.1)
	β	27.1	2.64 m	27.1	2.65 m
	γ	19.2, 19.5	0.83 d (6.6), 0.82 d (6.9)	19.2, 19.5	0.83 d (6.6), 0.82 d (7.0)
R4 Ile	N*H*		8.82 br s		8.81 br s
	CO	171.2		171.2	
	α	59.3[a]	3.79 m	59.3[a]	3.79 m

unit	position	synthetic δ_C	synthetic δ_H (*J* in Hz)	natural δ_C	natural δ_H (*J* in Hz)
	β	36.1	1.50 m	36.1	1.49 m
	γ	[d]	1.41 m, 1.16 m	[d]	1.40 m, 1.13 m
	γ′δ	15.2, 10.2	0.81 d (7.0), 0.78 t (7.3)	15.2, 10.2	0.81 d (6.9), 0.78 t (7.4)
R5 Leu	N*H*		7.45 d (7.0)		7.44 d (7.0)
	CO	172.3		172.3	
	α	49.1[b]	4.62 m	49.1[b]	4.61 m
	β	41.1	1.76 m, 1.25 m	41.1	1.77 m, 1.25 m
	γ	[d]	1.62 m	[d]	1.62 m
	δ, δ′	21.0[c], 21.0[c]	0.87 d (6.4), 0.86 d (6.6)	21.0[c], 21.0[c]	0.87 d (6.5), 0.86 d (6.6)
R6 Pro	CO	171.4		171.4	
	α	64.0	4.08 m	64.0 d	4.05 m
	β	26.2	2.27 m, 1.89 m	26.2	2.30 m, 1.91 m
	γ	[e]	2.00 m, 1.91 m	[e]	1.99 m, 1.91 m
	δ	46.1	3.61 m, 3.50 m	46.1	3.61 m, 3.47 m
R7 Pro	CO	171.4		171.4	
	α	62.5	4.26 m	62.5	4.27 m
	β	28.5	2.27 m, 1.62 m	28.5	2.25 m, 1.61 m
	γ	[e]	1.89 m	[e]	1.94 m, 1.86 m
	δ	47.0	3.61 m, 3.31 m	47.0	3.59 m, 3.31 m
R8 Leu	N*H*		6.73 d (10.0)		6.72 d (10.0)
	CO	172.4		172.4	
	α	50.0[b]	4.62 m	50.0[b]	4.61 m
	β	40.5	1.89 m, 1.57 m	40.5	1.89 m, 1.57 m
	γ	[d]	1.65 m	[d]	1.65 m
	δ, δ′	22.8[c], 23.2[c]	0.96 d (6.5), 0.85 d (6.5)	22.8[c], 23.2[c]	0.96 d (6.6), 0.85 d (6.6)

unit	position	synthetic δ_C	synthetic δ_H (*J* in Hz)	natural δ_C	natural δ_H (*J* in Hz)
C1 Pro	CO	172.7		172.7	
	α	61.9	4.26 m	61.9	4.25 m
	β	29.4	2.27 m, 1.50 m	29.4	2.26 m, 1.50 m
	γ	[e]	1.84 m, 1.72 m	[e]	1.83 m, 1.72 m
	δ	48.7	3.50 m, 3.22 m	48.7	3.51 m, 3.21 m
C2 Ile	N*H*		7.47 m		7.47 m
	CO	171.1		171.1	
	α	58.6[a]	3.79 m	58.6[a]	3.79 m
	β	34.9	1.67 m	34.9	1.67 m
	γ	[d]	1.16 m, 1.04 m	[d]	1.17 m, 1.05 m
	γ′δ	14.9, 11.0	0.39 d (6.7), 0.70 t (7.4)	14.9, 11.0	0.39 d (6.8), 0.70 t (7.3)
C3 Phe	N*H*		7.27 d (8.7)		7.27 d (8.6)
	CO	171.5		171.5	
	α	59.3	4.26 m	59.3	4.27 m
	β	39.9	3.09 dd (13.8, 2.9), 2.64 dd (13.8, 12.1)	39.9	3.09 dd (13.9, 2.9), 2.63 dd (14.0, 12.1)
	Others	C1:138.0, C2,6: 129.0, C3,5: 127.7, C4: 126.1	7.19–7.11 m	C1:138.0, C2,6: 129.0, C3,5: 127.7, C4: 126.1	7.19–7.11 m
C4 Gly	N*H*		8.16 t (6.3)		8.15 dd (6.8, 5.5)
	CO	170.8		170.8	
	α	42.0	3.92 dd (16.6, 7.1), 3.48 dd (16.5, 5.1)	42.0	3.91 dd (16.5, 7.0), 3.48 dd (16.5, 5.3)
	NH_2		7.25 br s, 6.98 br s		7.24 br s, 6.97 br s

[a,b,c] Interchangeable. [d] Overlapping signals at 24.6, 24.7, 24.8, 24.9.

[e] Overlapping signals at 25.0, 25.5, 25.8 ppm.

Finally, the biological activity of either synthetic and natural Callyaerin A was tested *in vitro* against the virulent wildtype strain H37Rv of *Mycobacterium tuberculosis* (see Figure 26) by Yvonne Gröner from the Kalscheuer lab at the HHU Düsseldorf, Germany. In this assay, synthetic Callyaerin A caused a highly comparable growth inhibition in the low micromolar range as natural Callyaerin A. In fact, synthetic Callyaerin showed slightly better growth inhibition properties than natural Callyaerin A. This small difference might result from a slight deviation of the natural Callyaerin A compound concentration in the stock solution. As can be seen in the LC-MS spectra in Figure 24, the natural Callyaerin A stock solution seemed to contain some impurities which may lower the final active compound content in the stock solution, resulting in a slightly lower growth inhibition as seen in Figure 26. Despite these differences in the curve progression, the resulting MIC_{90} value for both compounds was calculated to 3.125-6.25 µM.

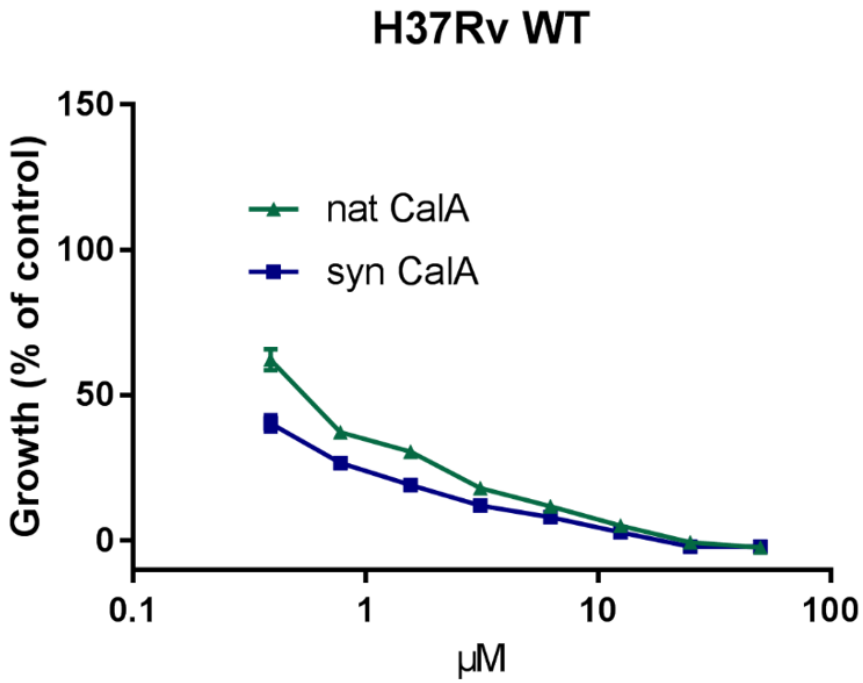

Figure 26: First biological evaluation of synthetic and natural Callyaerin A on virulent wildtype strain H37Rv of *Mycobacterium tuberculosis*. MIC_{90} = 3.125-6.25 µM.

Alltogether, all three independent methods, i. e. LC-MS, NMR and the biological evaluation, confirmed that synthetic Callyaerin A matched in structure and bioactivity to natural Callyaerin A which approved the feasibility of our developed synthetic route as well as the structure assignment of natural Callyaerin A.

The synthesis of all other Callyaerins and derivatives followed the same workflow of sequential linear solid phase peptide synthesis and subsequent ring closing reaction. Also, for these derivatives, their chemical structure and purity were evaluated by HRMS and LC-MS. An ^{1}H-NMR spectrum however was only acquired if the synthesis delivered enough material (> 5 mg). ^{13}C-NMR analysis was only performed for selected compounds.

3.1.8 NMR data comparison of other synthetic Callyaerins (B, C, D, E, F, G, H, I, J) with published data of the corresponding natural compound

Callyaerin A was previously described as the 'best' antitubercular natural product from the Callyaerin family[97]. Nevertheless, the chemical synthesis of the other Callyaerins allowed to validate these previous findings and to demonstrate the overall scope of the established synthesis approach. Therefore, the Callyaerins B, C, D, E, F, G, H, I, J, K and L were synthesized, and the identity of the synthetic compounds were determined by NMR analysis. Due to the unaccessiblity of these natural compounds, no additional LC-MS co-elution experiments for these Callyaerins were possible. A biological evalution of these compounds is described in section 3.2.

3.1.8.1 Callyaerin B

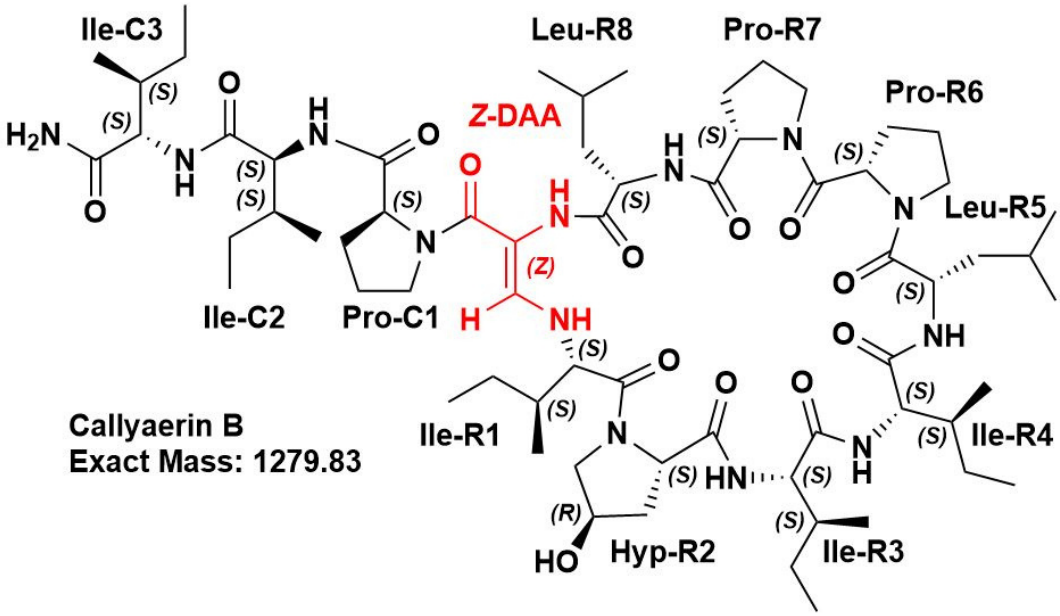

Figure 27: Chemical structure of Callyaerin B.

Table 5: ^{1}H and ^{13}C NMR data of synthetic Callyaerin B (400 MHz, DMSO-d_6) and natural Callyaerin B[95] (600 MHz, DMSO-d_6).

unit	position	synthetic δ_C	synthetic δ_H (J in Hz)	natural δ_C	natural δ_H (J in Hz)
DAA	NH		8.29 br s		8.28 br s
	CO	167.2		167.2	
	α	97.9		97.9	
	β	142.6	7.05 d (13.5)	142.6	7.04 d (13.6)
R1 Ile	NH		5.70 dd (13.0, 10.3)		5.70 dd (13.6, 10.8)
	CO	172.1		172.1	
	α	64.6	3.95 t (10.0)	64.6	3.94 t (9.8)
	β	37.9	1.44 m	37.9	1.45 m
	γ	29.7	1.40 m, 1.00 m	29.1	1.40 m, 1.00 m
	γ′δ	[b]	0.85[a], 0.76 t (7.5)	[b]	0.85[a], 0.76 t (7.5)
R2 Hyp	CO	173.5		173.4	
	α	59.2	4.24 m	59.2	4.24 m
	β	37.5	2.10 m,1.89 m	37.5 t	2.10 m,1.89 m
	γ	68.7	4.41 br s	68.7 d	4.40 br s
	δ	56.7	3.67 m, 3.80 m	56.7 t	3.67 m, 3.80 m
	OH		5.40 br s		5.40 d (2.4)
R3 Ile	NH		8.99 d (6.5)		9.00 br s
	CO	172.1		172.1 s	
	α	64.6	3.07 m	64.2 d	3.07 m
	β	32.4	2.55 m	32.4 d	2.55 m
	γ	24.6	1.40 m, 1.10 m	24.5 t	1.40 m, 1.10 m
	γ′δ	[b]	0.82[a] t, 0.78[a]	[b]	0.82[a] t, 0.78[a]
R4 Ile	NH		8.86 d (5.5)		8.86 br s
	CO	171.3		171.3 s	
	α	57.9	3.79 t (7.5)	57.8 d	3.81 (8.8)
	β	36.2	1.59 m	36.2 d	1.55 m
	γ	25.6	1.44 m, 1.15 m	25.5 t	1.45 m, 1.15 m
	γ′δ	[b]	0.85[a], 0.82[a] t	[b]	0.84[a], 0.81[a] t
R5 Leu	NH		7.37 d (7.0)		7.37 d (6.6)
	CO	171.4		171.4 s	
	α	49.2	4.62 q (6.6)	49.1 d	4.62 q (~6.7)
	β	41.2	1.76 m, 1.28 m	41.1 t	1.76 m, 1.30 m
	γ	24.8	1.60 m	24.7 d	1.60 m

unit	position	synthetic δ_C	synthetic δ_H (*J* in Hz)	natural δ_C	natural δ_H (*J* in Hz)
	δ, δ′	[b]	0.88[a]	[b]	0.88[a]
R6 Pro	CO	172.3		172.3	
	α	64.0	4.04 t (8.8)	63.9	4.03 t (8.2)
	β	24.9	2.30 m, 1.90 m	24.9	2.30 m, 1.90 m
	γ	28.5	2.00 m, 1.90 m	29.1	2.00 m, 1.90 m
	δ	46.1	3.60 m, 3.48 m	46.1	3.60 m, 3.48 m
R7 Pro	CO	171.4		171.4	
	α	61.4	4.25 m	61.3	4.25 m
	β	25.8	2.20 m, 1.85 m	25.7	2.20 m, 1.82 m
	γ	29.7	1.90 m, 1.48 m	29.7	1.90 m, 1.50 m
	δ	47.0	3.59 m, 3.35 m	47.0	3.55 m, 3.35 m
R8 Leu	NH		6.64 (10.0)		6.63 (10.0)
	CO	172.7		172.7	
	α	50.0	4.55 ddd (10.7, 10.1, 3.7)	50.0	4.55 ddd (10.7, 10.4, 3.7)
	β	40.5	1.70 m, 1.60 m	40.5	1.70 (m), 1.60 (m)
	γ	24.6	1.47 m	24.6	1.47(m)
	δ, δ′	[b]	0.88[a], 0.81[a]	[b]	0.88[a], 0.81[a]
C1 Pro	CO	171.2		171.2	
	α	62.5	4.25 m	62.5	4.25 m
	β	26.2	2.55 m, 1.77 m	26.2	2.55 m, 1.80 m
	γ	29.7	1.70 m, 1.44 m	29.7	1.70 m, 1.45 m
	δ	48.7	3.52 m, 3.15 m	48.6	3.52 m, 3.15 m
C2 Ile	NH		7.58 d (10.1)		7.58 d (10.4)
	CO	172.1		172.1	
	α	57.9	4.10 dd (10.0, 8.9)	57.8	4.10 dd (9.4, 9.2)
	β	36.4	1.84 m	36.4	1.82 m
	γ	25.1	1.44 m, 1.15 m	25.0	1.45 m, 1.15 m
	γ′δ	[b]	0.86[a], 0.82[a] t	[b]	0.86[a], 0.82[a] t
C3 Ile	NH		7.23 d (9.6)		7.23 d (9.5)
	CO	172.7		172.7	
	α	57.4	4.15 dd (9.7, 5.3)	57.4	4.15 dd (9.5, 5.0)
	β	36.2	1.90 m	36.2	1.90 m
	γ	23.5	1.25 m, 1.00 m	23.5	1.25 m, 1.00 m

unit	position	synthetic δ_C	synthetic δ_H (J in Hz)	natural δ_C	natural δ_H (J in Hz)
	γ′δ	[b]	0.77[a], 0.72 t (7.6)	[b]	0.78[a], 0.71 t (7.5)
	NH_2		7.16 s, 6.96 s		7.17 s, 6.97 s

[a] Signal overlap prevents determination of couplings.

[b] Specific assignments of the methyl signals are not possible. However, the relative assignments are 23.1, 22.7, 22.1, 20.8 (δ-Leu), 15.7 (×2), 15.3, 15.2, 14.4 (γ-Ile), and 11.4, 11.0, 10.7, 10.3, 9.8 ppm (δ-Ile).

3.1.8.2 Callyaerin C

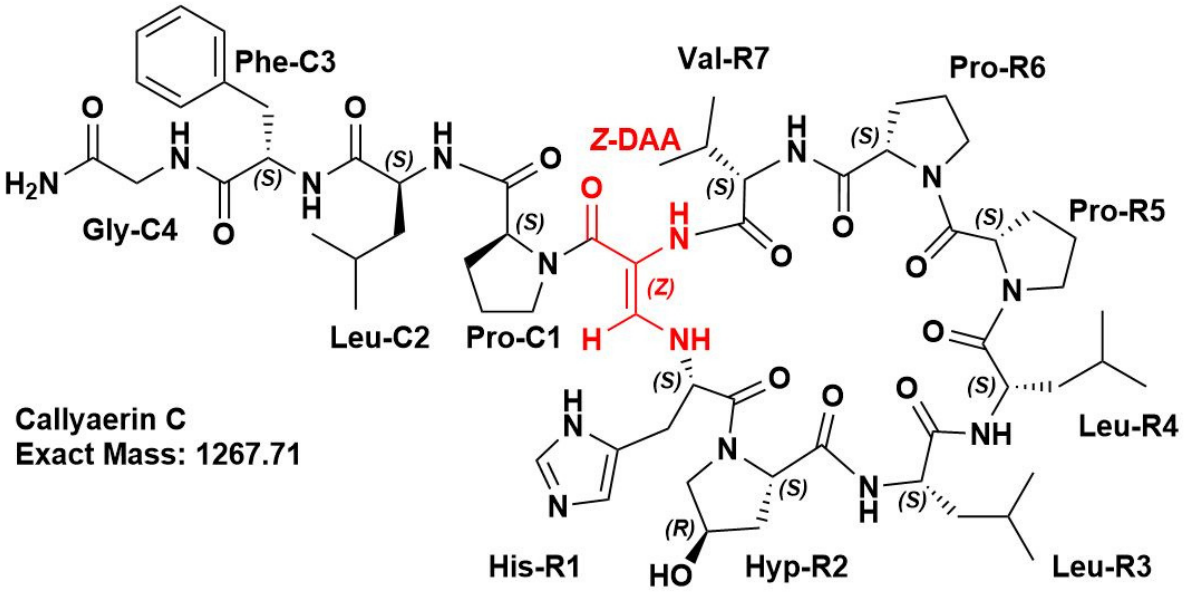

Figure 28: Chemical structure of Callyaerin C.

Table 6: ^{1}H NMR data of synthetic Callyaerin C (400 MHz, DMSO-d_6) and natural Callyaerin C[95] (600 MHz, DMSO-d_6).

unit	position	synthetic δ_H (J in Hz)	natural δ_H (J in Hz)
DAA	NH	8.57 s	8.57 s
	β	7.65 d (13.8)	7.65 d (13.7)
R1 His	NH	5.64 dd (13.8, 9.9)	5.64 dd (13.7, 9.9)
	α	4.48 m	4.48 ddd (10.5, 9.9, 4.0)
	β	2.33 m, 2.21 m	2.33 m, 2.20 m
	aromatic	NH1/3: 12.03 s, 2H: 7.39 s, 4H: 6.00 s	NH1/3: 12.03 s, 2H: 7.39 s, 4H: 6.01 s
R2 Hyp	α	4.14 m	4.14 dd (9.2, 4.3)
	β	2.09 m, 1.64 m	2.07 m, 1.64 m
	γ	4.07 m	4.06 m

unit	position	synthetic δ_H (J in Hz)	natural δ_H (J in Hz)
	δ	3.54 m, 1.81 m	3.54 m, 1.81 m
	OH	5.09 d (3.7)	5.09 d (3.8)
R3 Leu	NH	9.84 d (7.7)	9.84 d (7.7)
	α	4.16 m	4.16 ddd (11.4, 7.6, 3.9)
	β	1.59 m, 1.51 m	1.59 m, 1.51 m
	γ	1.73 m	1.73 m
	δ	0.86 d (6.6), 0.82 d (6.5)	0.86 d (6.6), 0.82 d (6.5)
R4 Leu	NH	7.57 d (6.3)	7.57 d (6.3)
	α	4.42 m	4.42 ddd (9.1, 6.1, 5.1)
	β	1.63 m, 1.22 m	1.63 m, 1.22 m
	γ	1.47 m	1.47 m
	δ	0.89 d (6.6)	0.89 d (6.6), 0.89 d (6.5)
R5 Pro	α	4.30 m	4.30 dd (9.0, 8.0)
	β	2.34 m, 1.58 m	2.34 m, 1.58 m
	γ	1.92 m	1.92 m
	δ	3.67 m, 3.19 m	3.67 m, 3.19 m
R6 Pro	α	4.39 m	4.39 dd (11.4, 7.2)
	β	2.21 m, 1.91 m	2.20 m, 1.89 m
	γ	2.00 m	2.00 m
	δ	3.56 m	3.56 m
R7 Val	NH	7.31 d (10.3)	7.32 d (10.3)
	α	4.67 dd (10.2, 4.4)	4.67 dd (10.2, 4.4)
	β	2.54 m	2.54 m
	γ	1.11 d (7.0), 0.97 d (6.9)	1.11 d (7.0), 0.97 d (6.9)
C1 Pro	α	4.32 dd (10.8, 6.9)	4.32 dd (10.8, 7.0)
	β	2.29 m, 1.53 m	2.29 m, 1.53 m
	γ	1.88 m, 1.77 m	1.88 m, 1.77 m
	δ	3.48 m, 3.28 m	3.48 m, 3.28 m
C2 Leu	NH	7.90 d (7.2)	7.90 d (6.2)
	α	3.90 m	3.90 ddd (11.1, 7.2, 3.8)
	β	1.64 m, 1.16 m	1.64 m, 1.16 m

unit	position	synthetic δ_H (J in Hz)	natural δ_H (J in Hz)
	γ	1.64 m	1.64 m
	δ	0.87 d (6.5), 0.75 d (6.5)	0.87 d (6.5), 0.75 d (6.5)
C3 Phe	NH	7.80 d (9.4)	7.80 d (9.3)
	α	4.24 m	4.24 ddd (12.1, 9.3, 3.1)
	β	3.30 m, 2.99 dd (13.3, 12.0)	3.30 m, 2.98 dd (13.3, 12.0)
	aromatic	C2,6: 7.35 m, C3,4,5: 7.16 m	2,6: 7.35 m, 3,4,5: 7.15 m
C4 Gly	NH	7.74 dd (7.1, 5.4)	7.74 dd (7.1, 5.1)
	α	3.88 dd (16.7, 7.0), 3.54 dd (16.6, 5.0)	3.88 dd (17.0, 7.2), 3.54 dd (16.8, 5.0)
	NH_2	7.20 br s, 7.09 br s	7.20 br s, 7.08 br s

3.1.8.3 Callyaerin D

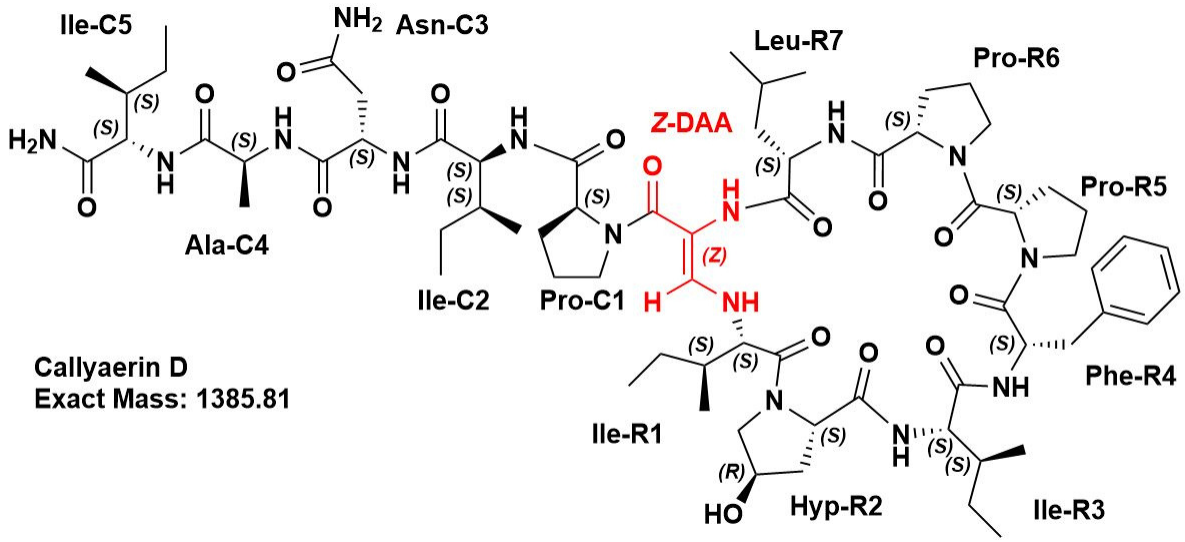

Figure 29: Chemical structure of Callyaerin D.

Table 7: ^{1}H data of synthetic Callyaerin D (400 MHz, DMSO-d_6) and natural Callyaerin D[95] (600 MHz, DMSO-d_6).

unit	position	synthetic δ_H (*J* in Hz)	natural δ_H (*J* in Hz)
DAA	N*H*	8.42 br s	8.42 br s
	β	7.38 d (3.2)	7.38 d (13.9)
R1 Ile	N*H*	5.30 dd (13.6, 10.3)	5.30 dd (13.9, 10.0)
	α	4.41 m	4.41 [a]
	β	1.98 m	1.98 m
	γ	0.94 m, 1.25 m	0.94 m, 1.25 m
	γ′δ	0.84 m	0.83[a], 0.84[a]
R2 Hyp	α	4.14 m	4.13 [a]
	β	2.06 m, 1.97 m	2.06 m, 1.97 m
	γ	4.40 m	4.40 [a]
	δ	3.66 br d (10.8), 3.93 t (6.3)	3.65 br d (10.9), 3.93 m
R3 Ile	N*H*	7.64 d (5.0)	7.64 d (4.9)
	α	4.00 dd (4.9, 3.5)	4.00 dd (4.9, 3.5)
	β	1.81 m	1.81 m
	γ	1.25 m, 1.30 m	1.25 m, 1.30 m
	γ′δ	0.82 m	0.82[a], 0.82[a]
R4 Phe	N*H*	7.50 d (6.0)	7.50 d (6.0)
	α	4.61 m	4.61 ddd (9.7, 6.0, 3.5)
	β	3.06 dd (13.1, 9.5), 2.77 dd (13.1, 3.0)	3.06 dd (13.1, 9.7), 2.77 dd (13.1, 3.5)
	aromatic	7.25 – 7.21 m	C2,6: 7.24 br d (7.2), C3,5: 7.30 br t (7.2), C4: 7.22 br t (7.2)
R5 Pro	α	4.17 m	4.16 [a]
	β	1.40 m, 2.23 m	1.40 m, 2.23 m
	γ	1.47 m, 1.69 m	1.47 m, 1.69 m
	δ	2.23 m, 3.27 m	2.23 m, 3.27 m
R6 Pro	α	4.16 m	4.16 [a]
	β	2.23 m, 1.40 m	2.23 m, 1.40 m
	γ	1.69 m, 1.47 m	1.69 m, 1.47 m

unit	position	synthetic δ_H (*J* in Hz)	natural δ_H (*J* in Hz)
	δ	3.27 m, 2.23 m	3.27 m, 2.23 m
R7 Leu	N*H*	7.54 d (9.0)	7.54 d (9.5)
	α	4.47 m	4.47 td (9.4, 5.5)
	β	1.85 m, 1.71 m	1.85 m, 1.71 m
	γ	1.76 m	1.76 m
	δ	0.85 m	0.85 [a], 0.87 [a]
C1 Pro	α	4.32 m	4.30 [a]
	β	1.60 m, 2.16 m	1.60 m, 2.17 m
	γ	1.80 m, 1.71 m	1.79 m, 1.71 m
	δ	3.53 br t (9.0), 3.30 m	3.53 br t (9.5), 3.30 m
C2 Ile	N*H*	7.76 d (6.7)	7.76 d (6.3)
	α	3.93 t (6.2)	3.93 t (6.3)
	β	1.90 m	1.90 m
	γ	1.40 m, 1.28 m	1.40 m, 1.28 m
	γ′δ	0.85 m	0.87[a], 0.82[a]
C3 Asn	N*H*	7.88 d (7.5)	7.88 d (7.6)
	α	4.55 q (7.0)	4.55 q (7.0)
	β	2.69 dd (15.2, 6.5), 2.34 dd (15.2, 7.1)	2.69 dd (15.1, 7.0), 2.35 dd (15.1, 7.0)
	NH_2	6.92 s, 7.30 s	6.93 s, 7.31 s
C4 Ala	N*H*	7.56 d (7.1)	7.57 d (6.9)
	α	4.16 m	4.17 [a]
	β	1.26 d (7.1)	1.25 d (6.9)
C5 Ile	N*H*	7.35 s br	7.34 d (6.7)
	α	4.05 dd (8.9, 6.9)	4.05 dd (8.9, 6.7)
	β	1.77 m	1.77 m
	γ	1.12 m, 1.45 m	1.12 m, 1.45 m
	γ′δ	0.85 m	0.83[a], 0.83[a]
	NH_2	7.11 s, 7.03 s	7.11 s, 7.03 s

[a] Signal overlap prevents determination of couplings.

3.1.8.4 Callyaerin E

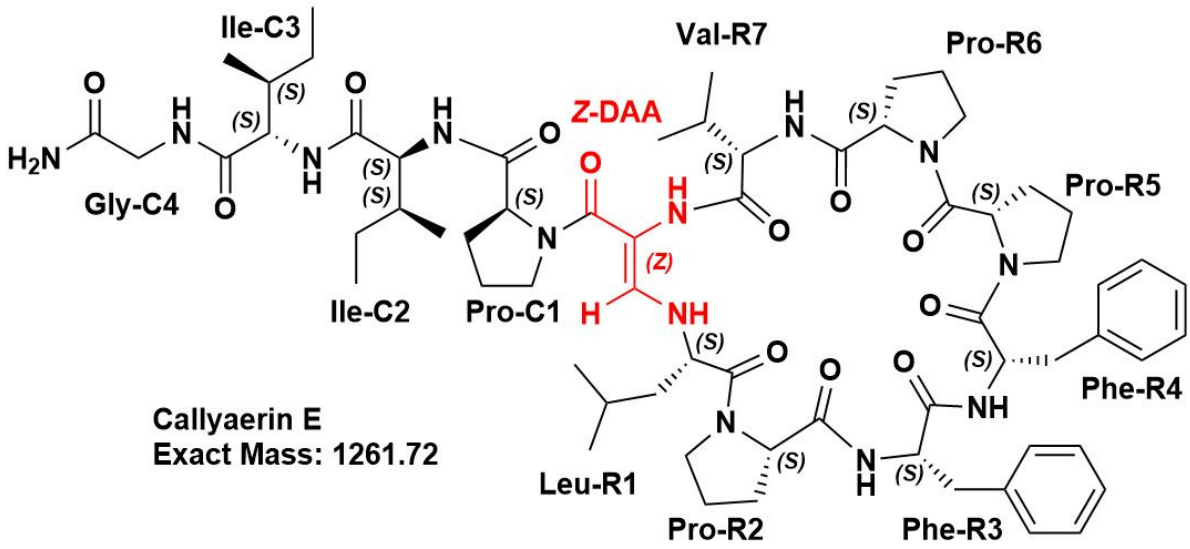

Figure 30: Chemical structure of Callyaerin E.

Table 8: ^{1}H and ^{13}C NMR data of synthetic Callyaerin E (400 MHz, DMSO-d_6) and natural Callyaerin E[95] (600 MHz, DMSO-d_6).

unit	position	synthetic δ_C (*J* in Hz)	synthetic δ_H (*J* in Hz)	natural δ_C (*J* in Hz)	natural δ_H (*J* in Hz)
DAA	N*H*		8.37 s		8.36 s
	CO	167.7		167.5	
	α	98.5		98.8	
	β	143.1	7.28 m	143.3	7.28 d (13.6)
R1 Leu	N*H*		5.27 dd (13.5, 9.8)		5.27 dd (13.3, 10.0)
	CO	171.0		170.8	
	α	57.8	4.38 m	57.9	4.36 m
	β	42.2	1.77 m, 1.23 m	41.8	1.77 m, 1.23 m
	γ	27.0	1.60 m	26.5	1.60 m
	δ, δ′	23.7, 24.4	0.96 d (6.7), 0.94 d (6.6)	22.5, 23.2	0.96 d (6.0), 0.94 d (6.6)
R2 Pro	CO	172.1		171.9	
	α	63.5	4.01 m	63.9	4.01 dd (9.9, 5.5)
	β	29.3	2.16 m, 1.67 m	29.1	2.16 m, 1.67 m
	γ	24.9	2.06 m, 1.88 m	24.9	2.06 m, 1.88 m
	δ	48.7	3.93 br t (8.3) 3.59 m	47.8	3.93 br t (8.8) 3.59 m

unit	position	synthetic δ_C (*J* in Hz)	synthetic δ_H (*J* in Hz)	natural δ_C (*J* in Hz)	natural δ_H (*J* in Hz)
R3 Phe	N*H*		7.72 d (6.8)		7.73 d (6.7)
	CO	169.0		168.9	
	α	54.0	4.39 m	54.1	4.39 m
	β	35.3	3.00 m	35.1	3.00 m
	aromatic	126.4, 128.4, 138.1	7.17–7.32 m	126.3, 128.5, 138.3	7.17–7.32 m
R4 Phe	N*H*		7.31 d (6.7)		7.31 d (6.9)
	CO	171.3		171.2	
	α	52.9	4.63 ddd (8.6, 6.2, 4.7)	53.1	4.63 ddd (8.8, 6.9, 4.7)
	β	36.1	3.01 m, 2.71 dd (13.4, 4.7)	36.1	3.00 m, 2.71 dd (13.3, 4.7)
	aromatic	C1: 137.9, C2,6: 129.0, C3,5: 128.4, C4: 126.5	7.17–7.30 m	C1: 137.3, C2,6: 129.5, C3,5: 129.1, C4: 126.5	7.17–7.30 m
R5 Pro	CO	171.6		171.3	
	α	63.1	4.41 m	62.8	4.41 m
	β	28.7	2.15 m, 1.82 m	28.4	2.15 m, 1.82 m
	γ	24.4	1.93 m, 1.89 m	24.5	1.93 m, 1.89 m
	δ	46.6	3.49 br t (8.4), 3.42 m	47.2	3.49 br t (8.8), 3.42 m
R6 Pro	CO	171.5		171.5	
	α	63.5	4.16 dd (7.5, 9.9)	64.0	4.16 dd (7.9, 9.8)
	β	29.9	2.22 m, 1.41 m	29.6	2.22 m, 1.41 m
	γ	25.7	1.74 m, 1.59 m	25.8	1.74 m, 1.59 m
	δ	48.7	3.34 m, 2.48 m	49.5	3.34 m, 2.48 m
R7 Val	N*H*		7.04 d (11.7)		7.03 d (10.1)
	CO	171.4		171.2	
	α	56.6	4.56 dd (10.2, 3.9)	56.5	4.56 dd (10.1, 3.9)
	β	28.8	2.33 m	28.8	2.33 m
	γ	18.3, 17.7	1.05 d (6.9), 0.97 d (6.7)	18.4, 18.3	1.06 d (6.9), 0.97 d (6.8)
C1 Pro	CO	172.6		172.4	
	α	61.0	4.38 m	59.5	4.36 m
	β	27.0	2.22 m, 1.57 m	26.6	2.22 m, 1.57 m
	γ	23.8	1.78 m, 1.68 m	23.8	1.78 m, 1.68 m
	δ	46.3	3.57 m, 3.21 m	45.8	3.57 m, 3.21 m

unit	position	synthetic δ_C (J in Hz)	synthetic δ_H (J in Hz)	natural δ_C (J in Hz)	natural δ_H (J in Hz)
C2 Ile	N*H*		7.63 d (8.0)		7.62 d (7.9)
	CO	171.3		171.1	
	α	58.4	3.99 m	58.3	3.99 dd (7.9, 7.3)
	β	35.3	1.95 m	35.3	1.95 m
	γ	24.4	1.45 m, 1.21 m	24.6	1.45 m, 1.21 m
	γδ	15.7, 11.2	0.88 d (6.6), 0.85 m	15.9, 11.4	0.88 d (6.9), 0.85 t (6.9)
C3 Ile	N*H*		7.37 d (8.2)		7.37 d (8.0)
	CO	171.0		170.8	
	α	57.8	4.09 t (7.7)	57.8	4.08 t (7.6)
	β	35.3	1.82 m	34.2	1.82 m
	γ	24.9	1.39 m, 1.27 m	25.1	1.39 m, 1.27 m
	γδ	15.5, 11.2	0.87 m 0.80 m	15.0, 10.8	0.87 d (6.9), 0.80 t (6.7)
C4 Gly	N*H*		7.89 t (6.1)		7.88 t (6.0)
	CO	171.0		170.9	
	α	42.3	3.71 dd (16.6, 6.2) 3.57 m	42.3	3.72 dd (16.7, 6.2) 3.57 dd (16.7, 5.9)
	NH_2		7.05 br s, 6.97 br s		7.04 br s, 6.97 br s

3.1.8.5 *Callyaerin F*

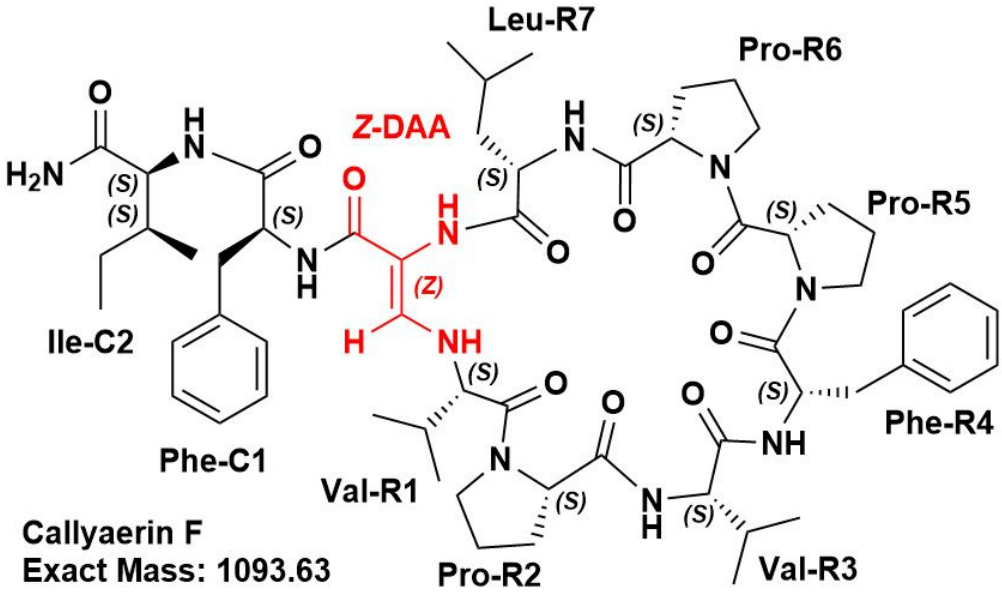

Figure 31: Chemical structure of Callyaerin F.

Table 9: ^{1}H data of synthetic Callyaerin F (400 MHz, DMSO-d_6) and natural Callyaerin F[95] (600 MHz, DMSO-d_6).

unit	position	synthetic δ_H (*J* in Hz)	natural δ_H (*J* in Hz)
DAA	N*H*	8.25 s	8.25 s
	β	7.25 m	7.25 d (14.0)
R1 Val	N*H*	5.14 dd (13.8, 10.0)	5.14 dd (14.0, 10.1)
	α	4.38 br d (10.0)	4.38 br d (9.8)
	β	2.31 m	2.31 m
	γ	0.86 d (6.9), 0.65 d (6.6)	0.87 d (6.9), 0.66 d (6.9)
R2 Pro	α	3.96 dd (10.3, 6.8)	3.95 dd (10.3, 6.7)
	β	2.17 m, 1.81 m	2.17 m, 1.81 m
	γ	2.03 m, 1.84 m	2.03 m, 1.84 m
	δ	3.86 m, 3.74 m	3.86 m, 3.74 m
R3 Val	N*H*	7.54 d (5.3)	7.54 d (5.1)
	α	3.86 m	3.86 m
	β	2.11 m	2.11 m
	γ	0.93 d (6.9), 0.86 d (6.9)	0.93 d (6.7), 0.86 d (6.7)
R4 Phe	N*H*	7.50 d (5.8)	7.50 d (6.1)
	α	4.54 ddd (9.7, 5.9, 3.5)	4.54 ddd (9.3, 6.1, 3.5)
	β	3.01 dd (12.9, 9.6) 2.74 dd (13.0, 3.5)	3.01 dd (12.9, 9.7) 2.71 dd (12.8, 3.1)
	aromatic	7.21–7.28 m	7.21–7.28 m
R5 Pro	α	4.28 m	4.28 m
	β	2.09 m, 1.80 m	2.09 m, 1.80 m
	γ	1.91 m, 1.83 m	1.91 m, 1.83 m
	δ	3.58 m, 3.35 m	3.58 m, 3.35 m
R6 Pro	α	4.26 m	4.26 m
	β	2.29 m, 1.42 m	2.29 m, 1.42 m
	γ	1.73 m, 1.45 m	1.73 m, 1.45 m
	δ	3.23 m, 2.31 m	3.23 m, 2.17 m
R7 Leu	N*H*	7.66 d (9.7)	7.66 d (9.6)
	α	4.62 td (10.1, 3.9)	4.62 td (10.1, 3.9)
	β	1.93 m, 1.67 m	1.93 m, 1.67 m
	γ	1.72 m	1.72 m
	δ	0.94 d (6.8), 0.84 d (6.8)	0.94 d (6.7), 0.84 d (6.2)
C1 Phe	N*H*	6.17 d (7.8)	6.17 d (7.8)

unit	position	synthetic δ_H (*J* in Hz)	natural δ_H (*J* in Hz)
	α	4.42 td (7.4, 4.6)	4.42 td (7.6, 4.5)
	β	2.93 m, 2.90 m	2.93 m, 2.90 m
	aromatic	7.15–7.28 m	7.15–7.28 m
C2 Ile	N*H*	7.52 d (8.5)	7.52 d (8.5)
	α	3.98 dd (8.3, 6.1)	3.98 dd (8.3, 6.1)
	β	1.73 m	1.73 m
	γ	1.29 m, 1.10 m	1.29 m, 1.10 m,
	γ′δ	0.76 d (7.1), 0.77 t (7.6)	0.76 d (6.8), 0.77 t (7.3)
	NH_2	7.03 br s, 6.97 br s	7.04 br s, 6.95 br s

3.1.8.6 Callyaerin G

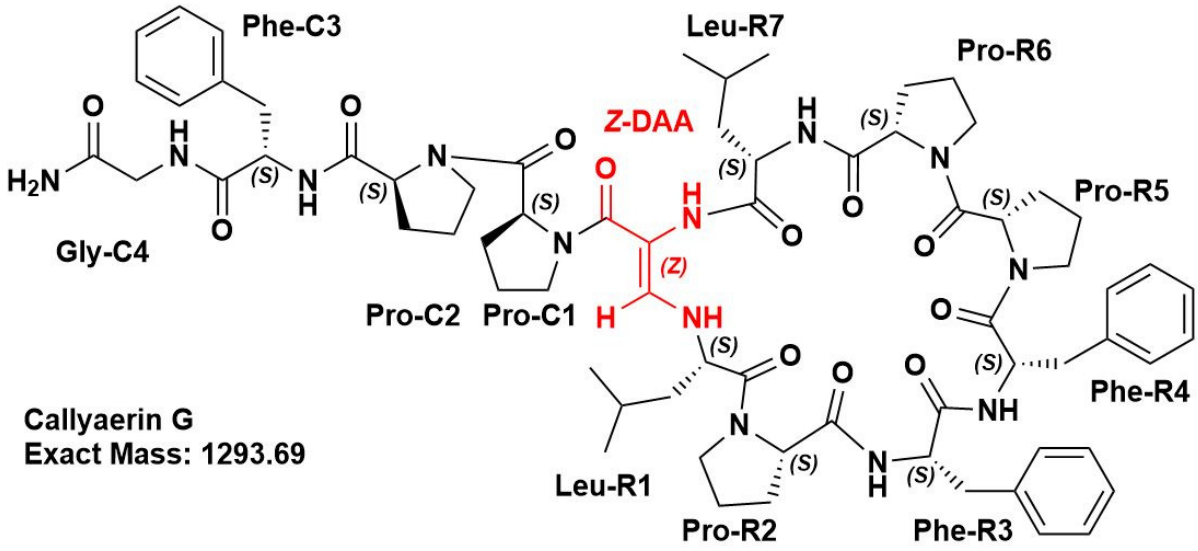

Figure 32: Chemical structure of Callyaerin G.

Table 10: ^{1}H data of synthetic Callyaerin G (400 MHz, DMSO-d_6) and natural Callyaerin G[97] (600 MHz, DMSO-d_6).

unit	position	synthetic δ_H (*J* in Hz)	natural δ_H (*J* in Hz)
DAA	N*H*	8.23 s	8.23 s
	β	7.46 d (13.5)	7.46 d (13.9)
R1 Leu	N*H*	5.32 d (13.5, 9.8)	5.30 d (13.9, 10.0)
	α	4.26 [a]	4.27 [a]
	β	1.62 m, 1.08 m	1.62 m, 1.08 m
	γ	1.33 m	1.33 m
	δ, δ′	0.53 d (6.6), 0.38 d (6.3)	0.53 d (6.7), 0.37 d (6.4)
R2 Pro	α	3.94 [a]	3.94 [a]
	β	2.10 m, 1.59 m	2.10 m, 1.59 m
	γ	2.01 m, 1.84 m	2.01 m, 1.84 m
	δ	3.92 m, 3.49 m	3.92 m, 3.49 m
R3 Phe	N*H*	7.70 d (7.2)	7.71 d (6.8)
	α	4.22 [a]	4.22 [a]
	β	2.86 m	2.86 m
	aromatic	7.28 – 7.10 m	C2,6: 7.12 br d (7.2) C3,5: 7.25 br t (7.2) C4: 7.19 br t (7.2)
R4 Phe	N*H*	7.19 [a]	7.21 [a]
	α	4.63 q (7.0)	4.63 q (7.1)
	β	2.96 m, 2.66 dd (13.1, 6.1)	2.96 m, 2.66 dd (13.4, 4.7)
	aromatic	7.28 – 7.10 m	C2,6: 7.18 br d (7.2) C3,5: 7.25 br t (7.2) C4: 7.22 br t (7.2)
R5 Pro	α	4.41 m	4.41 dd (9.8, 7.9)
	β	2.15 m, 1.83 m	2.15 m, 1.83 m
	γ	1.92 m, 1.90 m	1.92 m, 1.90 m
	δ	3.45 m, 3.38 m	3.45 m, 3.38 m
R6 Pro	α	4.24 m	4.24 dd (10.1, 7.4)
	β	2.28 m, 1.48 m	2.28 m, 1.48 m
	γ	1.78 m, 1.67 m	1.78 m, 1.67 m
	δ	3.40 m, 2.75 m	3.40 m, 2.74 td (10.3, 6.2)

unit	position	synthetic δ_H (*J* in Hz)	natural δ_H (*J* in Hz)
R7 Leu	N*H*	7.51 d (9.8)	7.51 d (10.1)
	α	4.46 m	4.46 dt (10.1, 3.8)
	β	1.92 m, 1.75 m	1.92 m, 1.75 m
	γ	1.75 m	1.75 m
	δ, δ’	0.87 d (6.1) 0.83 d (6.1)	0.86 d (6.5) 0.83 d (6.2)
C1 Pro	α	4.34 m	4.34 dd (9.8, 7.9)
	β	2.08 m, 1.83 m	2.08 m, 1.83 m
	γ	1.95 m, 1.78 m	1.95 m, 1.78 m
	δ	3.86 m, 3.36 m	3.86 m, 3.36 m
C2 Pro	α	4.11 dd (8.4, 6.6)	4.11 dd (10.0, 7.5)
	β	1.89 m, 1.06 m	1.89 m, 1.06 m
	γ	1.69 m	1.69 m
	δ	3.84 m, 3.37 m	3.84 m, 3.37 m
C3 Phe	N*H*	7.68 d (9.5)	7.67 d (7.0)
	α	4.23 [a]	4.23 [a]
	β	3.24 dd (13.2, 3.6), 2.92 m	3.23 dd (13.4, 2.7), 2.92 m
	aromatic	C2,6: 7.35 br d (7.2) 7.28 – 7.10 m	C2,6: 7.35 br d (7.2) C3,5: 7.25 br t (7.2) C4: 7.17 br t (7.2)
C4 Gly	N*H*	7.97 dd (7.9, 4.7)	7.96 dd (7.9, 5.0)
	α	3.91 m, 3.41 m	3.91 dd (17.2, 7.9), 3.41 dd (17.2, 5.0)
	NH_2	7.28 – 7.10 m	7.20 br s, 7.14 br s

3.1.8.7 Callyaerin H

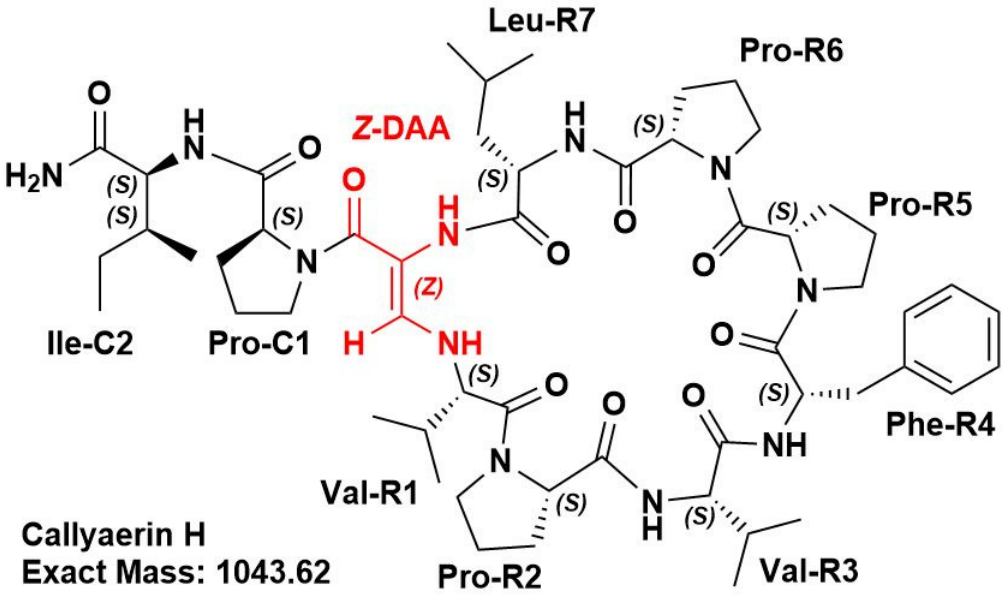

Figure 33: Chemical structure of Callyaerin H.

Table 11: 1H data of synthetic Callyaerin H (400 MHz, DMSO-d6) and natural Callyaerin H[95] (600 MHz, DMSO-d6).

unit	position	synthetic δ_H (J in Hz)	*natural* δ_H (J in Hz)
DAA	NH	8.47 br s	8.47 br s
	β	7.23 m	7.23 d
R1 Val	NH	5.26 dd (13.8, 9.9)	5.26 dd (13.7, 10.0)
	α	4.42 dd (10.0, 1.2)	4.42 dd (10.0, 1.4)
	β	2.35 m	2.35 m
	γγ′	0.68 d (6.6), 0.89 d (7.4)	0.68 d (6.7), 0.89 d (6.9)
R2 Pro	α	3.97 dd (10.2, 6.6)	3.97 dd (10.5, 6.8)
	β	2.03 m, 1.82 m	2.03 m, 1.82 m
	γ	2.18 m, 1.82 m	2.18 m, 1.82 m
	δ	3.82 m, 3.75 m	3.82 m, 3.75 m
R3 Val	NH	7.59 d (5.1)	7.59 d (5.1)
	α	3.86 t (4.7)	3.86 t (4.7)
	β	2.10 m	2.10 m
	γγ′	0.93 d (6.9), 0.86 d	0.93 d (7.0), 0.86 d
R4 Phe	NH	7.51 d (5.5)	7.51 d (5.8)
	α	4.57 ddd (9.3, 5.7, 3.5)	4.57ddd (9.6, 5.9, 3.8)
	β	3.04 dd (13.0, 9.5), 2.77 dd (13.0, 3.6)	3.03 dd (13.1, 9.7), 2.77 dd (13.1, 3.6)

unit	position	synthetic δ_H (J in Hz)	*natural* δ_H (J in Hz)
	aromatic	7.30 – 7.20 m	7.2 – 7.3 m
R5 Pro	α	4.34 m	4.34 dd (11.4, 7.5)
	β	2.40 – 1.60 m	1.80–2.10 m
	γ	2.40 – 1.60 m	1.80–2.10 m
	δ	3.63 m, 3.35 m	3.63 m, 3.35 m
R6 Pro	α	4.17 dd (9.5, 7.7)	4.17 dd (9.3, 7.7)
	β	2.21 m, 1.69 m	2.21 m, 1.69 m
	γ	1.45 m	1.45 m
	δ	3.27 m	3.27 m
R7 Leu	NH	7.55 d (9.5)	7.54 d (9.6)
	α	4.51 dd (9.8, 4.3)	4.51 ddd (9.8, 9.8, 4.3)
	β	1.77 m	1.77 m
	γ	1.85 m	1.85 m
	δ, δ′	0.87 – 0.80 m	0.86 d, 0.82 d
C1 Pro	α	4.34 m	4.34 dd (9.6, 7.8)
	β	2.16 m, 1.72 m	2.16 m, 1.72 m
	γ	1.81 m, 1.55 m	1.81 m, 1.55 m
	δ	3.48 m, 3.24 m	3.48 br t (8.0), 3.24 m
C2 Ile	NH	7.50 d (9.2)	7.50 d (9.1)
	α	4.01 dd (9.1, 6.0)	4.01 dd (9.2, 6.1)
	β	1.92 m	1.92 m
	γ	1.21 m, 1.40 m	1.21 m, 1.40 m
	γ′δ	0.87 – 0.80 m	0.85 d (6.6), 0.82 t (7.3)
	NH_2	6.97 br s, 6.89 br s	6.96 br s, 6.89 br s

3.1.8.8 Callyaerin I

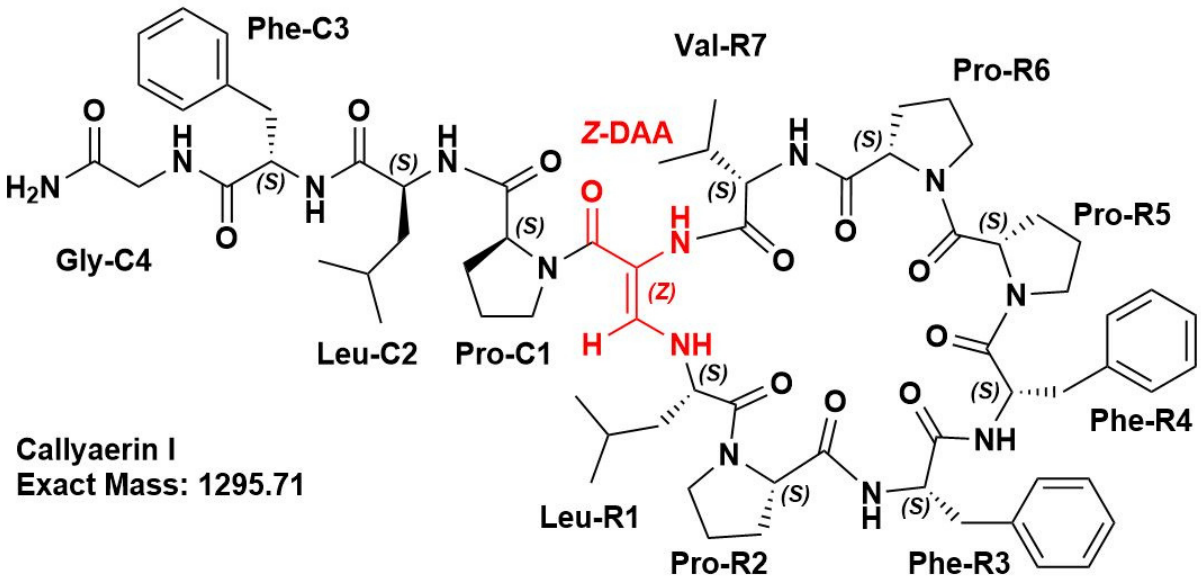

Figure 34: Chemical structure of Callyaerin I.

Table 12: ^{1}H NMR data of synthetic Callyaerin I (400 MHz, DMSO-d_6) and natural Callyaerin I[95] (600 MHz, DMSO-d_6).

unit	position	synthetic δ_H (*J* in Hz)	natural δ_H (*J* in Hz)
DAA	N*H*	8.45 br s	8.45 br s
	β	7.44 d (13.5)	7.43 d (13.5)
R1 Leu	N*H*	5.37 dd (13.6, 9.8)	5.36 dd (13.5, 9.8)
	α	4.39 [a]	4.39 [a]
	β	1.59 m, 1.0 m	1.59 m, 1.0 m
	γ	1.21 m	1.21 m
	δ	0.44 d (6.4)	0.45 d (6.4)
	δ′	0.32 d (6.6)	0.32 d (6.7)
R2 Pro	α	3.98 dd (10.0, 7.3)	3.98 dd (10.0, 7.3)
	β	2.14 m, 1.63 m	2.14 m, 1.63 m
	γ	2.02 m, 1.82 m	2.02 m, 1.82 m
	δ	3.96 m, 3.48 m	3.96 m, 3.48 m
R3 Phe	N*H*	7.67 dd (10.0, 8.2)	7.61 d (6.8)
	α	4.38 [a]	4.38 [a]
	β	2.96 m	2.96 m
	aromatic	7.32 – 7.10 m	C2,6: 7.25 C3,5: 7.15 C4: 7.18
R4 Phe	N*H*	7.25 [a]	7.25 [a]
	α	4.63 [a]	4.63 [a]
	β	2.96 m,	2.96 m,

unit	position	synthetic δ_H (*J* in Hz)	natural δ_H (*J* in Hz)
		2.68 dd (13.4, 4.7)	2.68 dd (13.4, 4.7)
	aromatic	7.32 – 7.10 m	C2,6: 7.25 C3,5: 7.29 C4: 7.23
R5 Pro	α	4.44 m	4.44 dd (11.1, 7.6)
	β	2.16 m, 1.81 m	2.16 m, 1.81 m
	γ	1.92 m, 1.90 m	1.92 m, 1.90 m
	δ	3.49 m, 3.41 m	3.49 m, 3.41 m
R6 Pro	α	4.18 dd (10.0, 7.4)	4.18 dd (10.1, 7.4)
	β	2.23 m, 1.42 m	2.23 m, 1.42 m
	γ	1.75 m, 1.59 m	1.75 m, 1.59 m
	δ	3.34 m, 2.49 m	3.34 m, 2.49 m
R7 Val	N*H*	7.03 d (10.2)	7.03 d (10.1)
	α	4.62 dd (10.0, 3.7)	4.62 dd (10.2, 3.8)
	β	2.48 m	2.48 m
	γ	1.20 d (7.0)	1.19 d (7.0)
	γ′	1.07 d (7.0)	1.06 d (7.0)
C1 Pro	α	4.30 dd (10.7, 7.2)	4.30 dd (10.8, 7.1)
	β	2.30 t (6.1), 1.52 m	2.30 dt (12.1, 6.4), 1.52 m
	γ	1.71 m, 1.85 m	1.71 m, 1.85 m
	δ	3.64 dd (10.9, 7.6), 3.24 m	3.64 dd (11.0, 7.7), 3.24 m
C2 Leu	N*H*	7.78 d (6.9)	7.78 d (7.0)
	α	3.82 ddd (11.4, 6.9, 4.1)	3.82 ddd (11.4, 7.0, 4.2)
	β	1.66 m, 1.12 m	1.66 m, 1.12 ddd (13.6, 9.3, 4.2)

3.1.8.9 Callyaerin J

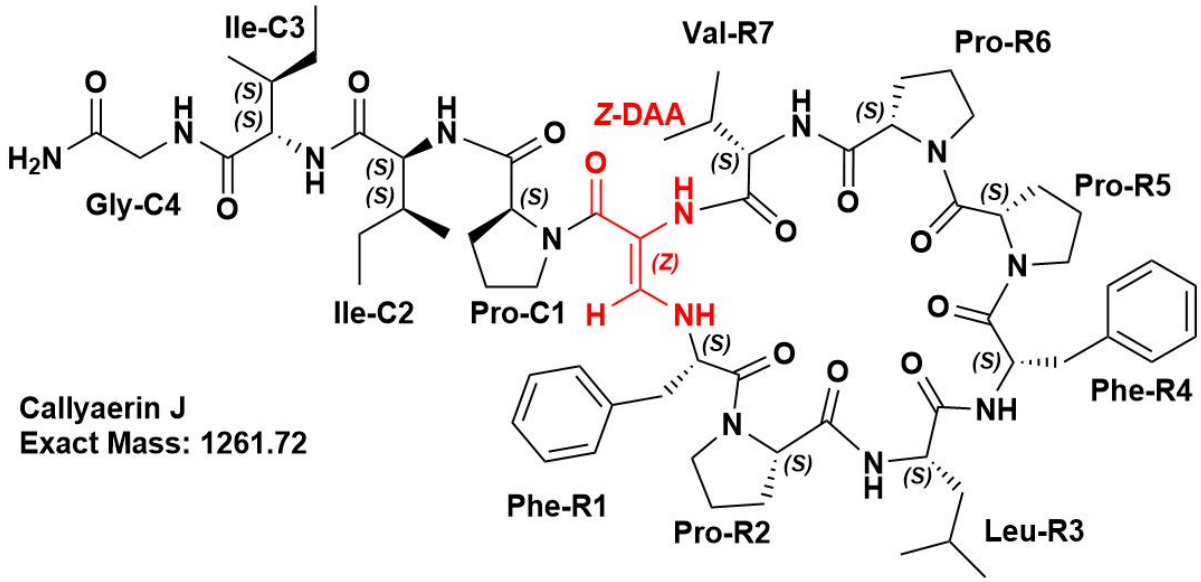

Figure 35: Chemical structure of Callyaerin J.

Table 13: ^{1}H NMR data of synthetic Callyaerin J (400 MHz, DMSO-d_6) and natural Callyaerin J[95] (600 MHz, DMSO-d_6).

unit	position	synthetic δ_H (*J* in Hz)	natural δ_H (*J* in Hz)
DAA	N*H*	8.21 br s	8.21 br s
	β	7.04 d (12.8)	7.04 d (13.4)
R1 Phe	N*H*	5.44 dd (13.5, 9.6)	5.44 dd (13.4, 9.7)
	α	4.60https://pubs.acs.org/doi/10.1021/acs.jnatprod.5b00266 - t2fn3 [a]	4.60https://pubs.acs.org/doi/10.1021/acs.jnatprod.5b00266 - t2fn3 [a]
	β	3.34 m, 2.67 m	3.34 dd (14.2, 3.1), 2.67 m
	aromatic	7.30 – 7.10 m	C2,6: 7.21 C3,5: 7.22 C4: 7.22
R2 Pro	α	4.02 dd (10.0, 6.9)	4.02 dd (10.5, 6.9)
	β	2.23 m, 1.81 m	2.23 m, 1.81 m
	γ	2.10 m, 1.90 m	2.10 m, 1.90 m
	δ	3.97 br t (9.3), 3.85 m	3.97 br t (9.7), 3.85 td (9.7, 6.5)
	N*H*	7.44 d (6.2)	7.41 d (6.2)
	α	4.08 [a]	4.08 [a]

unit	position	synthetic δ_H (*J* in Hz)	natural δ_H (*J* in Hz)
R3 Leu	β	1.47 m	1.47 m
	γ	1.63 m	1.63 m
	δ	0.92 d (6.4)	0.92 d (6.6)
	δ′	0.82 d (6.5)	0.82 d (6.6)
R4 Phe	N*H*	7.14 d (6.7)	7.13 d (6.5)
	α	4.60 [a]	4.60 [a]
	β	3.01 dd (13.4, 8.9), 2.64 dd (13.5, 4.9)	3.01 dd (13.5, 8.9), 2.64 dd (13.5, 4.9)
	aromatic	7.30 – 7.10 m	C2,6: 7.24 C3,5: 7.26 C4: 7.20
R5 Pro	α	4.36 dd (11.0, 7.6)	4.36 dd (11.3, 7.6)
	β	2.11 m, 1.80 m	2.11 m, 1.80 m
	γ	1.92 m, 1.90 m	1.92 m, 1.90 m
	δ	3.52 m, 3.34 m	3.52 m, 3.34 m
R6 Pro	α	4.15 dd (9.7, 7.6)	4.15 dd (9.8, 7.5)
	β	2.22 m, 1.42 m	2.22 m, 1.42 m
	γ	1.74 m, 1.58 m	1.74 m, 1.58 m
	δ	3.34 m, 2.51 m	3.34 m, 2.51 m
R7 Val	N*H*	7.10 d (10.1)	7.10 d (10.2)
	α	4.50 dd (10.2, 5.1)	4.50 dd (10.2, 5.2)
	β	2.33 m	2.33 m
	γ	1.05 d (6.8)	1.06 d (6.9)
	γ′	1.01 d (6.8)	1.01 d (6.9)
C1 Pro	α	4.30 dd (8.9, 7.9)	4.30 dd (9.7, 7.4)
	β	2.18 m, 1.54 m	2.18 m, 1.54 m
	γ	1.76 m, 1.65 m	1.76 m, 1.65 m
	δ	3.53 m, 3.14 td (10.7, 6.0)	3.53 m, 3.14 td (11.3, 6.7)

unit	position	synthetic δ_H (*J* in Hz)	natural δ_H (*J* in Hz)
C2 Ile	N*H*	7.69 d (7.5)	7.68 d (7.5)
	α	3.95 t (9.3)	3.95 t (7.5)
	β	1.92 m	1.92 m
	γ	1.46 m, 1.26 m	1.46 m, 1.26 m
	γ′	0.86 d (6.6)	0.86 d (6.8)
	δ	0.86 t (7.1)	0.86 t (7.4)
C3 Ile	N*H*	7.32 d (8.3)	7.31 d (8.4)
	α	4.08 [a]	4.08 [a]
	β	1.78 m	1.78 m
	γ	1.23 m, 1.06 m	1.23 m, 1.06 m
	γ′	0.69 d (6.8)	0.69 d (6.9)
	δ	0.65 t (7.3)	0.65 t (7.4)
C4 Gly	N*H*	7.84 t (6.1)	7.83 dd (6.5, 5.6)
	α	3.70 dd (16.7, 6.4)	3.70 dd (16.8, 6.5)
		3.50 m	3.50 dd (16.8, 5.6)
	NH_2	7.06 br s, 7.03 br s	7.04 br s, 7.01 br s

3.2 Biological evaluation of synthetic Callyaerins and derivatives

3.2.1 MIC_{90} determination of synthetic Callyaerins and derivatives on *M. tuberculosis* strain H37Rv

Daletos *et al.* published in 2015[97] that Callyaerin A and B shows potent anti-TB activity with MIC_{90} values of 2 and 5 µM, respectively, while all other tested natural Callyaerins have only weak or no anti-TB activity against the *M. tuberculosis* strain H37Rv. To corroborate these data and to determine bioactivities for all synthesized Callyaerins, we therefore performed further biological evaluations. Accordingly, the synthetic Callyaerins and derivatives of the present work were tested against different *M. tuberculosis* strains by Yvonne Gröner from the Kalscheuer lab at the HHU Düsseldorf, Germany. To this end, she first determined the MIC_{90} values of all synthetic Callyaerins and derivatives on *M. tuberculosis* strain H37Rv (Table 14).

Table 14: MIC_{90} values of all synthetic Callyaerins and derivatives on *M. tuberculosis* strain H37Rv.

#	substance	H37Rv MIC_{90} [µM]
0	natural CalA	6.25
1	Callyaerin A	3.125
2	Callyaerin B	0.39
3	Callyaerin C	>100
4	Callyaerin D	50
5	Callyaerin E	50
6	Callyaerin F	25
7	Callyaerin G	50
8	Callyaerin H	25
9	Callyaerin I	50
10	Callyaerin J	25
11	Callyaerin K	>100
12	Callyaerin L	>100
13	Callynormine A	>100
14	CalA_R1A	12.5
15	CalA_R2A	12.5
16	CalA_R2P	3.125
17	CalA_R3A	>50
18	CalA_R3F	3.125
19	CalA_R3I	0.78
20	CalA_R3L	3.125
21	CalA_R4A	3.125
22	CalA_R5A	6.25

#	substance	H37Rv MIC_{90} [µM]
23	CalA_R5D	>100
24	CalA_R6A	12.5
25	CalA_R7A	6.25
26	CalA_R8A	12.5
27	CalA_R8W	>100
28	CalA_R8V	3.125
29	CalA_C1A	12.5
30	CalA_C2A	>50
31	CalA_C3A	>50
32	CalA_C3L	3.125
33	CalA_C3I	1.56
34	CalA_C3W	1.56
35	CalA_C4A	12.5
36	CalA_C4X	1.56
37	CalA_C4Pra	1.56
38	CalA_C4Aha	3.125
39	CalA_C5A	3.125
40	CalA_C3X+C4X	25
41	CalA_C3I+C4X	3.125
42	CalA_R2P+C3I+C4X	6.25
43	CalA_R3I+R2P	3.125
44	CalB_C4Pra	3.125
45	Biotin-CalA probe	12.5

H37Rv MIC_{90} color code
≤ 0.78 µM
1.56 µM
3.12 µM
6.25 µM
12.5 µM
25 µM
≥ 50 µM

The obtained results are generally consistent with the former published MIC_{90} values. Accordingly, Callyaerin A and B were active in the low to submicromolar range while the other Callyaerins had no substantial anti-TB activity. A comparison of the activity of natural and synthetic Callyaerin A revealed, as previously described in section 3.1.7, that the synthetic compound had a slightly lower MIC_{90} value (3.125 µM vs. 6.25 µM) than previously reported for the natural product.

3.2.2 Structure-activity relationship of Callyaerin derivatives by comparison of MIC_{90} values on *M. tuberculosis* strain H37Rv

To obtain insights into the structure-activity relationships underlying Callyaerin A's bioactivity, an alanine scan was performed. Accordingly, all residues of Callyaerin A (R1-8, C1-C4) were individually replaced against an alanine in a systematic manner (see Table 14). This approach allowed to gain a first hint on the contribution of each amino acid for anti-mycobacterial activity. An alanine on positions R1, R2, R5 - R8, C1, C4 increased the MIC_{90} slightly to 6.25 µM - 12.5 µM, while *CalA_R4A* with a MIC_{90} of 3.125 µM retained its activity. On the contrary, an exchange to alanine on positions R3, C2 and C3 led to a loss of activity (MIC_{90} >50 µM).

Surprisingly, Callyaerin B exhibited the most potent antitubercular activity of all Callyaerins (MIC_{90} = 0.39 µM). Callyaerin B differs from Callyaerin A by a C3-Ile instead of a Phe and a R3-Ile instead of a Val. Interestingly, the Callyaerin A derivative *CalA_R3I* in which an isoleucine residue is also incorporated into the R3 position also had a comparably low MIC_{90} value (0.78 µM). We also tested other large hydrophobic residues on this ring position (e. g. Leu or Phe) which all retained or slightly improved bioactivity, although Ile remained the best choice for bioactivity. In contrast, incorporation of a small hydrophobic amino acid led to significantly reduced bioactivity (e. g. Ala). Overall, this indicates that the R3 position is important for bioactivity and favors the incorporation of large hydrophobic residues with Ile currently representing the best choice.

Callyaerin B differs from Callyaerin A also in position C3, harbouring an Ile instead of a Phe residue. Hence, the influence on bioactivity of amino acid substitutions in this position was also tested. We found that the presence of bulky hydrophobic amino acid residues (Phe, Trp, Leu, Ile) on position C3 is essential for a high activity, while the replacement with an alanine as an example of small hydrophobic amino acid leads to

a significant decrease of activity (*CalA_C3A* with MIC_{90} >50 µM). This is thus similar to the previous findings for position R3, where large hydrophobic amino acids such as Val, Leu, Ile and Phe conduce to and Ala abrogates activity.

In position C2, an exchange of the Ile residue to Ala also reduced the bioactivity. These data strongly suggest that Callyaerin A amino acid positions R3, C2 and C3 are crucial for antitubercular activity and that all three positions seem to require large hydrophobic amino acids. For C2, validation by further synthesis of derivatives is however pending.

To test the relevance of the terminal Callyaerin A chain position C4 (Gly) for bioactivity, Callyaerin A derivatives in which the terminal glycine was deleted (*CalA_C4X*) or modified with click tags (alkyne in *CalA_C4Pra*, azide in *CalA_C4Aha*) were also tested. These derivatives remained as active as the parent compound, indicating that this position is not essential for efficient target binding. Also, the addition of an extra amino acid (Ala) on Callyaerin A chain position C5 (*CalA_C5A*) that is not present in natural Callyaerin A has no significant influence on bioactivity.

From a synthetical point of view, it was also pleasant to see that the exchange of the most expensive amino acid hydroxyproline on position R2 against a standard proline moiety (*CalA_R2P*) basically had no effect on the bioactivity. This finding paves the way for the synthesis of active Callyaerin derivatives that can be economically produced, e.g. for the production of a Callyaerin-based inhibitor in a multi-gram scale, e. g. for mouse experiments. However, the additional replacement of Val → Ile also on position R3 besides the proline replacement (*CalA_R3I+R2P*) retained but did not increase the activity as for *CalA_R3I*. Accordingly, the structure-activity relationships are not only binary.

An alternative approach to reduce the synthetic efforts is the deletion of amino acids from the sequence which do not contribute to the activity, like the Gly residue of Callyaerin A chain position C4 (*CalA_C4X*) that is possible without significant loss of bioactivity. However, we found that this approach has its limitations because a further reduction of the exocyclic sequence as for example in Callyaerin A derivative *CalA_C3X+C4X* led to a decreased bioactivity (MIC_{90} = 25 µM).

All Callyaerins are highly hydrophobic due to the presence of many hydrophobic amino acids. This unfortunately leads to improper pharmacokinetic properties. To test if better water-soluble compounds can be obtained without significant loss of bioactivity, Asp

as a hydrophilic amino acid was implemented at ring position R5 which in the alanine scan was non-sensitive and which is rather distant to the DAA unit. However, the resulting compound was found to be inactive (MIC_{90} >100 µM for *CalA_R5D*). So far, it seems as the hydrophobic character of Callyaerins A and B is crucial for their activity.

We also tested the impact of the R8 position which is located vicinal to the DAA unit on bioactivity. We found that if for example a bulky tryptophan was built into the Callyaerin A ring position R8 (Leu → Trp), the bioactivity dropped significantly (*CalA_R8W* with MIC_{90} >100 µM). In contrast, a valine on ring position R8 is as good as the initial leucine (*CalA_R8V* with MIC_{90} = 3.125 µM) but a smaller alanine led to a slightly lower bioactivity (*CalA_R8A* with MIC_{90} = 12.5 µM). Overall, this demonstrates that also this position is important for bioactivity with a preference for large, aliphatic amino acids.

As also reported in 3.1.4, the click-tagged Callyaerin derivatives *CalA_C4Pra*, *CalA_C4Aha* and *CalB_C4Pra* all remained active (MIC_{90} ≤ 3.125 µM), which enables the functionalization with fluorescence or affinity tags *in vitro* or *in vivo*. For the first trial, an azide-PEG3-biotin conjugate was clicked with *CalA_C4Pra* to receive a *Biotin-CalA* probe. Even this voluminous molecule featured a moderate activity with a MIC_{90} value of 12.5 µM.

3.2.3 MIC_{90} determination of selected Callyaerin derivatives on other *M. tuberculosis* strains

All biological experiments were carried out by Yvonne Gröner from the Kalscheuer lab at the HHU Düsseldorf, Germany.

From the Callyaerin derivatives that had shown activity against the virulent strain H37Rv (see Table 14), a selection was tested against further mycobacteria including the *M. tuberculosis* strains HN878 Bejing, CDC1551 and mc²6230, the *Mycobacterium bovis* strains AF2122/97, BCG Pasteur, BCG Danish, BCG Birkhaug and BCG Copenhagen as well as the avirulent fast-growing species *Mycobacterium smegmatis* mc²155. The MIC_{90} values of selected Callyaerin derivatives are summarized in Table 15.

Table 15: MIC_{90} values [µM] of selected Callyaerin derivatives against different *Mycobacterium* strains.

#	**0**	**1**	**2**	**16**	**21**	**22**	**35**	**37**
substance	nat. CalA	syn. CalA	syn. CalB	CalA_ R2P	CalA_ R4A	CalA_ R5A	CalA_ C4A	CalA_ C4Pra
SPPS# (reactor)		R58	R57	R53	R51	R45	R39	R80
***M. tb.* H37Rv**	6.25	3.125	0.39	3.125	3.125	6.25	12.5	1.56
***M. tb.* HN878 Bejing**		12.5						
***M. tb.* CDC1551**		3.125						
***M. tb.* mc²6230**	3.125	0.78	<0.78	1.56	3.125	3.125	1.56	1.56
***M. bovis* (AF2122/97)**		>100						
BCG Pasteur	>100	>100	50	50	>100	>100	>100	50
BCG Danish		>100	50	50	>100	>100	>100	50
BCG Birkhaug		>100	50	>100	>100	>100	>100	100
BCG Copenhagen		>100	50	>100	>100	>100	>100	100
***M. smegmatis* mc²155**		>100	>50					

All selected compounds were also active against the attenuated strain mc²6230 that was originally obtained from W.R. Jacobs lab of the Albert Einstein College of Medicine, Bronx, NY, USA. This non-virulent strain is an auxotrophic double knock-out mutant of H37Rv harboring gene deletions of the genes *panCD* and the DRD region. This strain is not able to produce pantothenic acid, also called vitamine B5, which must be added to the growth medium.

Synthetic Callyaerin A also exhibited bioactivity against the hypervirulent *M. tuberculosis* strains HN878 Bejing and CDC1551. The HN878 strain is regarded as hypervirulent due to its rapid growth and the reduced survival of infected mice when compared with other clinical isolates[110]. Another strain of *M. tuberculosis* (CDC1551 or CSU 93) was responsible for an outbreak of tuberculosis in the 1990s in a rural area near the Kentucky-Tennessee border and is considered exceptionally virulent because of the high number of positive tuberculin reactions, skin test conversions, and infected casual contacts[111].

An astonishing result is the inactivity of all selected Callyaerin derivatives against *M. bovis* (AF2122/97) and all tested BCG strains. These attenuated Bacillus Calmette-Guerin strains were generated by serial passages of *M. bovis* and are used as vaccines against tuberculosis. The resistance of BCG strains against Callyaerin A and B may provide indications for their uptake, mode of action and target elucidation.

3.2.4 Test of selected Callyaerin derivatives on XDR *M. tuberculosis* isolates

Additionally, some compounds were tested against clinical isolates of extremely drug resistant (XDR) *M. tuberculosis* (KZN06, KZN13, KZN14, KZN16). These XDR *M. tuberculosis* clinical isolates were obtained from W.R. Jacobs lab at the Albert Einstein College of Medicine, Bronx, NY, USA.

All biological experiments were carried out by Yvonne Gröner from the Kalscheuer lab at the HHU Düsseldorf, Germany. An overview of the resistance of these strains against clinically used anti-tubercular antibiotics is listed in Table 16.

Table 16: Overview of antibiotic resistance of XDR clinical isolates. R = resistant, S = susceptible.

Anti-TB drug	**KZN06**	**KZN13**	**KZN14**	**KZN16**
Rifampicin	R	R	R	R
Isoniazid	R	R	R	R
Ethambutol	R	R	R	R
Pyrazinamide	R	R	R	R
Streptomycin	R	R	R	R
Ethionamide	R	R	R	R
Kanamycin	R	R	R	R
Amikacin	R	R	R	R
Capreomycin	R	R	R	R
Ofloxacin	R	R	R	R
Cycloserine	S	S	S	S
Para-aminosalicylic acid	S	S	S	S

Intriguingly, synthetic Callyaerin A and the other tested derivatives *CalA_R3I*, *CalA_C3I* and *CalA_C3W* showed activity against these XDR *M. tuberculosis* clinical isolates in the MIC_{90} range of 6.25 µM to 25 µM (see Figure 36).

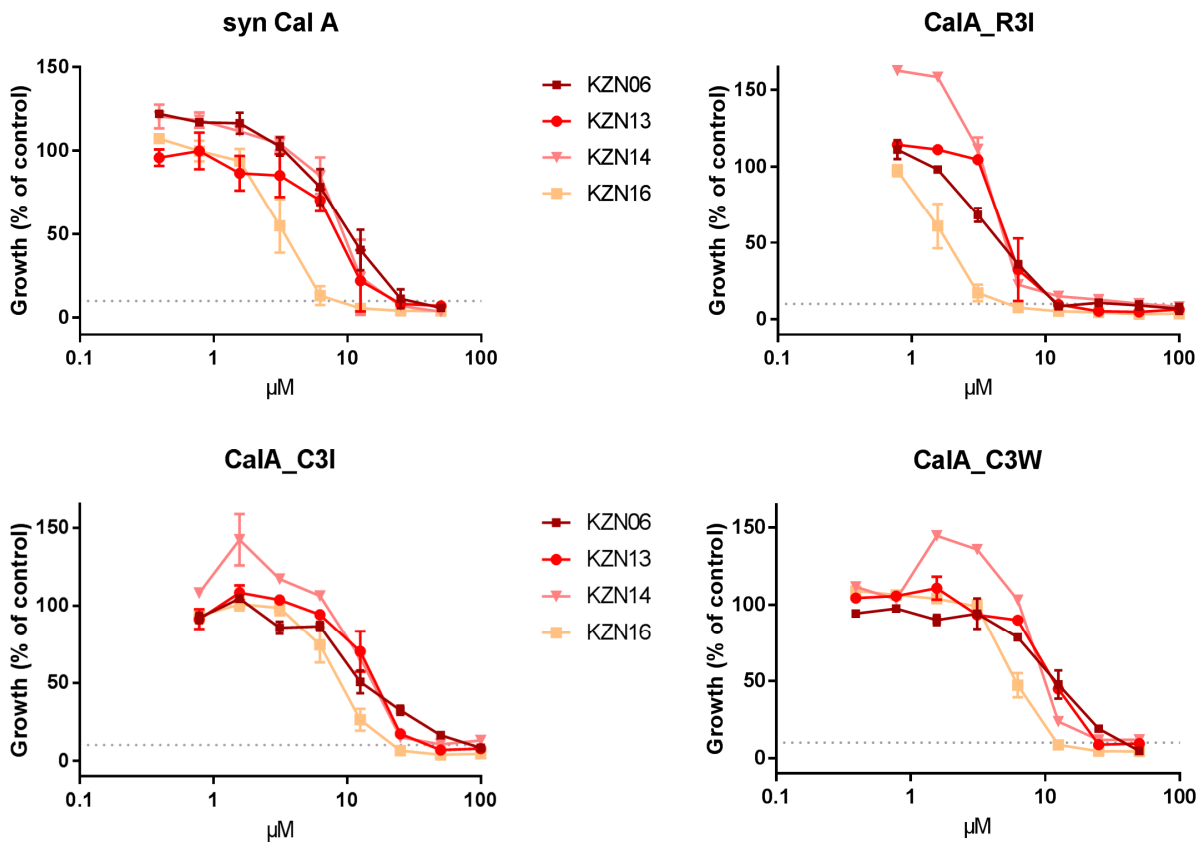

Figure 36: Growth inhibition of clinical isolates of XDR *M. tuberculosis* (KZN06, KZN13, KZN14, KZN16) from treatment with synthetic Callyaerin A and derivatives *CalA_R3I*, *CalA_C3I* and *CalA_C3W*.

The observed shift to higher MIC_{90} values of the XDR *M. tuberculosis* isolates in comparison to the wildtype strain H37Rv can thereby be explained by the slower growth rate *in vitro*. Due to a variety of mutations, XDR bacteria grow slowly in liquid culture. This effect may not occur *in vivo*, where the human host cells provide supplementary nutrients. Also, the difference of growth inhibition among the XDR isolates (e. g. KNZ06 vs. KNZ16) can be interpreted by various mutations effecting the growth rate. This problem could be overcome by an adaption of the assay, e. g. by prolongation of the incubation time or an increase of the CFU/mL; however, these adjustments would result in a loss of comparability to the wildtype assay and were therefore not implemented here.

The main conclusions from the observed activity against XDR *M. tuberculosis* is that Callyaerin derivatives also inhibited these clinically important strains which is a very promising trait for the development of a new antitubercular agent. In addition, the results suggest that Callyaerins may act *via* chemical modulation of a new target that differs from common antibiotics, which is not affected by known resistance mechanisms of XDR *M. tuberculosis* strains.

3.2.5 Generation of Callyaerin A resistant mutants

All biological experiments were carried out by Yvonne Gröner from the Kalscheuer lab at the HHU Düsseldorf, Germany. For elucidation of the Callyaerin resistance mechanism, the virulent *M. tuberculosis* strain H37Rv was plated out on Callyaerin A-containing agar culture media. Resistance occurred at a frequency of ~ 10^{-7}. After four weeks individual clones were picked, and their resistance was initially tested against natural Callyaerin A. Three resistant clones C1, C2 and C3 were chosen for genome sequencing (see Table 17).

Table 17: Genome sequencing results for three Callyaerin A resistant clones.

Callyaerin A resistant clone	**SNPs (single-nucleotide polymorphisms)**
C1	Rv2113 (T185A)
C2	Rv2113 (L28P)
C3	Rv2113 (L241P), Rv0236c/AftD (G882G)

All three clones had a mutation in gene Rv2113, which is not essential and has an unknown function. Gene dispensability suggests that the product of this gene is likely not the target but is involved in the resistance mechanism (e. g. due to efflux or impaired uptake).

Accordingly, besides Callyaerin A, also Callyaerin A derivatives were tested vs. these resistant H37Rv clones C1, C2, C3. These derivatives were *CalA_C4A*, *CalA_R4A*, *CalA_R5A*, *CalA_R2P*, *CalA_C4Pra* (see Figure 37). All clones showed cross-resistance to Callyaerin A and all tested derivatives (MIC_{90} > 100 µM). Only *CalA_R5A* and *CalA_R2P* had a slight inhibitory effect at higher concentrations.

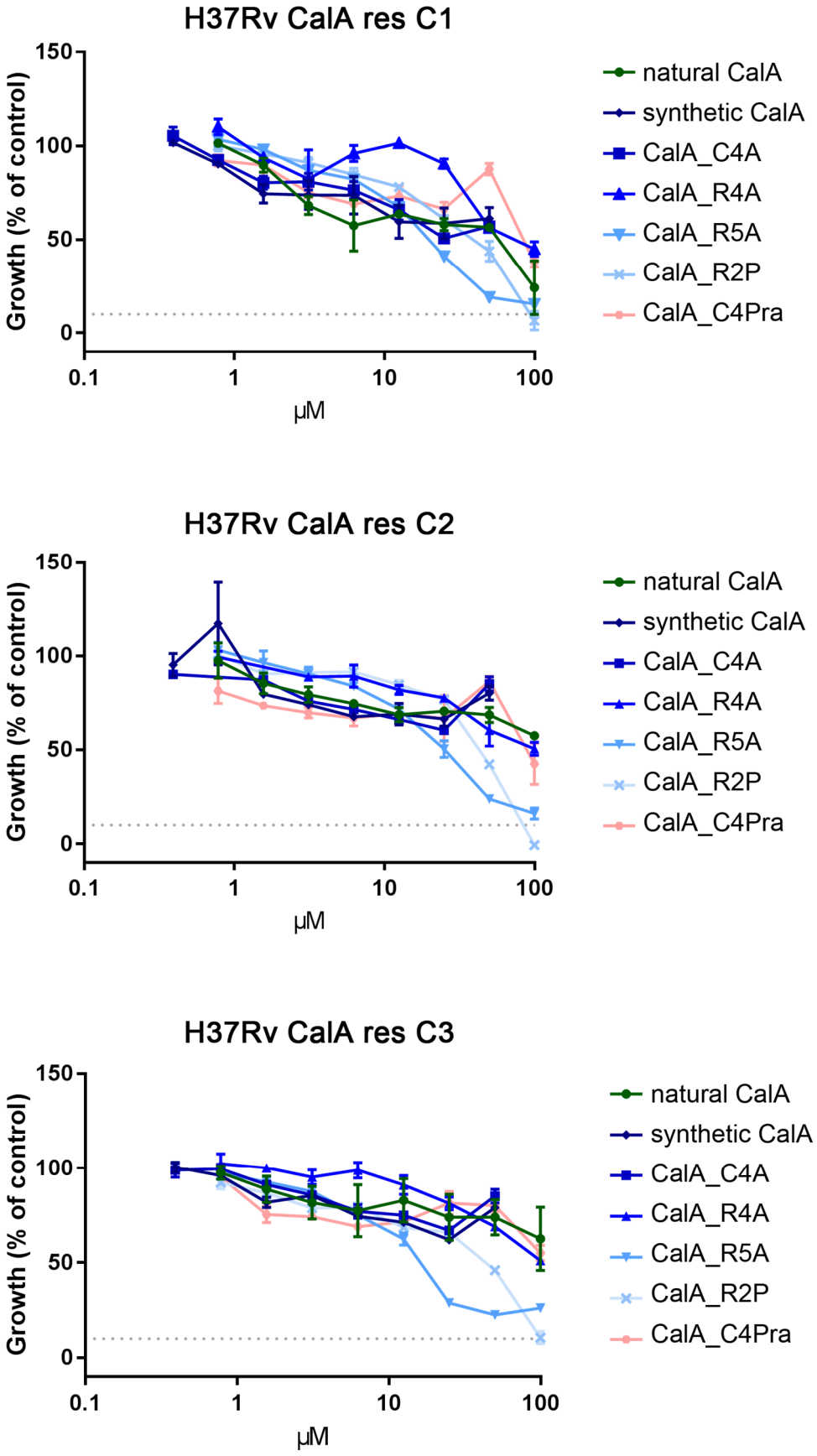

Figure 37: Growth inhibition of three Callyaerin A resistant H37Rv clones C1, C2, C3 by treatment with natural Callyaerin A, synthetic Callyaerin A and Callyaerin A derivatives *CalA_C4A*, *CalA_R4A*, *CalA_R5A*, *CalA_R2P*, *CalA_C4Pra*.

3.2.6 Cytotoxicity assay on human cell lines

To test a potential applicability of Callyaerins as chemotherapeutics, cytotoxicity assays with human cell lines were performed. All corresponding biological experiments were carried out by Yvonne Gröner from the Kalscheuer lab at the HHU Düsseldorf, Germany. To this end, the cytotoxicity of selected Callyaerin A derivatives and Callyaerin B was tested on human monocytic cell line THP-1, human liver cancer cell line HepG2 and human embryonic kidney cell line HEK293 *in vitro* (see Figure 38 and Table 18).

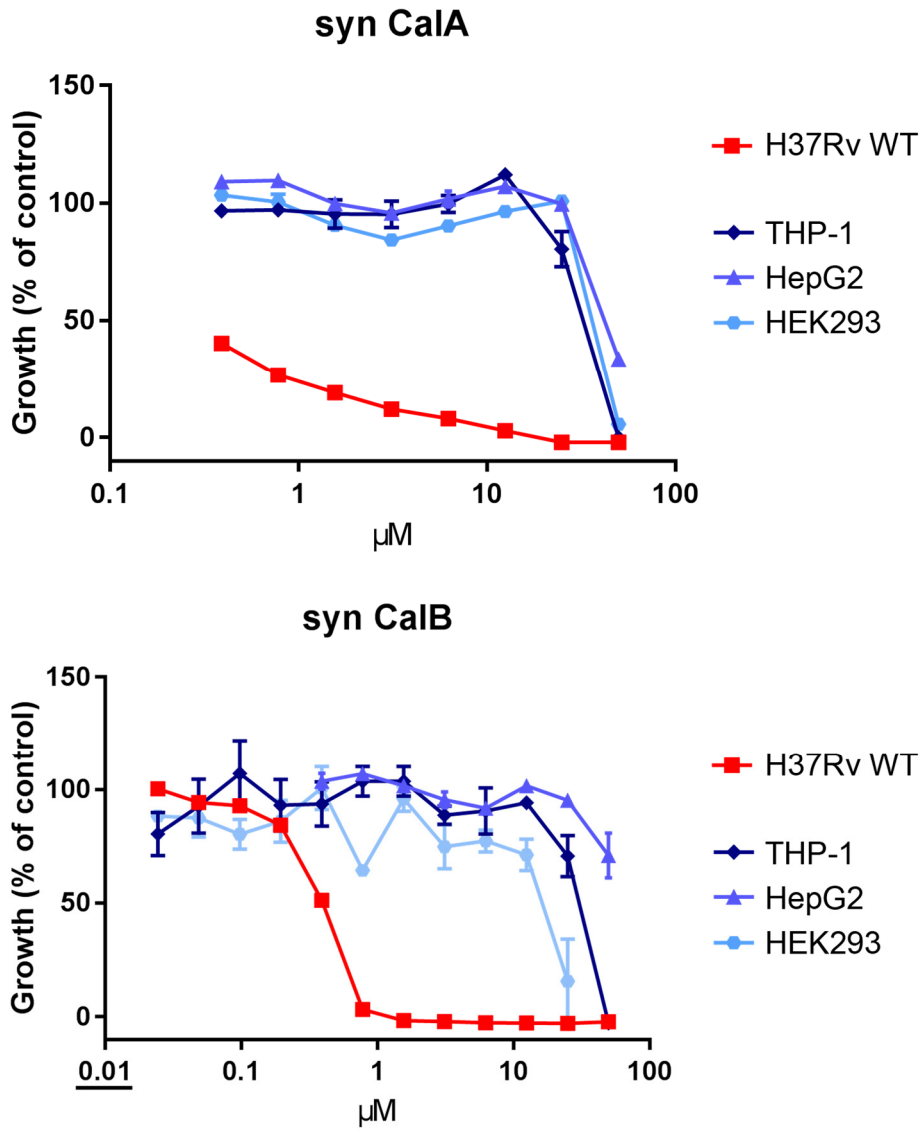

Figure 38: Growth inhibition of synthetic Callyaerin A and B against *M. tuberculosis* H37Rv and the three different human cell lines: human monocytic cell line THP-1, human liver cancer cell line HepG2 and human embryonic kidney cell line HEK293.

Table 18: Selectivity indices for selected CalA derivatives. SI values were calculated using IC_{50} values of THP-1.

	H37Rv MIC_{90}	**THP-1 IC_{50}**	**HepG2 IC_{50}**	**HEK293 IC_{50}**	**SI = IC_{50}/MIC_{90}**
natural CalA	6.25 µM	50 µM			8
synthetic CalA	3.13 µM	50 µM	50 µM	50 µM	16
synthetic CalB	0.39 µM	50 µM	>50 µM	25 µM	128
CalA_C3W	1.56 µM	50 µM			32
CalA_C4X	1.56 µM	20 µM			13
CalA_C3I	1.56 µM	100 µM			64
CalA_R3I	0.78 µM	50 µM			64

The IC_{50} values for the human cell lines were determined as 50 µM for synthetic Callyaerin A and B, resulting in selectivity indices of 16 and 128, respectively. The Callyaerin A derivatives *CalA_C3I* and *CalA_C3I* also exhibit a high selectivity index of 64. These findings indicate that Callyaerins may not display hepatotoxic and nephrotoxic effects which paves the way for further drug development.

3.2.7 Macrophage infection assay

Macrophages are among the very first cells that will encounter *M. tuberculosis* after inhalation into the lung and they play a crucial role in the process of infection. Therefore, *in vitro* models of macrophage infection are powerful tools for understanding host-pathogen interaction.

The human monocytic cell line THP-1 is the most widely used model for primary human macrophages. They acquire a macrophage-like phenotype following differentiation using phorbol 12-myristate 13-acetate (PMA) and mimic primary human macrophages in many respects.

All biological experiments were carried out by Yvonne Gröner from the Kalscheuer lab at the HHU Düsseldorf, Germany.

To this end, the effect of Callyaerins on PMA stimulated THP-1 cells that were infected with the virulent H37Rv reporter strain (MOI = 3) expressing the fluorescent protein mCherry was determined. After 3 h incubation, the extracellular bacteria were washed away and fresh media with compound (5x MIC) was applied. The microscopic analysis ensued after 5 days post infection. The results are shown in Figure 39.

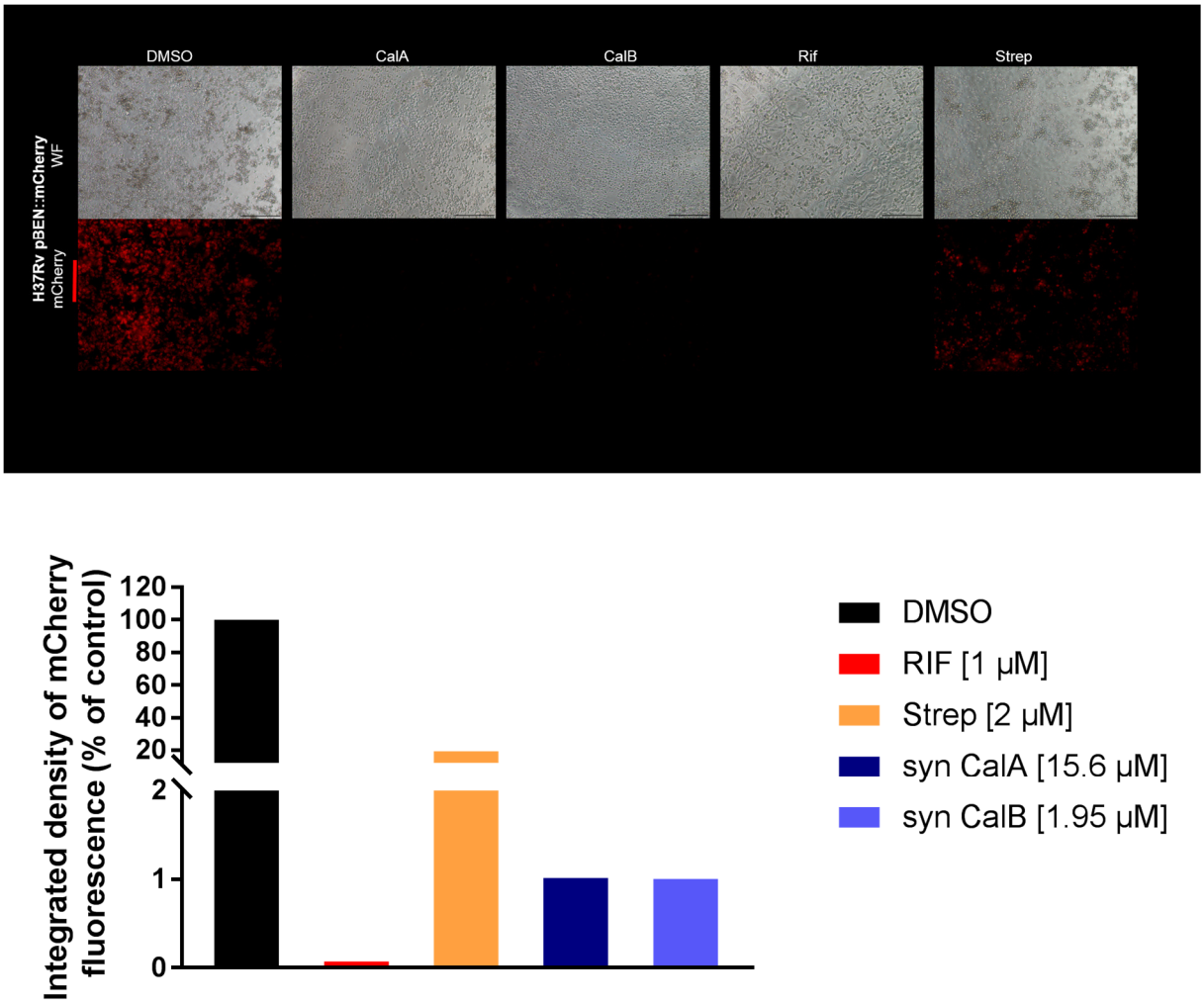

Figure 39: Microscopic analysis and resulting quantification of the macrophage infection assay.

The macrophages internalize the mycobacteria, which produce the fluorescent protein mCherry. A reduced integrated fluorescence intensity is thus a sign of impaired intracellular replication of the mycobacteria. Concurrently, the cell form in the wide field image serves to ensure the healthiness of the human macrophages.

The assay was carried out in five conditions: DMSO as a negative control, Rifampicin and Streptomycin as positive controls and synthetic Callyaerin A + B as test compounds. The integrated density of the fluorescence signal in relation to DMSO for incubation with both synthetic Callyaerins A and B was 1 %, which was slightly higher than the most active positive control Rifampicin (< 0.1 %) but substantially lower than Streptomycin (20 %), while the macrophages remained in a healthy form for all conditions except for the DMSO control which exhibited a heavy intracellular bacterial burden. These results underline the anti-TB activity of Callyaerins in combination with a high selectivity for *M. tuberculosis* in a human cell environment.

3.3 Proteomic affinity enrichment experiments for target elucidation of Callyaerin A and B

3.3.1 Workflow for proteomic affinity enrichment experiments

As shown in 3.2.1, Callyaerin A and B exhibit anti-tubercular activity in the low micromolar range. In order to determine their mode of action in living organisms, it is highly desirable to elucidate their molecular target(s). A first attempt to determine these was performed in the Kalscheuer laboratory by generating and sequencing of Callyaerin A resistant mutants (see 3.2.5), which resulted in the identification of genes that however seem to be involved in the uptake of Callyaerins and not as direct binding partners. More specific information about the binding partners of an active compound can however be gained on a protein level via affinity purification or enrichment strategies. Therefore, proteomic experiments were designed to find proteins which potentially interact with Callyaerin A and B.

A general workflow for the performed proteomic affinity enrichment experiments is shown in Figure 40. The detailed protocols for each experiment are described in section 5.8. Briefly, the cell lysate was incubated with the Biotin-tagged Callyaerin A or B probe (*Biotin-CalA, Biotin-CalB*) to reversibly bind potential protein targets of the active compound. Accordingly, these biotin-tagged proteins were then affinity enriched upon binding to avidin, which was immobilized on agarose beads. Mild washing steps were then performed to reduce unspecific protein binding.

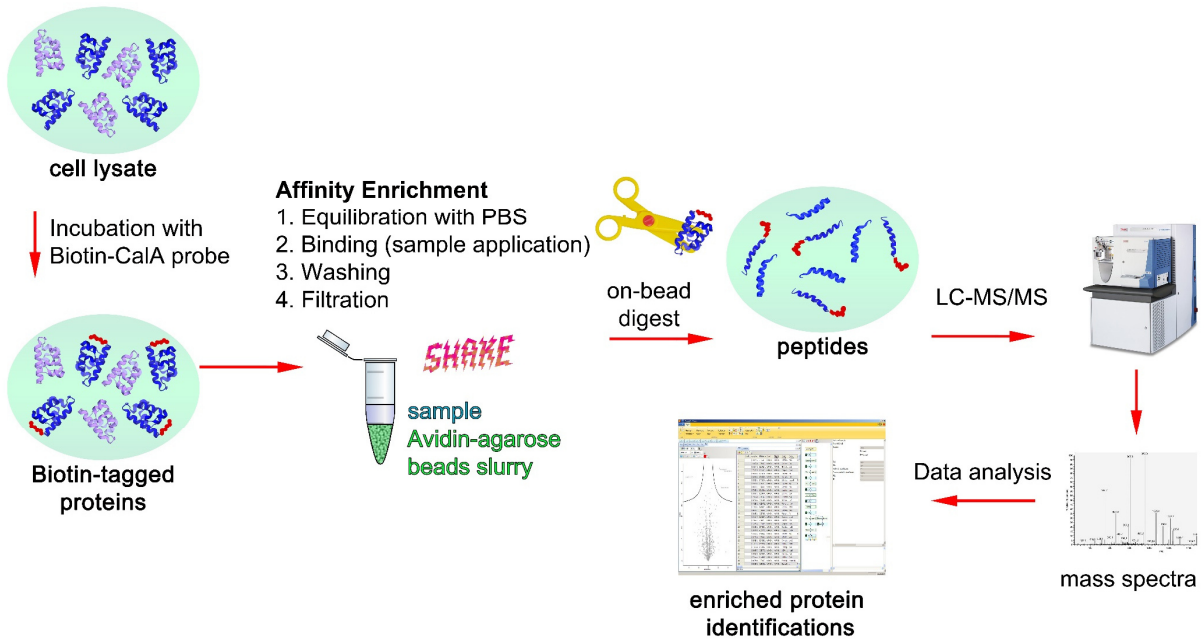

Figure 40: General workflow for proteomic affinity enrichment experiments.

The following on-bead digest with trypsin generated peptides that were measured by LC-MS/MS and quantified in a label-free approach *via* MaxQuant and the statistics software package Perseus. Statistical processing allowed the assignment of the identified peptides to their corresponding proteins, which were compared for different experimental conditions, for example the application of a biotin probe vs. a negative control. From the statistical point of view, it is desirable to perform a sample preparation with mild washing steps rather than a stringent purification of the biotin-tagged proteins on the beads, because with the label-free MS-settings a large protein background leads to more identifications which results in better statistics for the build-in algorithm calculating the label-free quantification (LFQ) intensities. The statistical outcome is depicted in a so called ‘vulcano plot’, in which the *p* value of each protein is plotted against the difference of its LFQ intensities for two experimental conditions. A comparison of the results of the pulldown from the use of a biotin probe against against a DMSO control thus reveals the enriched proteins with a high positive difference in LFQ intensities.

3.3.2 Proteomic affinity enrichment in *M. tuberculosis*

For target elucidation of Callyaerin A and B in *M. tuberculosis*, a *M. tuberculosis* cell lysate provided from the Kalscheuer laboratory at the HHU Düsseldorf was treated with the biotinylated Callyaerin A and B probes *Biotin-CalA* and *Biotin-CalB*, respectively, (see 3.1.4) as well as with controls. Avidin-agarose beads were added and after mild washing steps with PBS the bound proteins were denatured with urea und digested on-bead for LC-MS/MS analysis.

Five cell lysate treatment conditions with three replicates for each condition were overall submitted to this workflow. The exact conditions are reported in Table 2. These were DMSO as a negative control, 2 µM Tri-FP (a trifunctional fluorophosphonate probe that labels serine proteases) as a control for the affinity enrichment workflow, and the *Biotin-CalA* and *Biotin-CalB* probes at 2 µM. Additionally, one experimental condition included the competition of the bound proteins by washing the beads with Callyaerin A containing PBS.

Table 19: Employed experimental conditions for proteomic affinity enrichment experiment in *M. tuberculosis*.

sample#	**experimental condition**
#01-03	DMSO
#04-06	Tri-FP (2 µM)
#07-09	Biotin-CalA (2 µM)
#10-12	Biotin-CalA (2 µM) + bead washing with 20 µM CalA in washing solution
#13-15	Biotin-CalB (2 µM)

For evaluation of the resulting MS data, the LFQ intensities of the protein groups of each condition were compared vs. the DMSO control and plotted as scatter (or vulcano) plots (Figure 41). The results were remarkable for many reasons. First, only a handful of proteins were found as significantly enriched with a very high difference in intensity compared to the DMSO control. Second, not a single protein was depleted (i. e. no significant data points with negative difference). This was expected since an enrichment strategy was chosen. Third, both probes *Biotin-CalA* and *Biotin-CalB* basically delivered the same enriched proteins (labelled green in Figure 41). The most enriched protein was HRP1 which was enriched with a factor of $2^{6.23}$ (= 75)-fold by *Biotin-CalA* and $2^{7.53}$ (= 185)-fold by *Biotin-CalB*-treated samples.

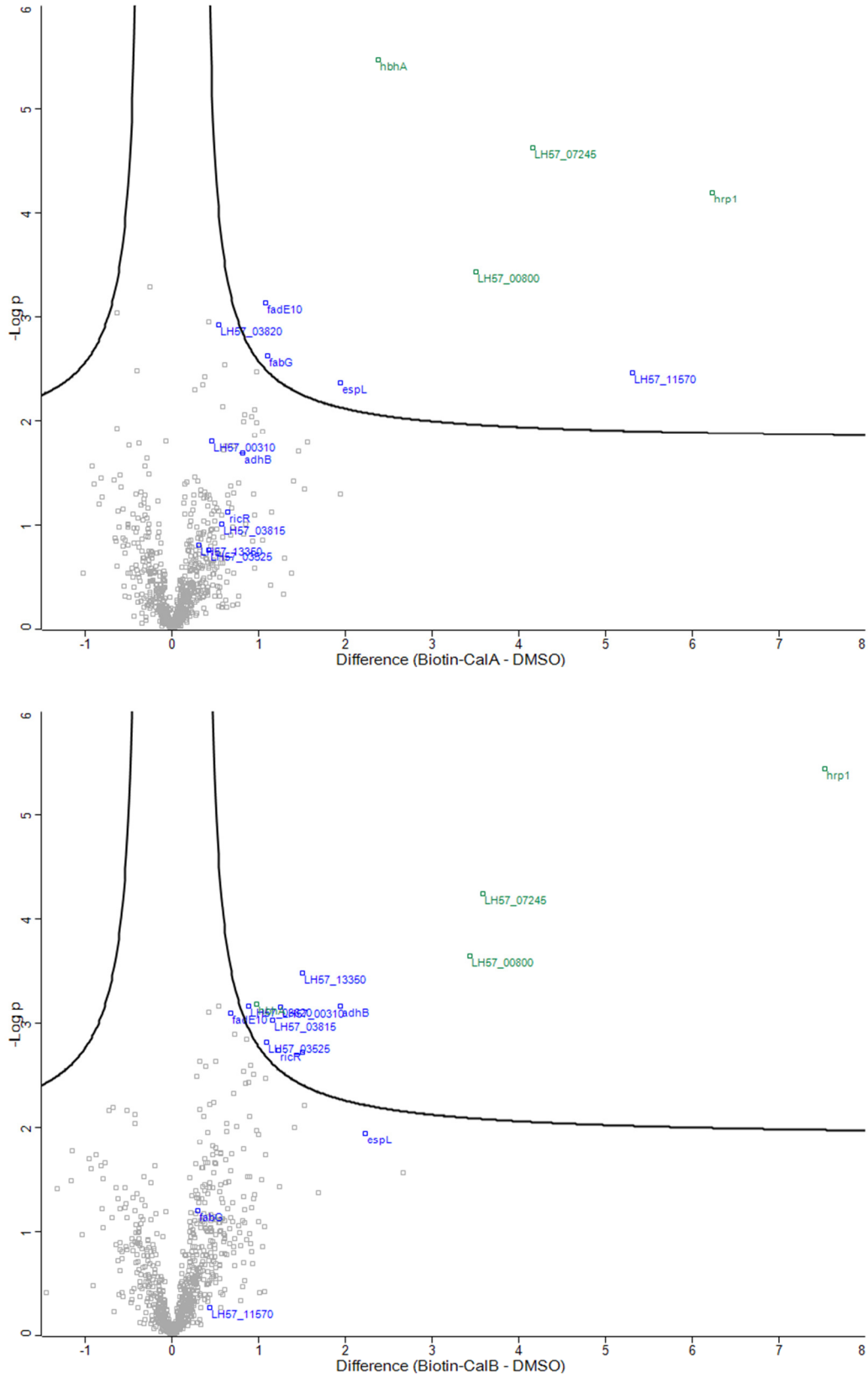

Figure 41: Scatter plots of *t*-test results from log_2 LFQ intensities of protein groups from each two different experimental conditions. Top: Biotin-CalA vs. DMSO. Bottom: Biotin-CalB vs. DMSO. Plotted is the -log(P-value) against the difference in log_2(LFQ intensity). Protein groups above the significance line in one of the two plots are colored in blue. Protein groups above the significance line in both plots are colored in green. The gene names are indicated. The sections cover all data points.

A visualization of the log_2 LFQ intensities across the sample numbers is shown in Figure 42. In this profile, the three most significant proteins, i. e. HRP1, P96821 and L7N6B1, were highlighted in green and are also reported in Table 20).

Table 20: Most significant proteins from the proteomic enrichment experiment in *M. tuberculosis*.

Uniprot names	**protein name**	**gene name; locus**
HRP1	Hypoxic response protein 1	LH57_14370; Rv2626c
P96821	Probable transcriptional regulatory protein (Possibly TetR-family)	LH57_00800; Rv0144
L7N6B1	Conserved protein	LH57_07245; Rv1322A

These three proteins exhibit a comparable LFQ intensity profile pattern in the different conditions. Accordingly, in presence of *Biotin-CalA* and *Biotin-CalB*, LFQ intensities significantly rise while a decreased intensity is observed for the condition in which the bead-bound proteins where washed with Callyaerin A in PBS buffer. The fact, that a 'simple' washing with Callyaerin A leads to lower intensities (see Figure 42), indicates that *Biotin-CalA* and thus Callyaerin A binds non-covalently to the analysed proteins.

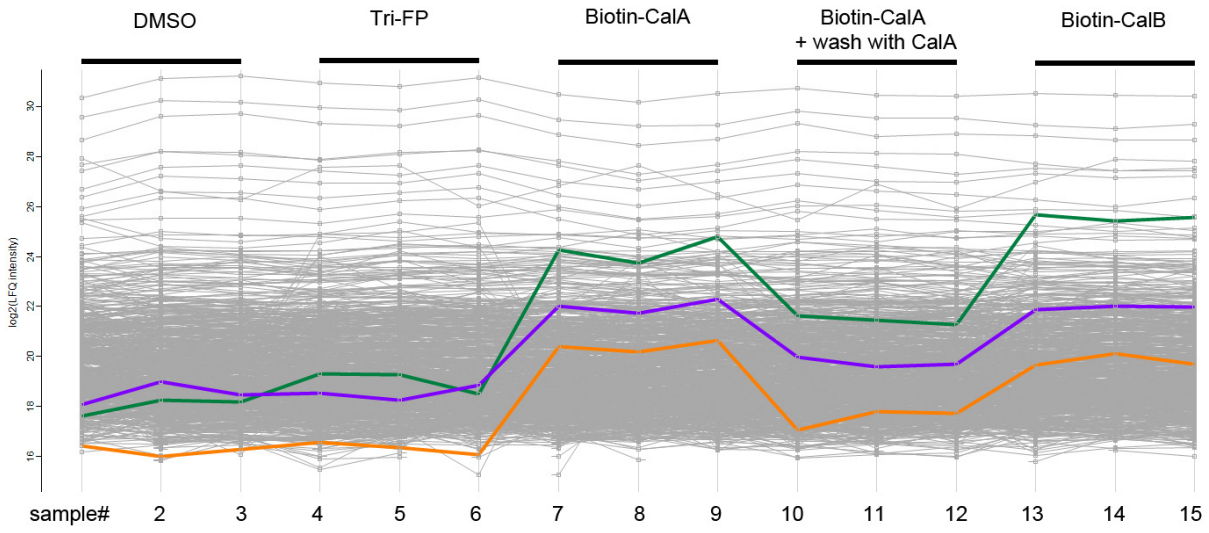

Figure 42: Profile plot of log_2 LFQ intensities across the sample numbers for all five experimental conditions in triplicates. The colored proteine groups are HRP1 (green), P96821 (violet) and L7N6B1 (orange).

3.3.3 Proteomic affinity enrichment in *H. sapiens*

We next went to also identify targets of Callyaerin A in human cell lines; these studies may help to validate the employed proteomics workflow and may also give insights into potential off-target effects of Callyaerins. To this end, a HeLa cell lysate was again either treated with *Biotin-CalA* (see 3.1.4) or with controls. Avidin-agarose beads were added and after mild washing steps with PBS, the bound proteins were denatured with urea und digested on-bead for LC-MS/MS analysis.

In these experiments, overall four conditions with four replicates each were chosen as reported in Table 21. These were DMSO as a negative control, again Tri-FP (trifunctional fluorophosphonate probe to label serine proteases) as a control for the enrichment workflow and the *Biotin-CalA* probe. Additionally, one experimental condition was a Callyaerin A competition of the bound proteins by washing the beads with Callyaerin A in PBS buffer.

Table 21: Employed experimental conditions used in the proteomic affinity enrichment experiment in *H. sapiens*.

sample#	**experimental condition**
#01-04	DMSO
#05-08	Tri-FP (2 µM)
#09-12	Biotin-CalA (2 µM)
#13-16	Biotin-CalA (2 µM) + bead washing with 20 µM CalA in washing solution

For evaluation of the MS data, the LFQ intensities of the protein groups in condition *Biotin-CalA* were taken for a *t*-test against the DMSO control and plotted as scatter (or vulcano) plot in Figure 43.

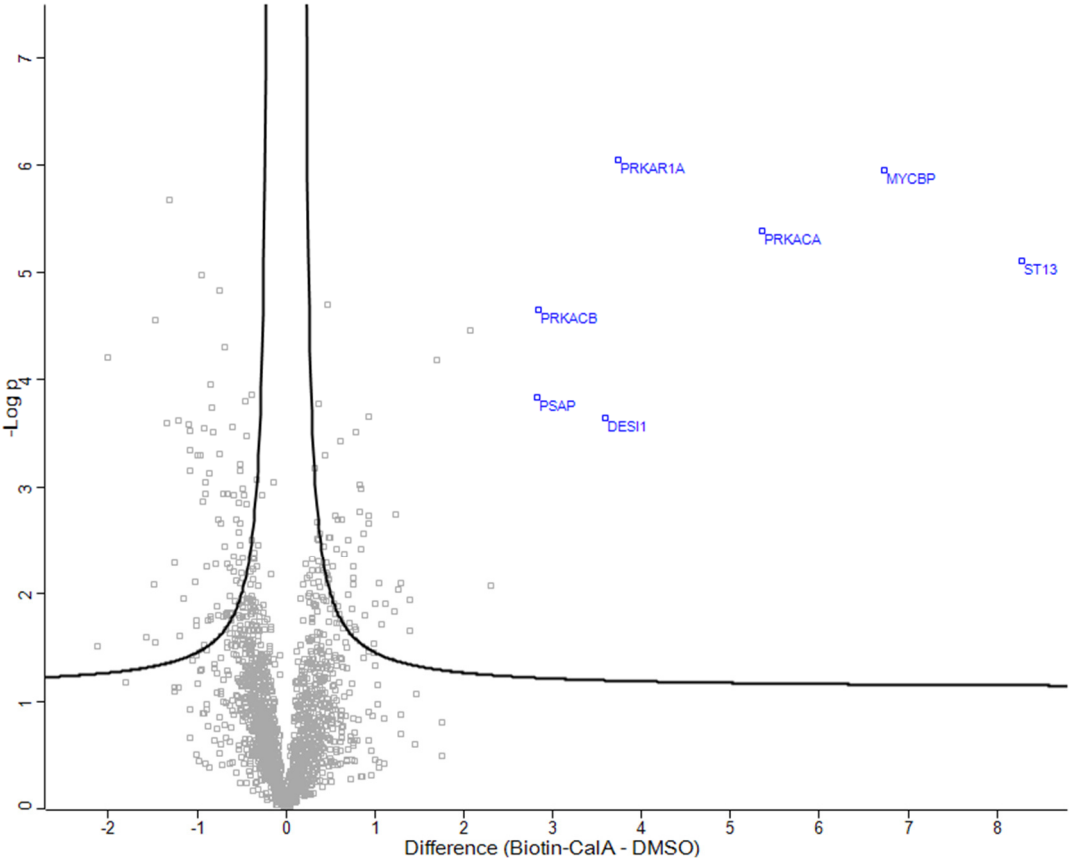

Figure 43: Scatter plot of *t*-test results from log_2 LFQ intensities of protein groups from experimental condition Biotin-CalA vs. DMSO. Plotted is the -log(P-value) against the difference in log_2(LFQ intensity). The gene names are indicated. The section covers all data points.

A visualization of the log_2 LFQ intensities across the sample numbers is shown in Figure 44. In this profile plot, the five most significant proteins from the vulcano plots are highlighted (also see Table 22).

Table 22: Most significant proteins from the proteomic enrichment experiment in *H. sapiens*.

Uniprot ID	protein name	gene
P50502	Hsc70-interacting protein	ST13
P10644	cAMP-dependent protein kinase type I-alpha regulatory subunit	PRKAR1A
P17612	cAMP-dependent protein kinase catalytic subunit alpha	PRKACA
P22694	cAMP-dependent protein kinase catalytic subunit beta	PRKACB
Q99417	c-Myc-binding protein	MYCBP

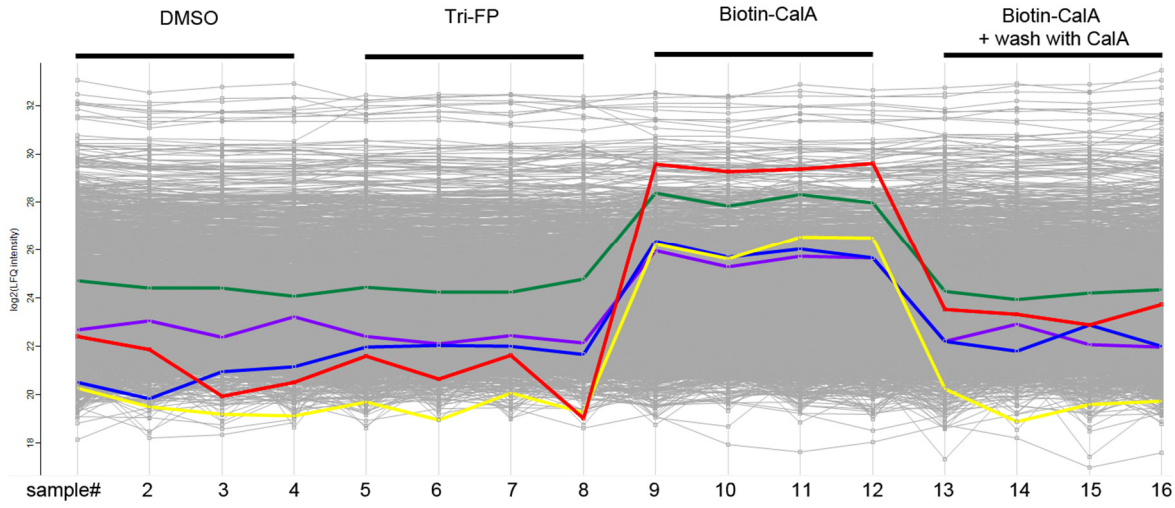

Figure 44: Profile plot of log_2 LFQ intensities across the sample numbers for all four experimental conditions in quadruplicates. The colored proteine groups are P50502 (red), P10644 (green) and P17612 (blue), P22694 (violet), Q99417 (yellow).

The most significant proteins from the proteomic enrichment experiment in *H. sapiens* were the Hsc70-interacting protein, cAMP-dependent protein kinase of which three out of four different subunits were found and the c-Myc-binding protein. The identification of these proteins demonstrates the first experimental evaluation of protein binding partners for Callyaerin A and may hint at possible side effects of Callyaerin treatment in the human organism. As well as for the proteomic experiment in *M. tuberculosis*, the interactions between these proteins and the Callyaerin A probe seem to be non-covalent due to the reduced intensities in the washing condition (sample #13-16).

4 Summary and outlook

The Callyaerins, a natural product family of cyclic peptides, were first isolated from the marine sponge *Callyspongia aerizusa* in 2010 by the Proksch group. Biological studies on the Callyaerins revealed that several Callyaerins, especially Callyaerins A and B, exhibit potent inhibitory activity against *M. tuberculosis*. Further biological assays however required a higher amount of these compounds, since the natural product isolates are limited.

The challenge for the chemical synthesis of Callyaerins is the formation of the structurally rare (*Z*)-2,3-diaminoacrylamide (DAA) moiety. Recently, a first total synthesis of Callyaerin A was described[101]; in this synthesis, a Fmoc-formylglycine-diethylacetal was used as a masked equivalent of formylglycine. Accordingly, this approach required the prior synthesis of a Fmoc-protected formylglycine-diethylacetal building block which was obtained in a 6-step synthesis.

In the present work, the synthesis of Callyaerins and derivatives was performed by oxidation of the hydroxyl group to an aldehyde of a ’standard’ serine residue in a linear precursor; this intermediate then reacted with the free N-terminal amine to form the desired cyclic peptide containing the DAA moiety. This synthesis route turned out to be very convenient and robust. It furthermore allowed the use of standard amino acids for the linear precursor peptide which is very convenient and cost effective. The cyclization reaction proceeded within 1 h at RT (10 min at 40 °C) and the crude product was directly purified by HPLC without extensive workup. Therefore, the established synthesis route represents a very practical and efficient approach, in particular vs. the previously reported synthesis procedure.

Once the synthesis route was established, the natural Callyaerins A – L were synthesized. Daletos *et al.* published in 2015 the structural characterization of the natural Callyaerins A – M[97]. In the present work, these structural assignments were confirmed by NMR and HRMS measurements of the synthetic Callyaerins A – L. Solely Callyaerin M was not chosen for synthesis due to its unusual AMOIPA amino acid residue.

In addition to the natural Callyaerins, the synthesis of more than 30 derivatives was performed. All of them were tested by Yvonne Gröner at the HHU Düsseldorf against the virulent *M. tuberculosis* strain H37Rv to elucidate the structure-activity relationship

underlying Callyaerins' antitubercular bioactivity. In this assay, synthetic Callyaerin B exhibited the most potent antitubercular activity (MIC_{90} = 0.39 µM) and hereby outvalued Callyaerin A (MIC_{90} = 3.125 µM), which was described before as the most active candidate from all natural Callyaerins[97]. The very low or even missing bioactivity of the other synthetic Callyaerins C – L (MIC_{90} > 25 µM) was also consistent with the prior published biological data[97].

Additionally, the antimycobacterial potential of selected synthetic Callyaerins was evaluated in different mycobacterial species (*M. tuberculosis, M. smegmatis* and *M. bovis*) *in vitro*. *M. tuberculosis* strains and also extremely drug resistant clinical isolates were susceptible for various tested Callyaerin derivates (*CalA*, *CalB*, *CalA_R2P*, *CalA_R4A*, *CalA_R5A*, *CalA_C4A* and *CalA_C4Pra*), while *M. smegmatis* and *M. bovis,* inclusively four BCG strains, exhibited higher MIC_{90} values > 50 µM. These findings underlined the selectivity of Callyaerins for virulent mycobacterial strains and their unique mode of action that differs from common antibiotics.

The pharmaco-therapeutic potential of Callyaerins hinges on the selective activity against *M. tuberculosis* in the human body. Therefore, the above-mentioned active Callyaerin derivatives were also assayed in different human cell lines (THP-1, HepG2 and HEK293), which all remained unaffected (most IC_{50} ≥ 50 µM) in the antitubercular concentration range. The calculated selectivity index SI = IC_{50}(THP-1)/MIC_{90}(H37Rv) was > 10 for all tested synthetic Callyaerin derivatives and highest for *CalB* (SI = 128) due to its low MIC_{90} value of 0.39 µM.

Further biological investigations included the conduction of a macrophage infection assay, in which PMA stimulated THP-1 cells were infected with a virulent H37Rv reporter strain expressing the fluorescent protein mCherry. In this experiment synthetic *CalB* outperformed the antibiotic positive control streptomycin (both at 2 µM) and *CalA* likewise exhibited a similar activity. This result confirmed the high selectivity of Callyaerins for *M. tuberculosis* in a human cell environment.

In order to obtain insights into the structure-activity relationship of Callyaerin A, each amino acid residue in ring positions R1-8 and chain positions C1-C4 was systematically replaced against alanine (also see 3.2.2). This synthetic derivatization allowed to estimate the contribution of each amino acid for antimycobacterial activity. An alanine on positions R1, R2, R5 - R8, C1, C4 increased the MIC_{90} slightly to 6.25 µM - 12.5 µM,

while an alanine on position R4 retained the activity. On the contrary, an exchange to alanine on positions R3, C2 and C3 led to a loss of activity (MIC_{90} > 50 µM). Therefore, the synthesis of further conceivable derivatives for structure-activity relationship considerations should therefore focus on these three amino acid residues.

From a synthetical point of view, it was pleasant to see that the exchange of the most expensive amino acid hydroxyproline on position R2 against a standard proline moiety basically had no effect on the bioactivity. This finding paves the way for the synthesis of active Callyaerin derivatives that can be economically produced, e. g. Callyaerin-based inhibitors on multi-gram scale for mouse experiments.

Amino acid modifications on the chain position C4 of Callyaerin A seemed to be uncritical for its bioactivity against *M. tuberculosis* – even the deletion of the glycine resulted in a derivative with MIC_{90} = 1.56 µM (*CalA_C4X*). Therefore, the synthetic implementation of modifications is possible at the C-terminal end of the chain. This was shown by generation of active Callyaerin derivatives with an alkyne or azide group (*CalA_C4Pra*, *CalB_C4Pra* and *CalA_C4Aha*; all MIC_{90} ≤ 3.125 µM), which were used for copper-catalyzed azide-alkyne click reactions with biotin or fluorescent dye conjugates.

The resulting probes *Biotin-CalA* and *Biotin-CalB* constituted valueable tools for target identification in a proteomic affinity enrichment approach. The incubation of *M. tuberculosis* cell lysates with these individual affinity probes, followed by immobilisation on avidin agarose resin and consecutive on-bead digest for LC-MS/MS whole proteome analysis revealed that only three proteins were highly enriched with both probes. The most enriched protein was Hypoxic response protein 1 (HRP1). The other two were a probable transcriptional regulatory protein (Possibly TetR-family, P96821, *Rv0144*) and a conserved protein (L7N6B1, *Rv1322A*) - both are unreviewed in UniProtKB so far. Hypoxic response protein 1 is coded by gene *hrp1* (*Rv2626c*) and its function is to date unknown. Hrp1 is one of the most highly upregulated genes in the DosR regulon and may participate in host-pathogen interactions.[112] The DosR regulatory system has been found to be involved in the response of bacilli to hypoxia, nitric oxide and carbon monoxide stresses, while it is thought to be crucial for the long-term survival of mycobacteria in the host organism.[113]

A similar proteomic experiment in human HeLa cell lysates with *Biotin-CalA* as an affinity probe resulted in the identification of a handful of enriched proteins. These were

the Hsc70-interacting protein, c-Myc-binding protein and cAMP-dependent protein kinase, also known as Protein kinase A, which was found as three different subunits: type I-alpha regulatory subunit (*PRKAR1A*), catalytic subunit alpha (*PRKACA*) and beta (*PRKACB*). Although the biological relevance of these identified proteins as targets of Callyaerins in humans remains unknown so far, the experiment demonstrates an effect on the protein level of Callyaerin A treatment in human organism.

The present thesis thus has provided many new insights into the chemical biology of the Callyaerin natural product family. Nevertheless, several questions have remained open that should be addressed in the future:

- Further lead optimization and definition of the structure activity relationship for the most active compound Callyaerin B. Derivatives including the replacement of the diaminoacrylic acid group with a thioenamine group may broaden the scope of cyclic peptides with a highly rigid structure.
- Validation of the molecular targets obtained from the chemoproteomic approach. To this end, e. g. knockout strains of the identified target proteins and subsequent Callyaerin sensitivity assays can be performed.
- Drug metabolism pharmacokinetic (ADME) profiling of the most active compounds.
- Evaluation of the *in vivo* antimycobacterial activity and toxicity of the most active compounds against *Mtb* infected mice as a proof of concept study (PoC).

5 Materials and methods

5.1 Chemicals

Chemicals were purchased from following companies: VWR, Sigma Aldrich, ABCR, Acros, Novabiochem, Merck, Alfa Aesar, Iris Biotech, Bachem. All the reagents purchased from commercial sources were reagent grade and were used without further purification. Rink Amide resin (100-200 mesh) for SPPS was purchased from Merck Millipore. Solvents for peptide synthesis and RP-HPLC were purchased as synthesis and HPLC grade, respectively.

5.2 Solid-phase synthesis of Callyaerins

5.2.1 General SPPS methods for linear precursor peptides of Callyaerins

The syntheses of the linear precursors for all Callyaerins and derivatives were assisted by a fully automated computer-controlled peptide synthesizer, model 'Syro I' purchased from MultiSynTech GmbH, Witten, Germany. All linear amino acid sequences were built up by alternating steps of Fmoc-protected amino acid coupling via method B and Fmoc deprotection via method C. After Fmoc deprotection of the last N-terminal amio acid, the linear peptide was cleaved and purified via method D.

Rink-amide resin was used without pre-treatment as the solid support for the synthesis of all substances, excepting Callyaerin K and Callynormine A, where 2-chlorotrityl resin was used with the following preparation method A for the first C-terminal amino acid of the sequence:

Method A: Manual loading of a Fmoc-amino acid onto 2-chlorotrityl resin

2-Chlorotrityl resin was transferred to a glass solid-phase reactor under an argon atmosphere. To the resin was added a solution of the Fmoc-aa-OH (4 eq.) and DIPEA (4 eq.) in DCM and the resin was shaken gently at RT overnight. The resin was capped with a solution of DIPEA/MeOH/DCM (1:2:17) which was applied 2 x for 10 min. The resin was washed with DMF (3 x 1 min) and DCM (3 x 1 min).

All following amino acid coupling and Fmoc deprotection steps were assisted by the peptide synthesizer using the standard protocol methods B and C:

Method B: Amino acid coupling

The resin was allowed to swell in DMF for 10 min followed by washing steps (3 x DMF for 10 min). The Fmoc-protected amino acid (4 eq.) and HOBt (4 eq.) were dissolved in an appropriate amount of DMF. This solution, HBTU (4 eq. in DMF) and DIPEA (4 eq.) were successively added to the resin. The resulting reaction suspension was shaken for 45 min at RT. The solution was removed by suction, and the resin was washed with DMF (3 x 1 min).

Method C: Fmoc deprotection

A solution of 40% piperidine in DMF was added to the resin and the resulting suspension was shaken for 3 min. The solution was removed by suction, a solution of 20 % piperidine in DMF was added and the suspension was shaken for 12 min. The solution was removed by suction and the resin was washed with DMF (6 x 1 min).

Method D: Cleavage and purification of the linear precursor peptide

The resin was allowed to swell in DCM and washed with DCM (3x 1 min). A cleavage cocktail containing 95 % TFA, 2.5 % TIPS and 2.5 % water was added, and the suspension was shaken for 30 min. The solution was filtrated and directly added to cold diethylether (10x volume). The resulting suspension with the precipitated crude peptide was stored overnight at -20 °C and thereafter centrifugated at 4000 rpm for 15 min. The supernatant was discarded, and the sediment was allowed to dry at ambient conditions for 10 min. The crude peptide was dissolved in ACN/water (lowermost ACN percentage) and purified by preparative RP-HPLC (ACN/water, 10 % to 100 % in 20 min, also see 5.3.1). Pure fractions were combined and freeze dried to obtain a white powder.

5.2.2 Cyclisation reaction of linear precursor peptides to Callyaerins

Method E: Dess-Martin Oxidation and final synthesis of Callyaerins

The purified linear precursor peptide (1 eq.) and Dess-Martin periodinane (4 eq.) were suspended in ACN (10 mL) and shaken for 30 min. After centrifugation for 10 min at 4000 rpm the supernatant was directly injected into preparative HPLC (also see 5.3.1). Pure fractions were combined and freeze dried to obtain a white soft foam.

5.2.3 Synthesis of Callyaerins A+B derived affinity and fluorescence probes

Method F: Copper(I)-catalyzed alkyne-azide cycloaddition (CuAAC)

The alkyne function bearing Callyaerin derivate *CalB_C4Pra* was solved in a buffer containing 100 mM $CuSO_4$, 4 eq. TBTA, 4 eq. TCEP and 50 mM ascorbic acid. For the synthesis of the affinity and fluorescence probe, 1.2 eq. of the corresponding azide conjugate (Biotin PEG3 azide or Cy3 azide) was added and shaken at 800 rpm at room temperature. After 30 min the reaction solution was directly injected into the preparative HPLC (also see 5.3.1). Pure fractions were combined and freeze dried.

5.2.4 Method overview for all synthesized Callyaerins and derivatives

The syntheses of the single Callyaerins and derivatives were performed by the methods described in 5.2. Table 23 lists the applied synthesis methods for each compound. For most of the substances, the combination of methods B, C, D, E leads to the desired cyclized product. Exceptions are Callyaerin K and Callynormine A with a carboxylic acid moiety at the C-terminus, for which method A was used instead of method B. The probes *Biotin_CalA*, *Biotin_CalB* and *Cy3-CalA* were synthesized by method F from the alkyne derivate *CalA_C4Pra*.

Table 23:Method overview for all synthesized Callyaerins and derivatives

#	substance	linear sequence 1=Hyp,2=Pra,3=Aha	synthesis by methods
1	Callyaerin A	I1VILPPLSPIFG	B, C, D, E
2	Callyaerin B	I1IILPPLSPII	B, C, D, E
3	Callyaerin C	H1LLPPVSPLFG	B, C, D, E
4	Callyaerin D	I1IFPPLSPINAI	B, C, D, E
5	Callyaerin E	LPFFPPVSPIIG	B, C, D, E
6	Callyaerin F	VPVFPPLSFI	B, C, D, E
7	Callyaerin G	LPFFPPLSPPFG	B, C, D, E
8	Callyaerin H	VPVFPPLSPI	B, C, D, E
9	Callyaerin I	LPFFPPVSPLFG	B, C, D, E
10	Callyaerin J	FPLFPPVSPIIG	B, C, D, E
11	Callyaerin K	FPFGLPPFSPFID	A, C, D, E
12	Callyaerin L	I1EIVPPLSPLF	B, C, D, E
13	Callynormine A	I1VLPPLSPFL	A, C, D, E
14	CalA_R1A	A1VILPPLSPIFG	B, C, D, E
15	CalA_R2A	IAVILPPLSPIFG	B, C, D, E
16	CalA_R2P	IPVILPPLSPIFG	B, C, D, E
17	CalA_R3A	I1AILPPLSPIFG	B, C, D, E
18	CalA_R3F	I1FILPPLSPIFG	B, C, D, E

#	substance	linear sequence 1=Hyp,2=Pra,3=Aha	synthesis by methods
19	CalA_R3I	I1IILPPLSPIFG	B, C, D, E
20	CalA_R3L	I1LILPPLSPIFG	B, C, D, E
21	CalA_R4A	I1VALPPLSPIFG	B, C, D, E
22	CalA_R5A	I1VIAPPLSPIFG	B, C, D, E
23	CalA_R5D	I1VIDPPLSPIFG	B, C, D, E
24	CalA_R6A	I1VILAPLSPIFG	B, C, D, E
25	CalA_R7A	I1VILPALSPIFG	B, C, D, E
26	CalA_R8A	I1VILPPASPIFG	B, C, D, E
27	CalA_R8W	I1VILPPWSPIFG	B, C, D, E
28	CalA_R8V	I1VILPPVSPIFG	B, C, D, E
29	CalA_C1A	I1VILPPLSAIFG	B, C, D, E
30	CalA_C2A	I1VILPPLSPAFG	B, C, D, E
31	CalA_C3A	I1VILPPLSPIAG	B, C, D, E
32	CalA_C3L	I1VILPPLSPILG	B, C, D, E
33	CalA_C3I	I1VILPPLSPIIG	B, C, D, E
34	CalA_C3W	I1VILPPLSPIWG	B, C, D, E
35	CalA_C4A	I1VILPPLSPIFA	B, C, D, E
36	CalA_C4X	I1VILPPLSPIF	B, C, D, E
37	CalA_C4Pra	I1VILPPLSPIF2	B, C, D, E
38	CalA_C4Aha	I1VILPPLSPIF3	B, C, D, E
39	CalA_C5A	I1VILPPLSPIFGA	B, C, D, E
40	CalA_C3X+C4X	I1VILPPLSPI	B, C, D, E
41	CalA_C3I+C4X	I1VILPPLSPII	B, C, D, E
42	CalA_R2P+C3I+C4X	IPVILPPLSPII	B, C, D, E
43	CalA_R3I+R2P	IPIILPPLSPIFG	B, C, D, E
44	CalB_C4Pra	I1IILPPLSPII2	B, C, D, E
45	Biotin_CalA probe	from *CalA_C4Pra*	F
46	Biotin_CalB probe	from *CalB_C4Pra*	F
47	Cy3-CalA probe	from *CalA_C4Pra*	F

5.3 Chromatographic methods

5.3.1 Preparative high-performance liquid chromatography (HPLC)

Instruments:	Shimadzu Prominence UFLC pump, UV detector and fraction collector
Column:	Phenomenex Luna® 5 µm C18, 100 x 21.20 mm
LC-Method:	solvent A – water (0.1 % TFA), solvent B – ACN (0.1 % TFA)
	flow rate = 20 mL/min, linear gradient (20 min)
	0 min / 10 % B –> 2 min / 10 % B –>
	18 min / 100 % B –> 20 min/ 100 % B
UV detection:	UV-channel A: 210 nm, B: 254 nm

5.3.2 Analytical HPLC coupled with mass spectrometry (LC-MS)

Instruments:	Thermo Scientific Accela autosampler, pump and PDA detector
	Thermo Scientific LCQ Fleet^{TM} Mass Spectrometer
Column:	Agilent Eclipse XDB-C18 (particle size = 5 µm)
LC-Method:	solvent A – water (0.1 % FA), solvent B – ACN (0.1 % FA)
	flow rate = 1 mL/min, linear gradient (15 min)
	0 min / 10 % B –> 1 min / 10 % B –>
	10 min / 100 % B –> 12 min/ 100 % B –> 15 min / 10 % B
UV detection:	UV-channel A: 210 nm, B: 254 nm, C: 280 nm
Mass range:	m/z = 130-2000
MS-Method:	Heated Electrospray Ionization (HESI)
Software:	Thermo Xcalibur Qual Browser 2.2

5.4 High resolution mass spectrometry (HR-MS)

Instrument:	Bruker maXis 4G UHR-TOF Mass Spectrometer
Mass range:	m/z = 100-2800
Reference substance:	Reserpin ($C_{33}H_{40}N_2O_9$)
MS-Method:	ESI
LC-Method:	C18 – Gradient (5 min)
Software:	Bruker Compass DataAnalysis 4.1

5.5 Nuclear magnetic resonance spectroscopy (NMR)

Nuclear magnetic resonance (NMR) spectra were acquired on a Bruker Avance II 400 System (400 MHz for ^{1}H-NMR and 101 MHz for ^{13}C-NMR) or on a Bruker Avance II 700 System (700 MHz for ^{1}H-NMR and 176 MHz for ^{13}C-NMR).

^{1}H-NMR spectra are described with the following nomenclature: chemical shift (δ) in [ppm], determined by the residual signal of non-deuterated solvent; multiplicity (s - singlet, d - doublet, t - triplet, q - quartet, dd - doublet of doublets, m - multiplet; coupling constant (J) in [Hz] and number of protons (H).

5.6 Biological methods

All biological experiments were carried out by Yvonne Gröner from the Kalscheuer lab at the HHU Düsseldorf, Germany.

5.6.1 Bacterial growth conditions

Liquid cultures of several *M. tuberculosis* strains (listed below) as well as *M. smegmatis* mc²155, *M. bovis* AF2122/97 and BCG strains Pasteur, Danish, Birkhaug and Copenhagen were grown aerobically in Middlebrook 7H9 Media (BD Diagnostics) supplemented with 10 % (*V*/*V*) ADS (5 %, w/v, bovine serum albumin fraction V; 2 %, w/v, glucose; 0.85%, w/v, sodium chloride), 0.5 % (*V*/*V*) glycerol and 0.05 % tyloxapol at 37 °C and 80 rpm. Selective media for growth of *M. tuberculosis* mc² 6230 and H37Rv reporter strain pBEN::mCherry (Hsp60) was supplemented with 100 mg/L pantothenic acid or 50 µg/mL hygromycin, respectively.

M. tuberculosis strains used in this study:

- H37Rv
- HN878
- CDC1551
- XDR *M. tuberculosis* clinical isolates KZN06, KZN13, KZN14, KZN16
- H37Rv pBEN::mCherry (Hsp60)
- mc²6230 ΔpanCD

5.6.2 Determination of minimal inhibitory concentration (MIC)

MIC values were determined in a 96-well round bottom microtiter plate. Precultured *M. tuberculosis* H37Rv cells were seeded at a density of $1x10^5$ cells per well in a total volume of 100 µL per well containing 2-fold serial diluted compounds. Plates were incubated at 37 °C for five days. 10 µL of a 100 µg/mL resazurin solution were added per well and plates were incubated at room temperature overnight. Afterwards, cells were fixed for 30 min with a final concentration of 5 % (*V*/*V*) formalin. Fluorescence (excitation 540 nm, emission 590 nm) was quantified using the Tecan infinite F200 Pro reader. MIC_{90} values were calculated in relation to DMSO treated (= 100 % growth) and rifampicin treated bacteria (= 0 % growth).

5.6.3 Generation of spontaneous resistant mutants

Spontaneous resistant mutants were generated by plating approximately $1x10^8$ cells on Middlebrook 7H10 (BD Diagnostics) agar plates supplemented with 10 % (*V*/*V*) ADS and 0.5 % (*V*/*V*) glycerol containing four to five times the MIC_{90} of selected compounds. Colonies were picked after four weeks of incubation at 37 °C. Resistance was quantified by determination of the MIC_{90} as described above.

5.6.4 Growth conditions of human cell lines THP-1, HepG2 and HEK293

Cell lines were cultivated at 37 °C in a humidified atmosphere of 5 % CO_2. Medium for human monocytic cell line THP-1 (Deutsche Sammlung von Mikroorganismen und Zellkulturen GmbH) consists of RPMI 1640 medium containing 10 % (*V*/*V*) fetal bovine serum (FBS). HepG2 cells were cultivated using Ham's F12 medium supplemented with 2 mM L-glutamine and 10 % (*V*/*V*) FBS. HEK293 cells were cultivated using EMEM medium supplemented with 2 mM L-glutamine, 1 % (*V*/*V*) non-essential amino acids, 1 mM sodium pyruvate and 10 % (*V*/*V*) FBS.

5.6.5 Determination of cytotoxicity and selectivity indices

Cytotoxicity was determined by seeding $5x10^4$ cells per well in a 96-well flat bottom microtiter plate in a total volume of 100 µL containing 2-fold serial dilutions of selected compounds. Cells were incubated at 37 °C, 5 % CO_2 for 48 h. Afterwards, 10 µL of a 100 µg/mL resazurin solution was added per well and plates were incubated at 37 °C, 5 % CO_2 for two hours. Fluorescence (excitation 540 nm, emission 590 nm) was quantified using the Tecan infinite F200 Pro reader. IC_{50} values were calculated in relation to DMSO-treated (= 100 % growth) and Titron-X 100-treated cells (= 0 % growth). Selectivity indices were described as the ratio between IC_{50} and MIC_{90} values.

5.6.6 Macrophage infection assay

For differentiation into macrophage-like cells, THP-1 cells were seeded at a density of $1x10^5$ cells per well in a total volume of 100 µL RPMI 1640 supplemented with 10 % (*V*/*V*) FBS and 50 nM phorbol-12-myristate-13-acetate in a 96-well flat bottom microtiter plate and incubated over night at 37 °C, 5 % CO_2. The next day, cells were washed with PBS twice and medium was replaced with fresh RPMI 1640 medium supplemented with 10 % (*V*/*V*) FBS containing $3x10^5$ cells of precultured H37Rv pBEN::mCherry (Hsp60) resulting in a multiplicity of infection of three (MOI=3). After three hours, cells were washed with PBS twice and medium was replaced with fresh RPMI 1640 medium supplemented with 10 % (*V*/*V*) FBS containing either 15.6 µM of synthetic Callyaerin A or 1.95 µM of synthetic Callyaerin B respectively, DMSO or antibiotics (1 µM of rifampicin or 2 µM of streptomycin). After five days of cultivation at 37 °C and 5 % CO_2, cells were fixed with a final concentration 5 % (*V*/*V*) formalin and incubated for 30 min at room temperature. Fluorescence was quantified using a Nikon Eclipse TS100 (100x magnification, 500 ms exposure time). Integrated density of red fluorescence was calculated using Fiji (ImageJ).

5.6.7 Isolation of total cytosolic protein of *M. tuberculosis* H37Rv

Precultured H37Rv cells were collected by centrifugation (4000 x *g*, 10 min, 4 °C), washed twice with PBS and finally resuspended in 1/20 PBS of culture volume. Cells were lysed using Percellys tubes containing a mixture of 0.5 mm and 0.1 mm glass beads and the Qiagen TissueLyser LT three times for 3 min at 50 Hz. Afterwards samples were centrifuged at 14000 x *g*, 1 min at 4 °C. Supernatants of the samples were sterilized by threefold filtration using 0.22 µm cellulose acetate low protein binding filters. Total cytosolic protein lysate was stored on ice and used directly for protein quantification assays and affinity enrichment.

5.8 Proteomic methods

5.8.1 Bradford assay

The protein concentration was measured using a modified Bradford assay, called RotiNanoquant®. The assay was conducted according to the instruction given by the supplier (https://www.carlroth.com/downloads/ba/de/K/BA_K880_DE.pdf).

5.8.2 Proteomic sample preparation for *M. tuberculosis* lysate

1. Freshly prepared *M. tuberculosis* H37Rv lysate (double sterile filtrated, ~11 mL, 0.444 µg/µL total protein measured by inhouse Bradford assay = ~4.8 mg total protein) was received from Yvonne Gröner (Kalscheuer lab, HHU Düsseldorf, Germany).

2. On the same day, the samples were immediately processed on ice (or 4 °C temperatured shaker). The lysate was aliquoted into 15 samples (676 µL lysate = 300 µg total protein per sample). The five conditions á three replicates were:

    - DMSO
    - Tri-FP (2 µM)
    - Biotin-CalA (2 µM)
    - Biotin-CalA (2 µM) + bead washing with 20 µM CalA in washing solution (PBS)
    - Biotin-CalB (2 µM)

3. To each Eppendorf tube was added 1.352 µL of either DMSO, Tri-FP (1 mM), Biotin-CalA (1 mM) or Biotin-CalB (1 mM) (all in DMSO, resulting in a total DMSO concentration of 0.2 %).

4. The samples were incubated for 60 min at 4 °C and 600 rpm.

5. Pierce Avidin-Agarose beads (bed volume ~ 50 µL, total suspension volume in PBS = 100 µL) were aliquoted into each sample Eppendorf-tube and incubated for 30 min at 4 °C and 1100 rpm and for 30 min at RT and 1100 rpm.

6. After centrifugation for 5 min at 600 x *g*, the supernatant was transferred into a fresh Eppendorf-tube and stored at -20 °C as backup.

7. The beads were washed 3x with 1 mL PBS at RT (each time shaking at 1100 rpm followed by centrifugation for 5 min at 600 x *g* and discarding the supernatant). Samples #10-#12 were washed with PBS containing 20 µM CalA in washing steps 2 and 3.

8. The beads were taken up in 100 µL of 6 M urea (in 50 mM ABC containing 10 mM DTT) followed by incubation for 30 min at RT shaking at 1100 rpm.

9. IAM was added (6 µL of 0.5 M stock solution in 50 mM ABC) followed by incubation for 30 min at RT shaking at 1100 rpm.

10. DTT was added (6 µL of 0.5 M stock solution in 50 mM ABC) followed by incubation for 5 min at RT shaking at 1100 rpm.

11. Samples were diluted with 470 µL of 50 mM ABC.

12. 1 µg trypsin was added per sample (10 µL of 100 ng/µL stock solution in 50 mM acetic acid) followed by incubation for 16 h at 37 °C shaking at 1100 rpm.

13. 10 µL of 50 % formic acid was added followed by incubation for 10 min at 37 °C shaking at 1100 rpm.

Stagetipping:

14. 1000 µL Eppendorf LoRetention epTIPS with double layer of glass fibre membrane (pore size 1.2 µm) was used for separating the agarose beads. Elution ensued into 5 mL Eppendorf Protein LoBind Tubes with the help of a custom made teflon centrifuge adapter at RT with 800 x *g* for 5 min.

15. 200 µL pipette tips (Eppendorf LoRetention epTIPS) with double layer of C18 membrane (Empore™ SPE Disks C18) were equilibrated consecutively with each 100 µL MeOH, STSB (80 % acetonitrile, 0.1 % formic acid in water) and STSA (0.1 % formic acid in water). The sample

volume of ~760 µL was applied in two steps (2x ~380 µL) and centrifuged at RT with 800 x *g* for 5 min followed by washing with 1x 100 µL STSA.

16. Elution of the peptides on the C18 membrane ensued into a 96-well plate with 200 µL STSB at RT with 800 x *g* for 5 min.
17. The solutions in the 96-well plate were reduced *in vacuo* to dryness.
18. The residues were solved in 35 µL 0.1 % FA in water and transferred to the autosampler 96-well plate.

5.8.3 Proteomic sample preparation for HeLa cell experiments

1. HeLa cells were cultivated in a 15 cm petri dish to 100 % confluency and harvested by trypsination. The cell pellet was washed 3x with PBS, suspended in PBS and disrupted by sonification. After centrifugation the supernatant cell lysate had a total protein concentration of 5.96 µg/µL (Bradford) and was immediately processed on ice.
2. The lysate was aliquoted into 16 samples (168 µL lysate = 1000 µg total protein per sample). The four conditions á four replicates were:
    - DMSO
    - Tri-FP (2 µM)
    - Biotin-CalA (2 µM)
    - Biotin-CalA (2 µM) + bead washing with 20 µM CalA in washing solution (PBS)
3. Each Eppendorf-tube was filled up to 499 µL PBS and 1 µL was added of either DMSO, Tri-FP (1 mM) or Biotin-CalA (1 mM). All compounds were solved in DMSO, resulting in a total DMSO concentration of 0.2 %.
4. The samples were incubated for 60 min at 4 °C and 600 rpm.
5. Pierce Avidin-Agarose beads (bed volume ~ 50 µL, total suspension volume in PBS = 100 µL) were aliquoted into each sample Eppendorf-tube and incubated for 30 min at 4 °C and 1100 rpm and for 30 min at RT and 1100 rpm.

6. After centrifugation for 5 min at 600 x *g*, the supernatant was transferred into a fresh Eppendorf-tube and stored at -20 °C as backup.
7. The beads were washed 3x with 1 mL PBS at RT (each time shaking at 1100 rpm followed by centrifugation for 5 min at 600 x *g* and discarding the supernatant). Samples #13-#16 were washed with PBS containing 20 µM CalA in washing steps 2 and 3.
8. The beads were taken up in 100 µL of 6 M urea (in 50 mM ABC containing 10 mM DTT) followed by incubation for 30 min at RT shaking at 1100 rpm.
9. IAM was added (6 µL of 0.5 M stock solution in 50 mM ABC) followed by incubation for 30 min at RT shaking at 1100 rpm.
10. DTT was added (6 µL of 0.5 M stock solution in 50 mM ABC) followed by incubation for 5 min at RT shaking at 1100 rpm.
11. Samples were diluted with 470 µL of 50 mM ABC.
12. 1 µg trypsin was added per sample (10 µL of 100 ng/µL stock solution in 50 mM acetic acid) followed by incubation for 16 h at 37 °C shaking at 1100 rpm.
13. 10 µL of 50 % formic acid was added followed by incubation for 10 min at 37 °C shaking at 1100 rpm.

Stagetipping:

14. 1000 µL Eppendorf LoRetention epTIPS with double layer of glas fibre membrane (pore size 1.2 µm) was used for separating the agarose beads. Elution ensued into 5 mL Eppendorf Protein LoBind Tubes with the help of a custom made teflon centrifuge adapter at RT with 800 x *g* for 5 min.
15. 200 µL pipette tips (Eppendorf LoRetention epTIPS) with double layer of C18 membrane (Empore™ SPE Disks C18) were equilibrated consecutively with each 100 µL MeOH, STSB (80 % acetonitrile, 0.1 % formic acid in water) and STSA (0.1 % formic acid in water). The sample volume of ~760 µL was applied in two steps (2x ~380 µL) and centrifuged at RT with 800 x *g* for 5 min followed by washing with 1x 100 µL STSA.
16. Elution of the peptides on the C18 membrane ensued into a 96-well plate with 200 µL STSB at RT with 800 x *g* for 5 min.

17. The solutions in the 96-well plate were reduced *in vacuo* to dryness.
18. The residues were solved in 35 µL 0.1 % FA in water and transferred to the autosampler 96-well plate.

5.8.4 Proteomic LC-MS/MS instrument methods

Experiments were performed on an Orbitrap Elite instrument (Thermo Fisher Scientific, Waltham, MA) that was coupled to an EASY-nLC 1000 liquid chromatography system. The LC was operated in the two-column mode. The homemade fused silica column equipped with a glass fiber frit was packed with Reprosil-Pur 120 C18-AQ 3 µm resin and connected to the analytical column *via* an ultra high-pressure liquid chromatography (UHPLC) union. The analytical column was a fused silica capillary (75 µm × 25 cm) with integrated PicoFrit emitter packed in-house with Reprosil-Pur 120 C18-AQ 3 µm resin. The analytical column was attached to a nanospray flex ion source (Thermo Fisher Scientific). Peptides were delivered to the precolumn *via* the integrated autosampler at a flow rate of 2–3 µL/min in 100 % solvent A (0.1 % FA, in HPLC grade water). Peptides were subsequently separated on the analytical column by running a 140-min gradient of solvent A and solvent B (start with 7 % B; gradient 7 %-35 % B [0.1 % FA in acetonitrile, ACN] for 120 min; gradient 35 %-80 % B for 10 min; and 80 % B for 10 min) at a flow rate of 300 nL/min.

The mass spectrometer (positive ion mode) was operated using Xcalibur software (version 2.2 SP1.48). Precursor ion scanning was performed in the Orbitrap analyzer Fourier transform-based mass spectrometers (FTMS) in the scan range of *m/z* 300-1800 and at a resolution of 60,000. Product ion spectra were recorded in a data-dependent manner in the ion trap mass spectrometer (ITMS) at a rapid scan rate. The spray voltage was set to 1.6-2.0 kV. Peptides were analyzed using a repeating cycle consisting of a full precursor ion scan followed by 12 product ion scans where peptides are isolated based on their intensity in the full survey scan for tandem mass spectrum generation that permits peptide sequencing and identification. Collision-induced dissociation (CID) collision energy was set to 35 % for the generation of MS2 spectra. During MS2 data acquisition, dynamic ion exclusion was set to 120 s with a maximum list of excluded ions consisting of 500 members and a repeat count of 1. Only charge states >1 were considered for fragmentation.

6 Appendix

6.1 LC-MS and NMR spectra of all synthetic Callyaerins and derivatives

6.1.1.1 Callyaerin A

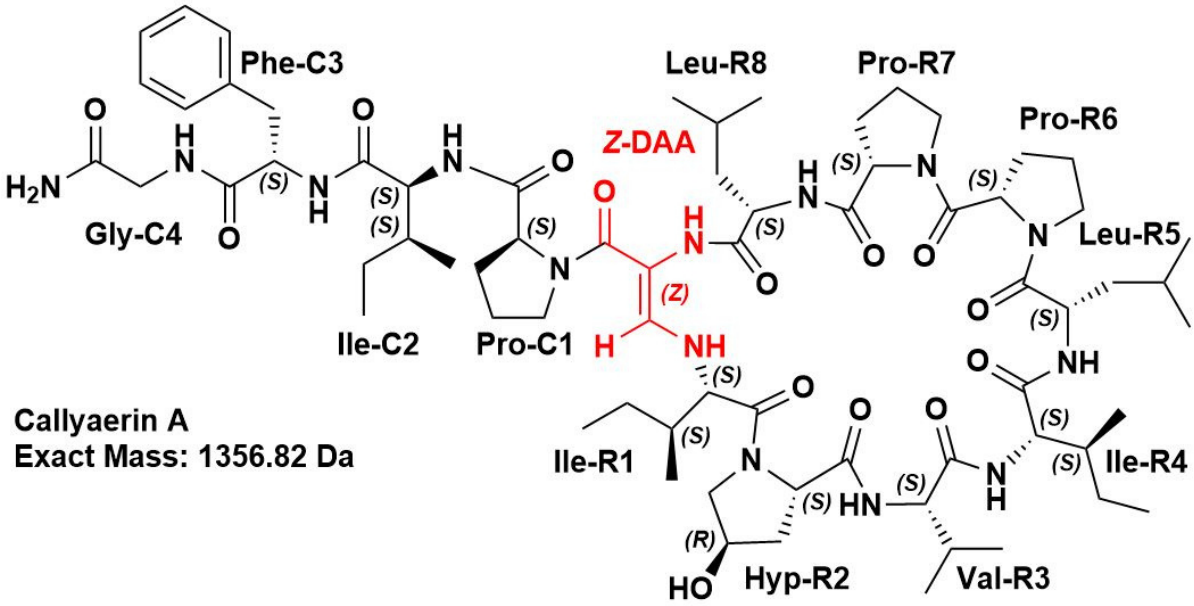

Figure 45: Chemical structure of Callyaerin A

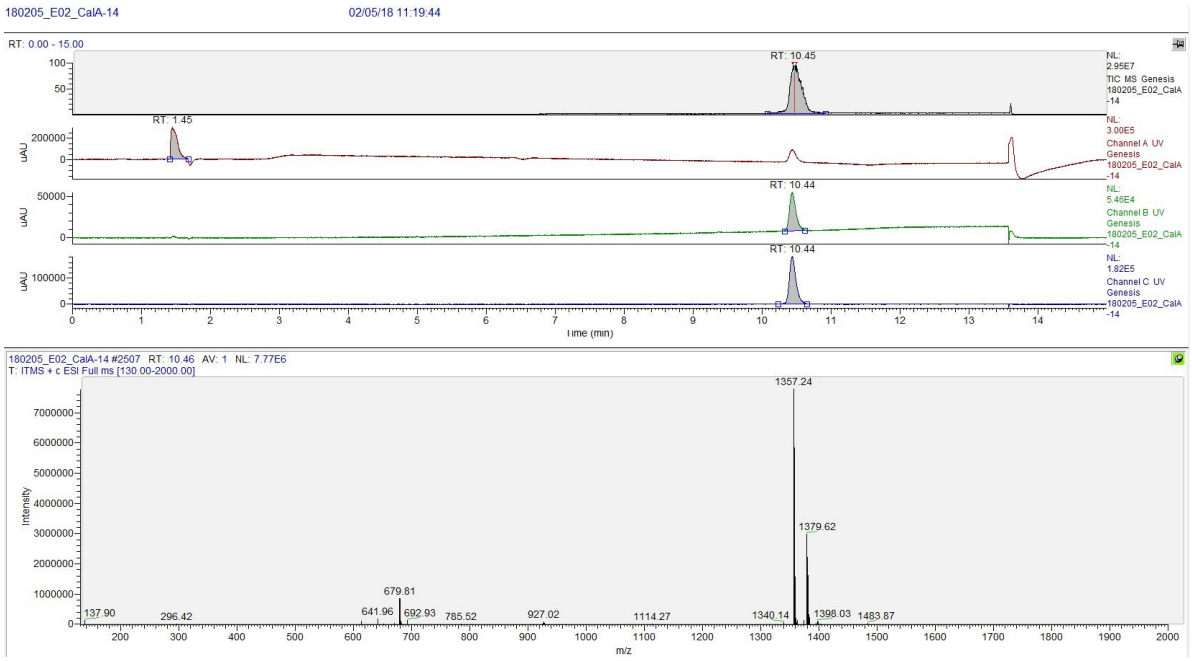

Figure 46: LC-MS spectrum of synthetic Callyaerin A. From top to bottom: TIC (ESI+), UV channel A (λ = 210 nm), UV channel B (λ = 254 nm), UV channel C (λ = 280 nm), mass spectrum of highest peak from chromatogram.

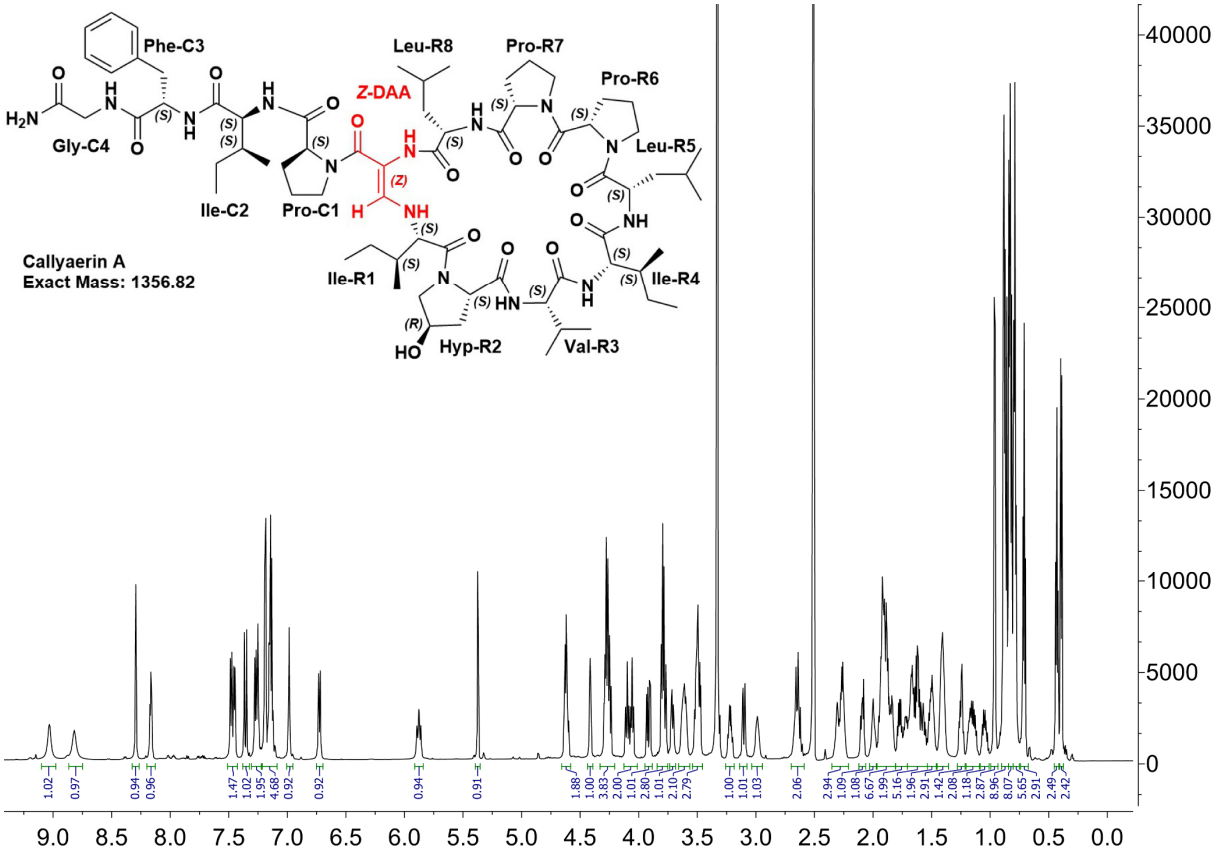

Figure 48: ^{1}H NMR spectrum (700 MHz, DMSO-d_6) of synthetic Callyaerin A.

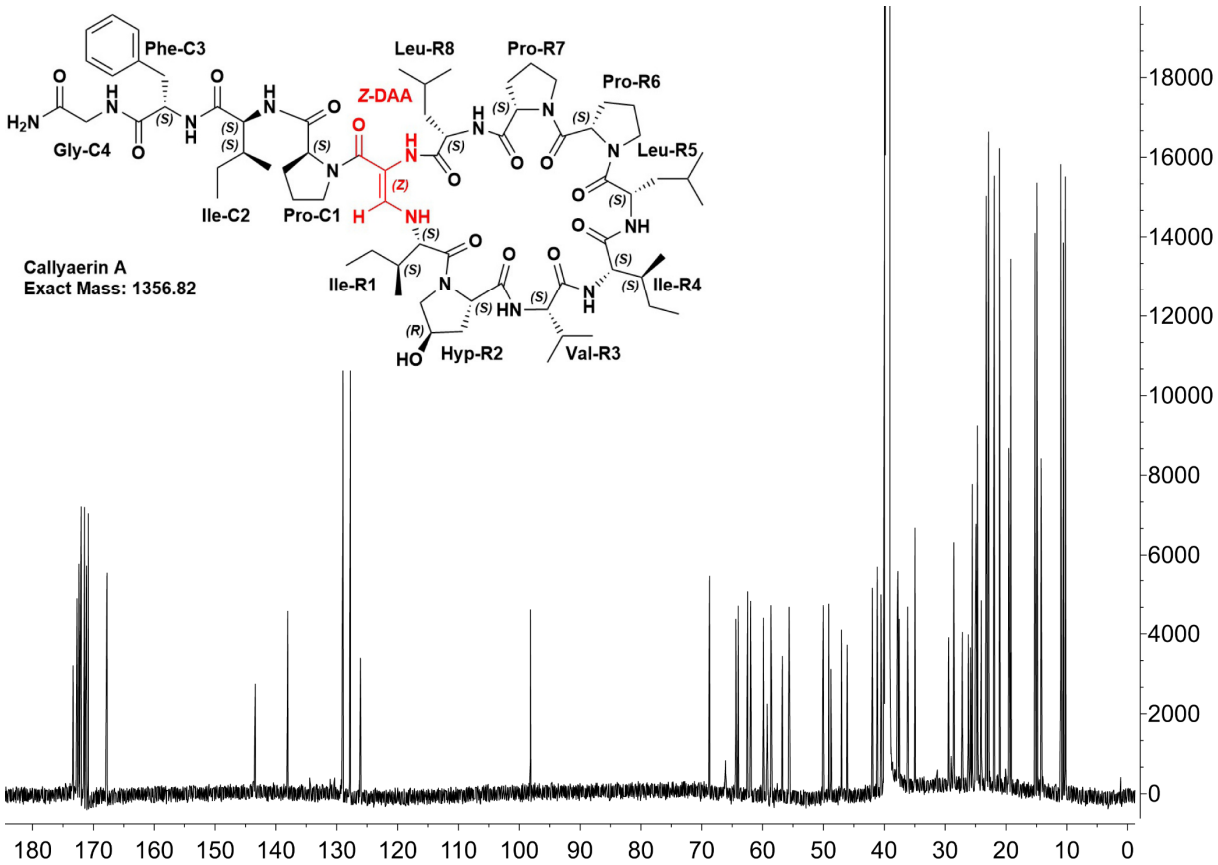

Figure 47: ^{13}C NMR spectrum (176 MHz, DMSO-d_6) of synthetic Callyaerin A.

6.1.1.2 Callyaerin B

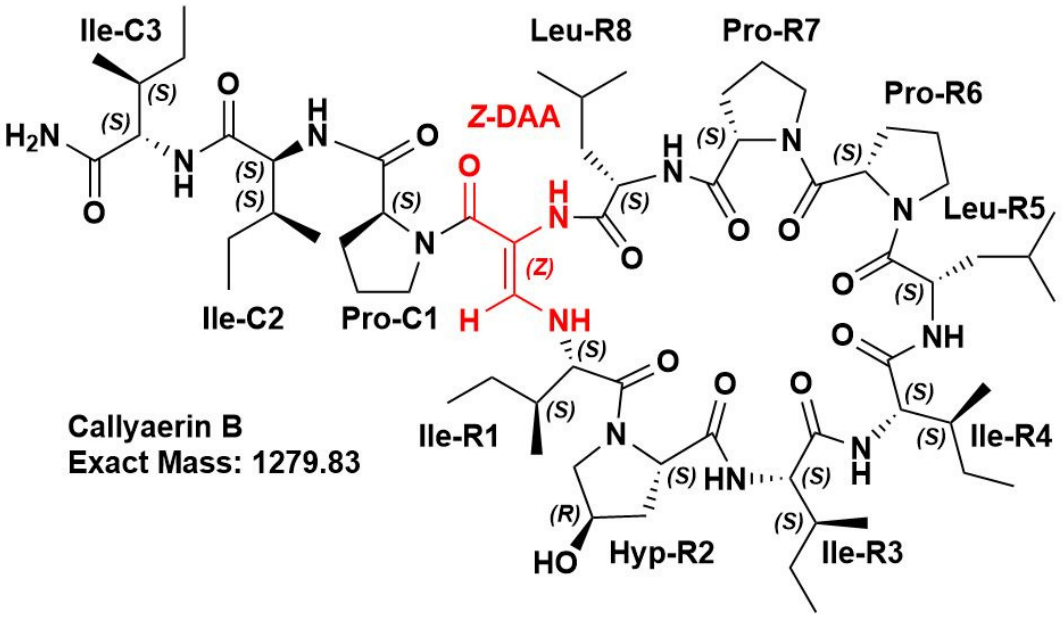

Figure 49: Chemical structure of Callyaerin B

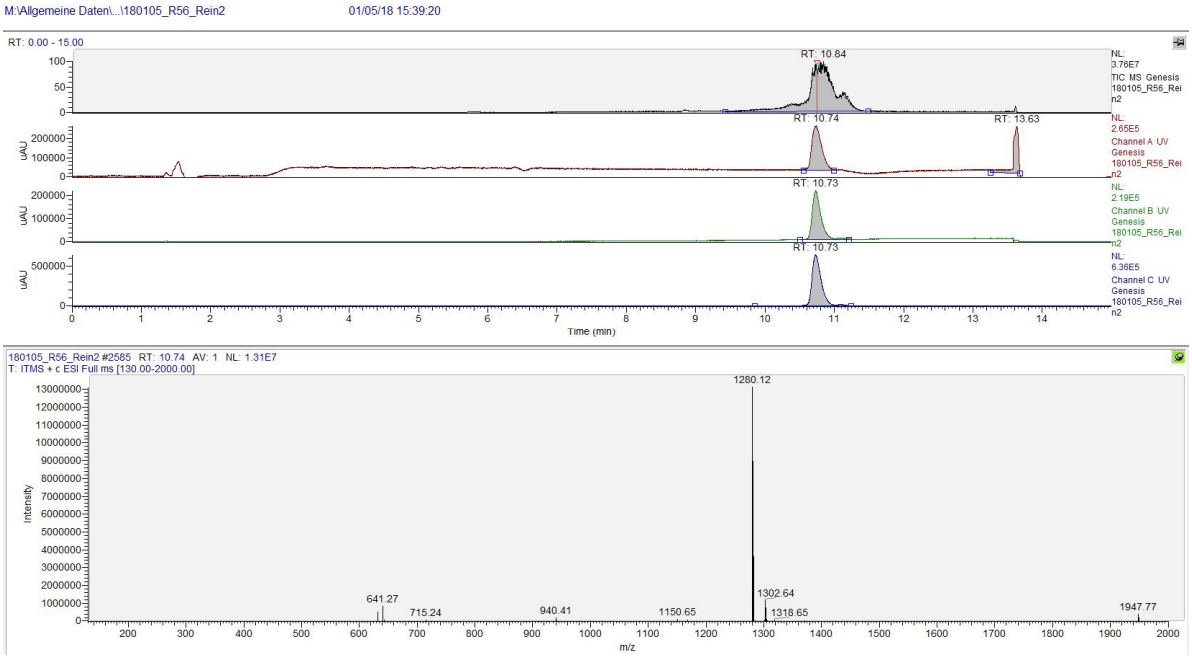

Figure 50: LC-MS spectrum of synthetic Callyaerin B. From top to bottom: TIC (ESI+), UV channel A (λ = 210 nm), UV channel B (λ = 254 nm), UV channel C (λ = 280 nm), mass spectrum of highest peak from chromatogram.

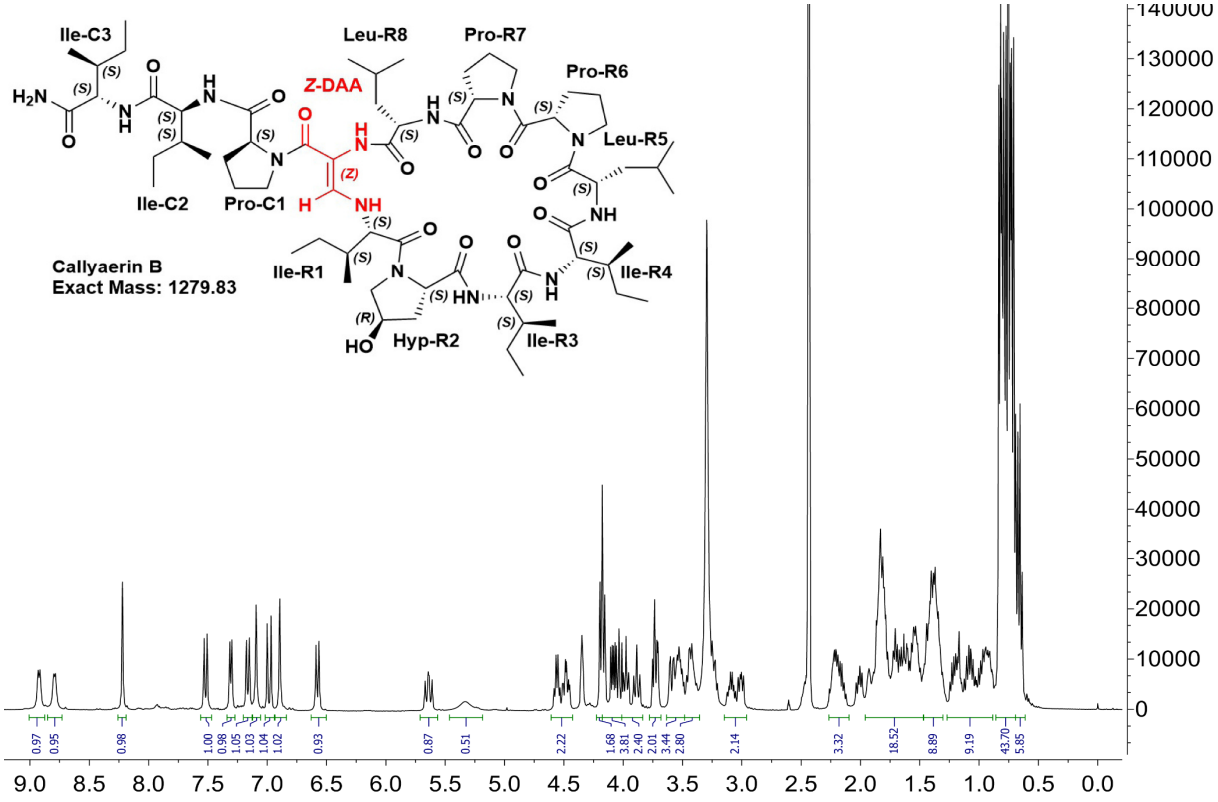

Figure 51: ^{1}H NMR spectrum (400 MHz, DMSO-d_6) of synthetic Callyaerin B.

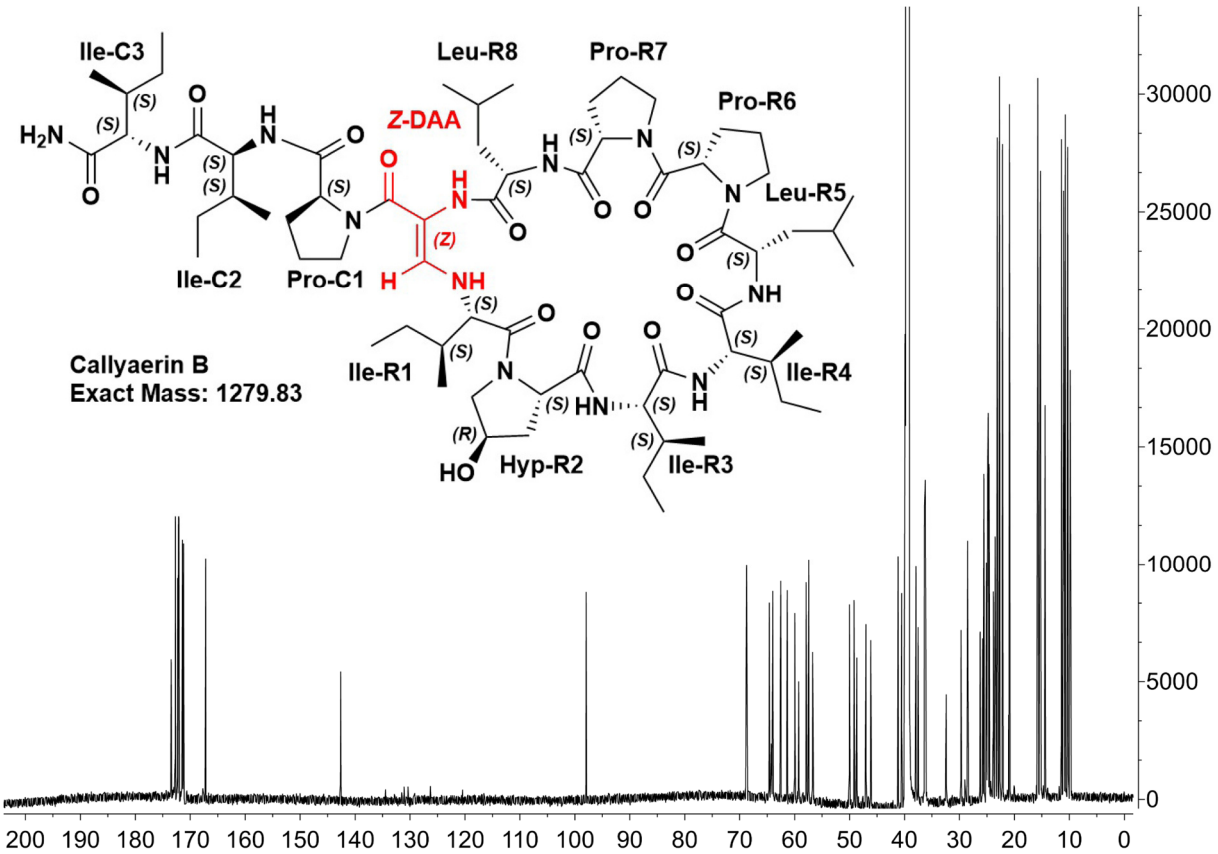

Figure 52: ^{13}C NMR spectrum (176 MHz, DMSO-d_6) of synthetic Callyaerin B.

6.1.1.3 Callyaerin C

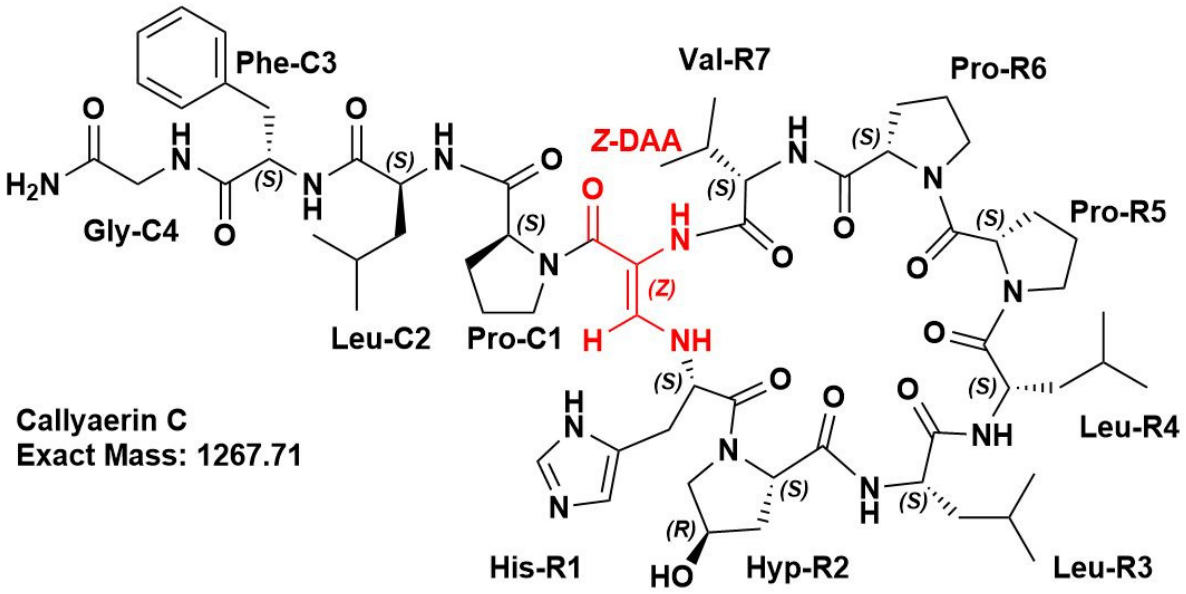

Figure 54: Chemical structure of Callyaerin C

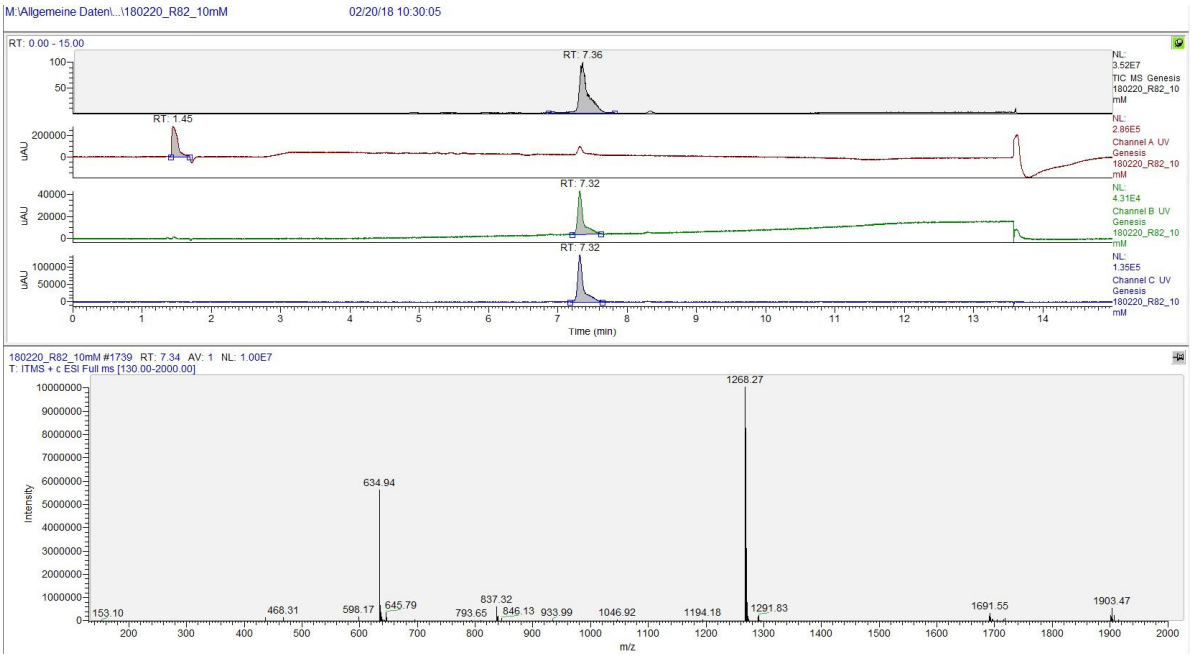

Figure 53: LC-MS spectrum of synthetic Callyaerin C. From top to bottom: TIC (ESI+), UV channel A (λ = 210 nm), UV channel B (λ = 254 nm), UV channel C (λ = 280 nm), mass spectrum of highest peak from chromatogram.

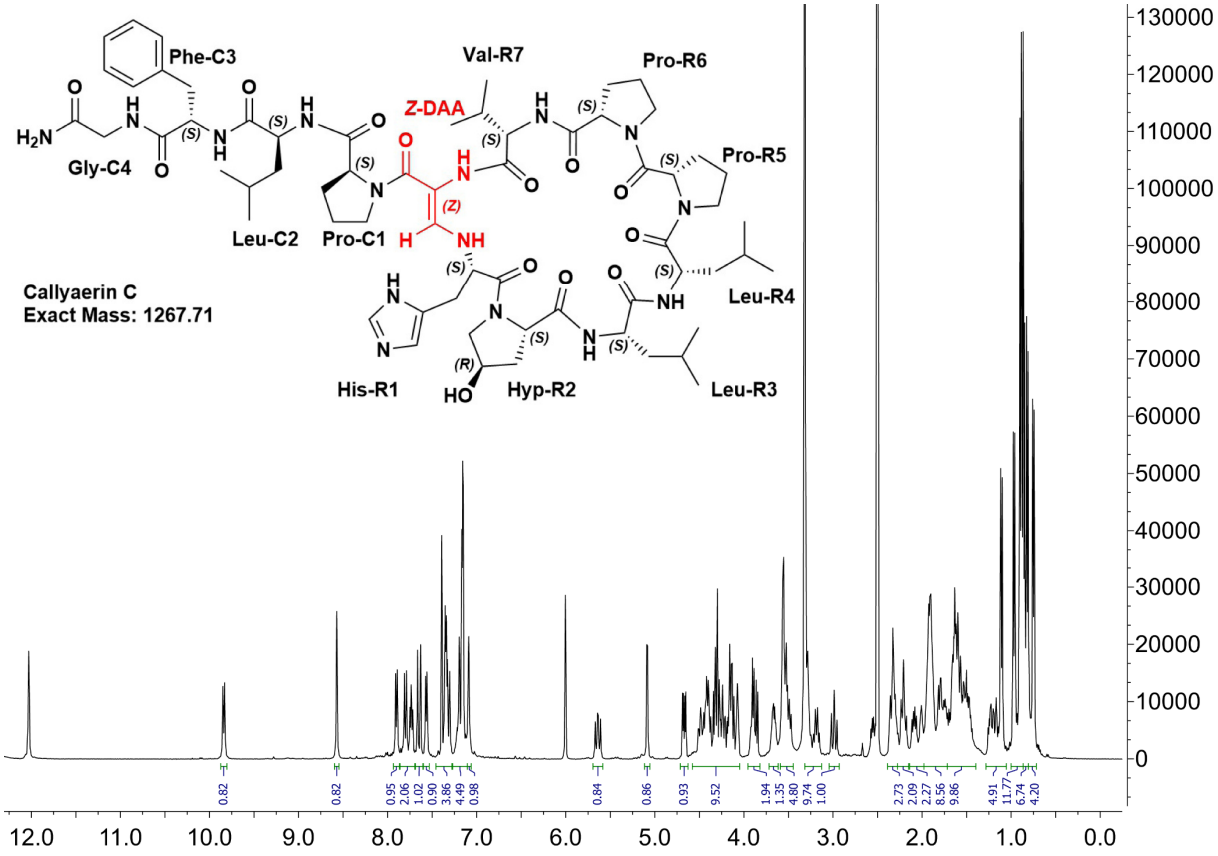

Figure 55: ^{1}H NMR spectrum (400 MHz, DMSO-d_6) of synthetic Callyaerin C.

6.1.1.4 Callyaerin D

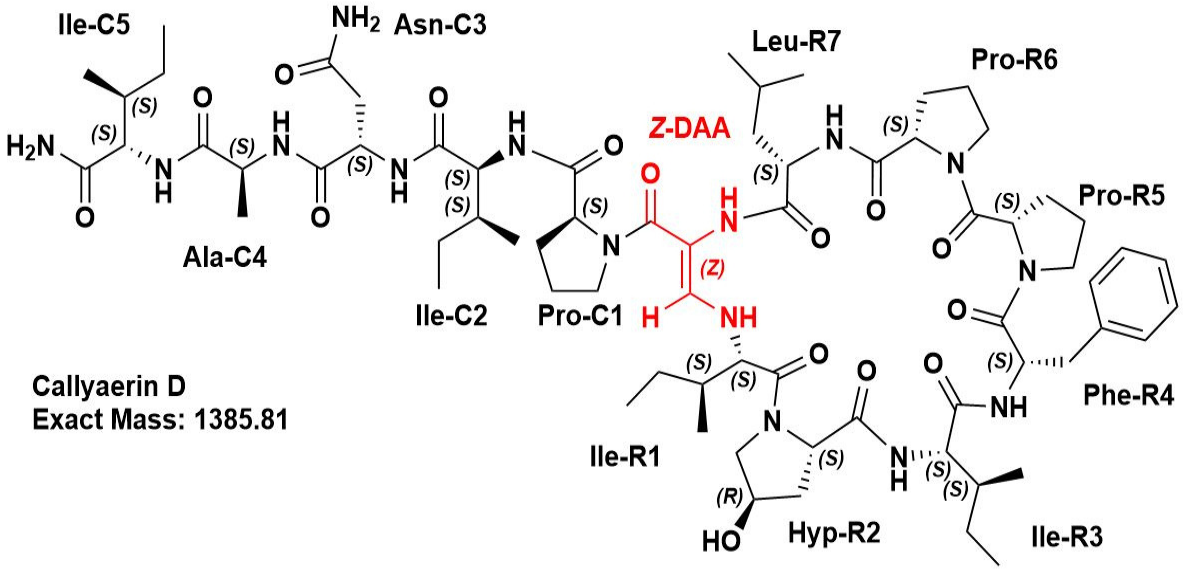

Figure 57: Chemical structure of Callyaerin D

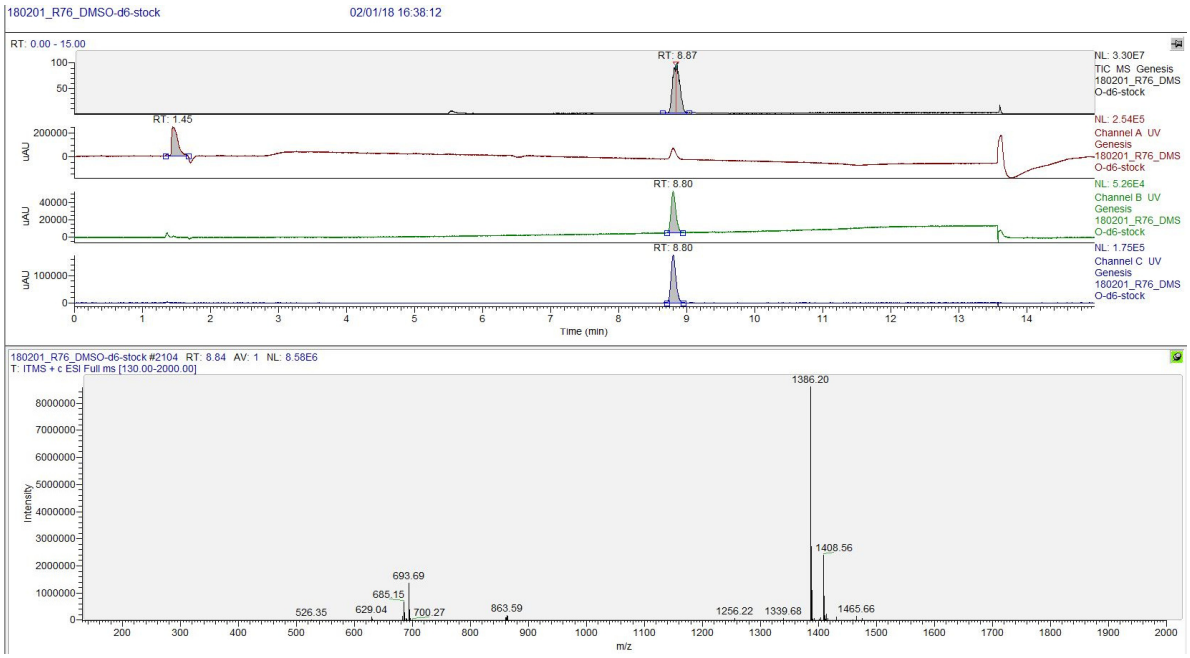

Figure 56: LC-MS spectrum of synthetic Callyaerin D. From top to bottom: TIC (ESI+), UV channel A (λ = 210 nm), UV channel B (λ = 254 nm), UV channel C (λ = 280 nm), mass spectrum of highest peak from chromatogram.

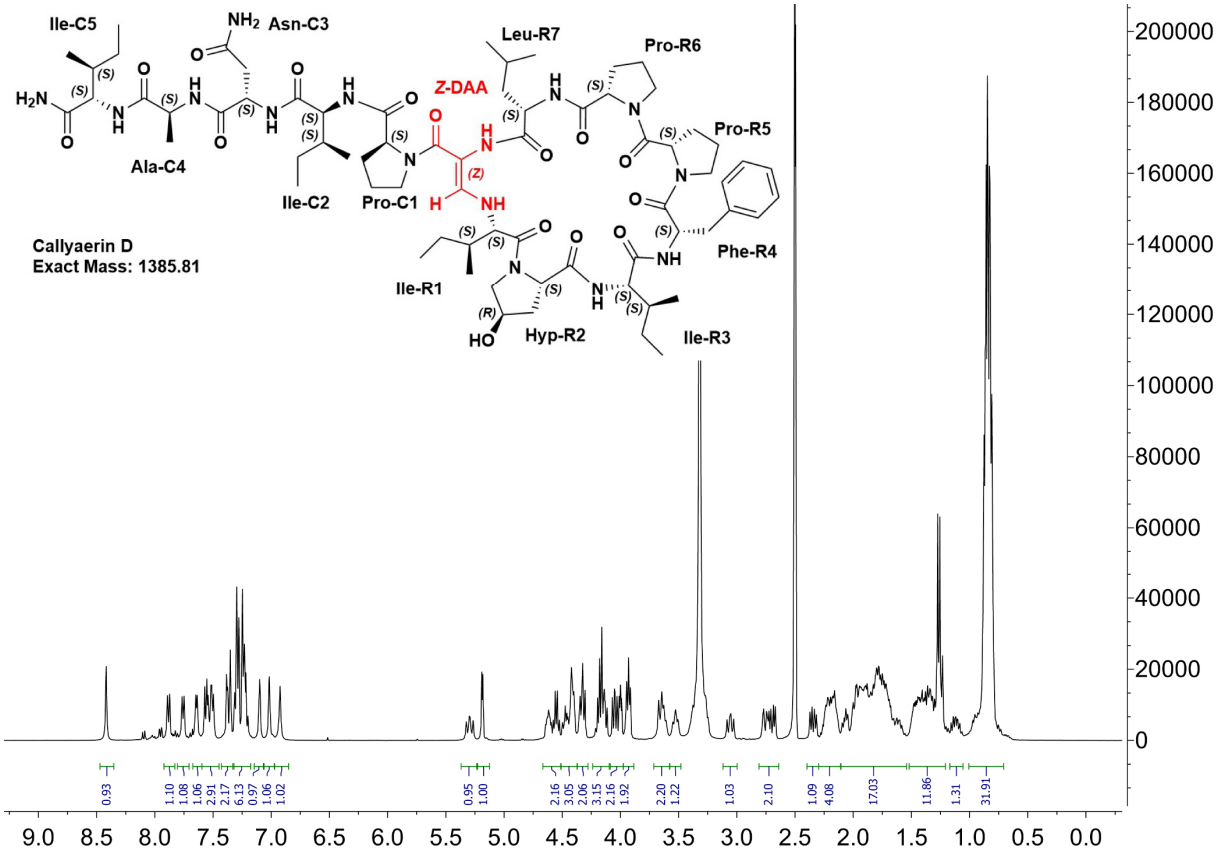

Figure 58: ^{1}H NMR spectrum (400 MHz, DMSO-d_6) of synthetic Callyaerin D.

6.1.1.5 Callyaerin E

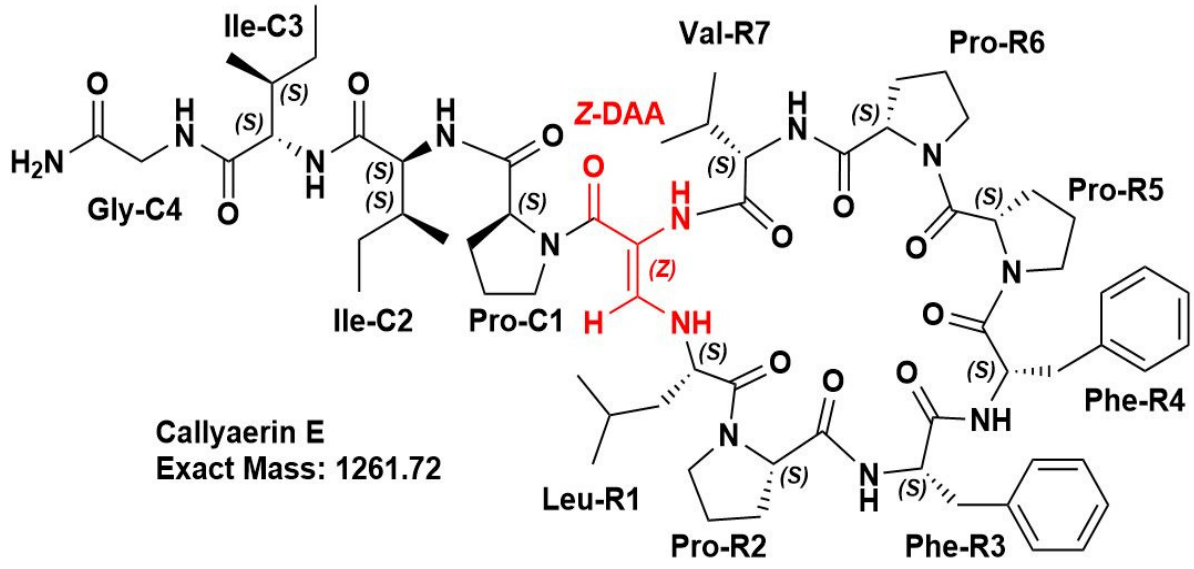

Figure 59: Chemical structure of Callyaerin E

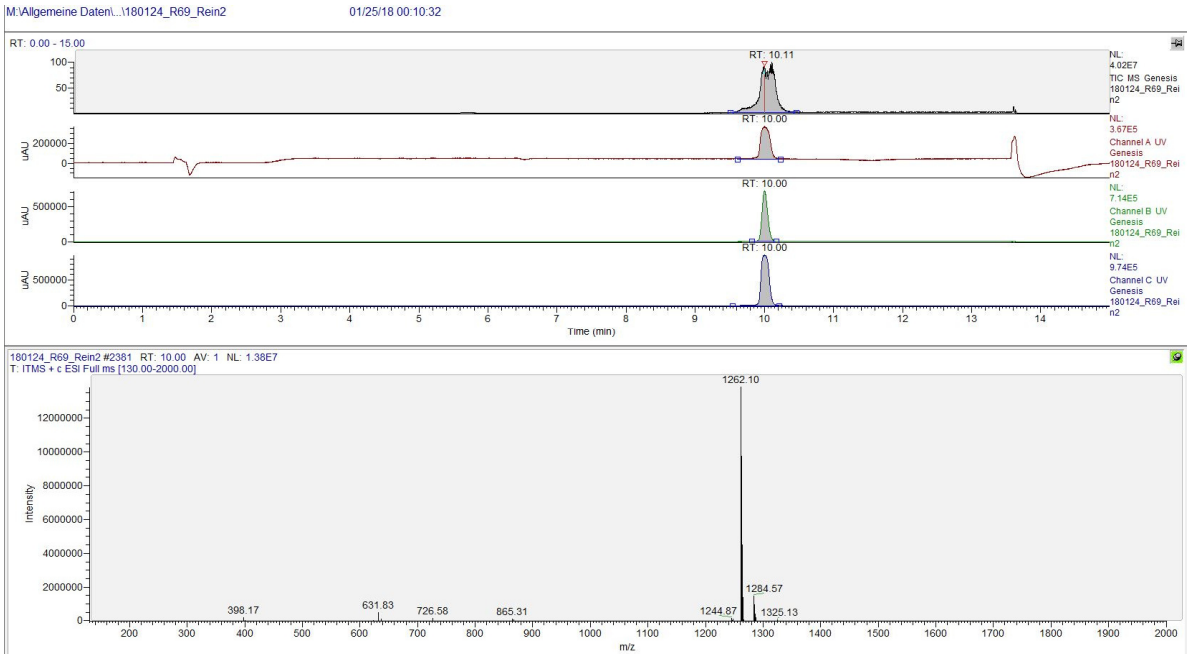

Figure 60: LC-MS spectrum of synthetic Callyaerin E. From top to bottom: TIC (ESI+), UV channel A (λ = 210 nm), UV channel B (λ = 254 nm), UV channel C (λ = 280 nm), mass spectrum of highest peak from chromatogram.

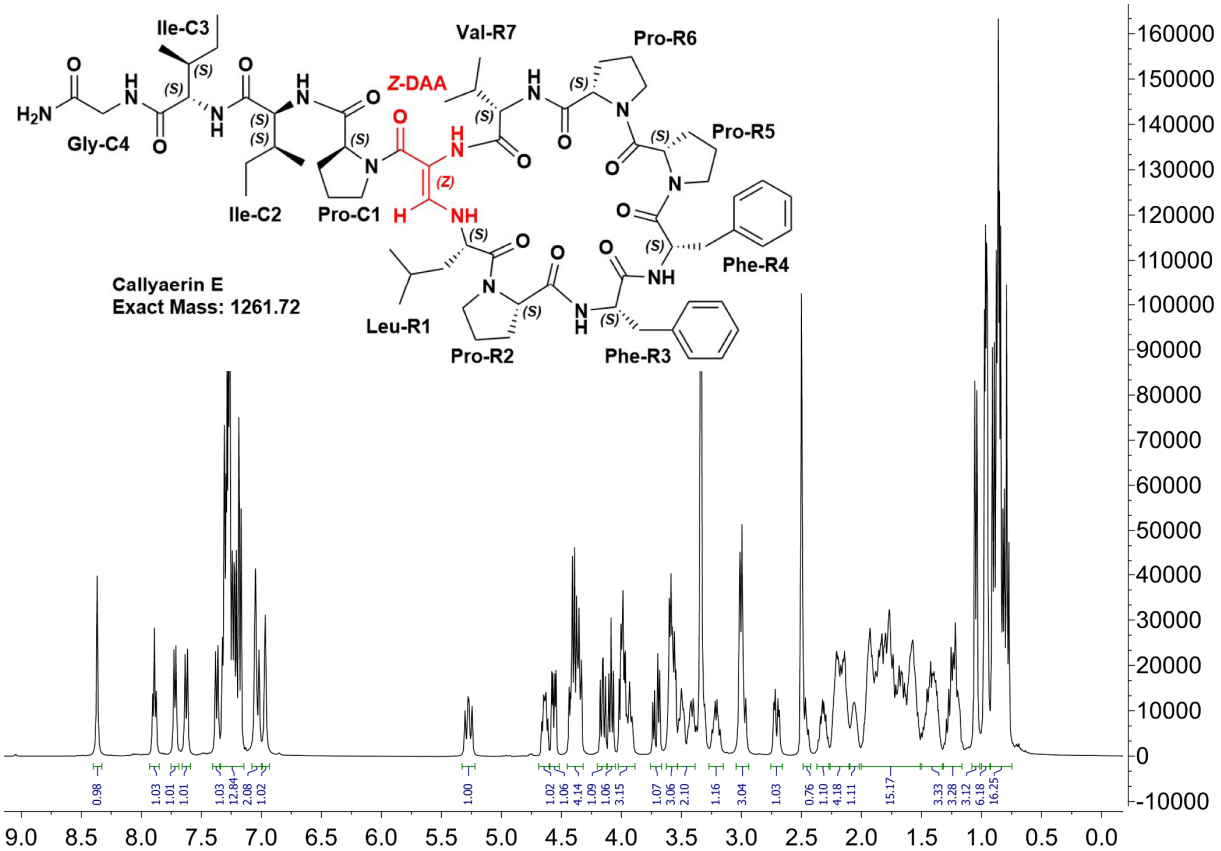

Figure 61: ^{1}H NMR spectrum (400 MHz, DMSO-d_6) of synthetic Callyaerin E.

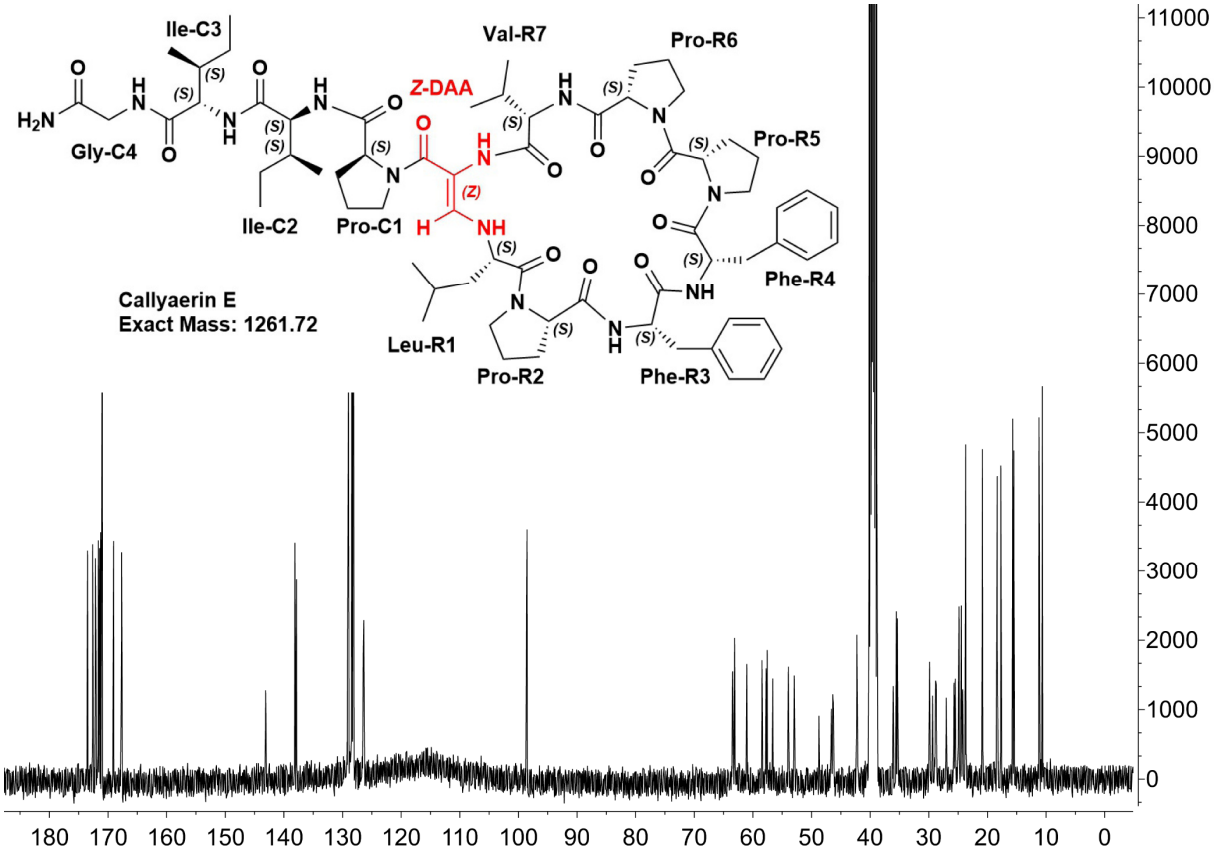

Figure 62: ^{13}C NMR spectrum (100 MHz, DMSO-d_6) of synthetic Callyaerin E.

6.1.1.6 Callyaerin F

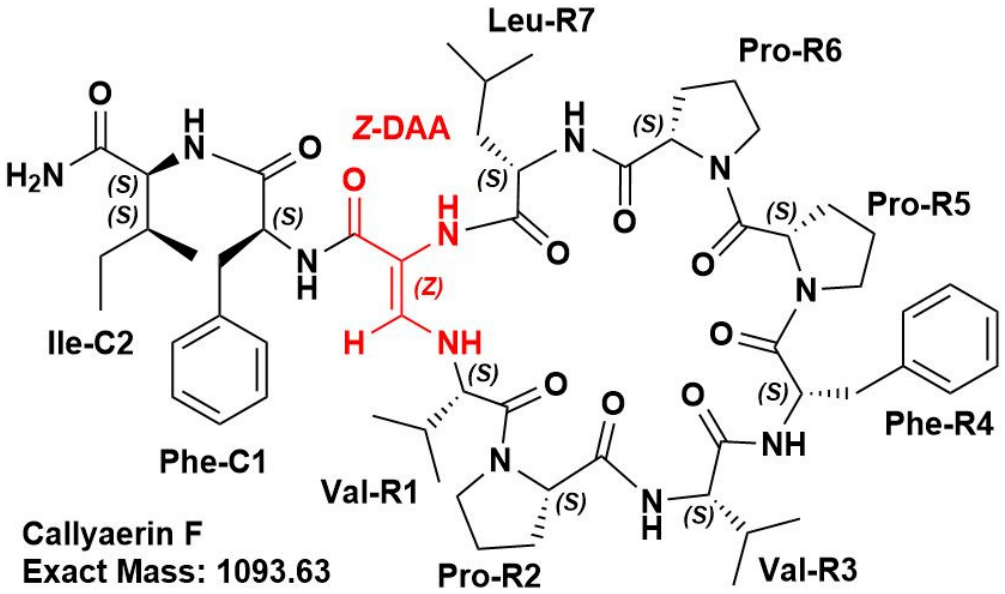

Figure 63: Chemical structure of Callyaerin F

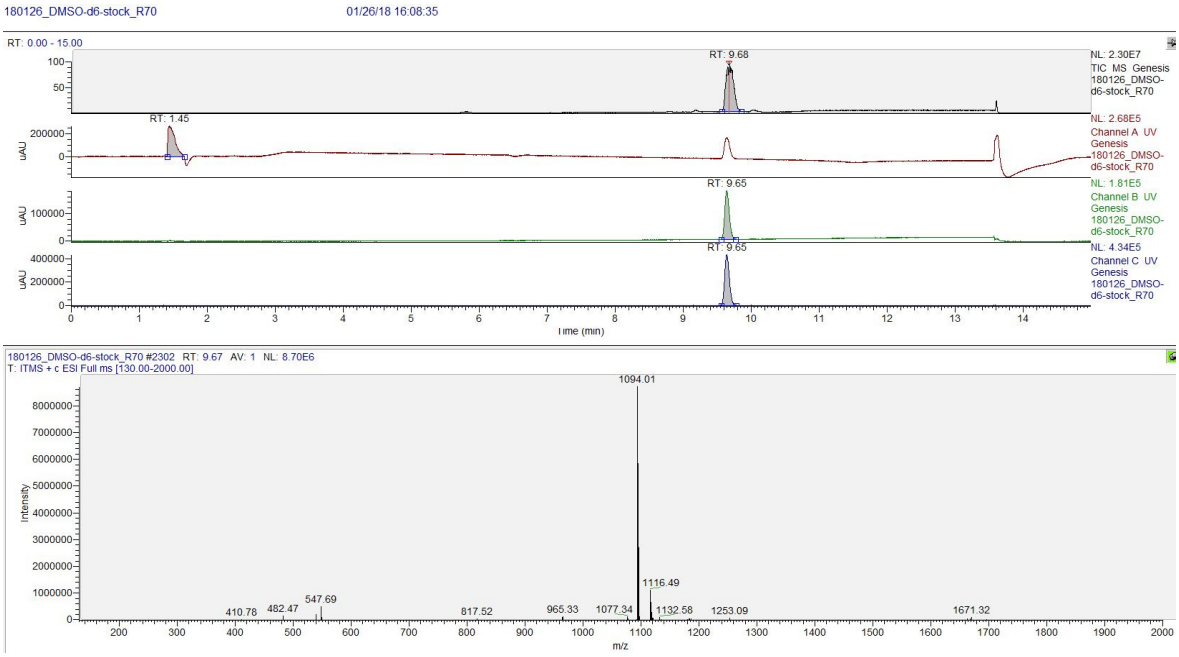

Figure 64: LC-MS spectrum of synthetic Callyaerin F. From top to bottom: TIC (ESI+), UV channel A (λ = 210 nm), UV channel B (λ = 254 nm), UV channel C (λ = 280 nm), mass spectrum of highest peak from chromatogram.

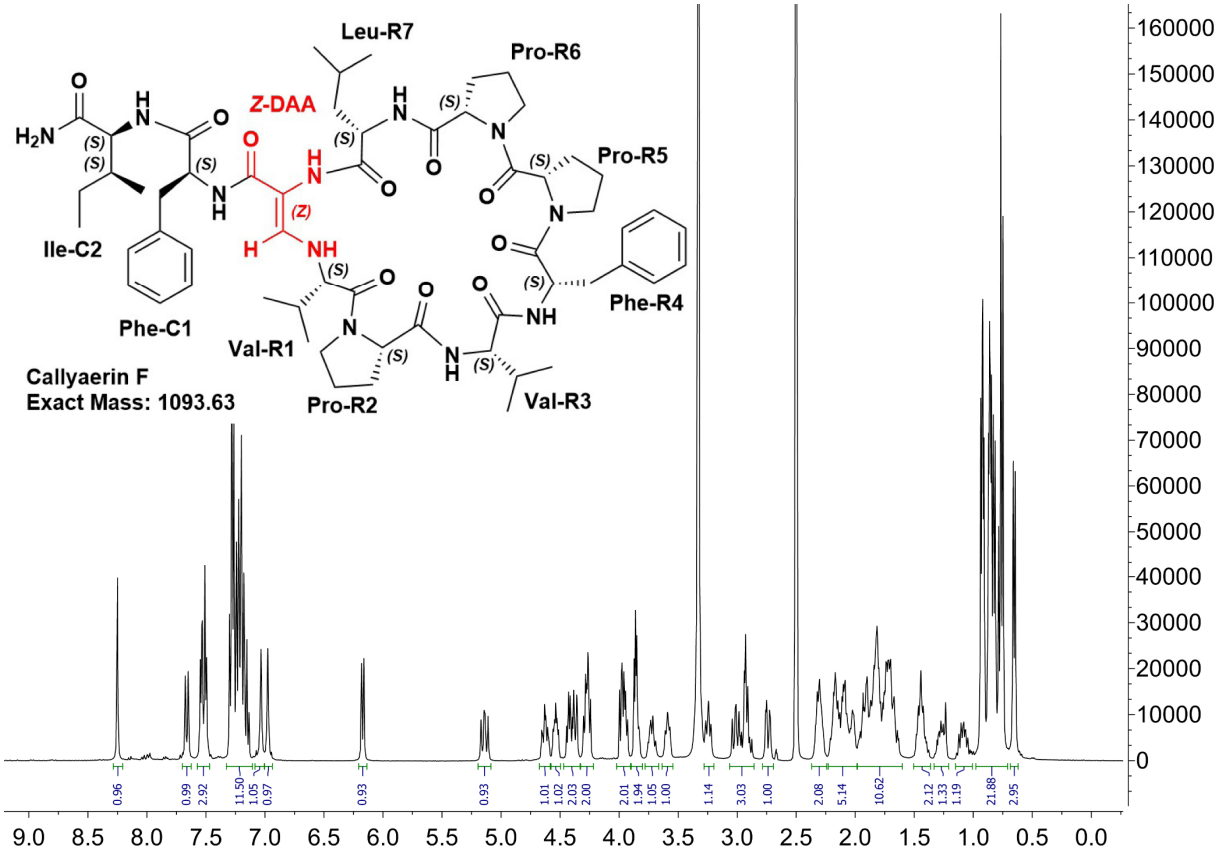

Figure 65: ^{1}H NMR spectrum (400 MHz, DMSO-d_6) of synthetic Callyaerin F.

6.1.1.7 Callyaerin G

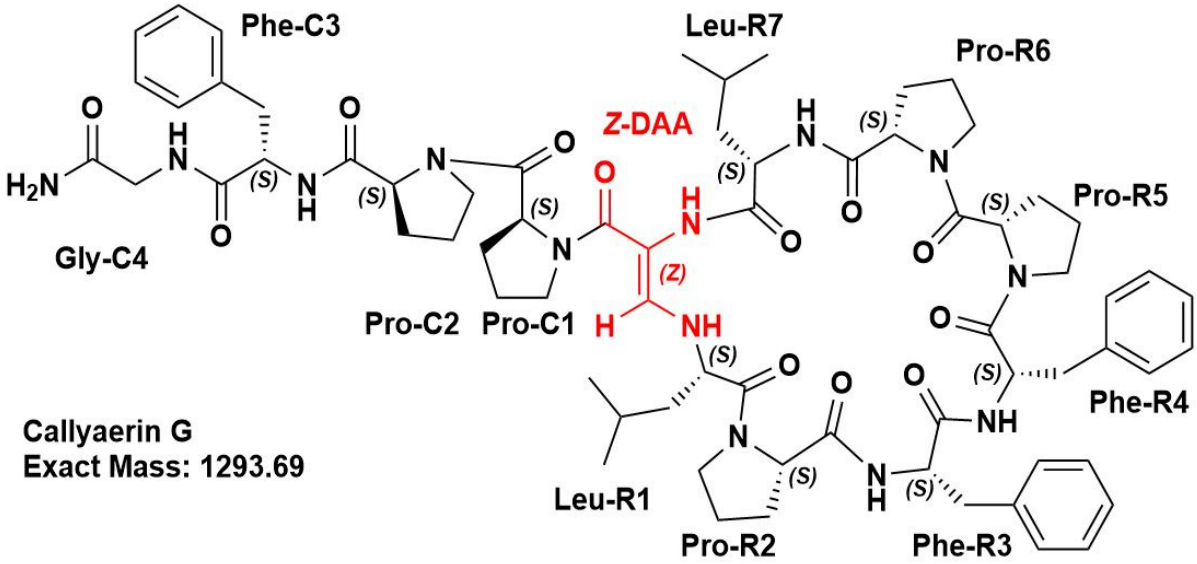

Figure 66: Chemical structure of Callyaerin G

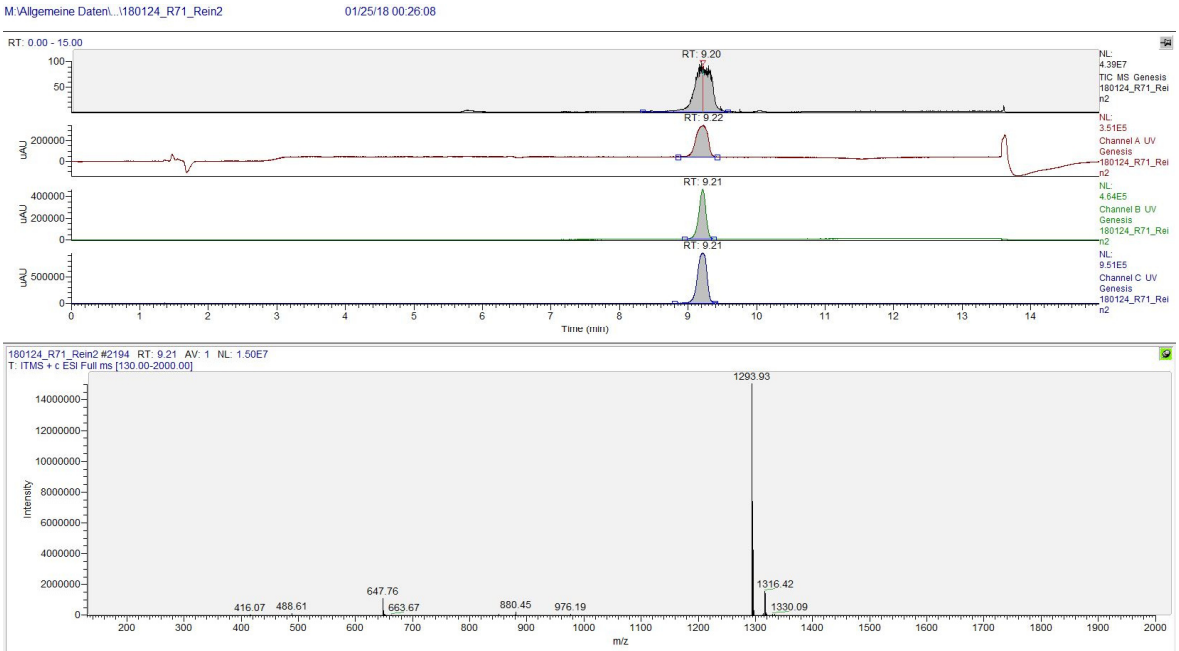

Figure 67: LC-MS spectrum of synthetic Callyaerin G. From top to bottom: TIC (ESI+), UV channel A (λ = 210 nm), UV channel B (λ = 254 nm), UV channel C (λ = 280 nm), mass spectrum of highest peak from chromatogram.

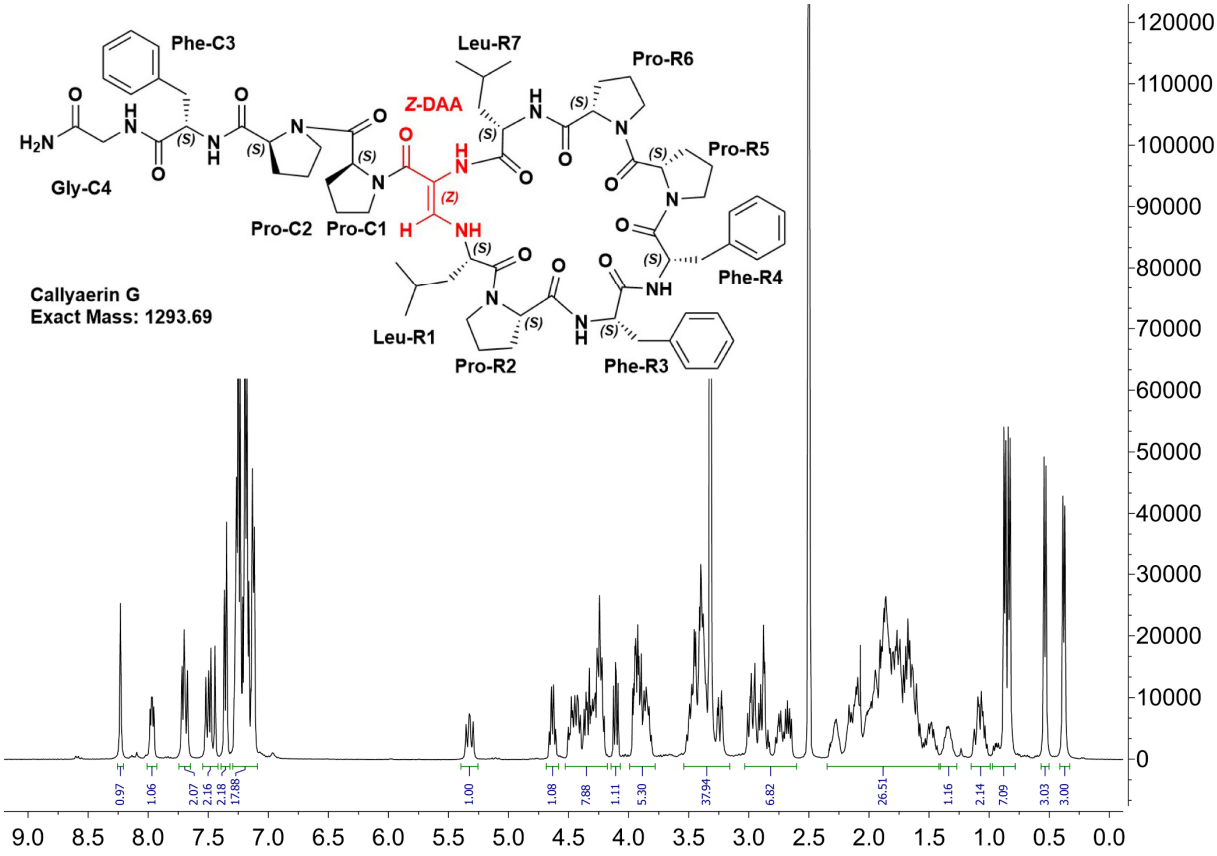

Figure 68: ^{1}H NMR spectrum (400 MHz, DMSO-d_6) of synthetic Callyaerin G.

6.1.1.8 Callyaerin H

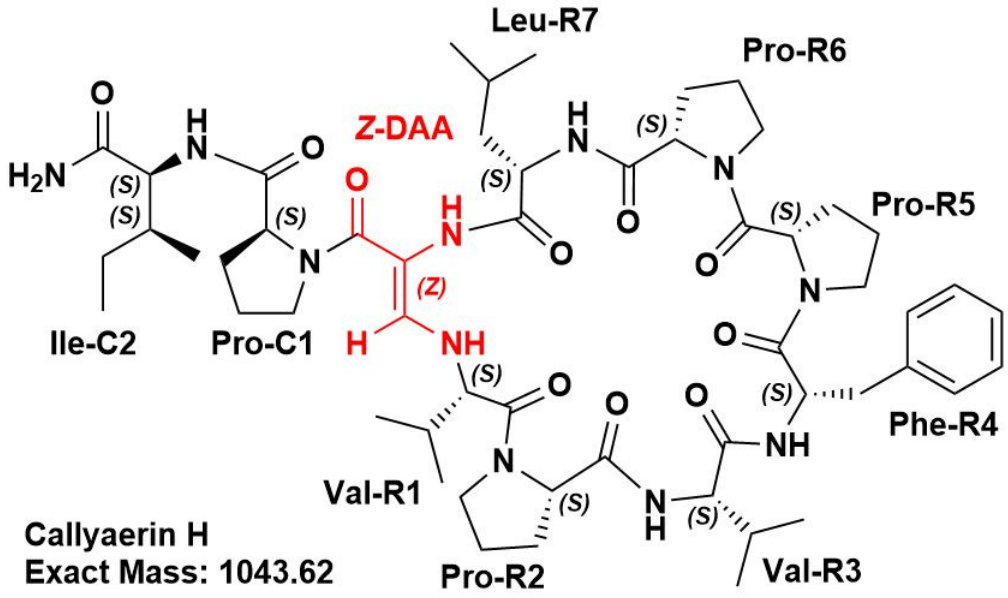

Figure 69: Chemical structure of Callyaerin H

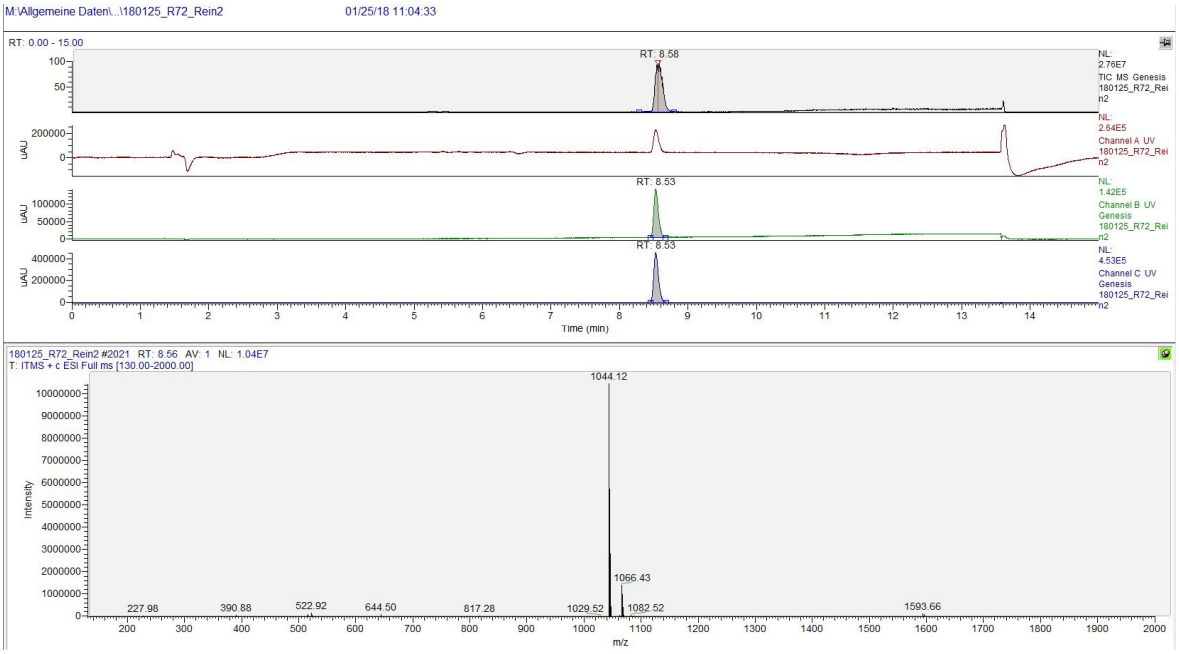

Figure 70: LC-MS spectrum of synthetic Callyaerin H. From top to bottom: TIC (ESI+), UV channel A (λ = 210 nm), UV channel B (λ = 254 nm), UV channel C (λ = 280 nm), mass spectrum of highest peak from chromatogram.

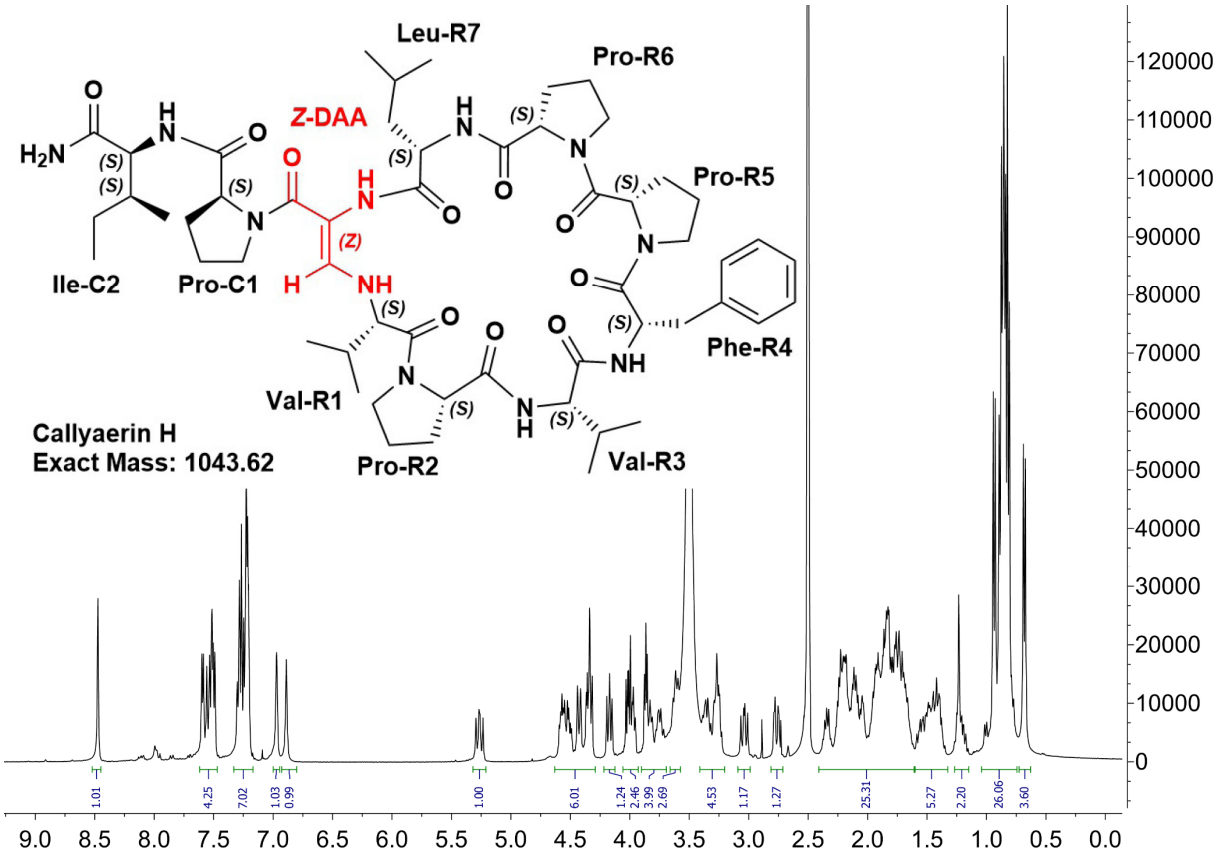

Figure 71: ^{1}H NMR spectrum (400 MHz, DMSO-d_6) of synthetic Callyaerin H.

6.1.1.9 Callyaerin I

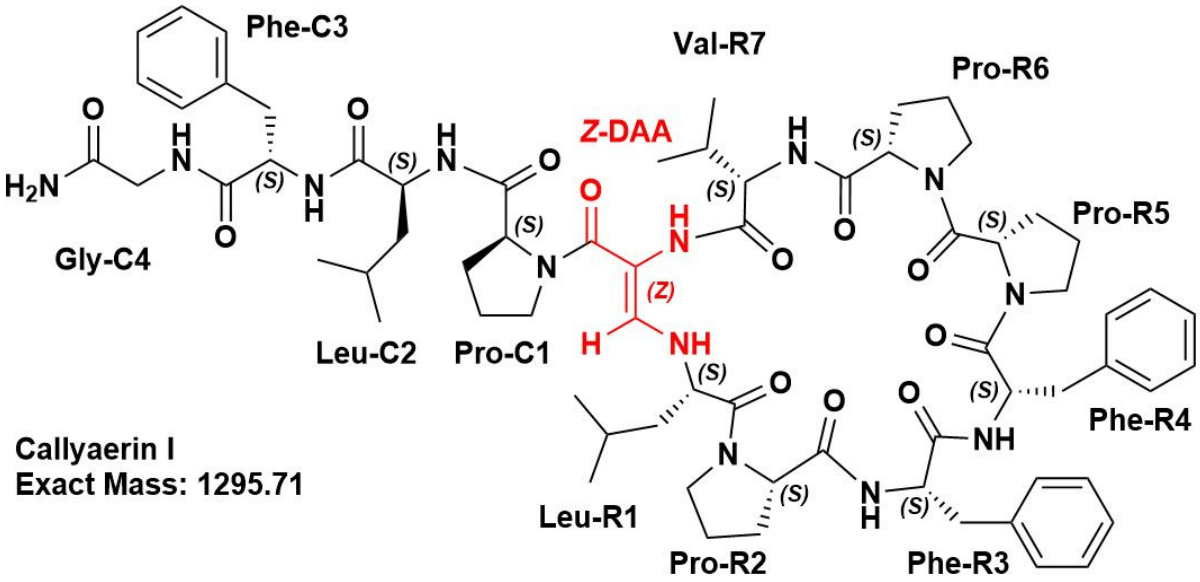

Figure 72: Chemical structure of Callyaerin I

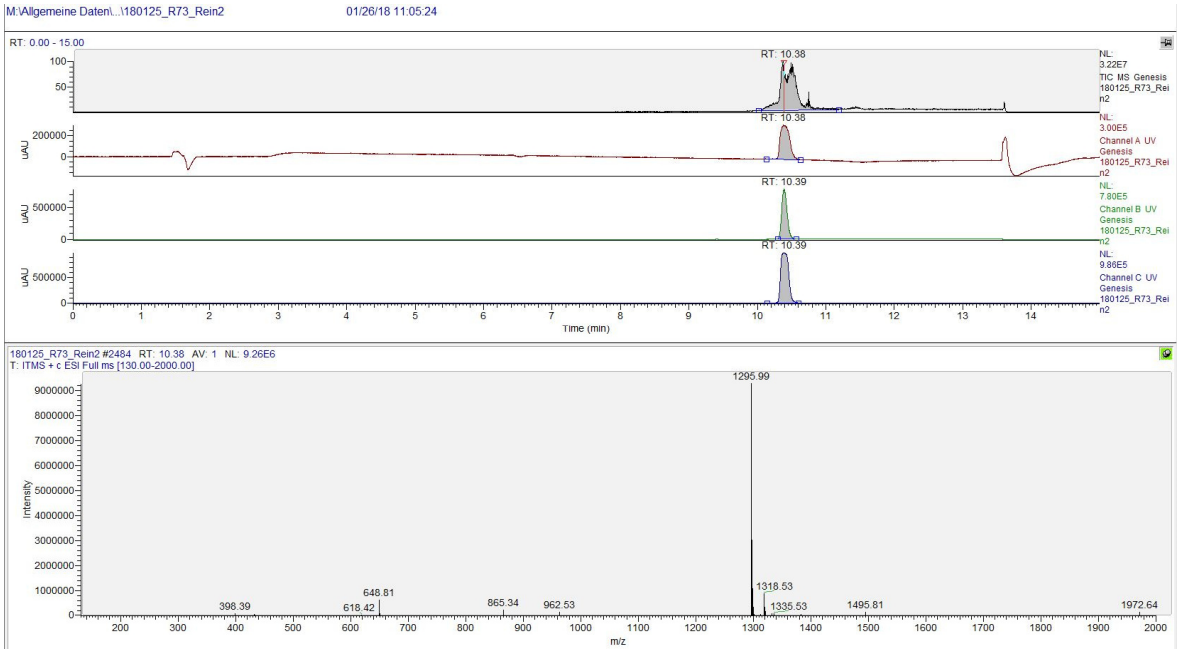

Figure 73: LC-MS spectrum of synthetic Callyaerin I. From top to bottom: TIC (ESI+), UV channel A (λ = 210 nm), UV channel B (λ = 254 nm), UV channel C (λ = 280 nm), mass spectrum of highest peak from chromatogram.

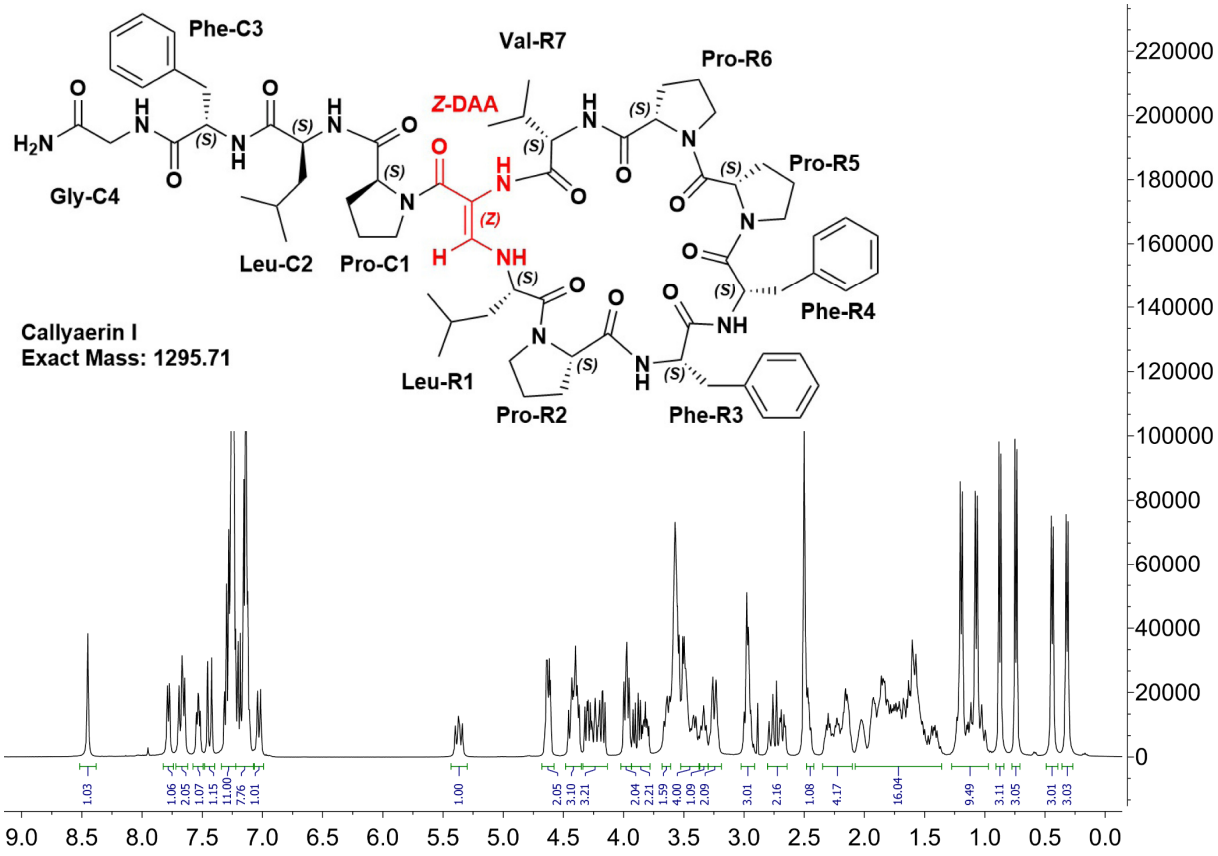

Figure 74: ^{1}H NMR spectrum (400 MHz, DMSO-d_6) of synthetic Callyaerin I.

6.1.1.10 Callyaerin J

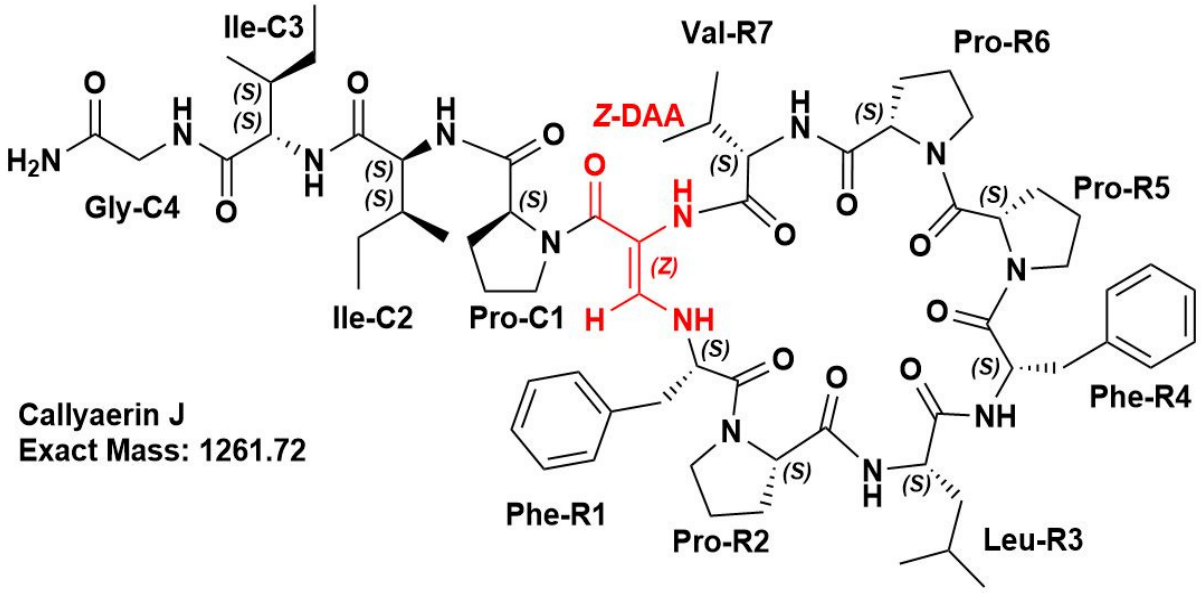

Figure 75: Chemical structure of Callyaerin J

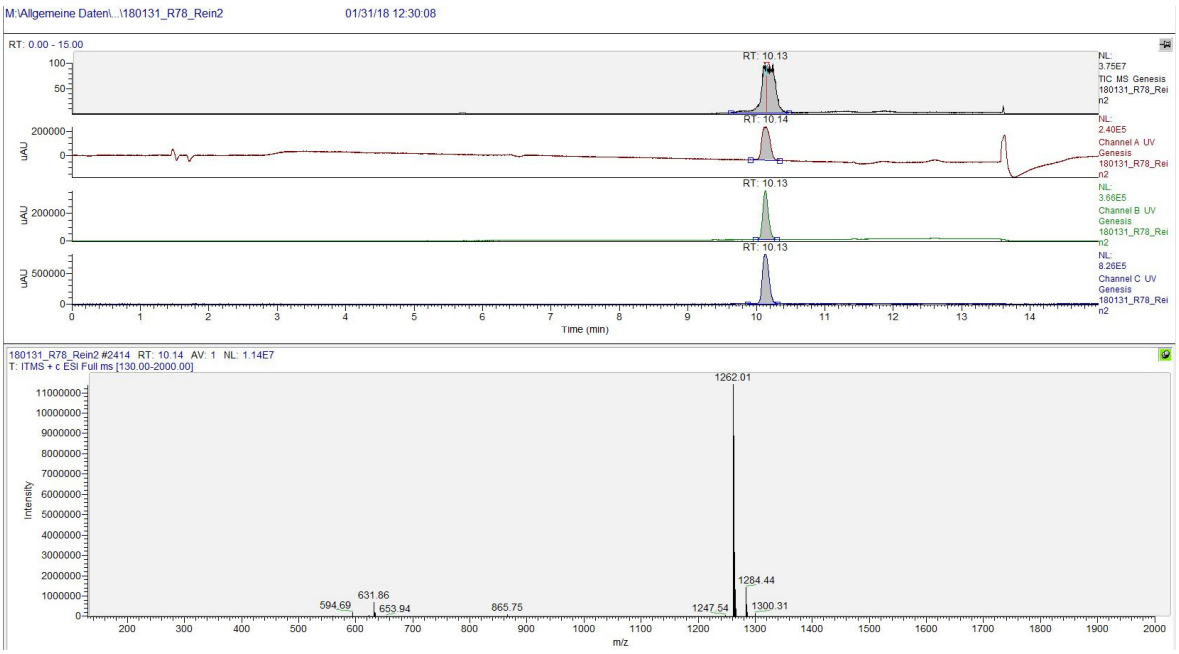

Figure 76: LC-MS spectrum of synthetic Callyaerin J. From top to bottom: TIC (ESI+), UV channel A (λ = 210 nm), UV channel B (λ = 254 nm), UV channel C (λ = 280 nm), mass spectrum of highest peak from chromatogram.

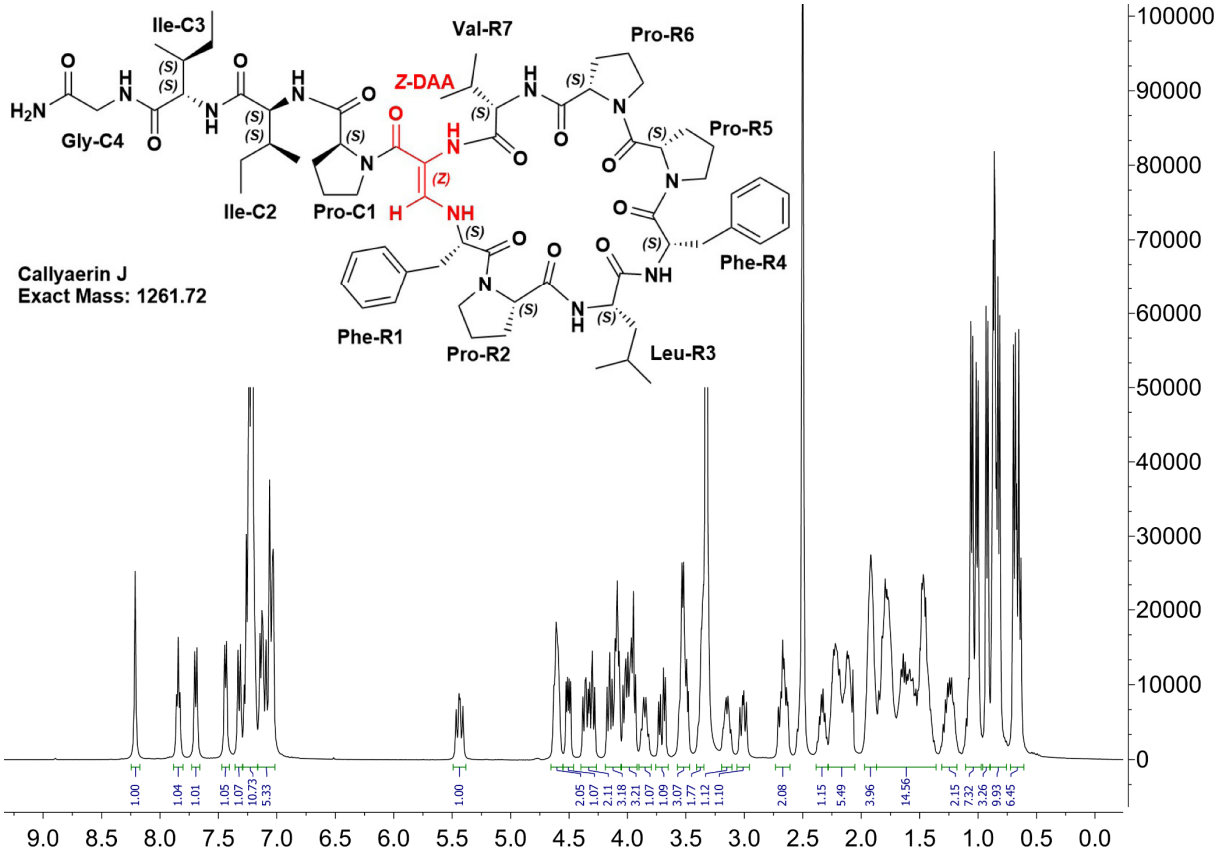

Figure 77: ^{1}H NMR spectrum (400 MHz, DMSO-d_6) of synthetic Callyaerin J.

6.1.1.11 Callyaerin K

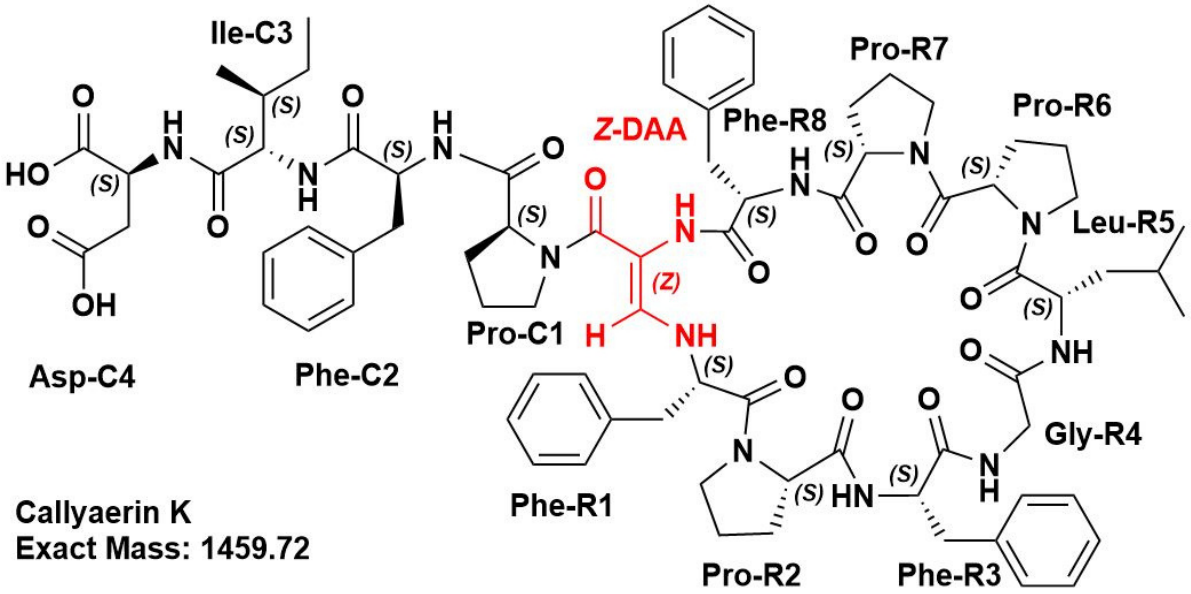

Figure 78: Chemical structure of Callyaerin K

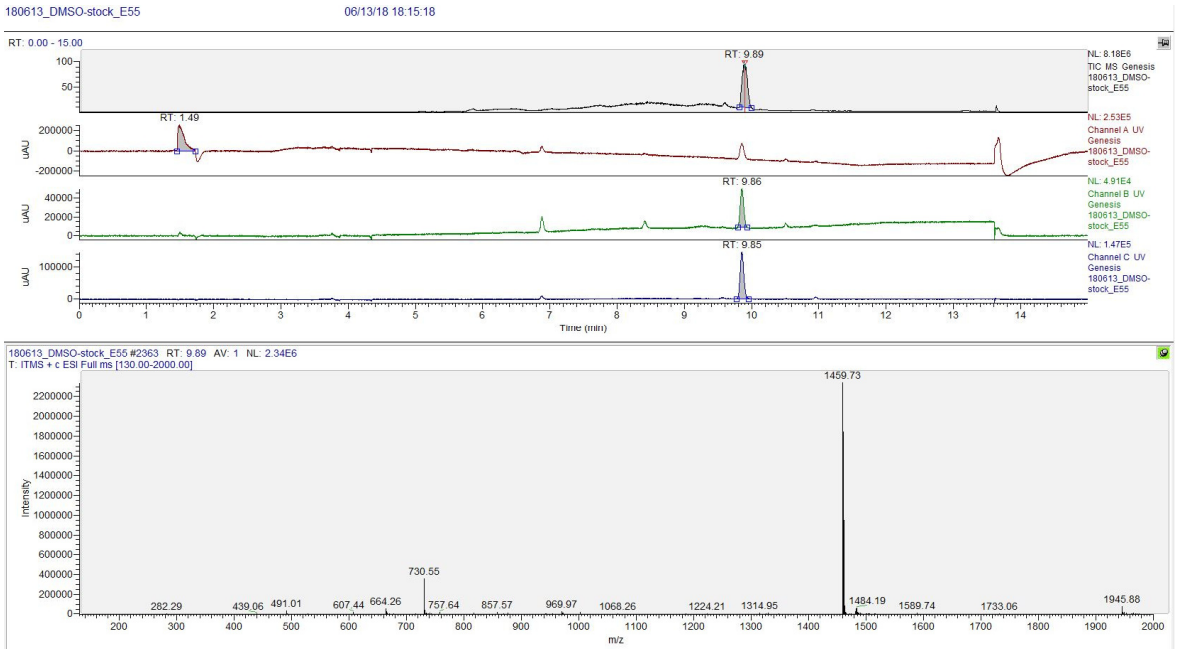

Figure 79: LC-MS spectrum of synthetic Callyaerin K. From top to bottom: TIC (ESI+), UV channel A (λ = 210 nm), UV channel B (λ = 254 nm), UV channel C (λ = 280 nm), mass spectrum of highest peak from chromatogram.

6.1.1.12 Callyaerin L

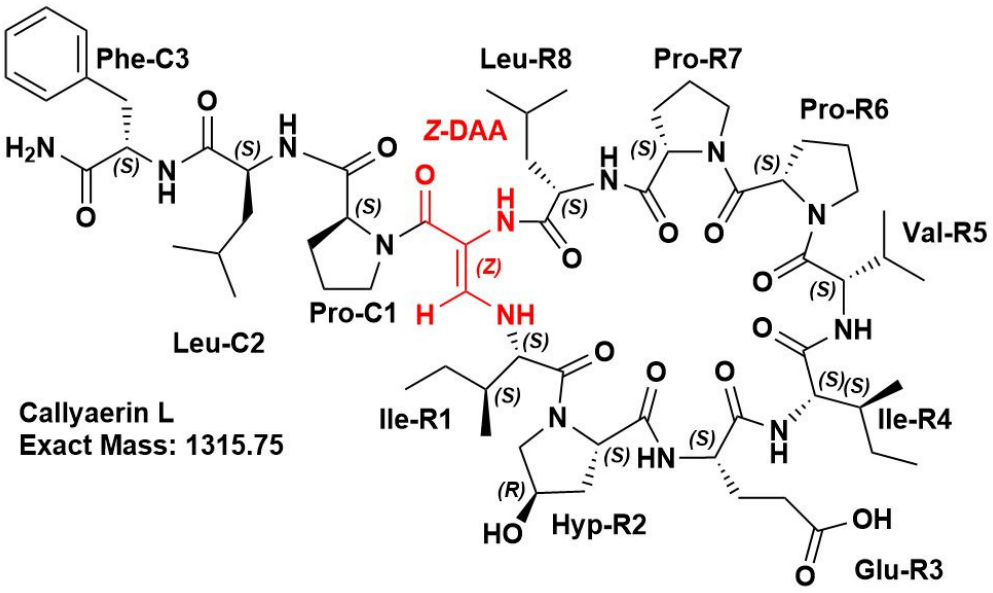

Figure 80: Chemical structure of Callyaerin L

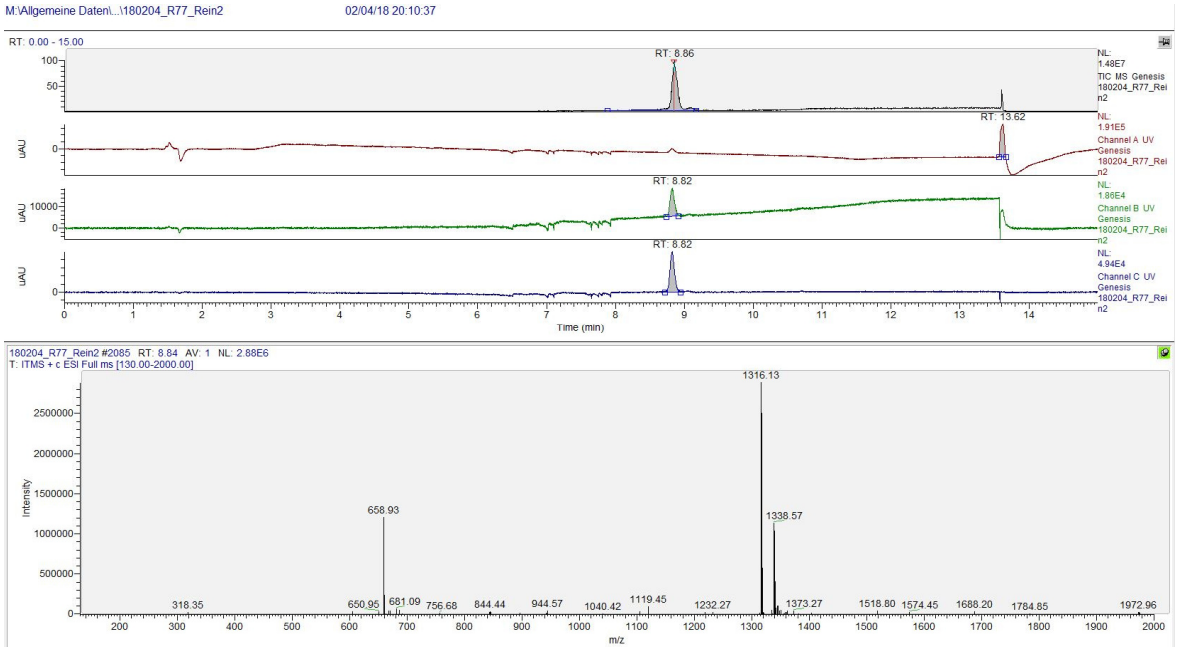

Figure 81: LC-MS spectrum of synthetic Callyaerin L. From top to bottom: TIC (ESI+), UV channel A (λ = 210 nm), UV channel B (λ = 254 nm), UV channel C (λ = 280 nm), mass spectrum of highest peak from chromatogram.

6.1.1.13 Callynormine A

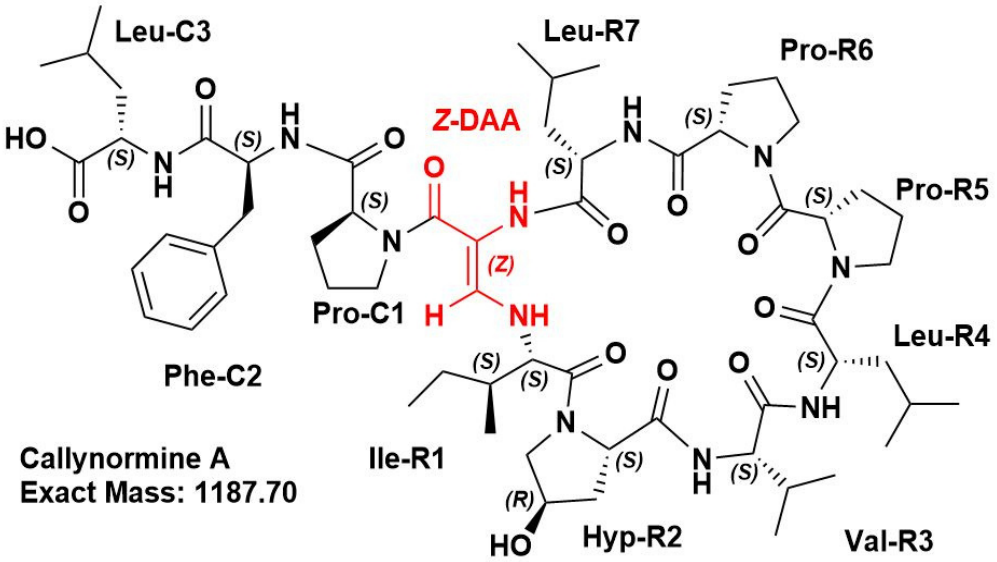

Figure 82: Chemical structure of Callynormine A

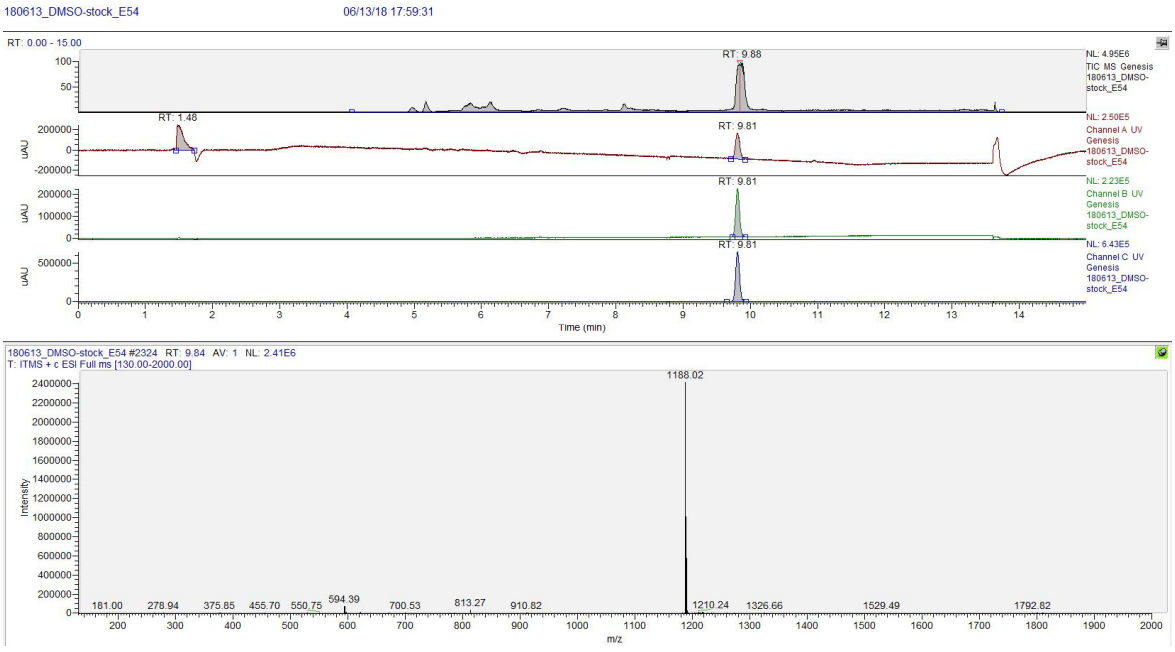

Figure 83: LC-MS spectrum of synthetic Callynormine A. From top to bottom: TIC (ESI+), UV channel A (λ = 210 nm), UV channel B (λ = 254 nm), UV channel C (λ = 280 nm), mass spectrum of highest peak from chromatogram.

6.1.1.14 CalA_R1A

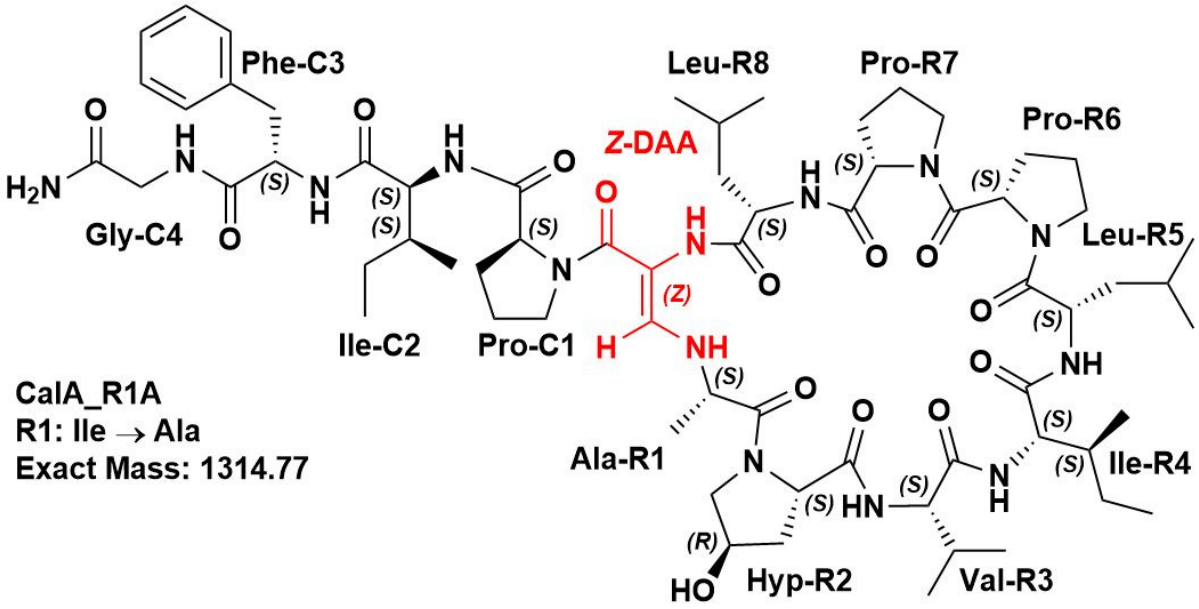

Figure 84: Chemical structure of derivative *CalA_R1A*

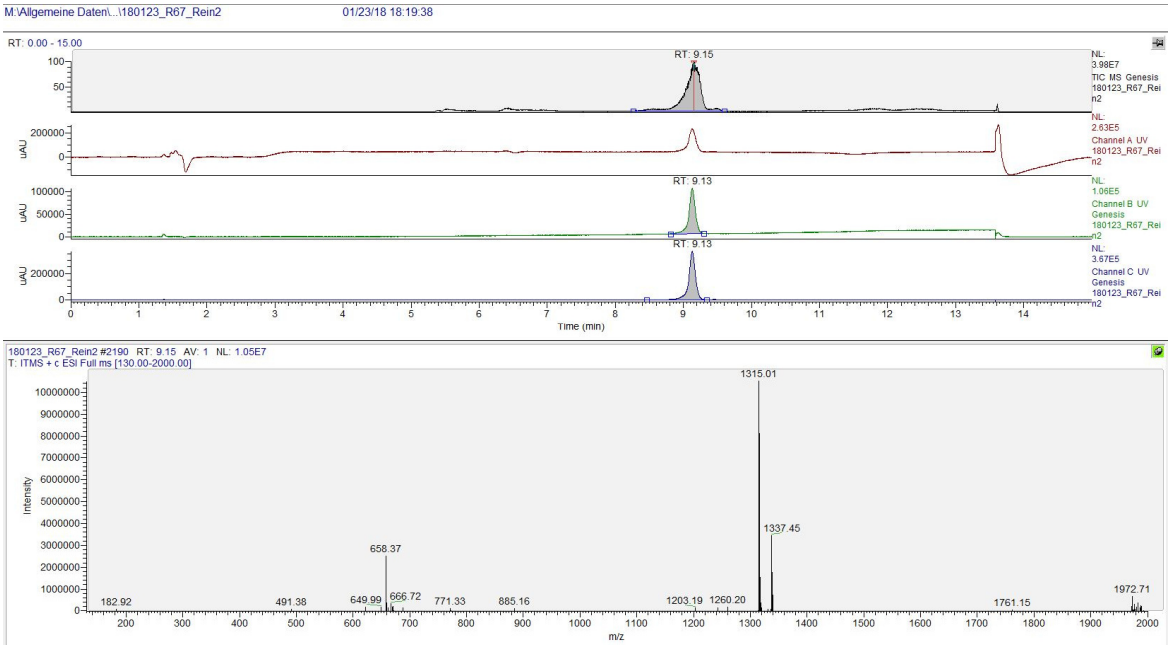

Figure 85: LC-MS spectrum of synthetic derivative *CalA_R1A*. From top to bottom: TIC (ESI+), UV channel A (λ = 210 nm), UV channel B (λ = 254 nm), UV channel C (λ = 280 nm), mass spectrum of highest peak from chromatogram.

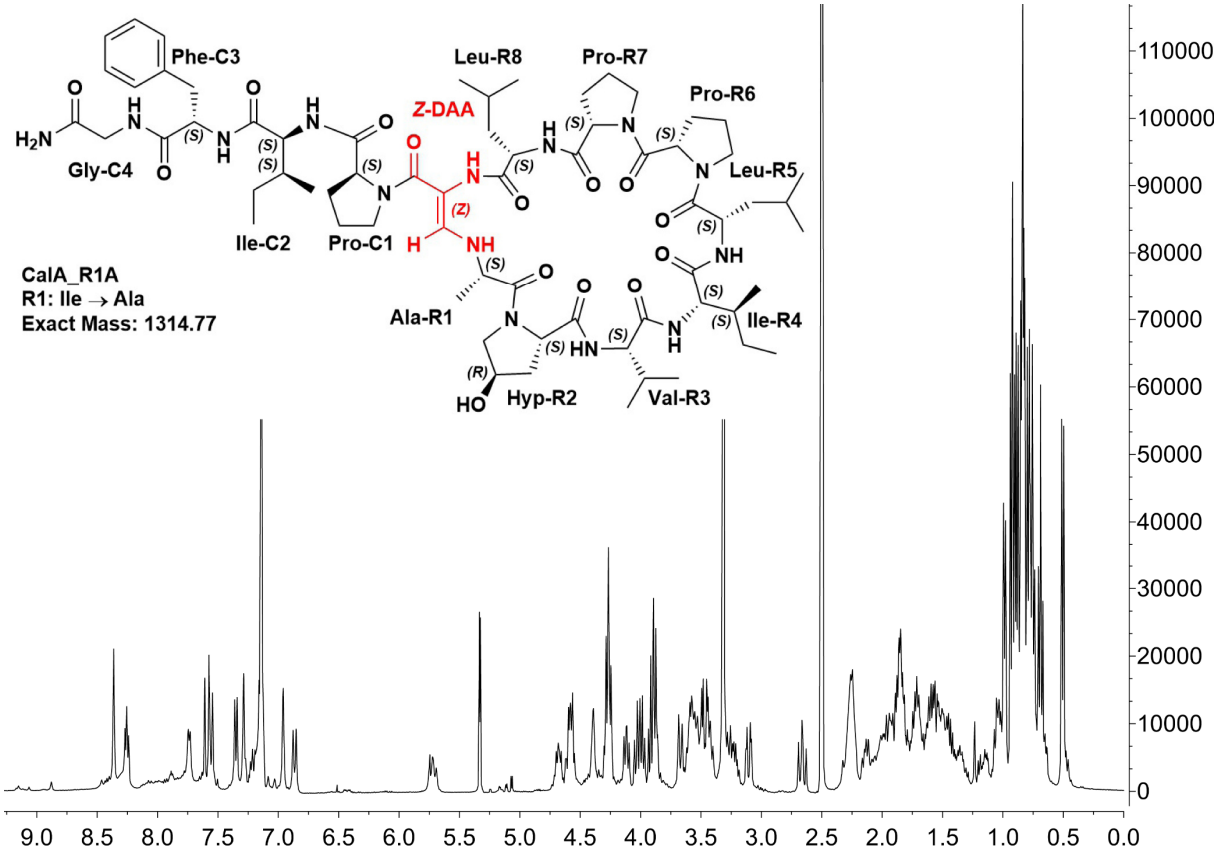

Figure 86: ^{1}H NMR spectrum (400 MHz, DMSO-d_6) of derivative *CalA_R1A*.

6.1.1.15 CalA_R2A

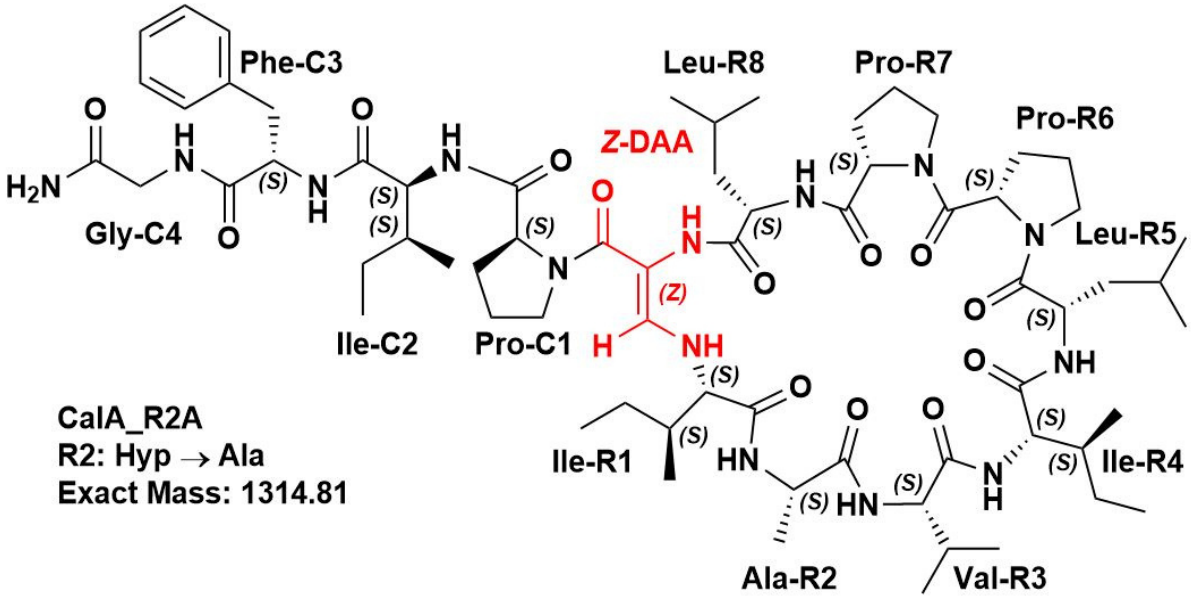

Figure 87: Chemical structure of derivative *CalA_R2A*

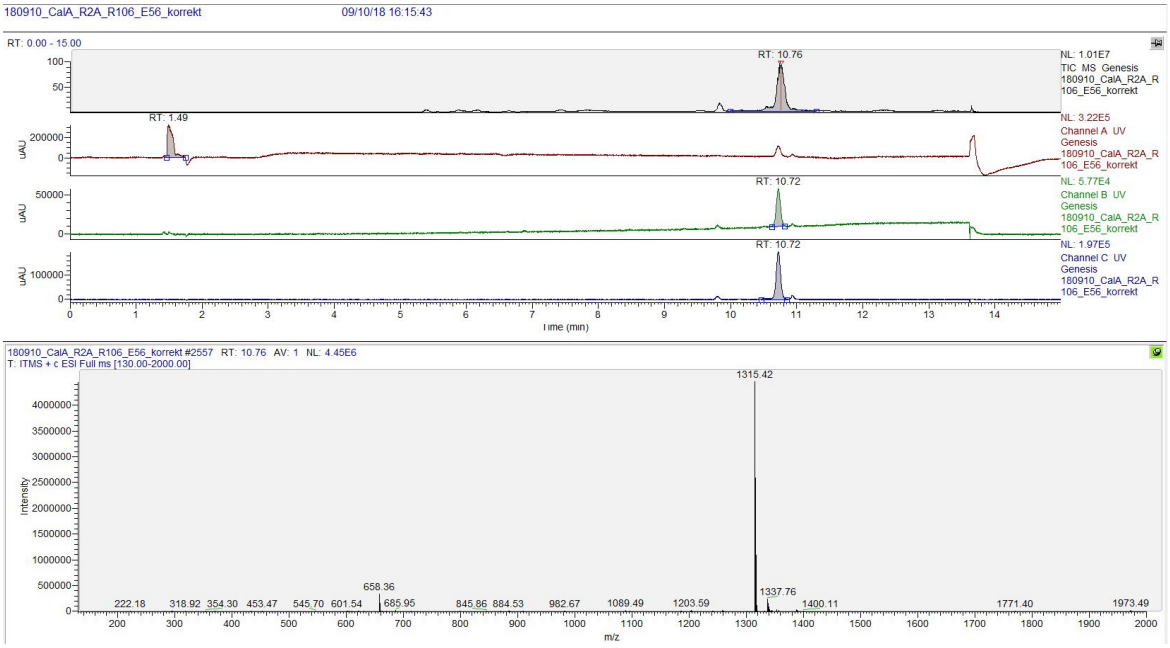

Figure 88: LC-MS spectrum of synthetic Callyaerin A derivative *CalA_R2A*. From top to bottom: TIC (ESI+), UV channel A (λ = 210 nm), UV channel B (λ = 254 nm), UV channel C (λ = 280 nm), mass spectrum of highest peak from chromatogram.

6.1.1.16 *CalA_R2P*

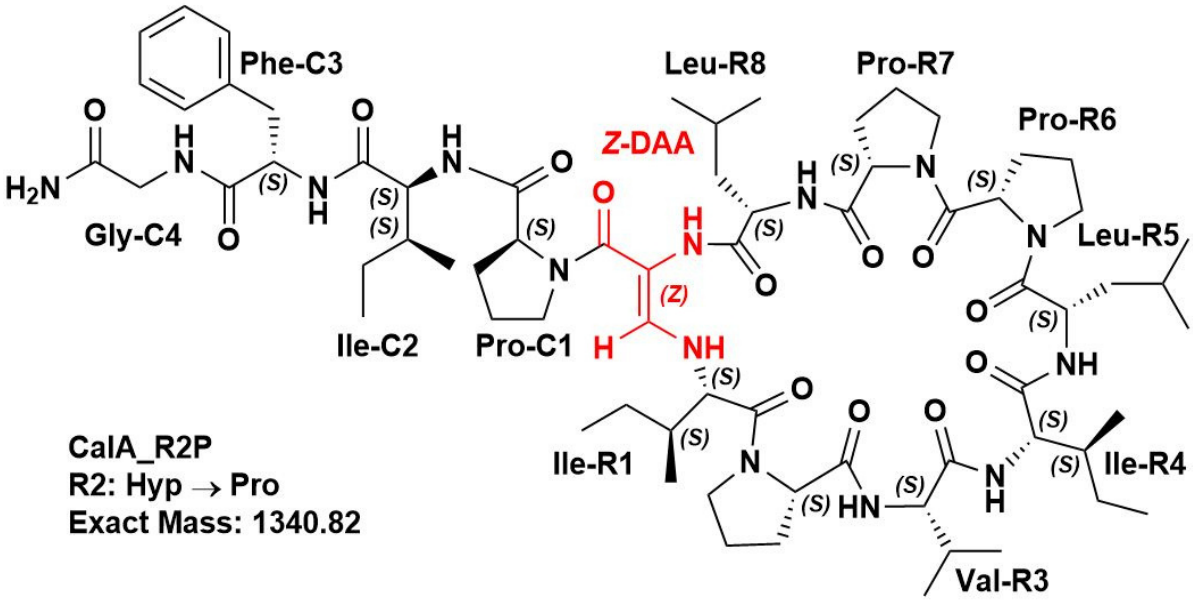

Figure 89: Chemical structure of derivative *CalA_R2P*

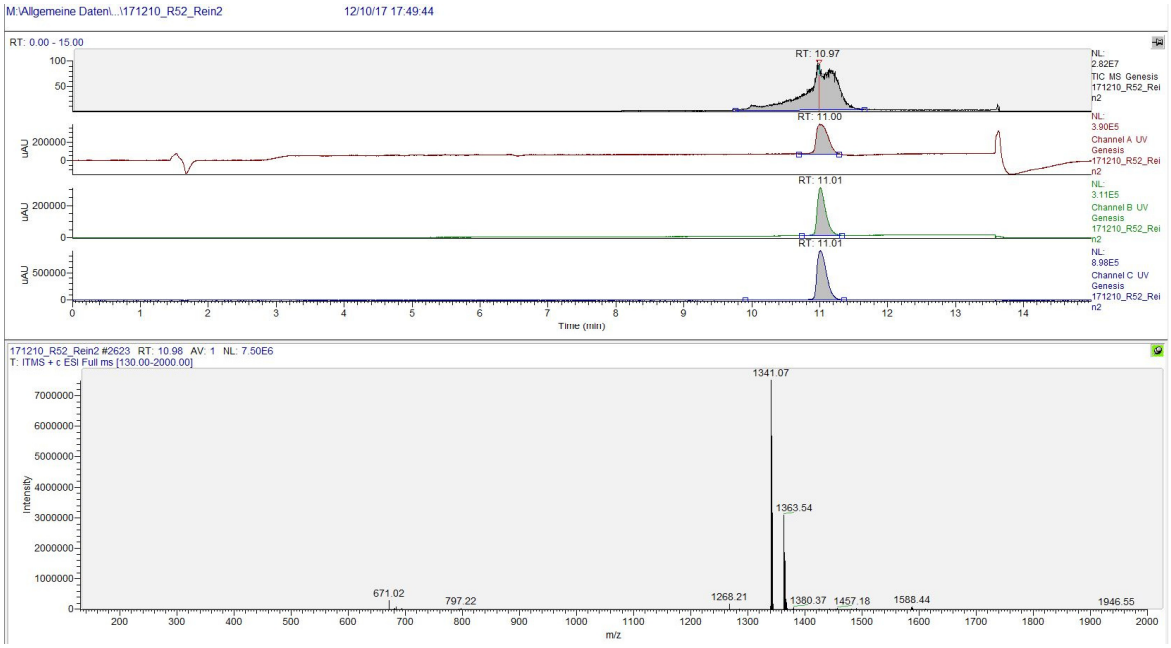

Figure 90: LC-MS spectrum of synthetic Callyaerin A derivative *CalA_R2P*. From top to bottom: TIC (ESI+), UV channel A (λ = 210 nm), UV channel B (λ = 254 nm), UV channel C (λ = 280 nm), mass spectrum of highest peak from chromatogram.

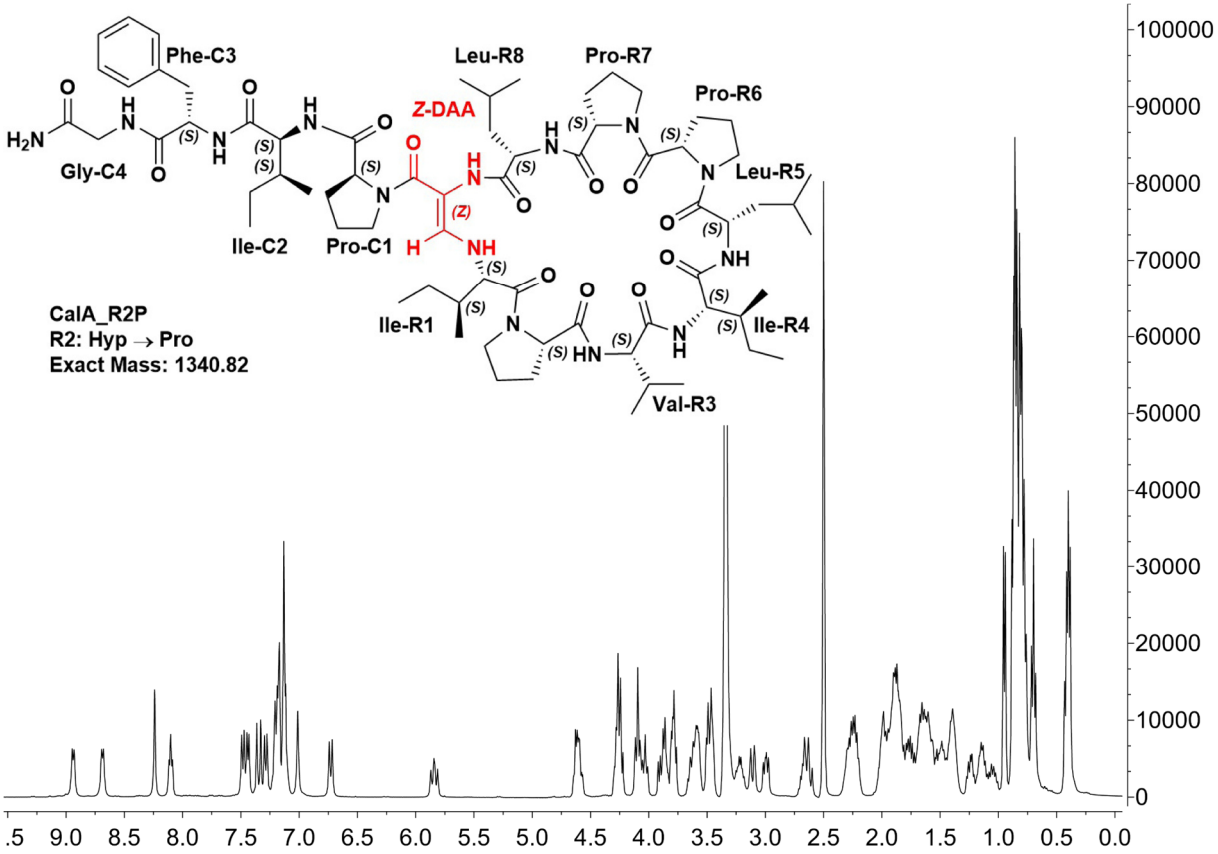

Figure 91: ^{1}H NMR spectrum (400 MHz, DMSO-d_6) of derivative *CalA_R2P*.

6.1.1.17 CalA_R3A

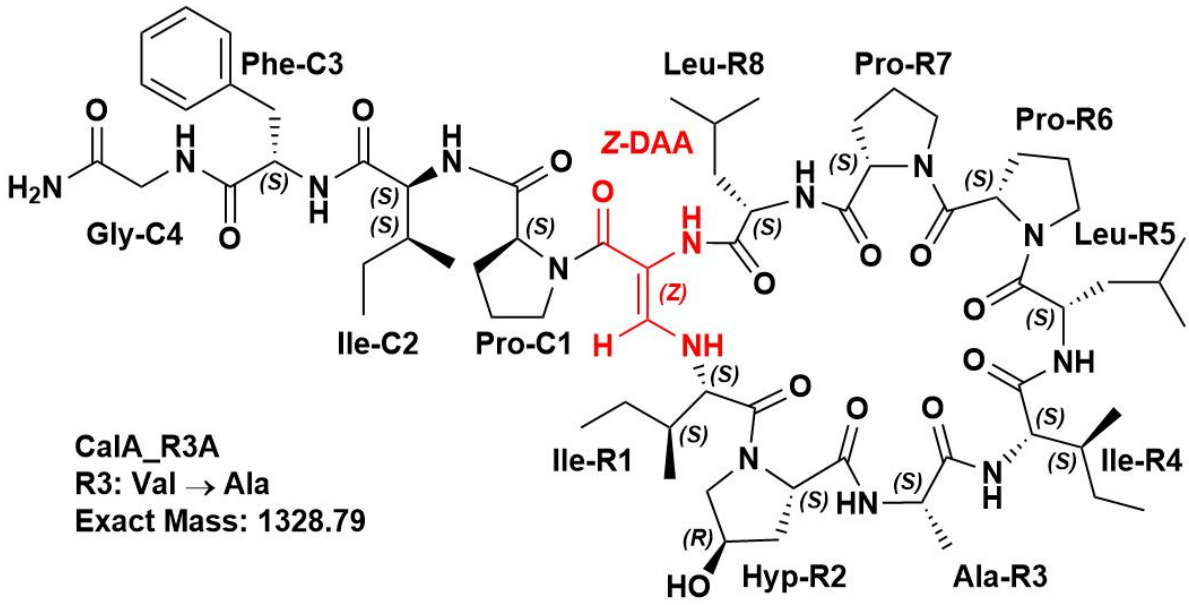

Figure 92: Chemical structure of derivative *CalA_R3A*

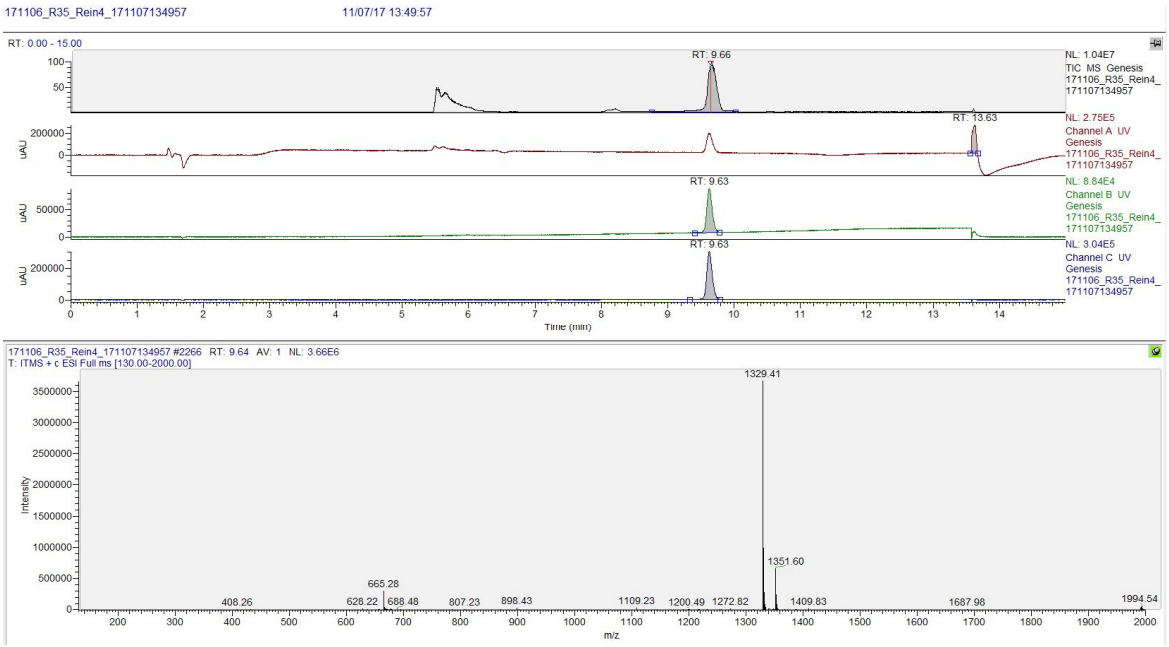

Figure 93: LC-MS spectrum of synthetic Callyaerin A derivative *CalA_R3A*. From top to bottom: TIC (ESI+), UV channel A (λ = 210 nm), UV channel B (λ = 254 nm), UV channel C (λ = 280 nm), mass spectrum of highest peak from chromatogram.

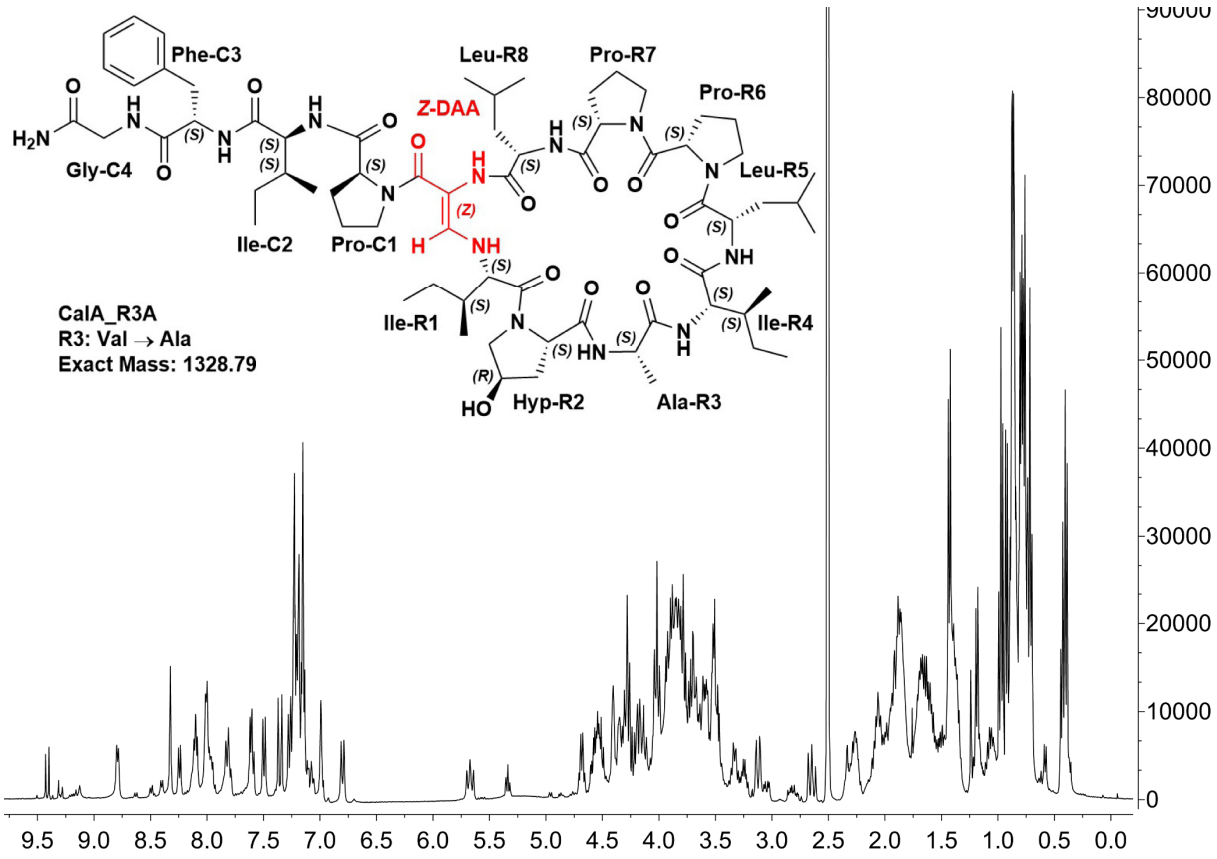

Figure 94: ^{1}H NMR spectrum (400 MHz, DMSO-d_6) of derivative *CalA_R3A*.

6.1.1.18 CalA_R3F

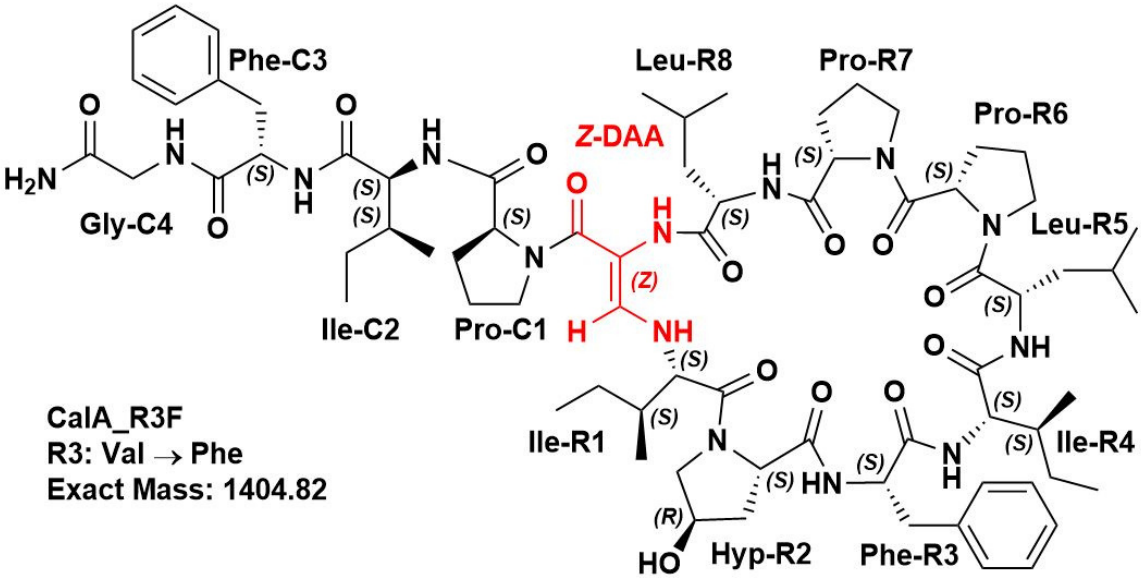

Figure 95: Chemical structure of derivative *CalA_R3F*

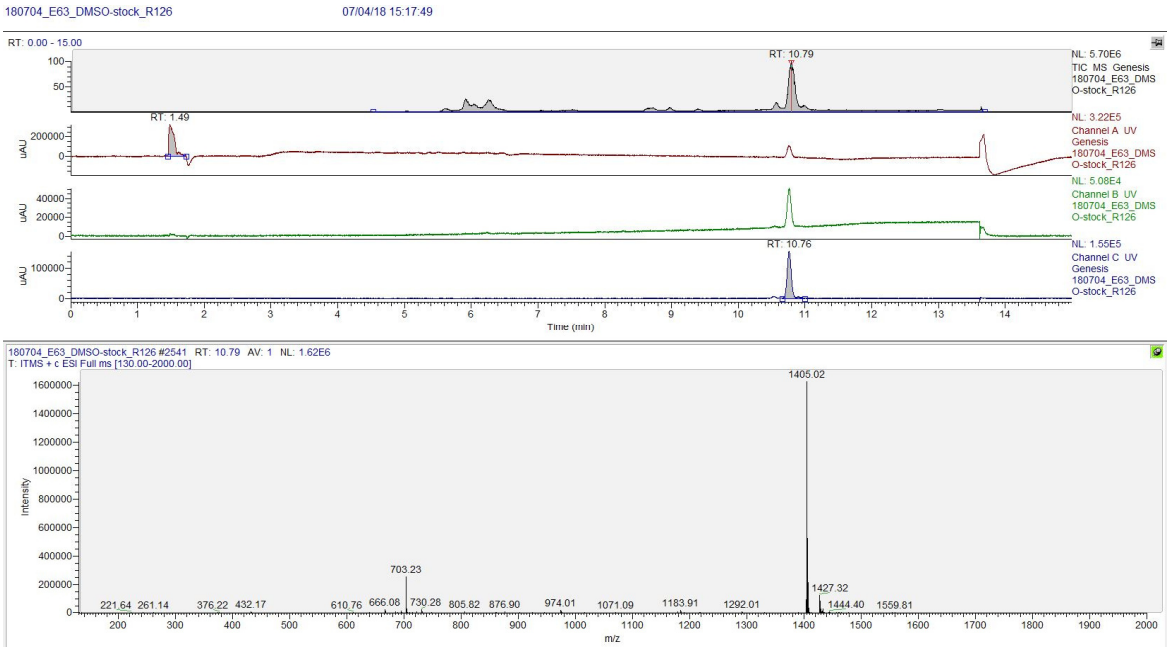

Figure 96: LC-MS spectrum of synthetic Callyaerin A derivative *CalA_R3F*. From top to bottom: TIC (ESI+), UV channel A (λ = 210 nm), UV channel B (λ = 254 nm), UV channel C (λ = 280 nm), mass spectrum of highest peak from chromatogram.

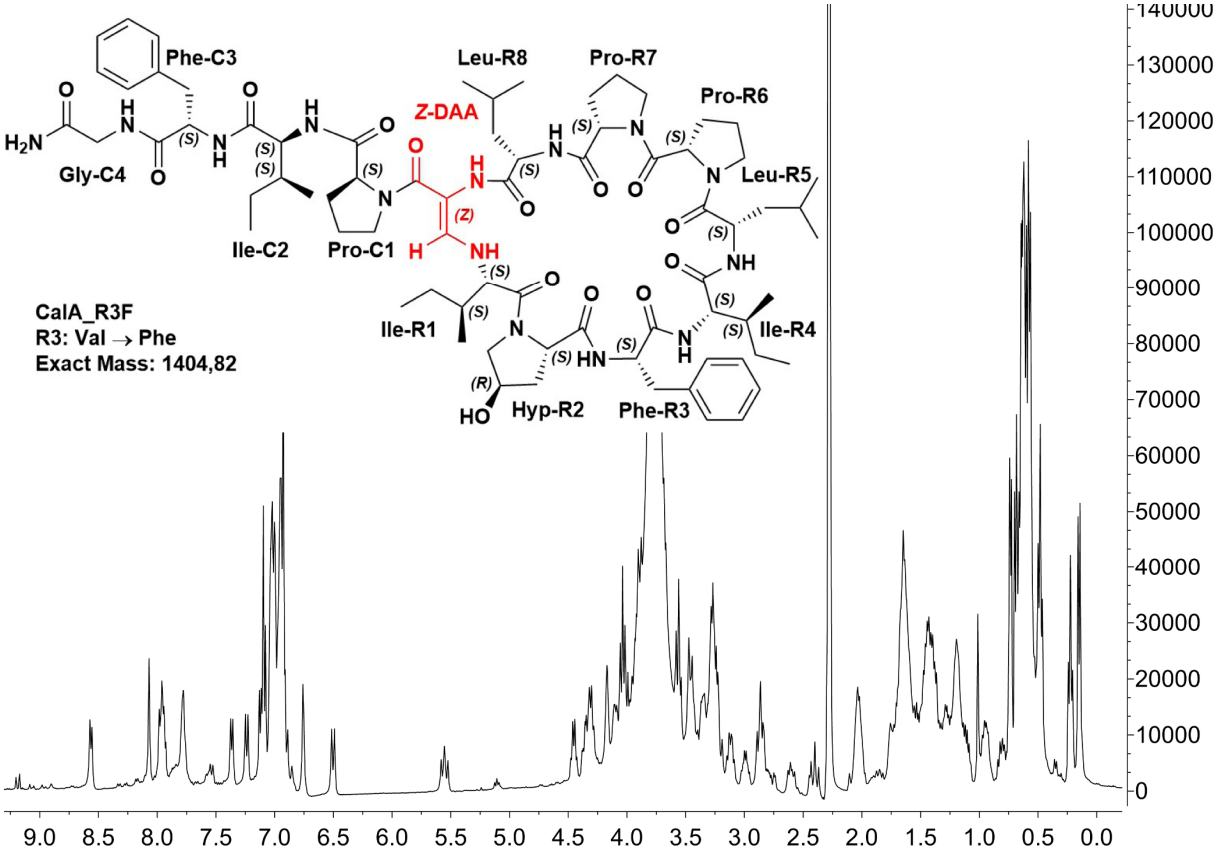

Figure 97: ^{1}H NMR spectrum (400 MHz, DMSO-d_6) of derivative *CalA_R3F*.

6.1.1.19 CalA_R3I

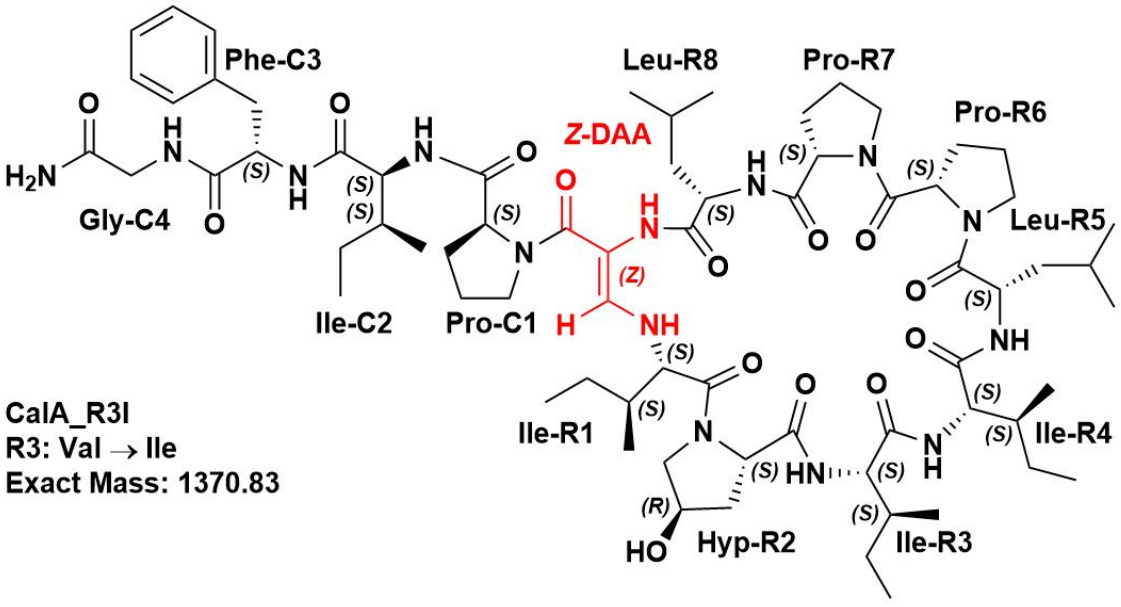

Figure 98: Chemical structure of derivative *CalA_R3I*

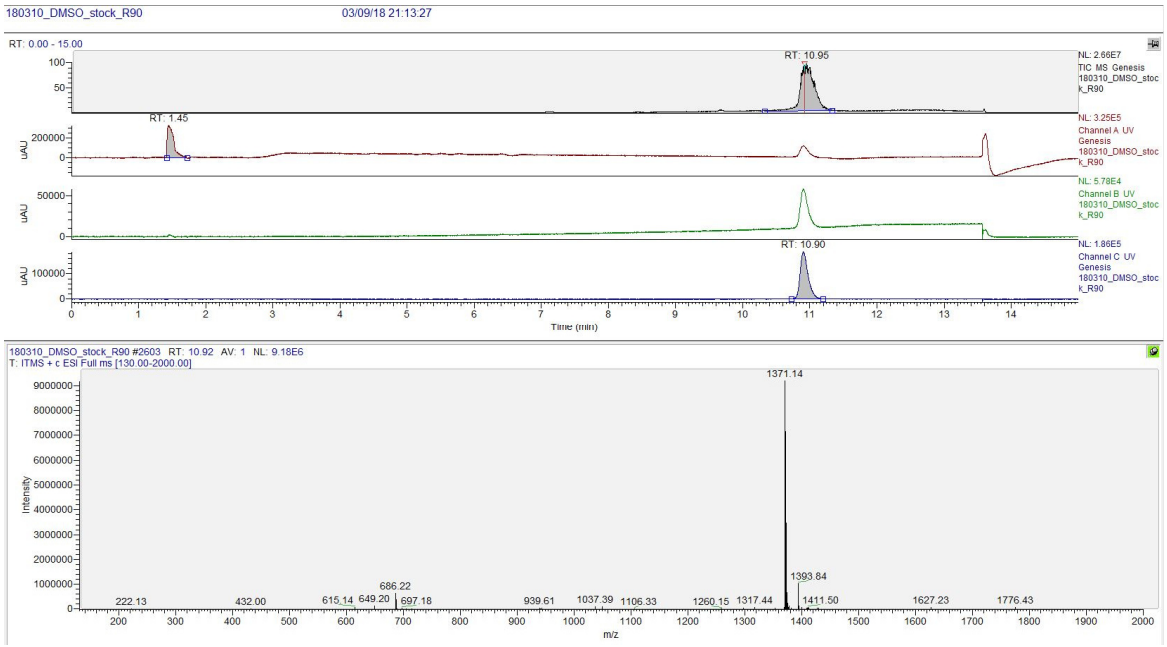

Figure 99: LC-MS spectrum of synthetic Callyaerin A derivative *CalA_R3I*. From top to bottom: TIC (ESI+), UV channel A (λ = 210 nm), UV channel B (λ = 254 nm), UV channel C (λ = 280 nm), mass spectrum of highest peak from chromatogram.

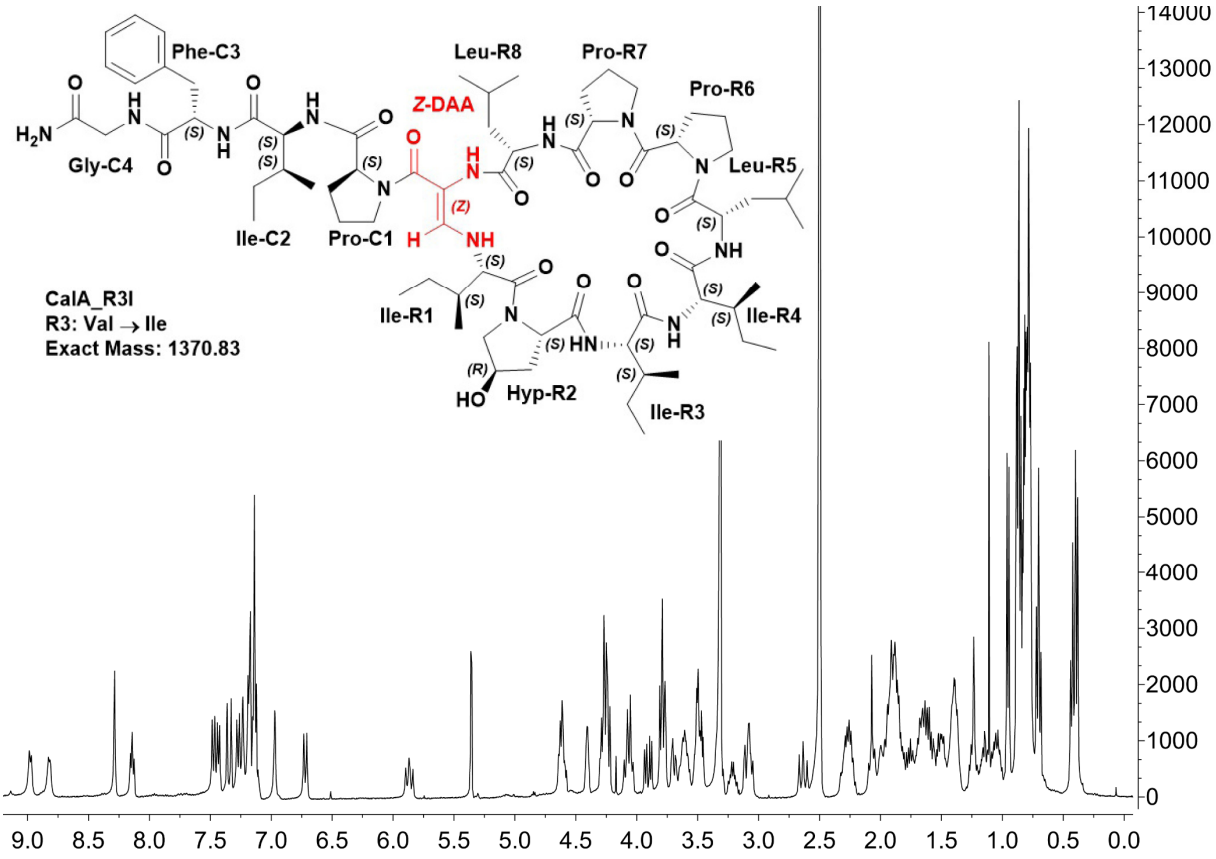

Figure 100: ^{1}H NMR spectrum (400 MHz, DMSO-d_6) of derivative *CalA_R3I*.

6.1.1.20 CalA_R3L

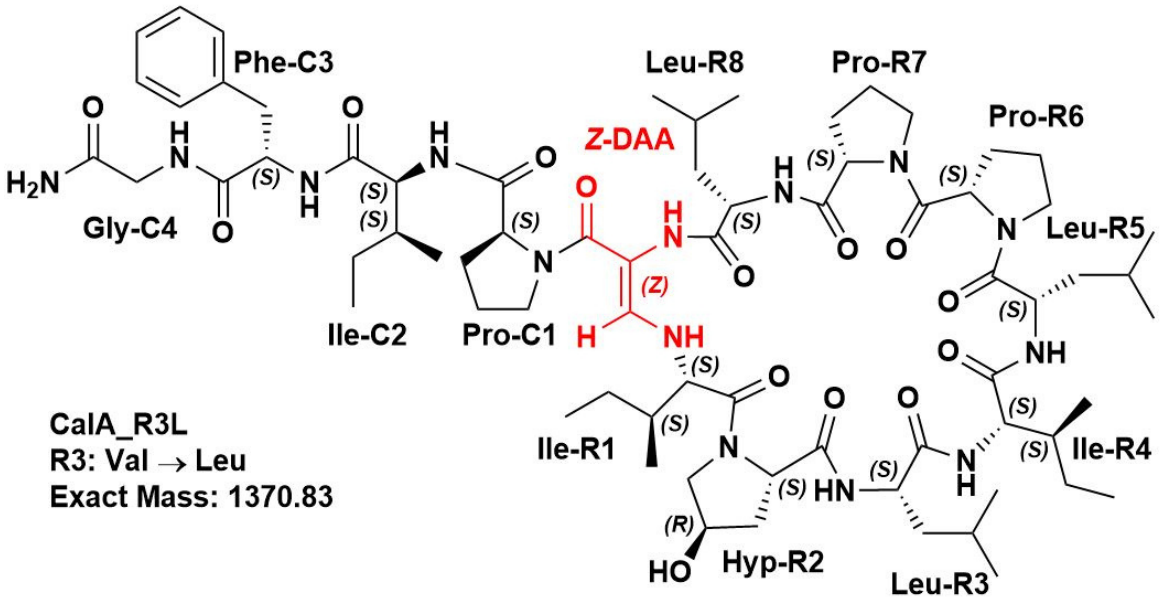

Figure 101: Chemical structure of derivative *CalA_R3L*

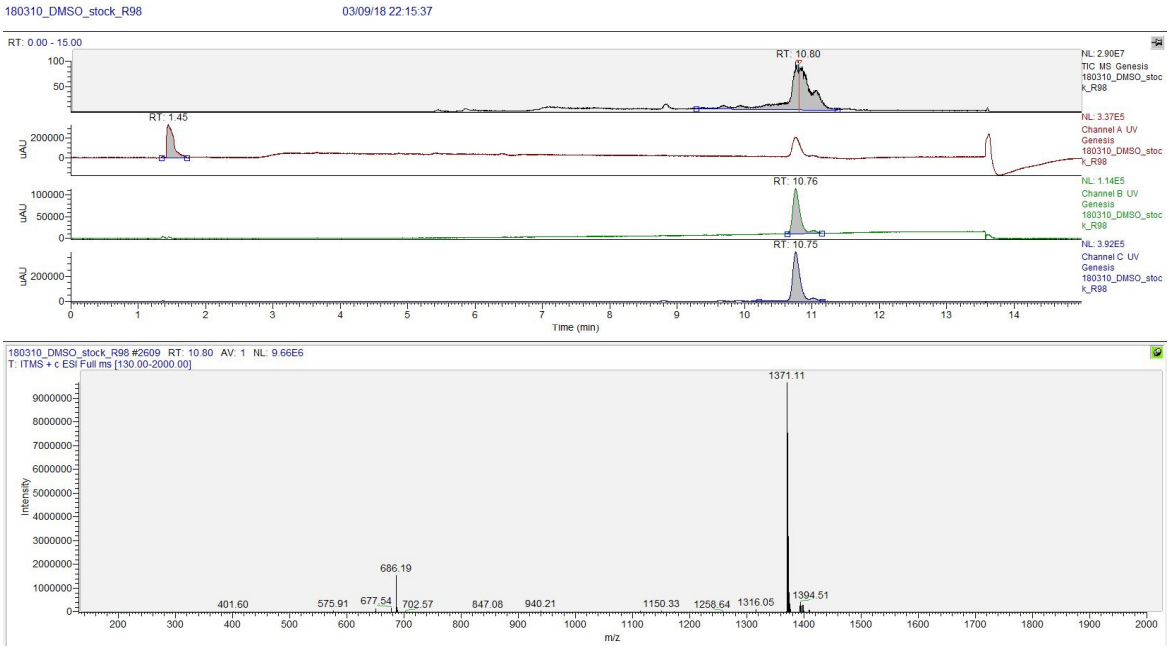

Figure 102: LC-MS spectrum of synthetic Callyaerin A derivative *CalA_R3L*. From top to bottom: TIC (ESI+), UV channel A (λ = 210 nm), UV channel B (λ = 254 nm), UV channel C (λ = 280 nm), mass spectrum of highest peak from chromatogram.

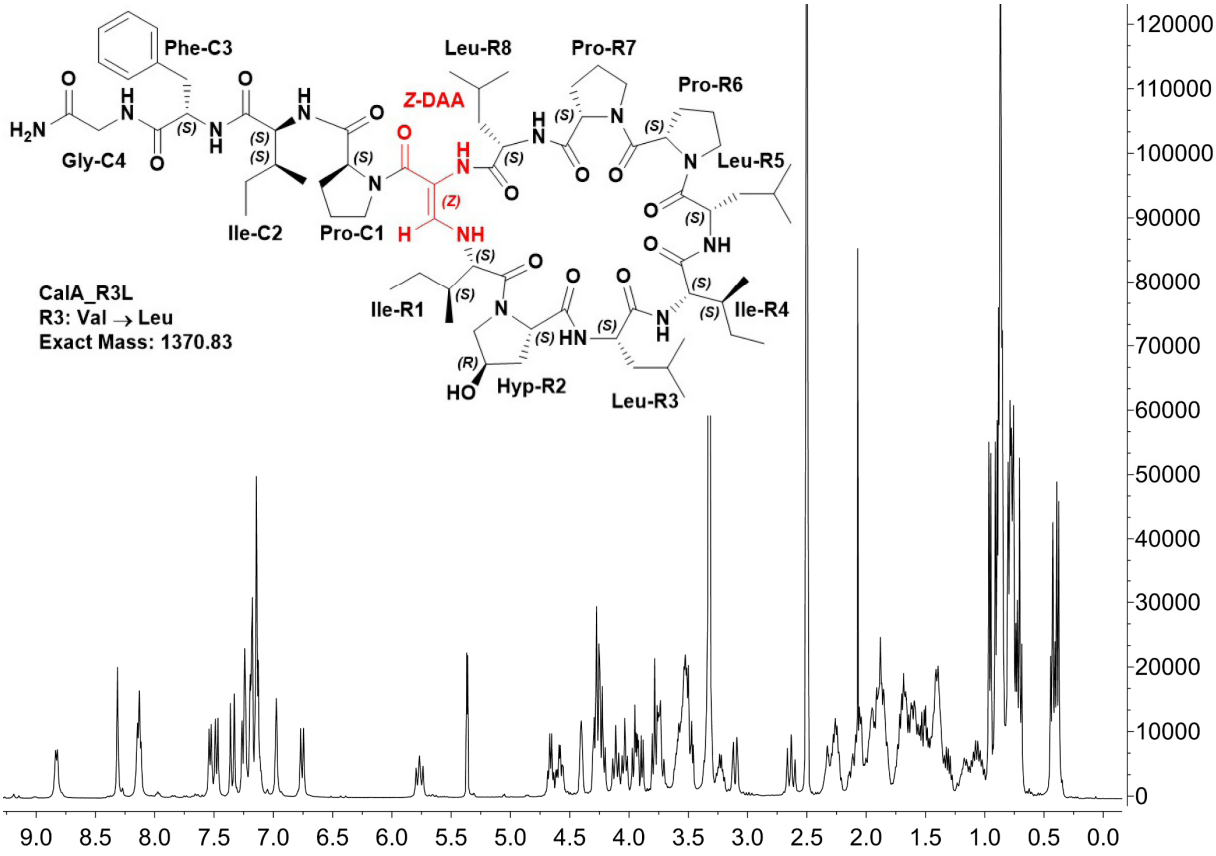

Figure 103: ^{1}H NMR spectrum (400 MHz, DMSO-d_6) of derivative *CalA_R3L*.

6.1.1.21 CalA_R4A

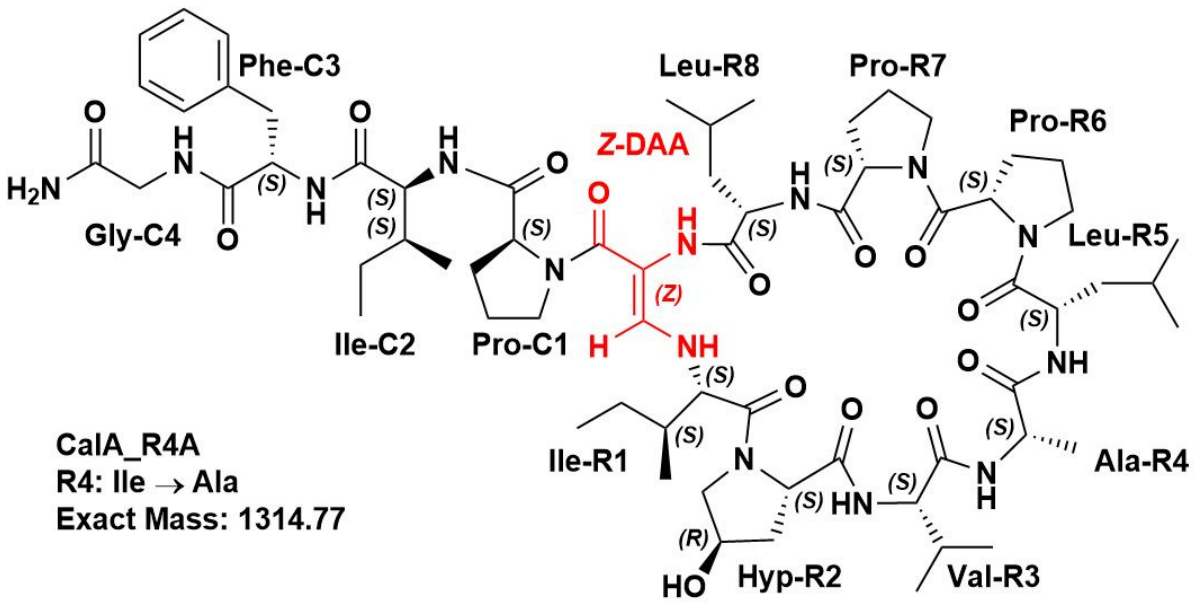

Figure 104: Chemical structure of derivative *CalA_R4A*

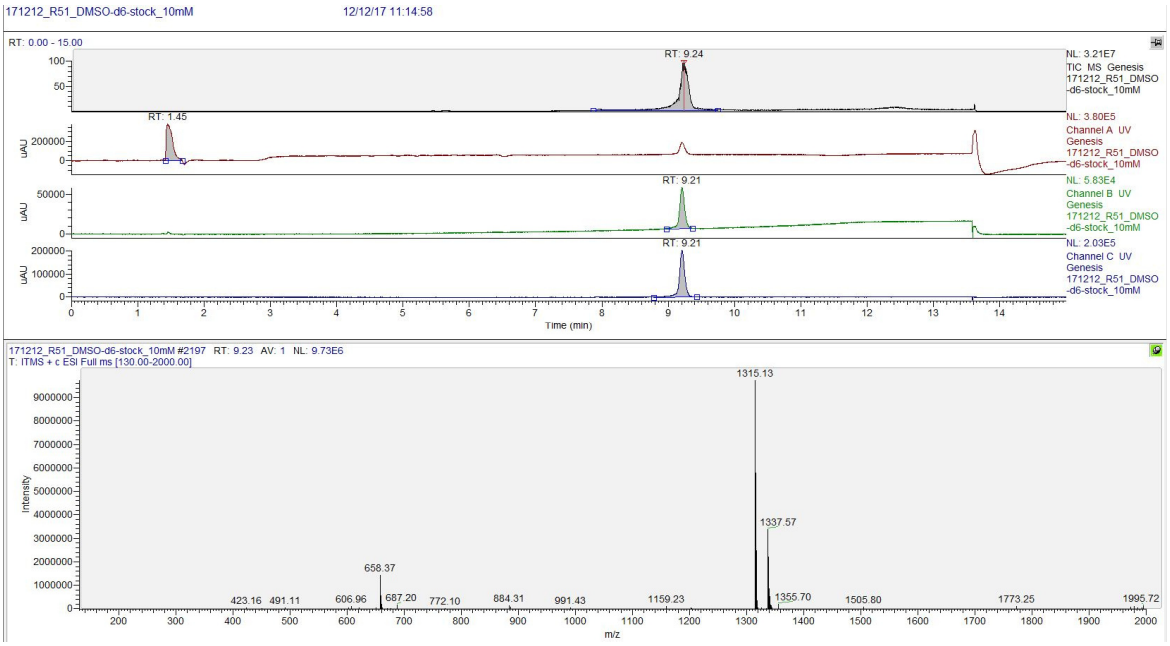

Figure 105: LC-MS spectrum of synthetic Callyaerin A derivative *CalA_R4A*. From top to bottom: TIC (ESI+), UV channel A (λ = 210 nm), UV channel B (λ = 254 nm), UV channel C (λ = 280 nm), mass spectrum of highest peak from chromatogram.

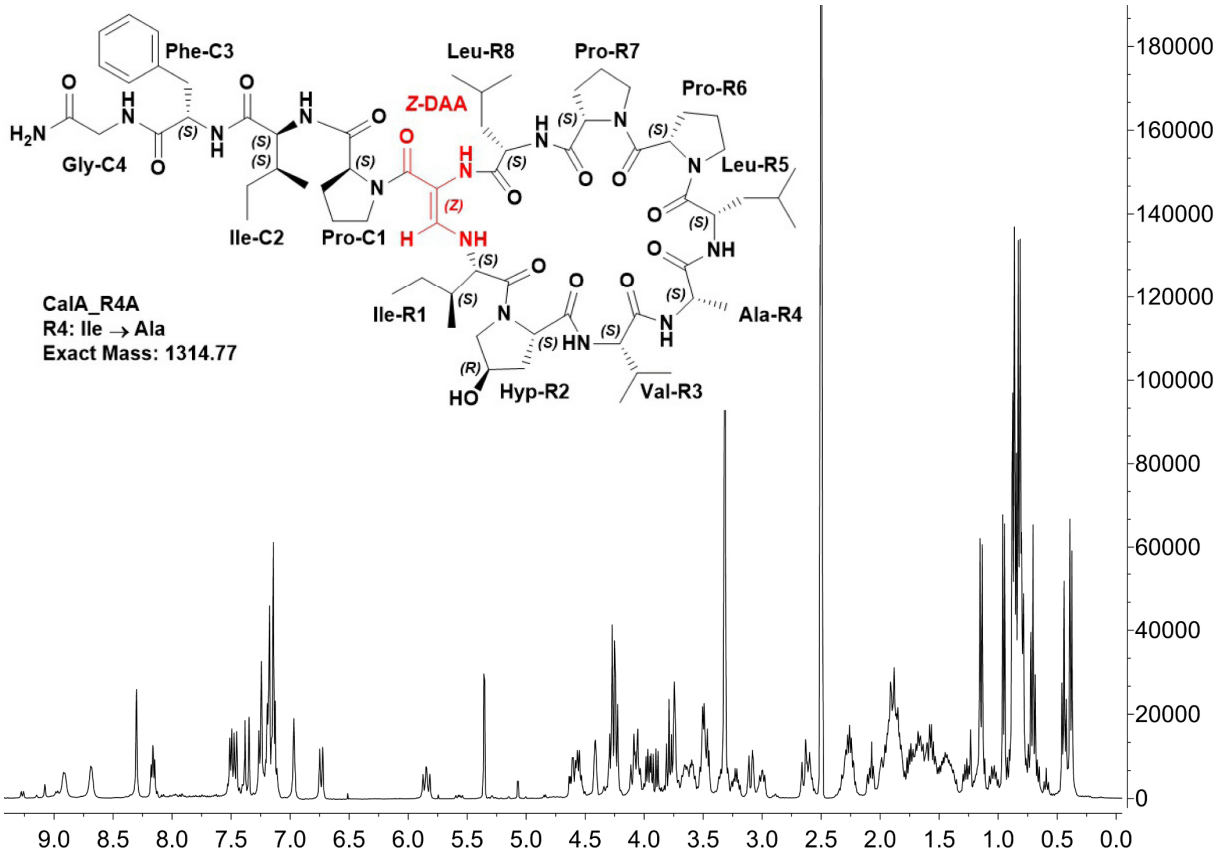

Figure 106: ^{1}H NMR spectrum (400 MHz, DMSO-d_6) of derivative *CalA_R4A*.

6.1.1.22 CalA_R5A

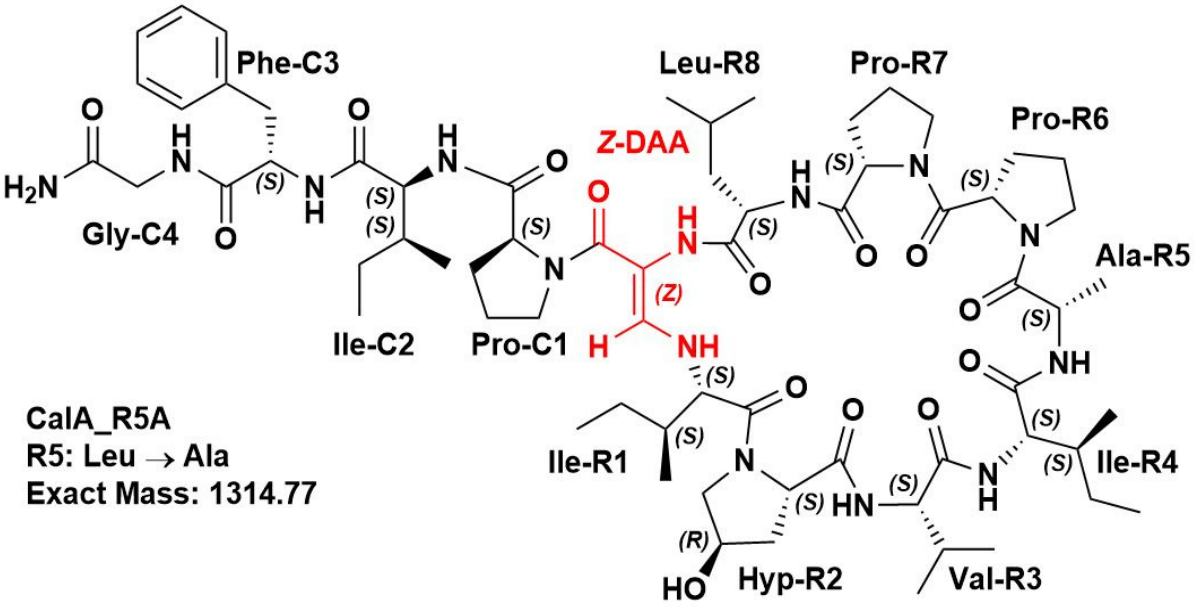

Figure 107: Chemical structure of derivative *CalA_R5A*

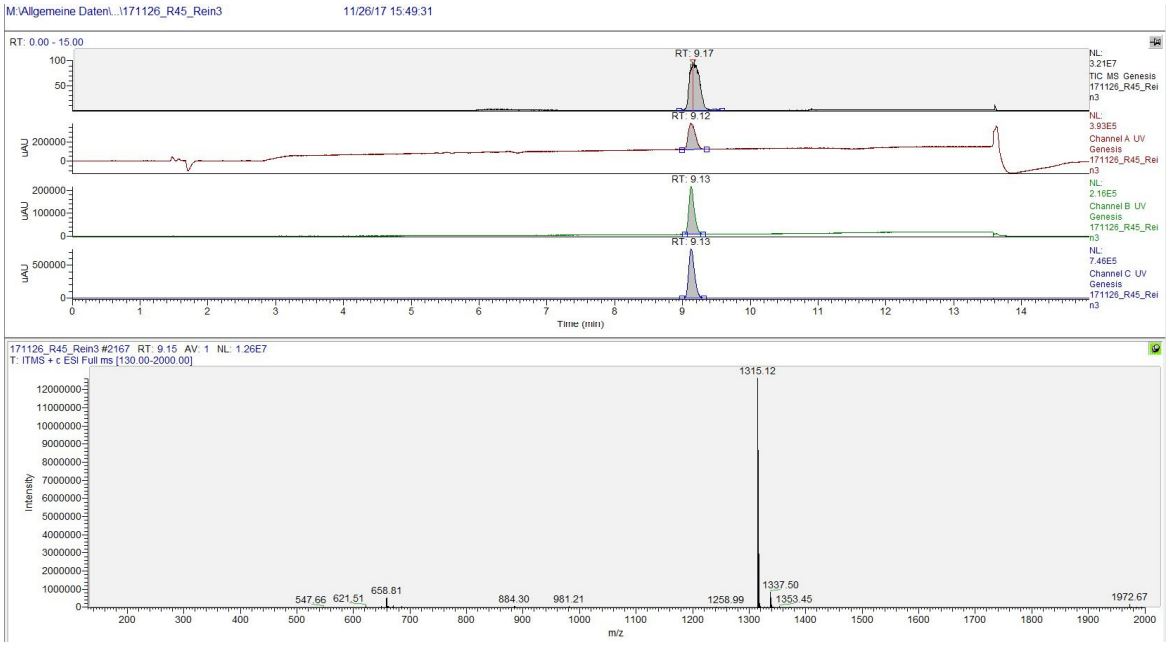

Figure 108: LC-MS spectrum of synthetic Callyaerin A derivative *CalA_R5A*. From top to bottom: TIC (ESI+), UV channel A (λ = 210 nm), UV channel B (λ = 254 nm), UV channel C (λ = 280 nm), mass spectrum of highest peak from chromatogram.

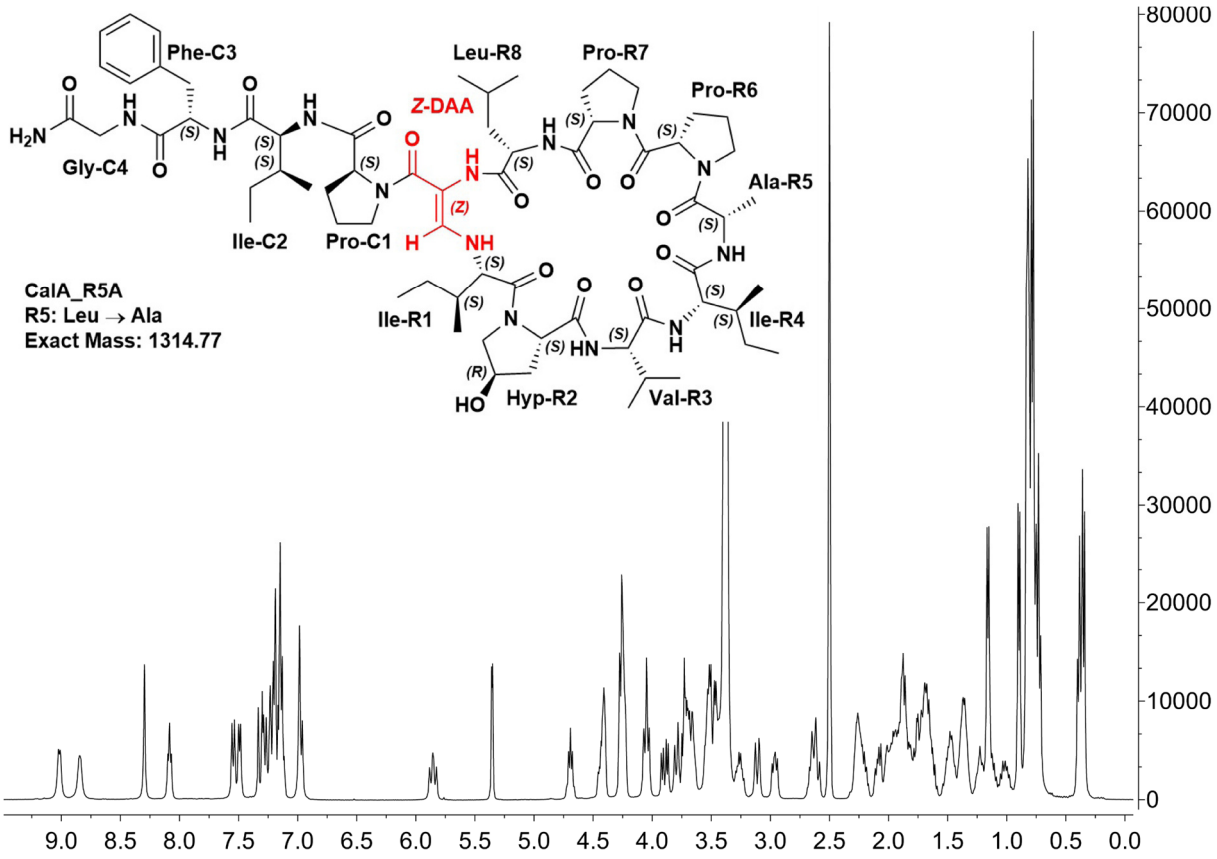

Figure 109: ^{1}H NMR spectrum (400 MHz, DMSO-d_6) of derivative *CalA_R5A*.

6.1.1.23 CalA_R5D

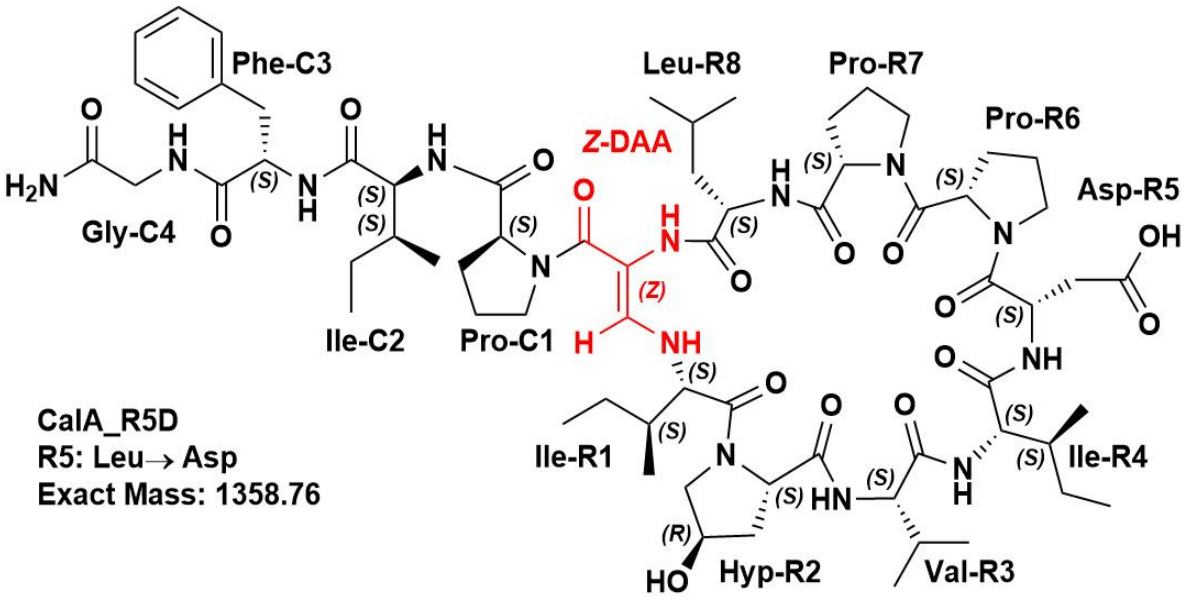

Figure 110: Chemical structure of derivative *CalA_R5D*

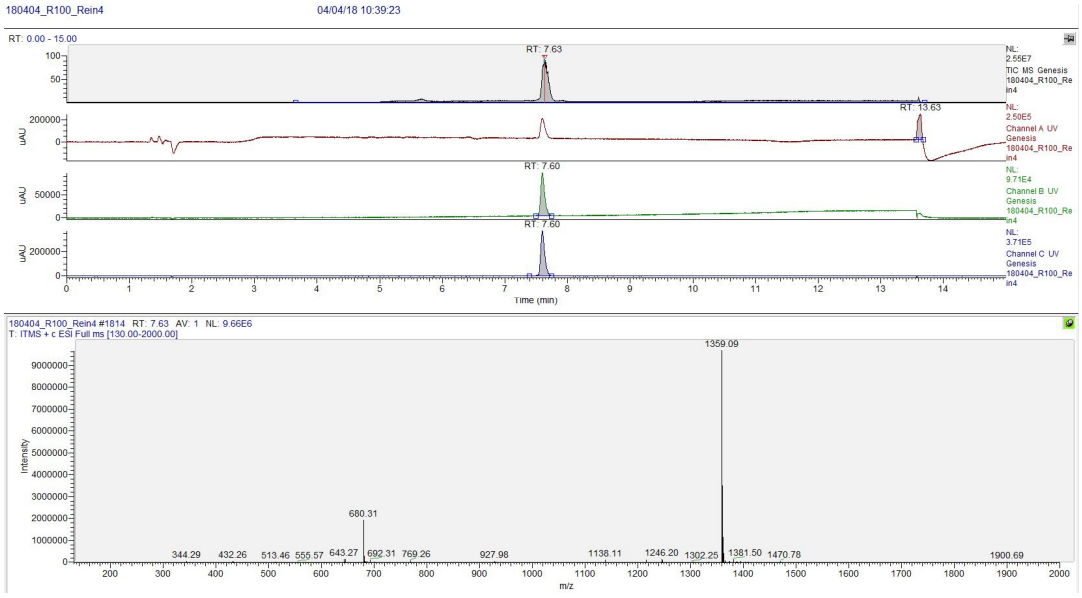

Figure 111: LC-MS spectrum of synthetic Callyaerin A derivative *CalA_R5D*. From top to bottom: TIC (ESI+), UV channel A (λ = 210 nm), UV channel B (λ = 254 nm), UV channel C (λ = 280 nm), mass spectrum of highest peak from chromatogram.

6.1.1.24 CalA_R6A

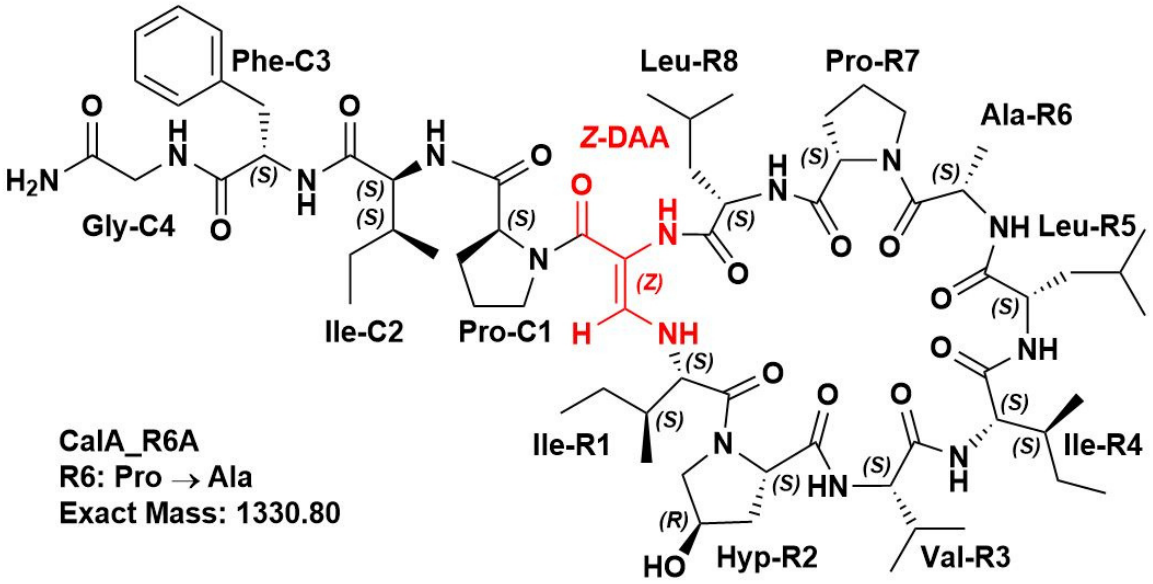

Figure 112: Chemical structure of derivative *CalA_R6A*

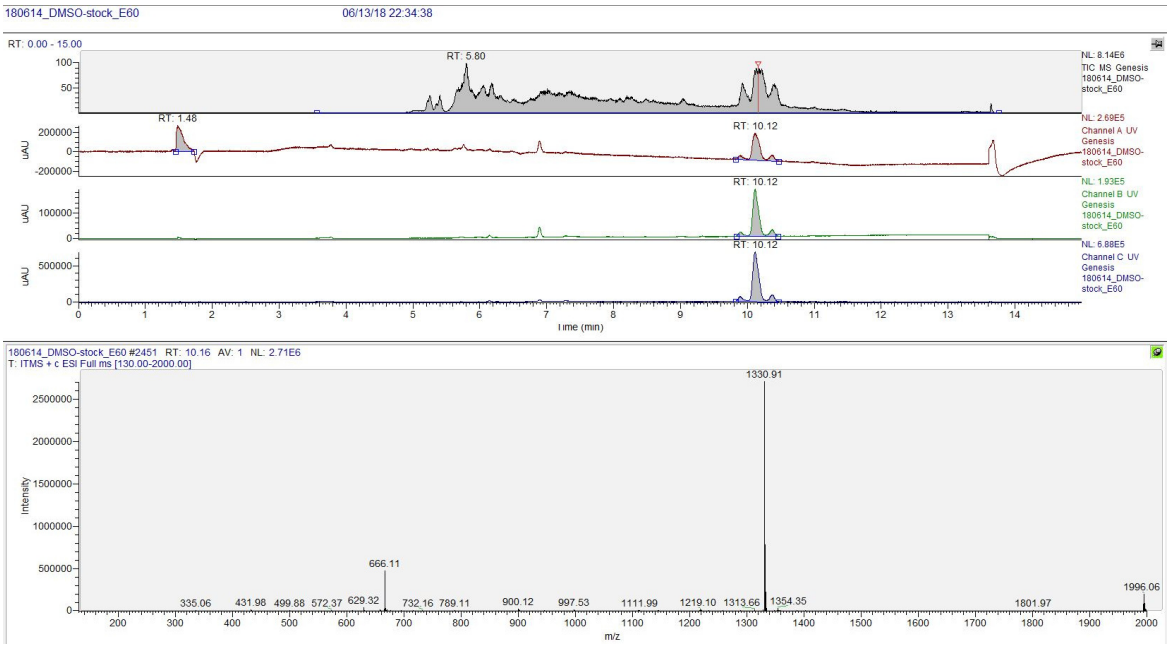

Figure 113: LC-MS spectrum of synthetic Callyaerin A derivative *CalA_R6A*. From top to bottom: TIC (ESI+), UV channel A (λ = 210 nm), UV channel B (λ = 254 nm), UV channel C (λ = 280 nm), mass spectrum of highest peak from chromatogram.

6.1.1.25 CalA_R7A

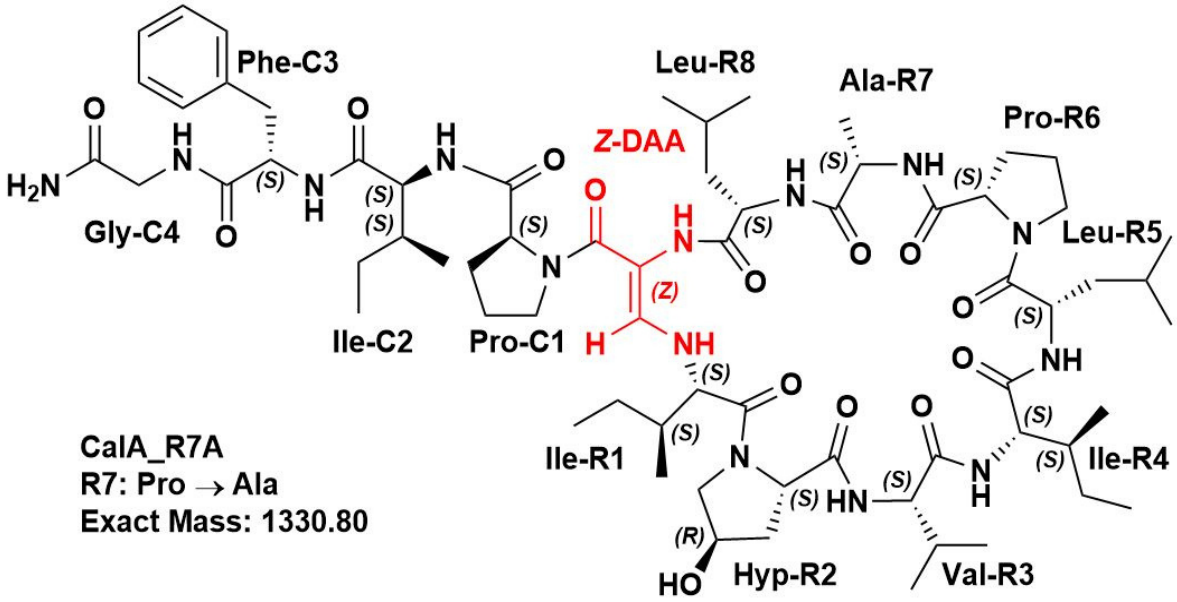

Figure 114: Chemical structure of derivative *CalA_R7A*

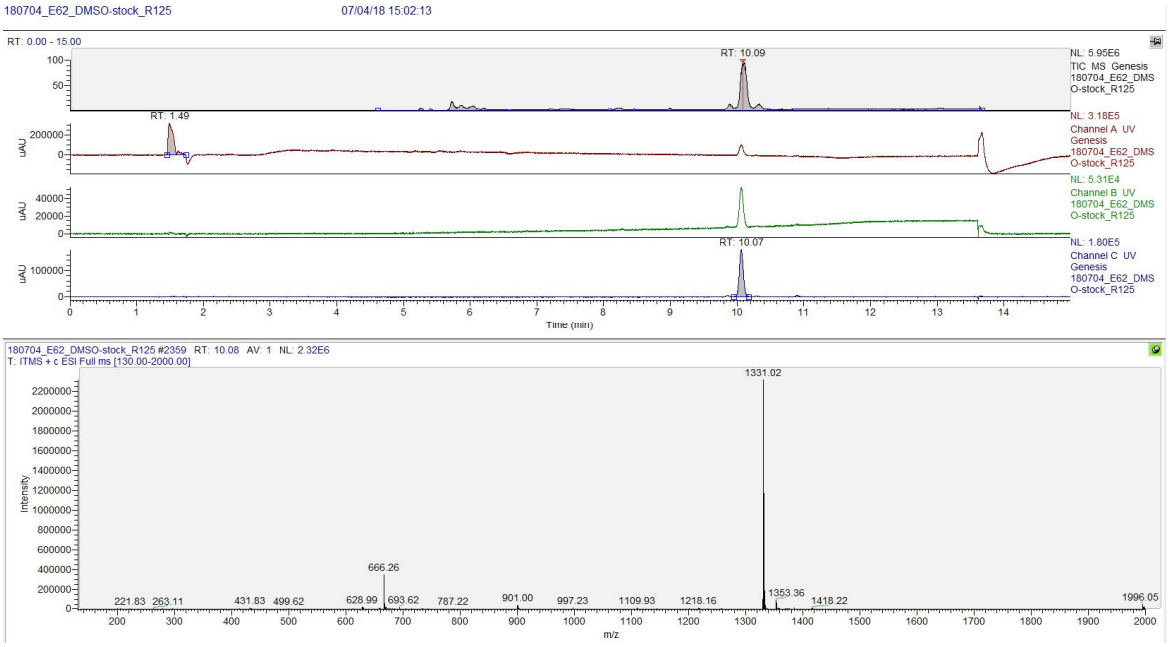

Figure 115: LC-MS spectrum of synthetic Callyaerin A derivative *CalA_R7A*. From top to bottom: TIC (ESI+), UV channel A (λ = 210 nm), UV channel B (λ = 254 nm), UV channel C (λ = 280 nm), mass spectrum of highest peak from chromatogram.

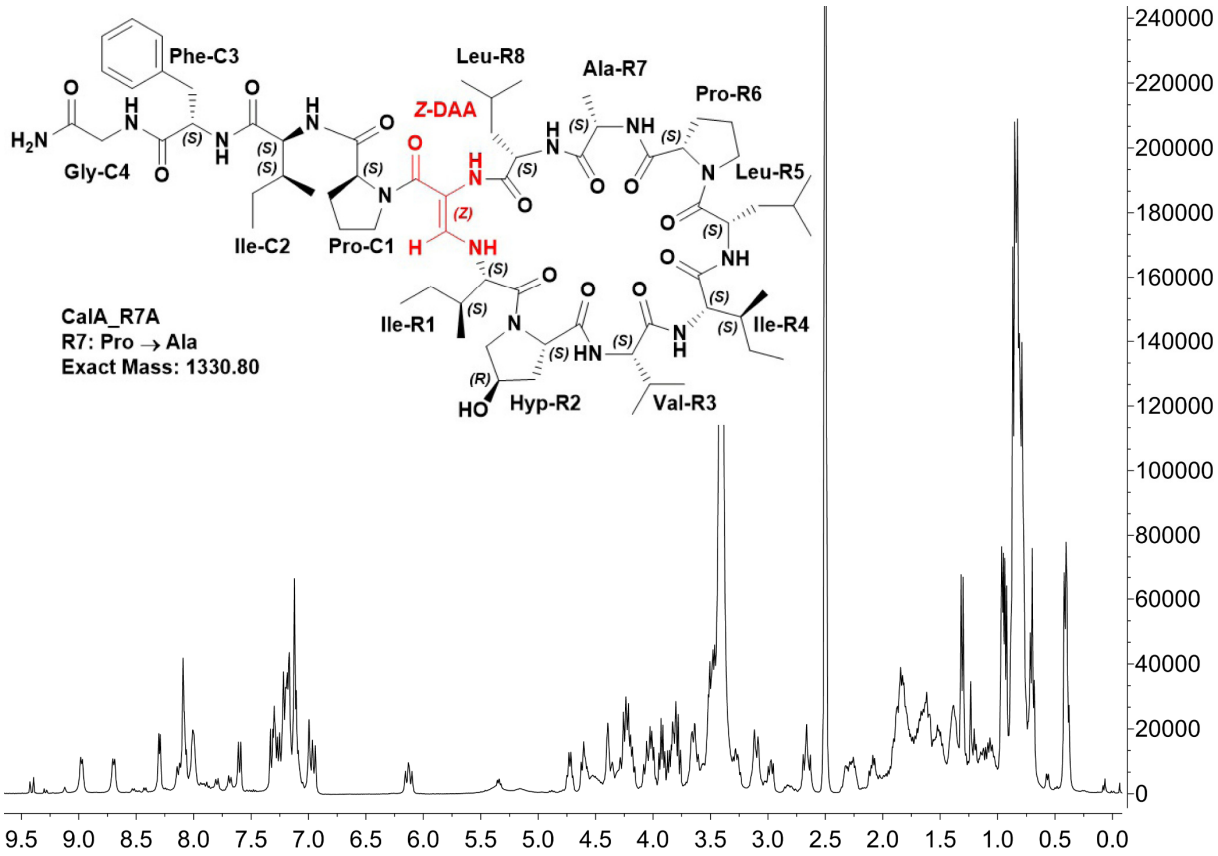

Figure 116: ^{1}H NMR spectrum (400 MHz, DMSO-d_6) of derivative *CalA_R7A*.

6.1.1.26 CalA_R8A

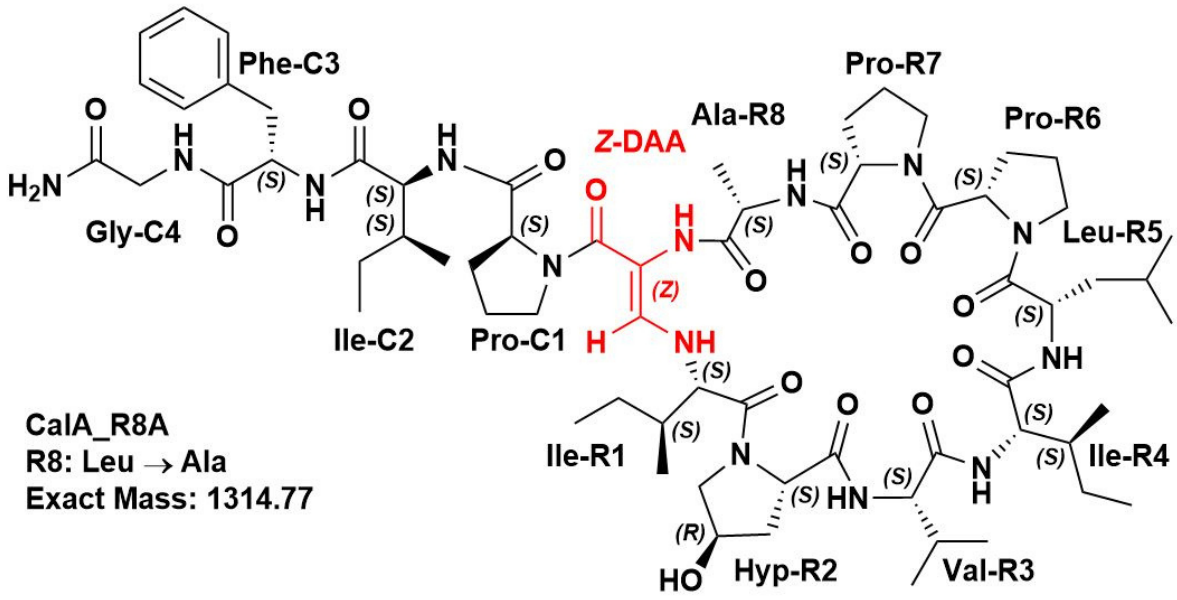

Figure 117: Chemical structure of derivative *CalA_R8A*

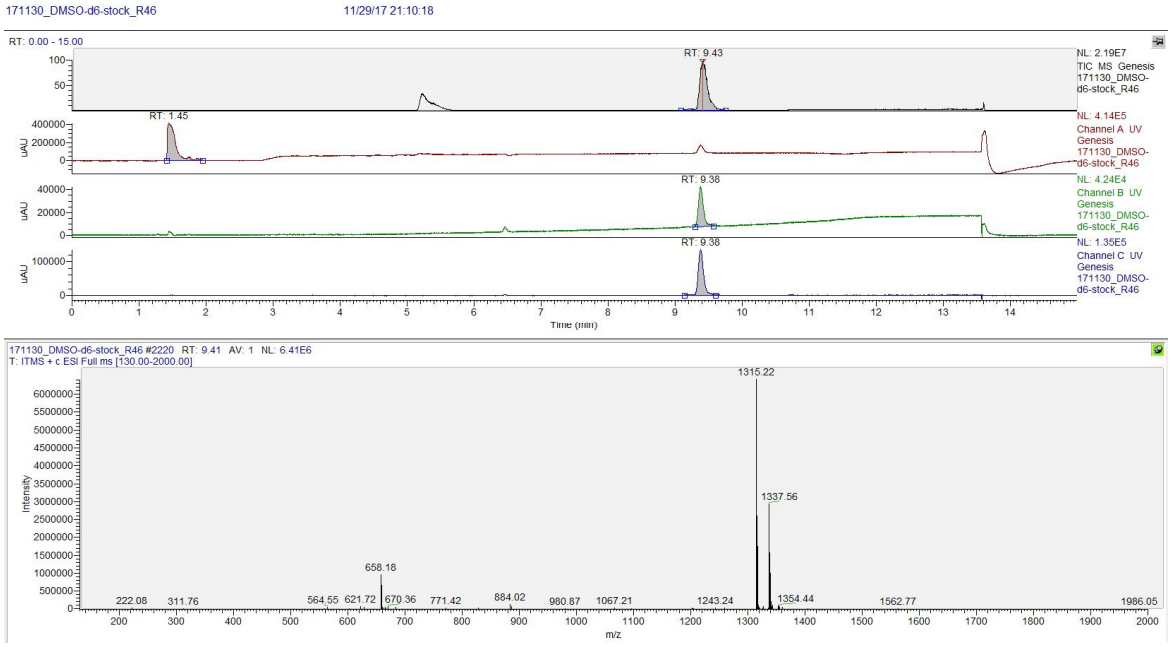

Figure 118: LC-MS spectrum of synthetic Callyaerin A derivative *CalA_R8A*. From top to bottom: TIC (ESI+), UV channel A (λ = 210 nm), UV channel B (λ = 254 nm), UV channel C (λ = 280 nm), mass spectrum of highest peak from chromatogram.

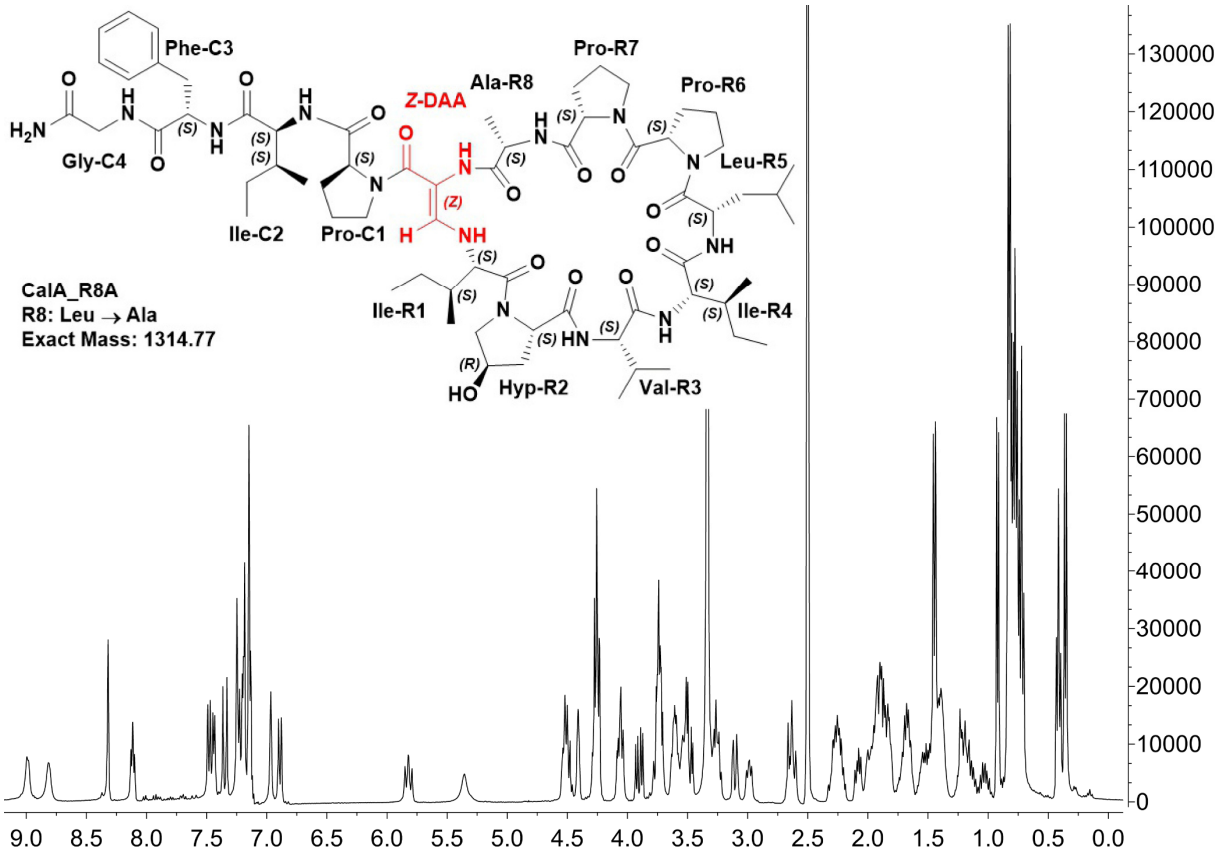

Figure 119: ^{1}H NMR spectrum (400 MHz, DMSO-d_6) of derivative *CalA_R8A*.

6.1.1.27 CalA_R8W

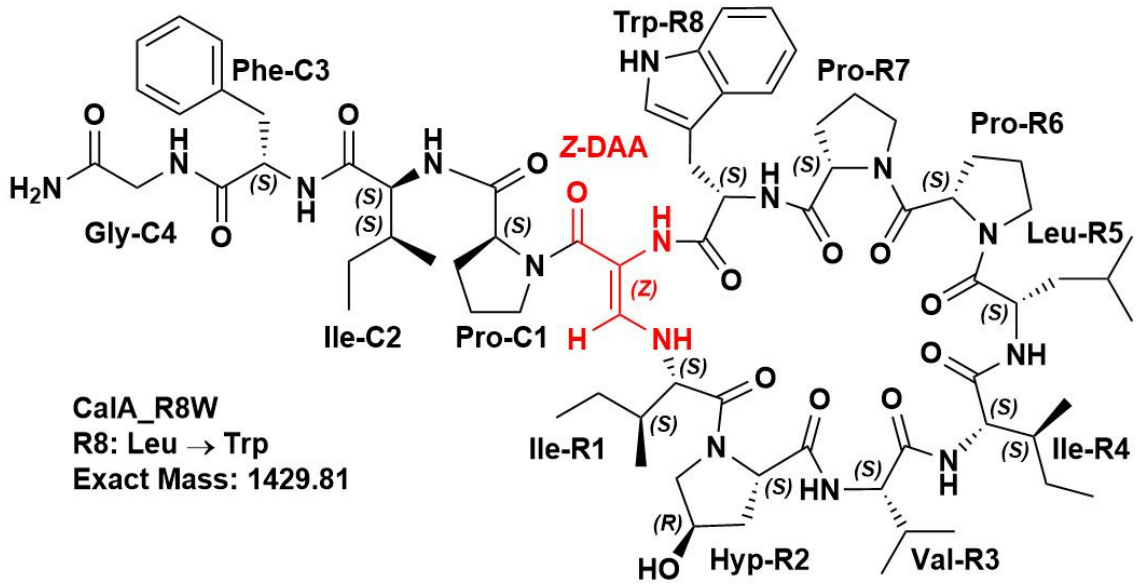

Figure 120: Chemical structure of derivative *CalA_R8W*

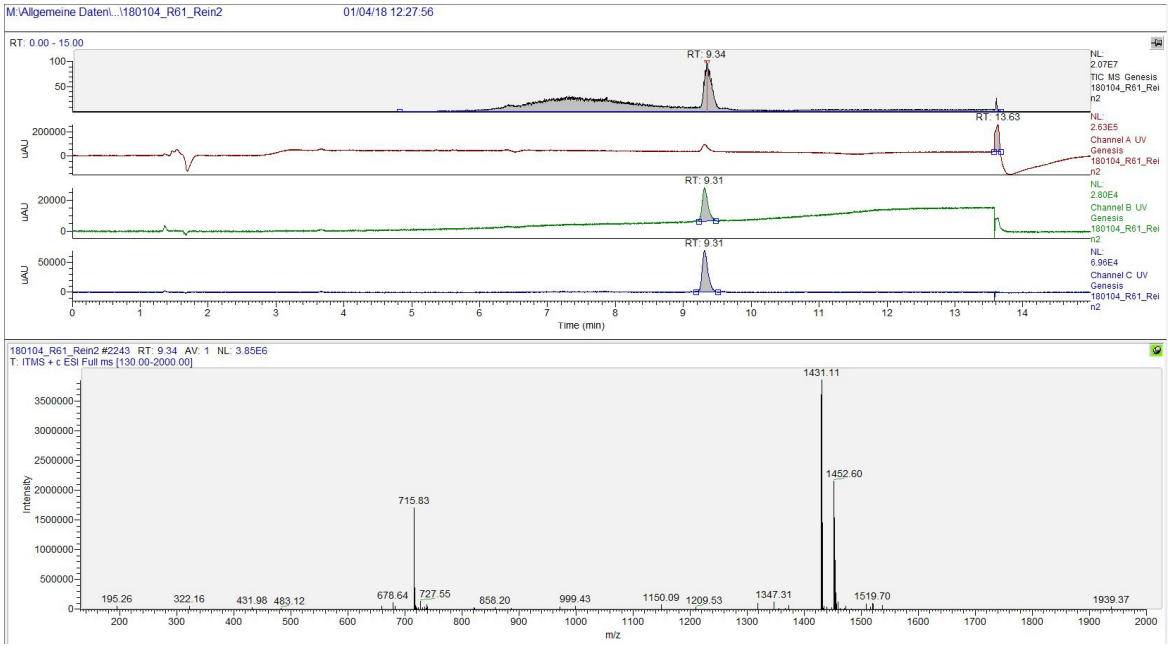

Figure 121: LC-MS spectrum of synthetic Callyaerin A derivative *CalA_R8W*. From top to bottom: TIC (ESI+), UV channel A (λ = 210 nm), UV channel B (λ = 254 nm), UV channel C (λ = 280 nm), mass spectrum of highest peak from chromatogram.

6.1.1.28 CalA_R8V

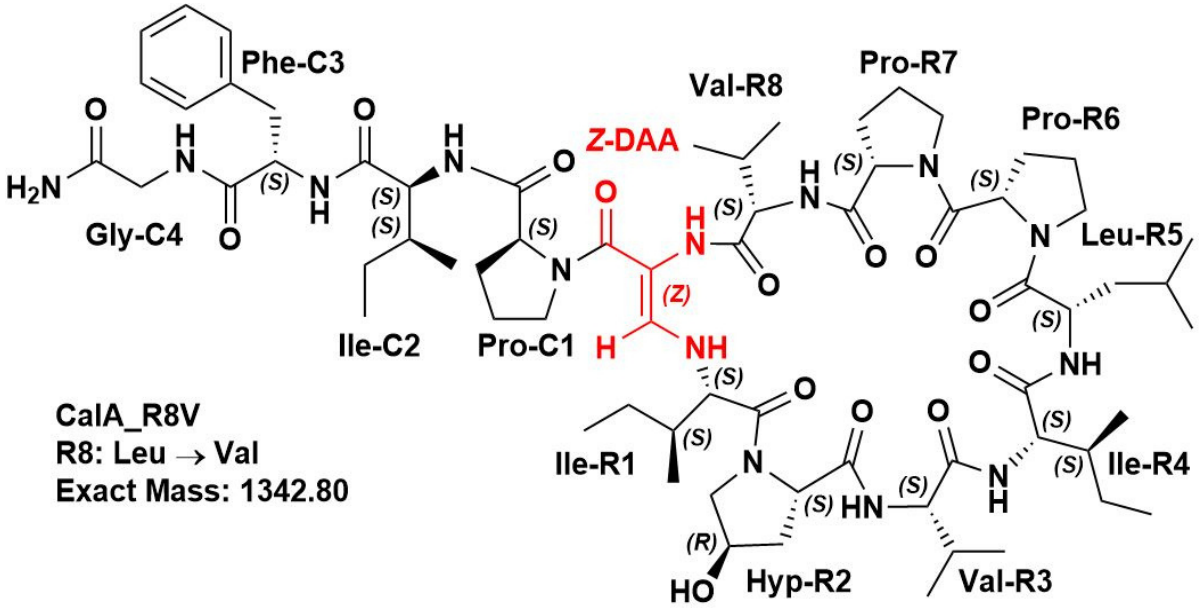

Figure 122: Chemical structure of derivative *CalA_R8V*

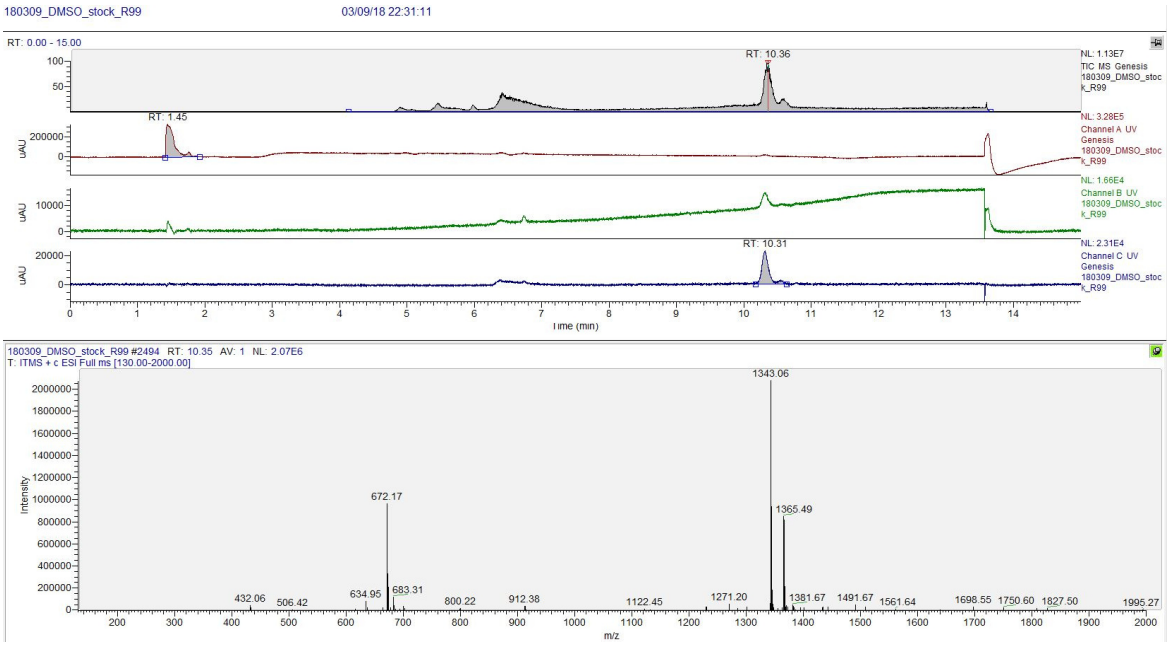

Figure 123: LC-MS spectrum of synthetic Callyaerin A derivative *CalA_R8V*. From top to bottom: TIC (ESI+), UV channel A (λ = 210 nm), UV channel B (λ = 254 nm), UV channel C (λ = 280 nm), mass spectrum of highest peak from chromatogram.

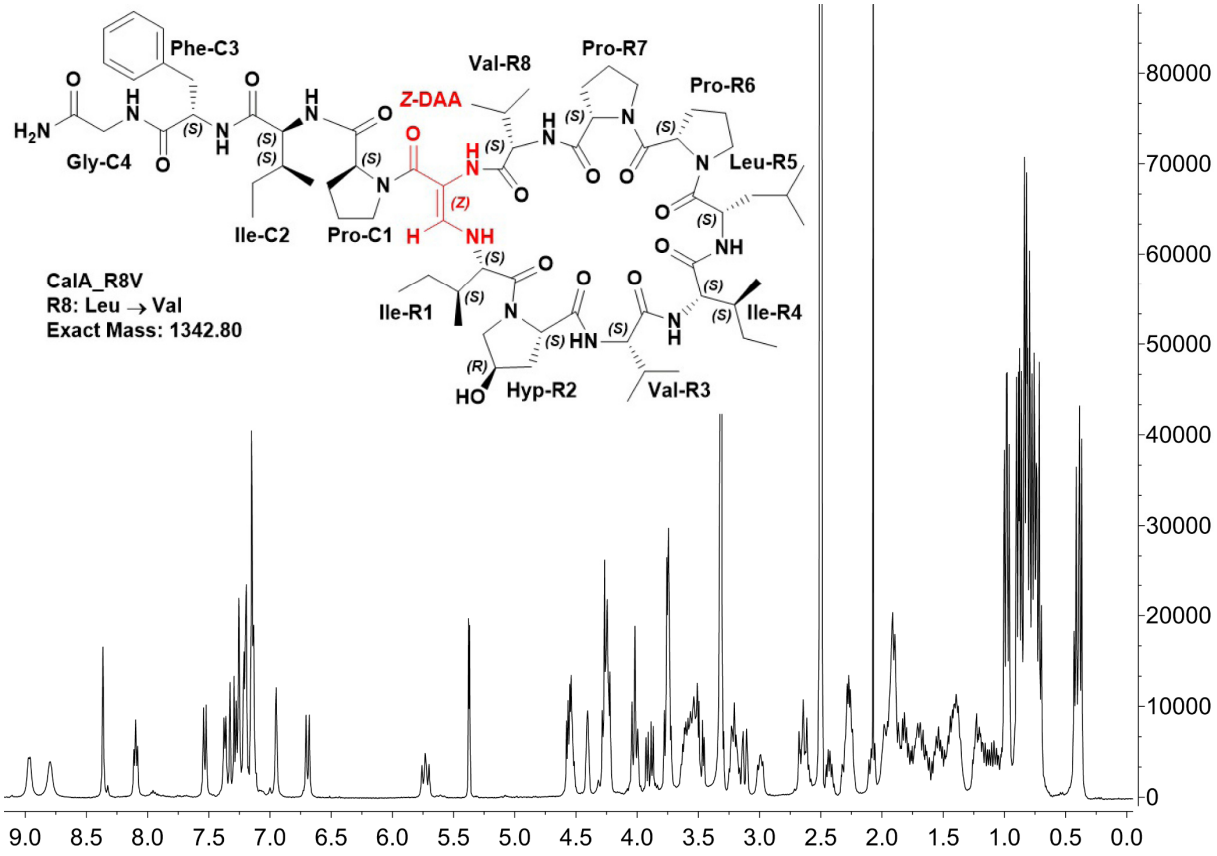

Figure 124: ^{1}H NMR spectrum (400 MHz, DMSO-d_6) of derivative *CalA_R8V*.

6.1.1.29 CalA_C1A

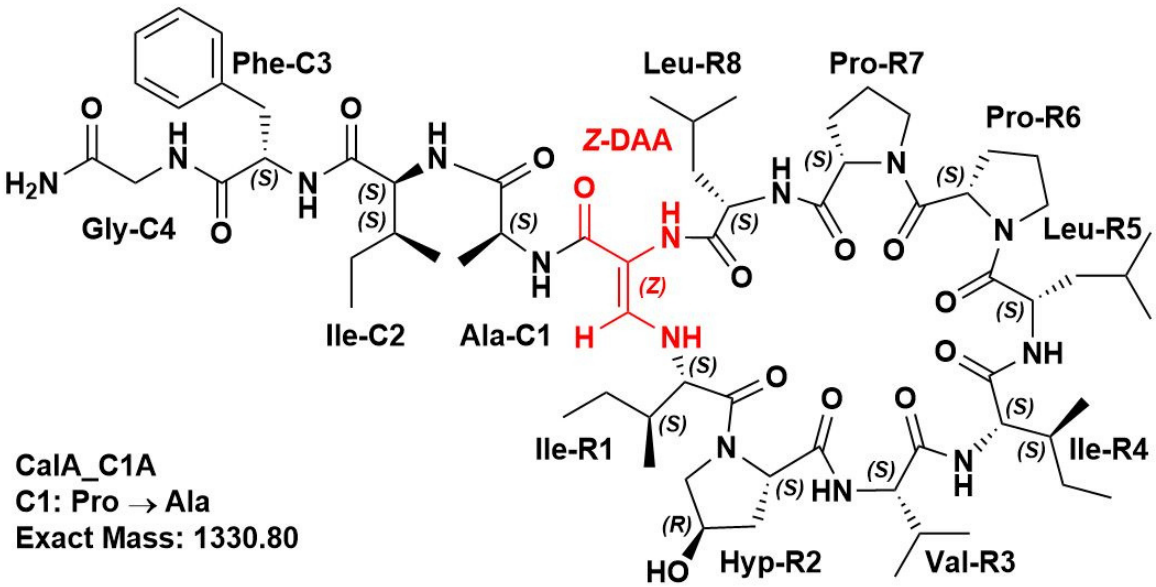

Figure 125: Chemical structure of derivative *CalA_C1A*

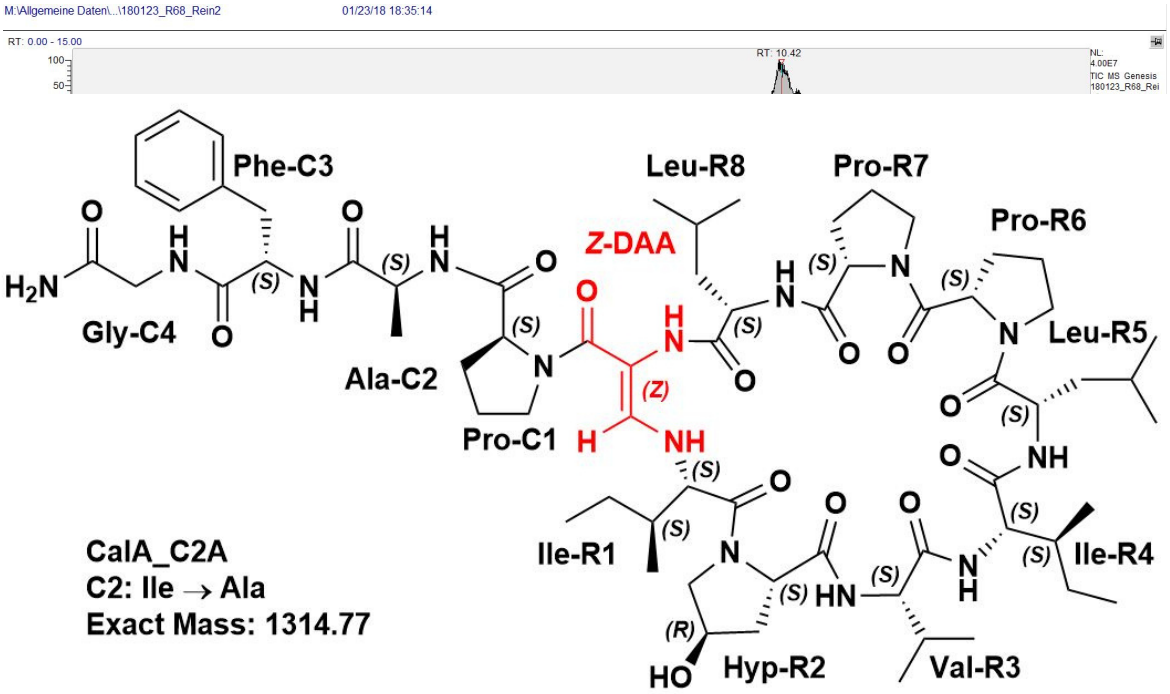

(ESI+), UV channel A (λ = 210 nm), UV channel B (λ = 254 nm), UV channel C (λ = 280 nm), mass

Figure 127: Chemical structure of derivative *CalA_C2A*

6.1.1.30 CalA_C2A

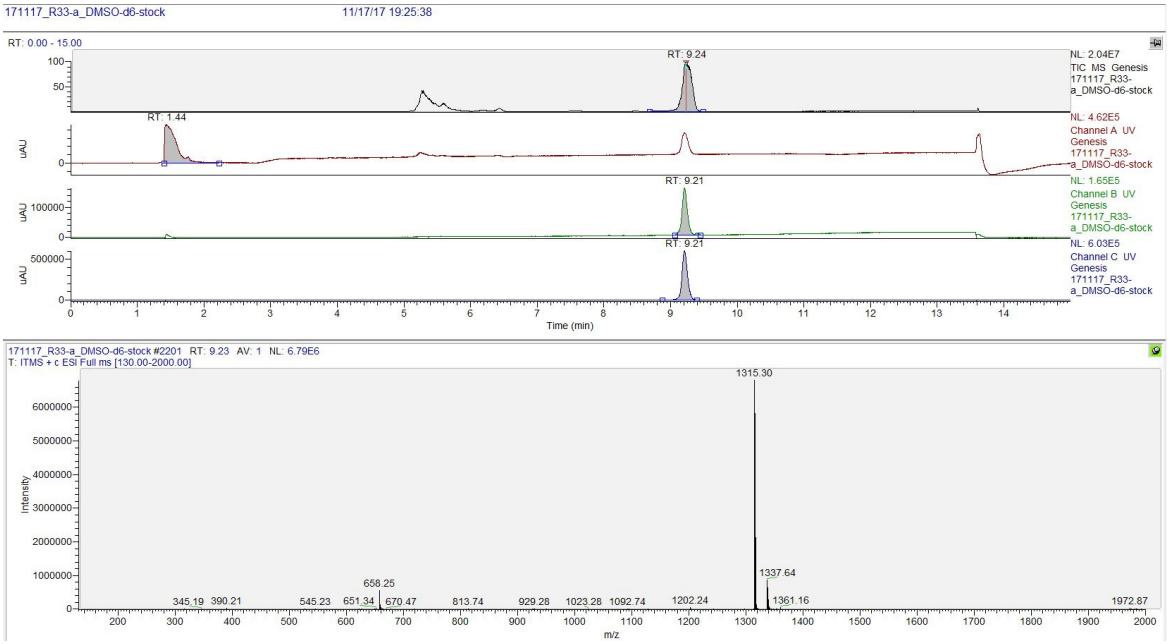

Figure 128: LC-MS spectrum of synthetic Callyaerin A derivative *CalA_C2A*. From top to bottom: TIC (ESI+), UV channel A (λ = 210 nm), UV channel B (λ = 254 nm), UV channel C (λ = 280 nm), mass spectrum of highest peak from chromatogram.

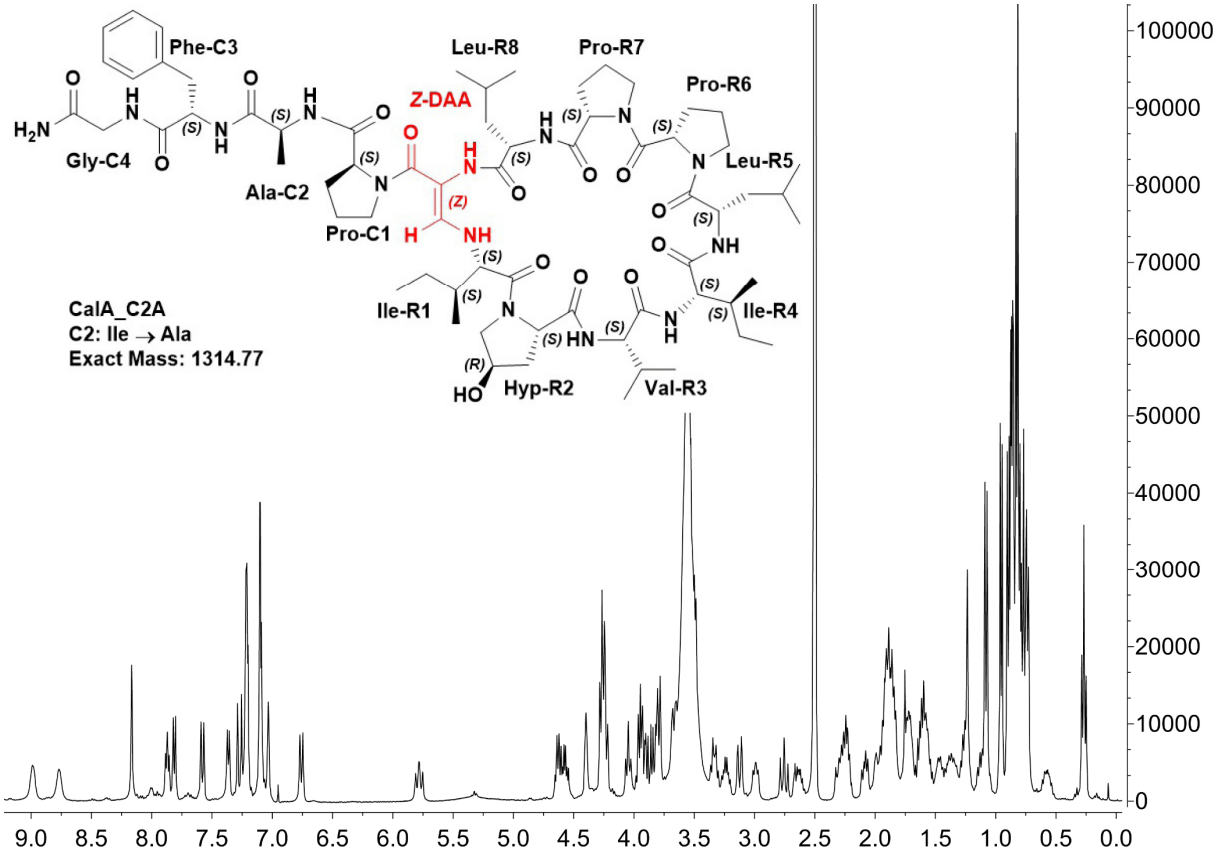

Figure 129: ^{1}H NMR spectrum (400 MHz, DMSO-d_6) of derivative *CalA_C2A*.

6.1.1.31 CalA_C3A

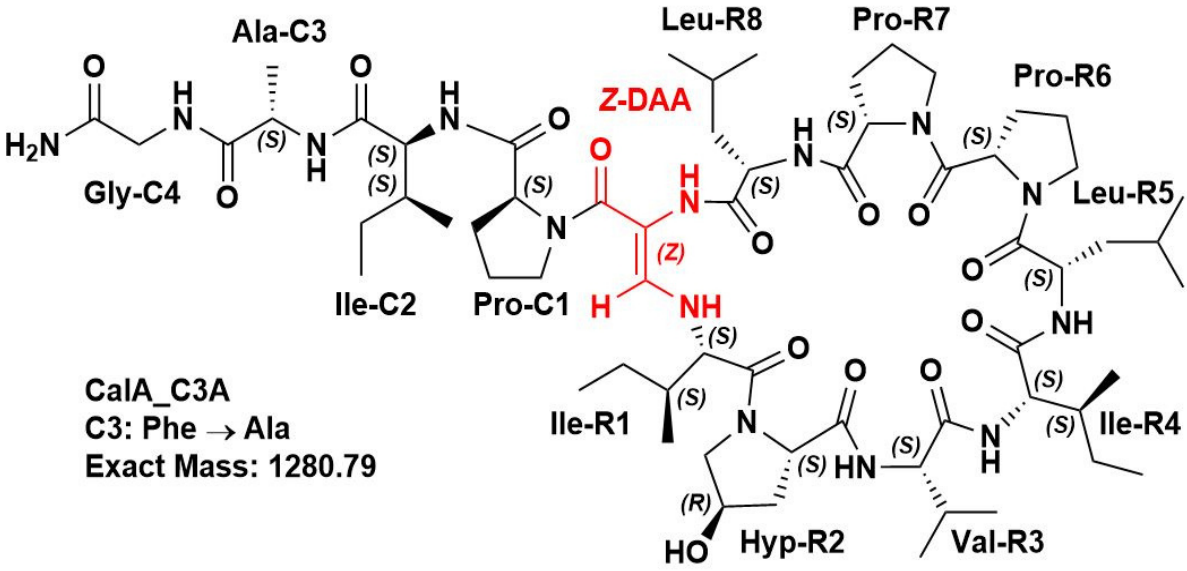

Figure 130: Chemical structure of derivative *CalA_C3A*

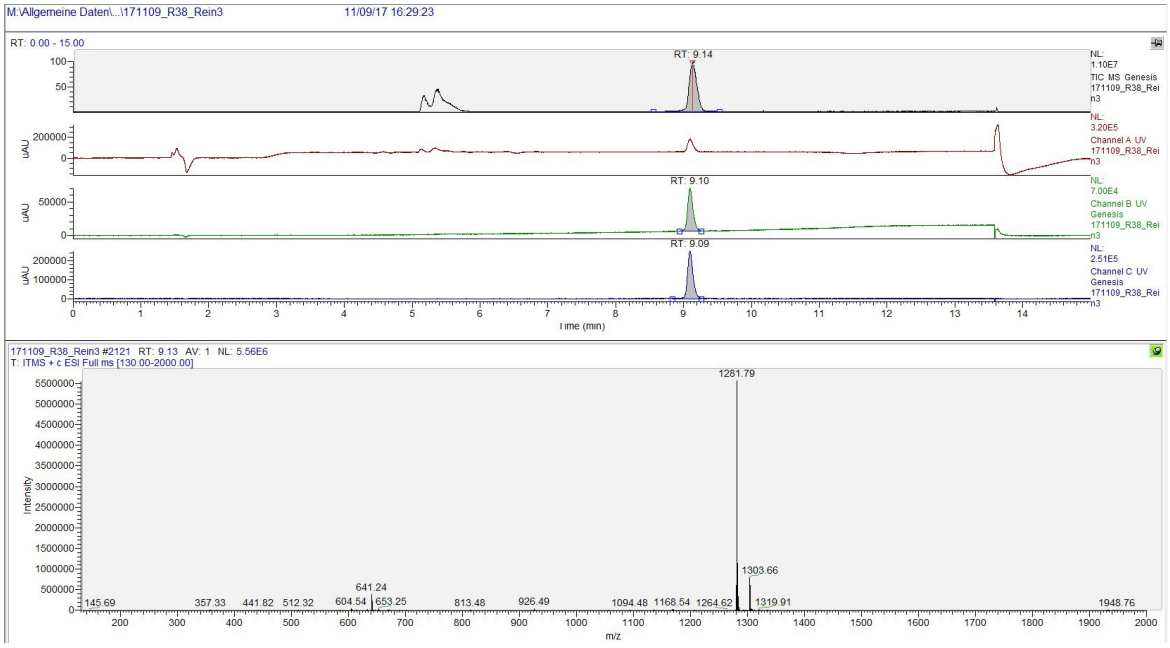

Figure 131: LC-MS spectrum of synthetic Callyaerin A derivative *CalA_C3A*. From top to bottom: TIC (ESI+), UV channel A (λ = 210 nm), UV channel B (λ = 254 nm), UV channel C (λ = 280 nm), mass spectrum of highest peak from chromatogram.

6.1.1.32 CalA_C3L

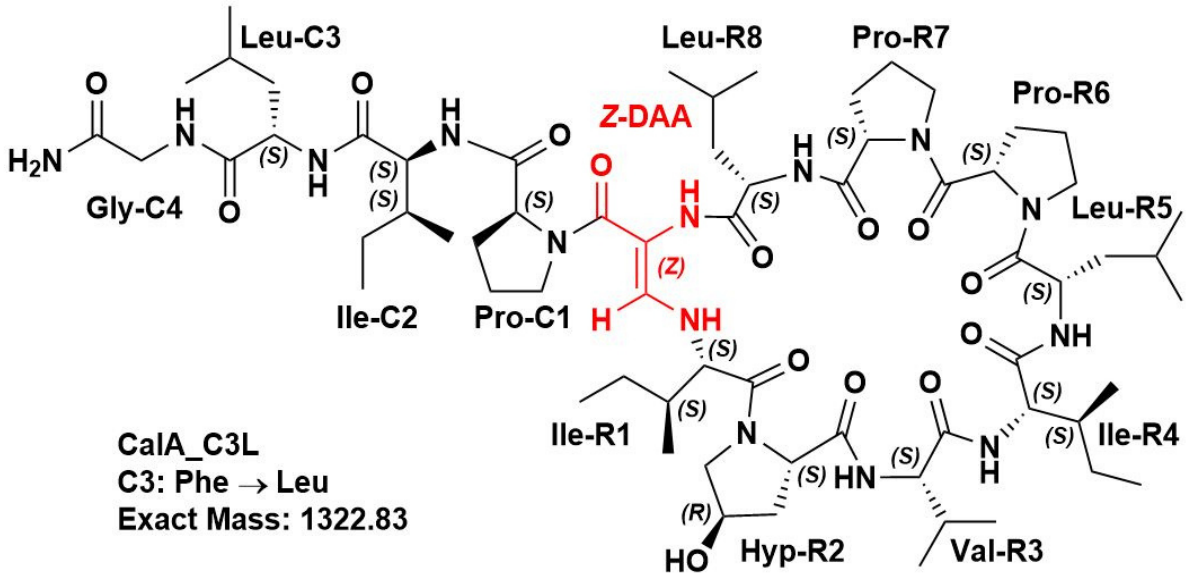

Figure 132: Chemical structure of derivative *CalA_C3L*

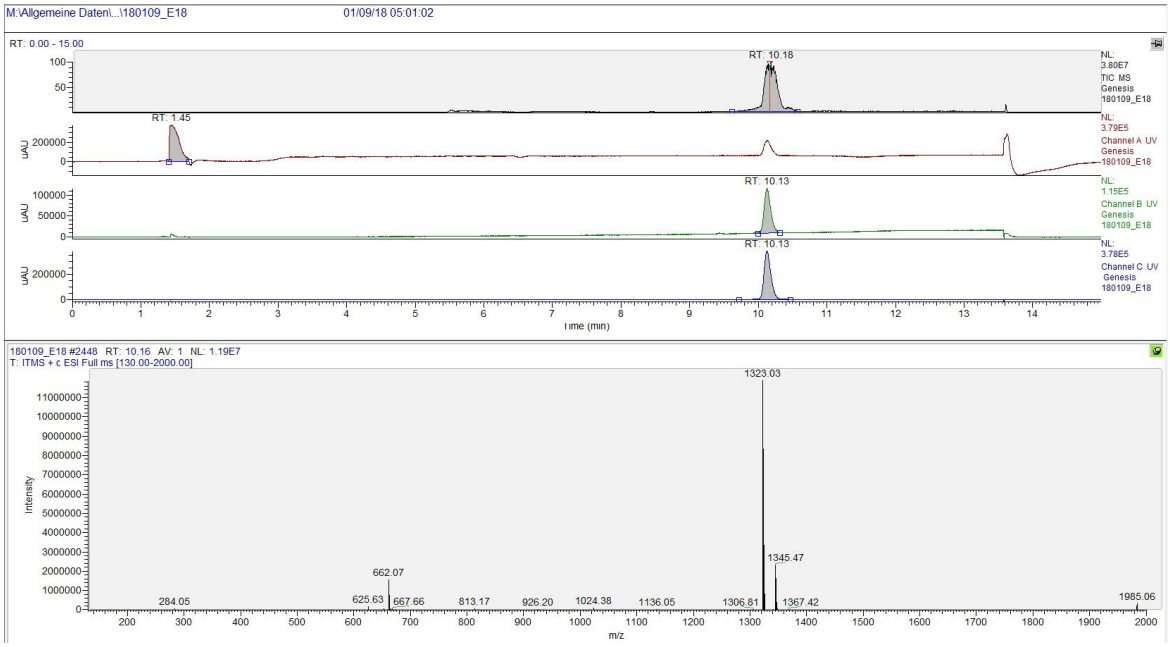

Figure 133: LC-MS spectrum of synthetic Callyaerin A derivative *CalA_C3L*. From top to bottom: TIC (ESI+), UV channel A (λ = 210 nm), UV channel B (λ = 254 nm), UV channel C (λ = 280 nm), mass spectrum of highest peak from chromatogram.

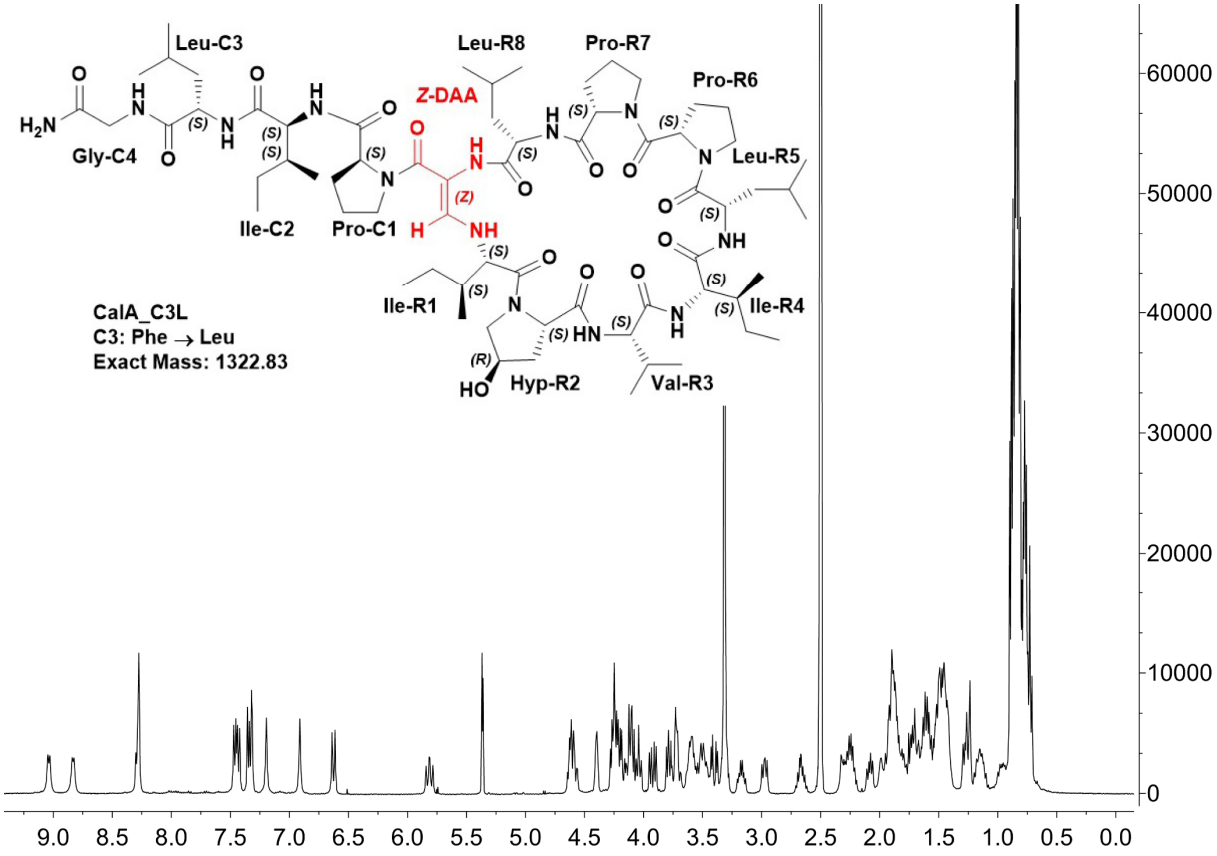

Figure 134: ^{1}H NMR spectrum (400 MHz, DMSO-d_6) of derivative *CalA_C3L*.

6.1.1.33 CalA_C3I

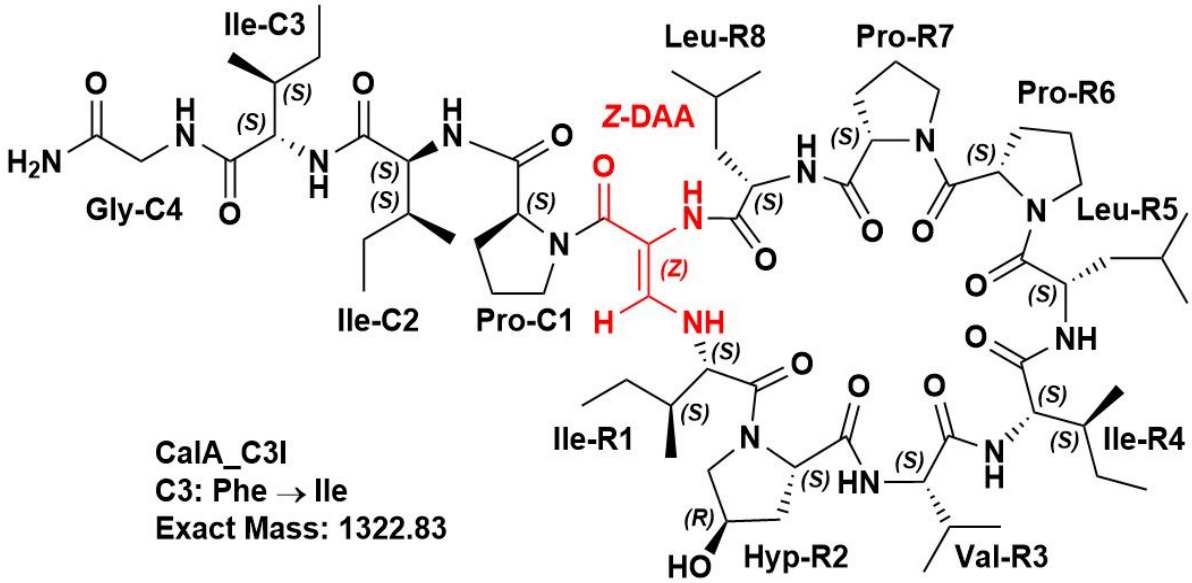

Figure 135: Chemical structure of derivative *CalA_C3I*

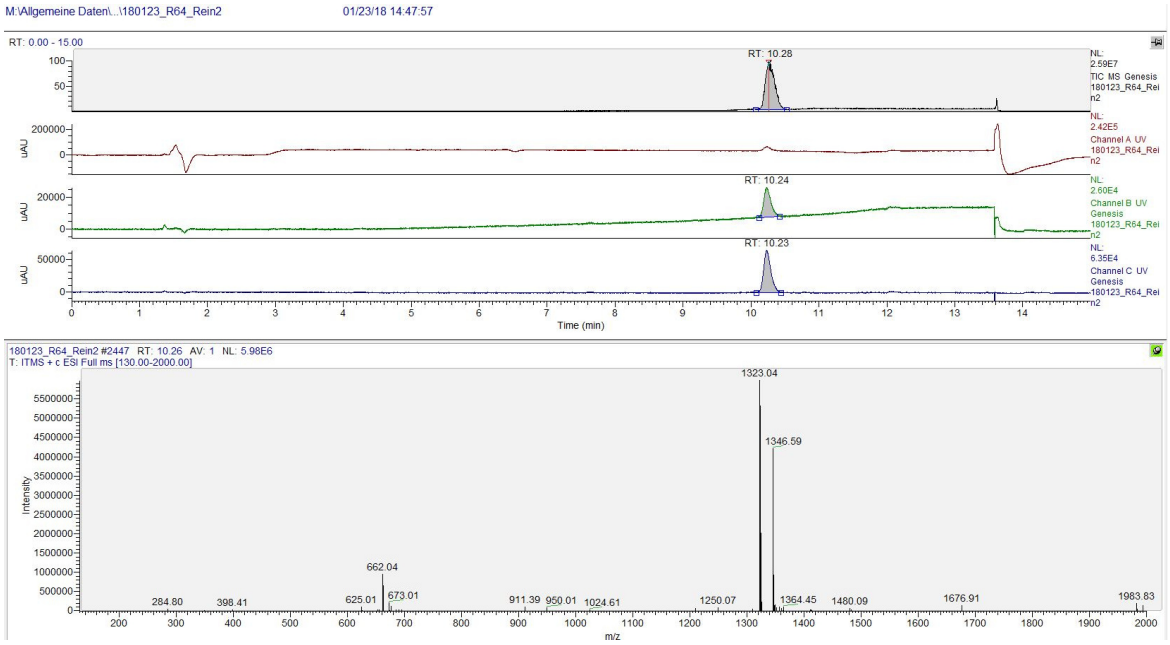

Figure 136: LC-MS spectrum of synthetic Callyaerin A derivative *CalA_C3I*. From top to bottom: TIC (ESI+), UV channel A (λ = 210 nm), UV channel B (λ = 254 nm), UV channel C (λ = 280 nm), mass spectrum of highest peak from chromatogram.

6.1.1.34 *CalA_C3W*

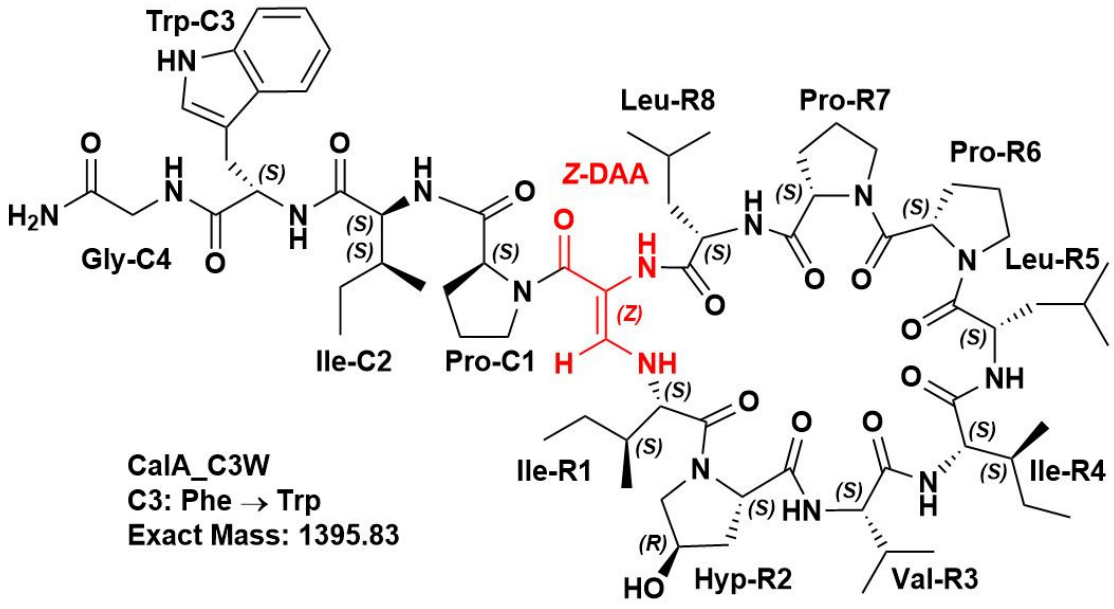

Figure 137: Chemical structure of derivative *CalA_C3W*

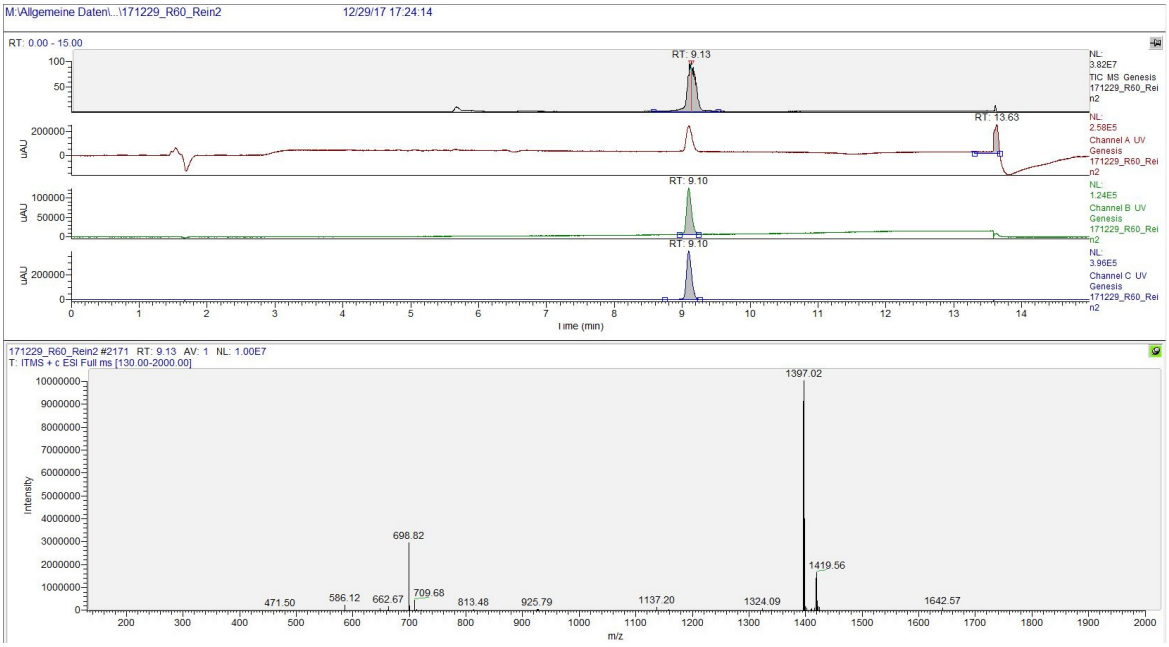

Figure 138: LC-MS spectrum of synthetic Callyaerin A derivative *CalA_C3W*. From top to bottom: TIC (ESI+), UV channel A (λ = 210 nm), UV channel B (λ = 254 nm), UV channel C (λ = 280 nm), mass spectrum of highest peak from chromatogram.

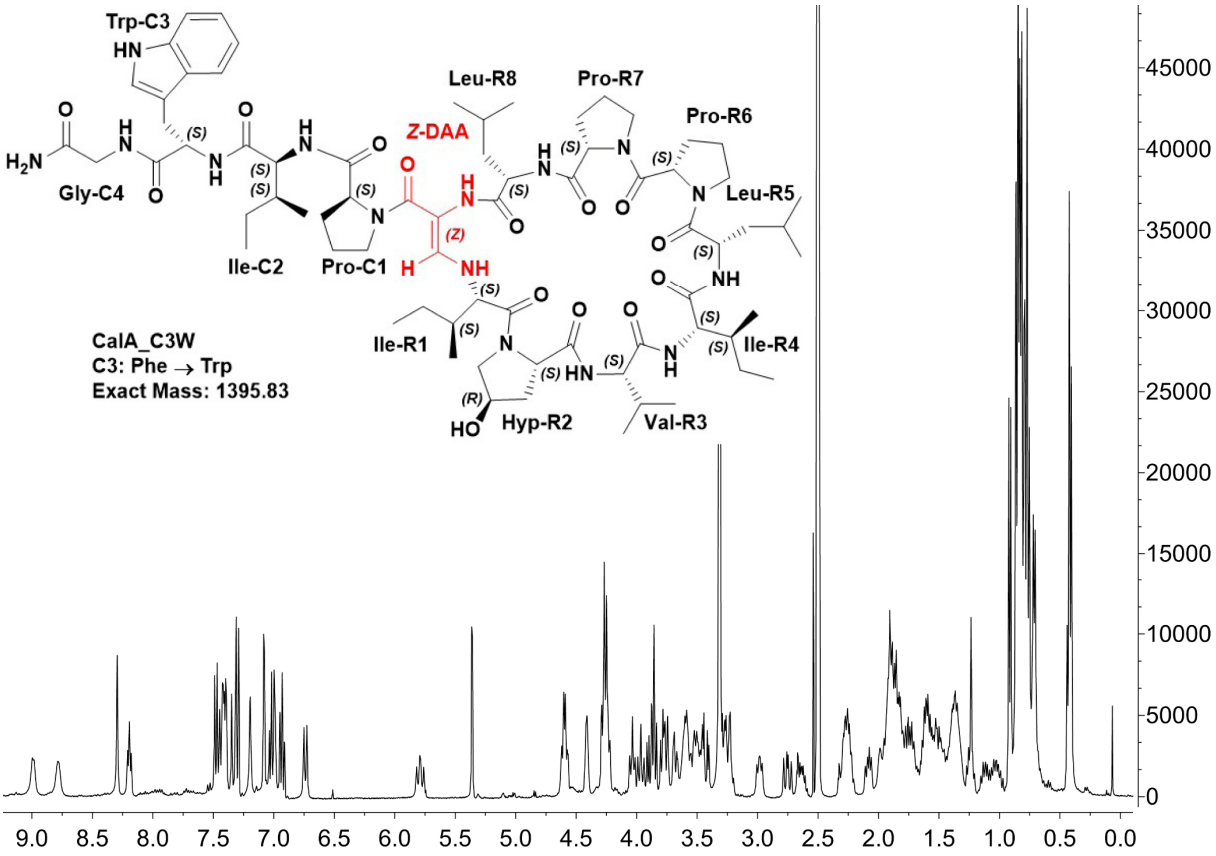

Figure 139: ^{1}H NMR spectrum (400 MHz, DMSO-d_6) of derivative *CalA_C3W*.

6.1.1.35 CalA_C4A

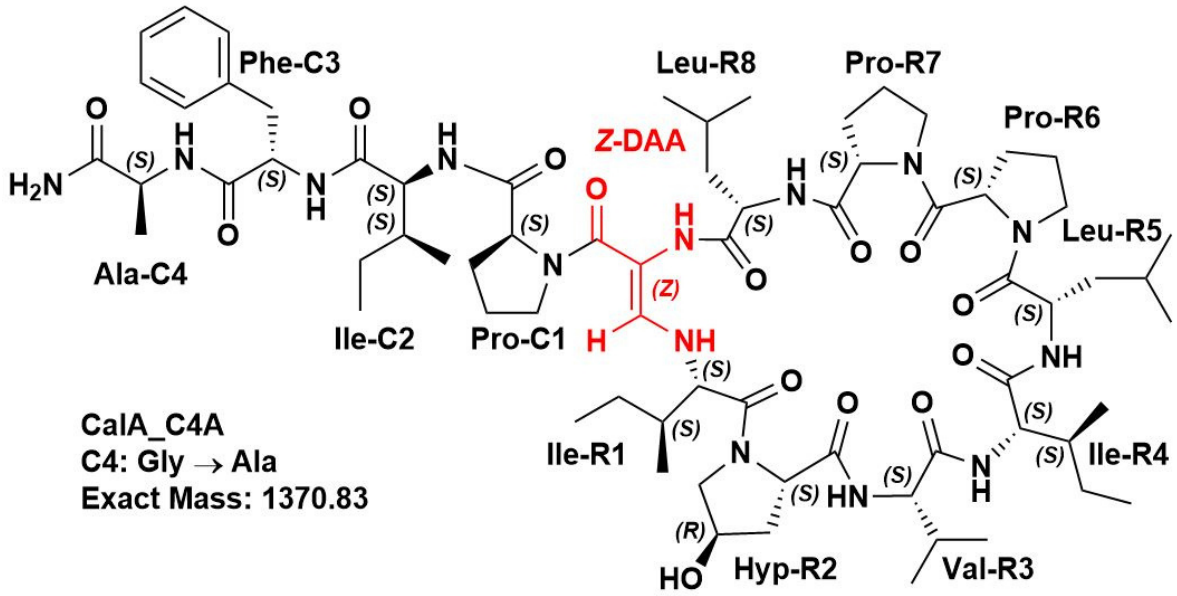

Figure 140: Chemical structure of derivative *CalA_C4A*

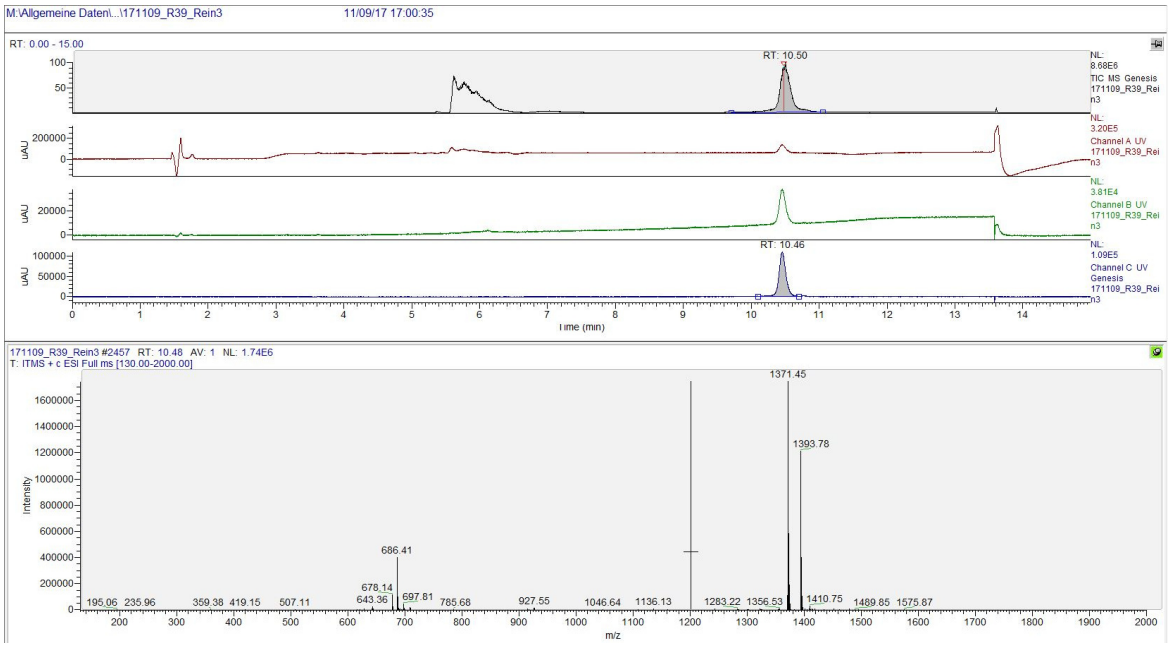

Figure 141: LC-MS spectrum of synthetic Callyaerin A derivative *CalA_C4A*. From top to bottom: TIC (ESI+), UV channel A (λ = 210 nm), UV channel B (λ = 254 nm), UV channel C (λ = 280 nm), mass spectrum of highest peak from chromatogram.

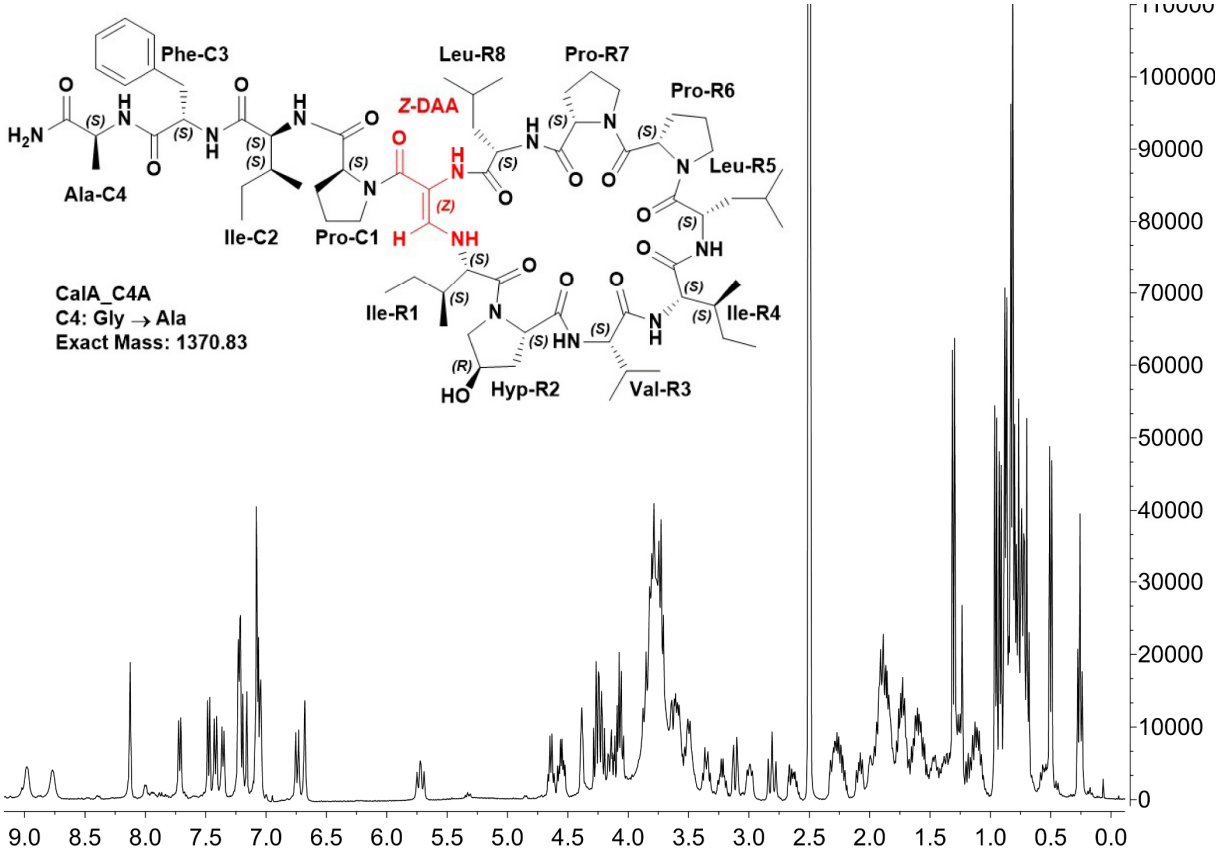

Figure 142: ^{1}H NMR spectrum (400 MHz, DMSO-d_6) of derivative *CalA_C4A*.

6.1.1.36 CalA_C4X

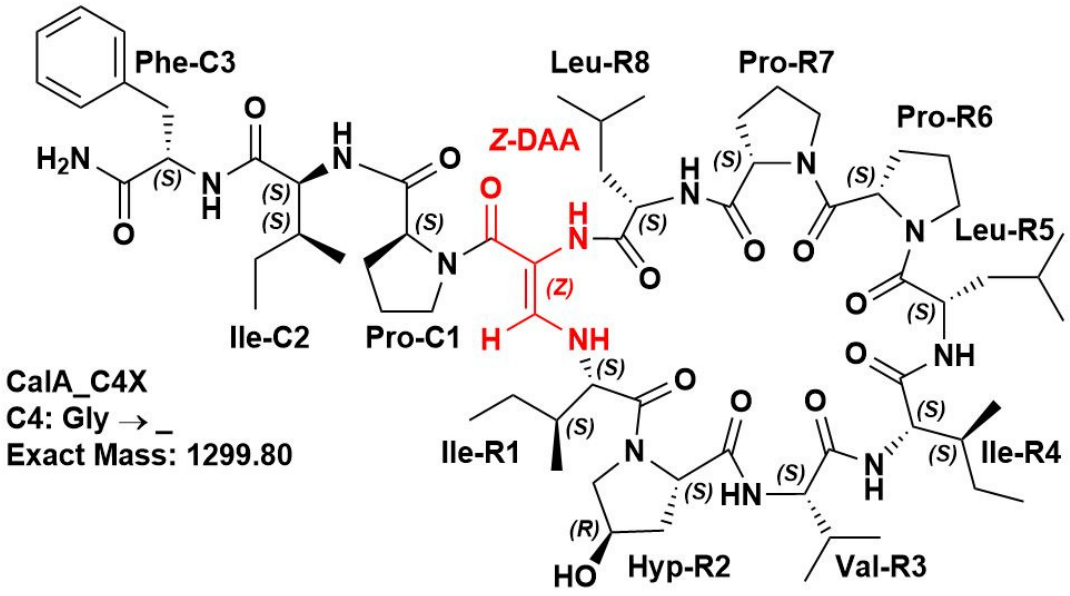

Figure 143: Chemical structure of derivative *CalA_C4X*

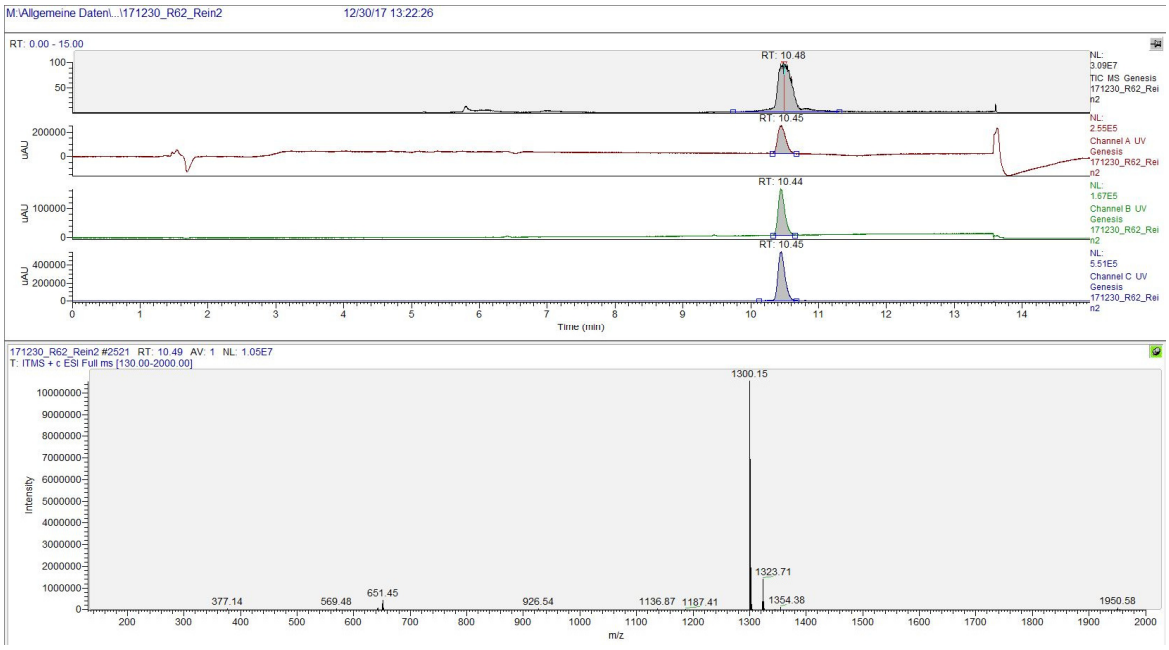

Figure 144: LC-MS spectrum of synthetic Callyaerin A derivative *CalA_C4X*. From top to bottom: TIC (ESI+), UV channel A (λ = 210 nm), UV channel B (λ = 254 nm), UV channel C (λ = 280 nm), mass spectrum of highest peak from chromatogram.

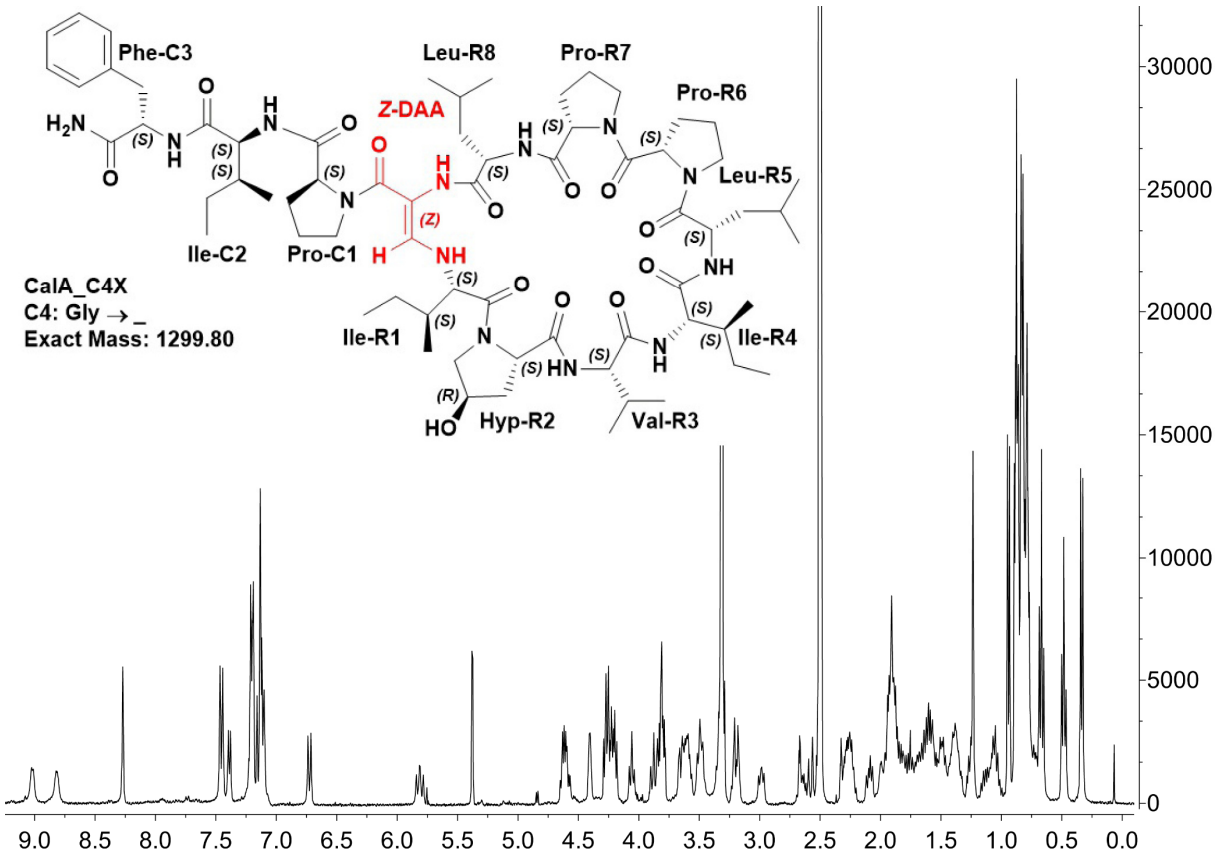

Figure 145: ^{1}H NMR spectrum (400 MHz, DMSO-d_6) of derivative *CalA_C4X*.

6.1.1.37 CalA_C4Pra

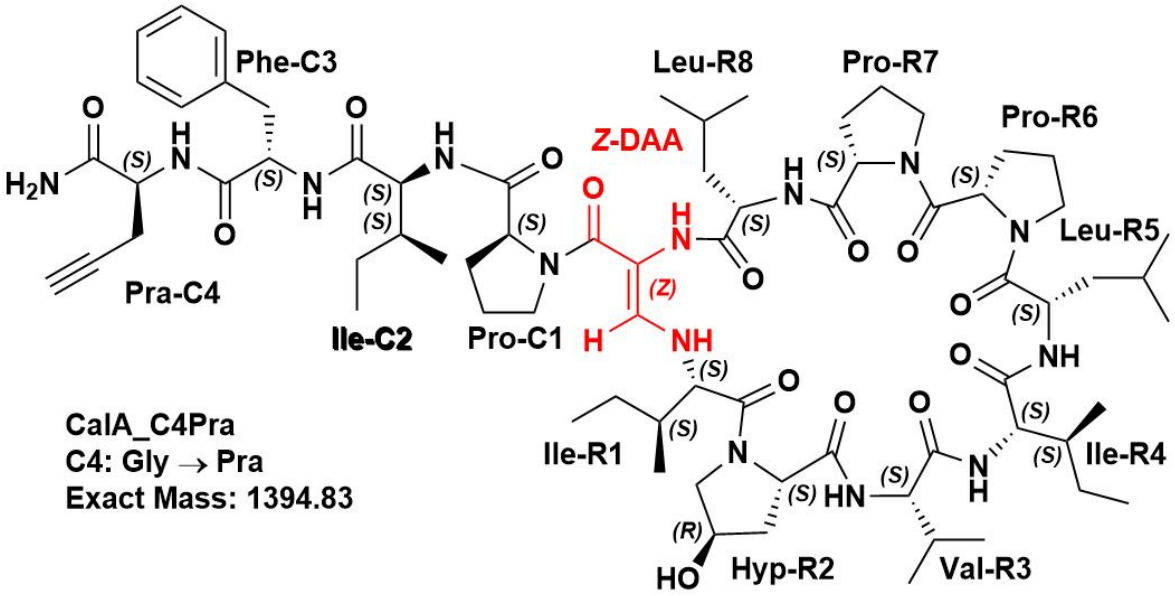

Figure 146: Chemical structure of derivative *CalA_C4Pra*

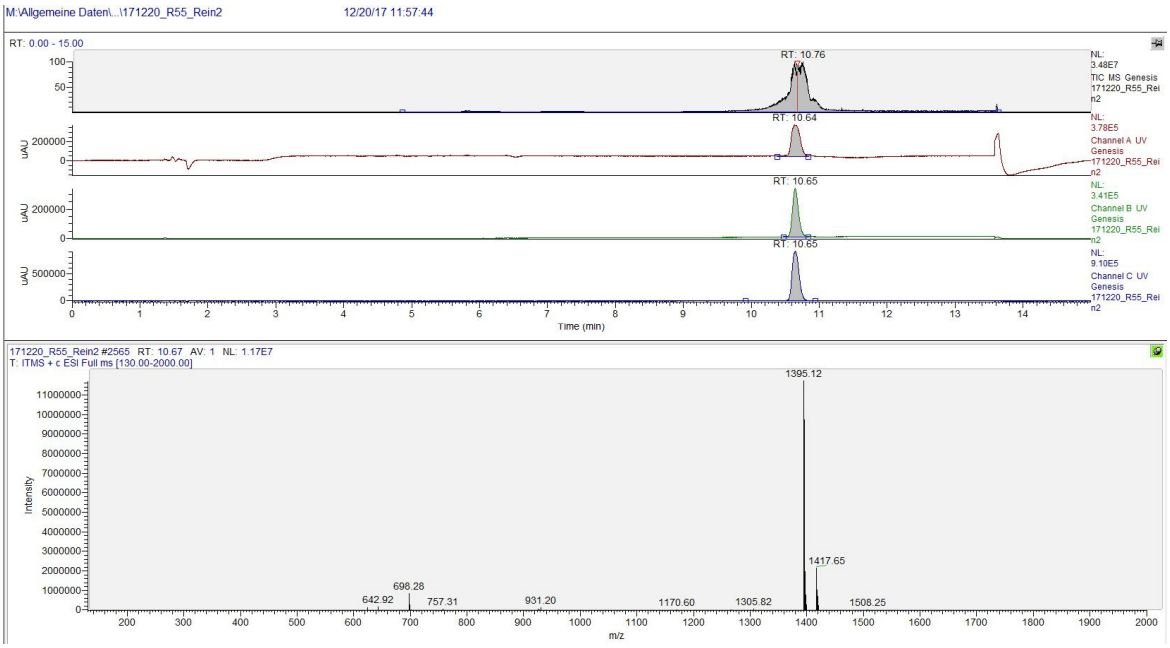

Figure 147: LC-MS spectrum of synthetic Callyaerin A derivative *CalA_C4Pra*. From top to bottom: TIC (ESI+), UV channel A (λ = 210 nm), UV channel B (λ = 254 nm), UV channel C (λ = 280 nm), mass spectrum of highest peak from chromatogram.

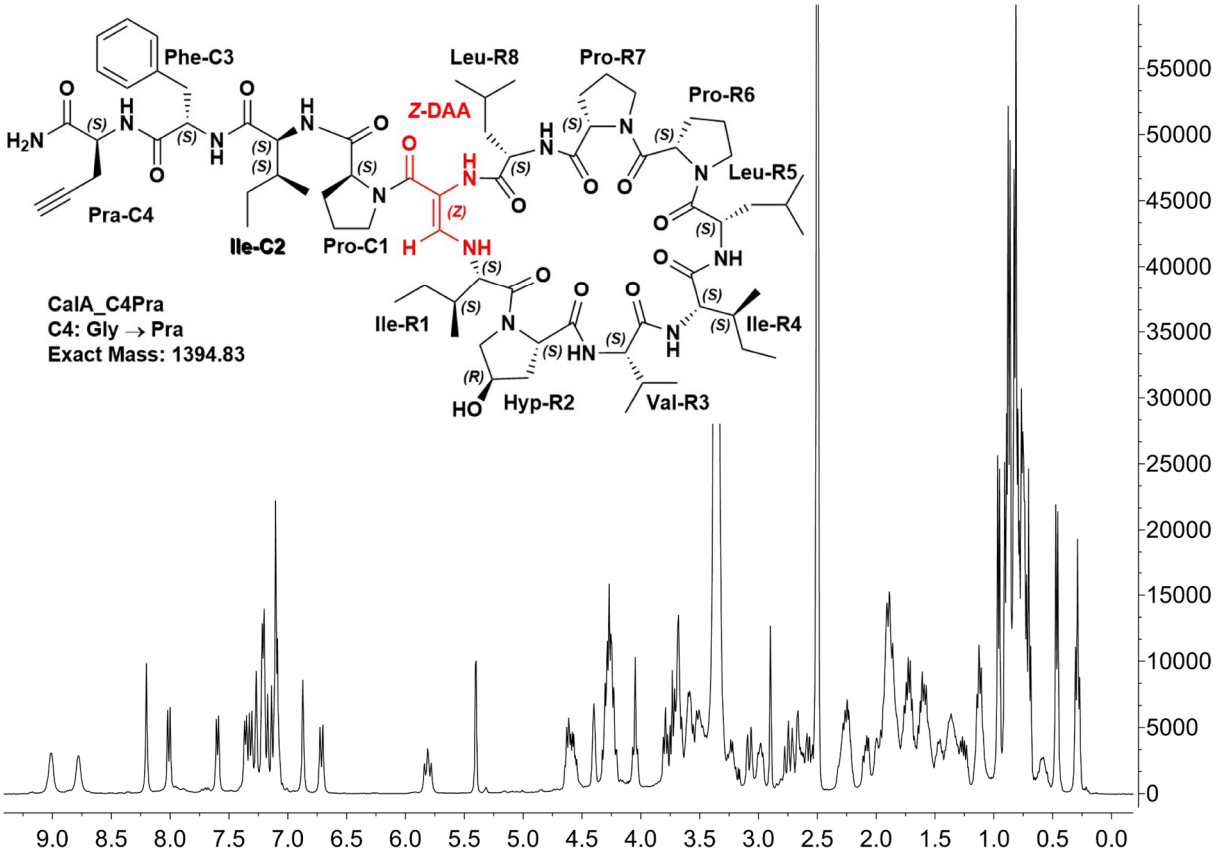

Figure 148: ^{1}H NMR spectrum (400 MHz, DMSO-d_6) of derivative *CalA_C4Pra*.

6.1.1.38 CalA_C4Aha

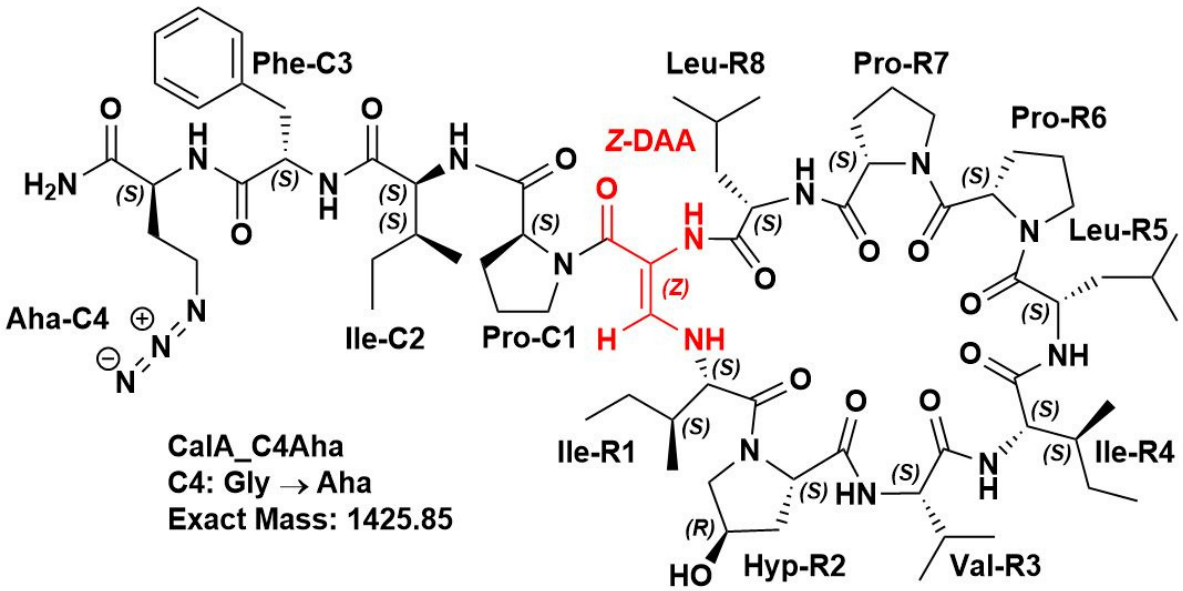

Figure 149: Chemical structure of derivative *CalA_C4Aha*

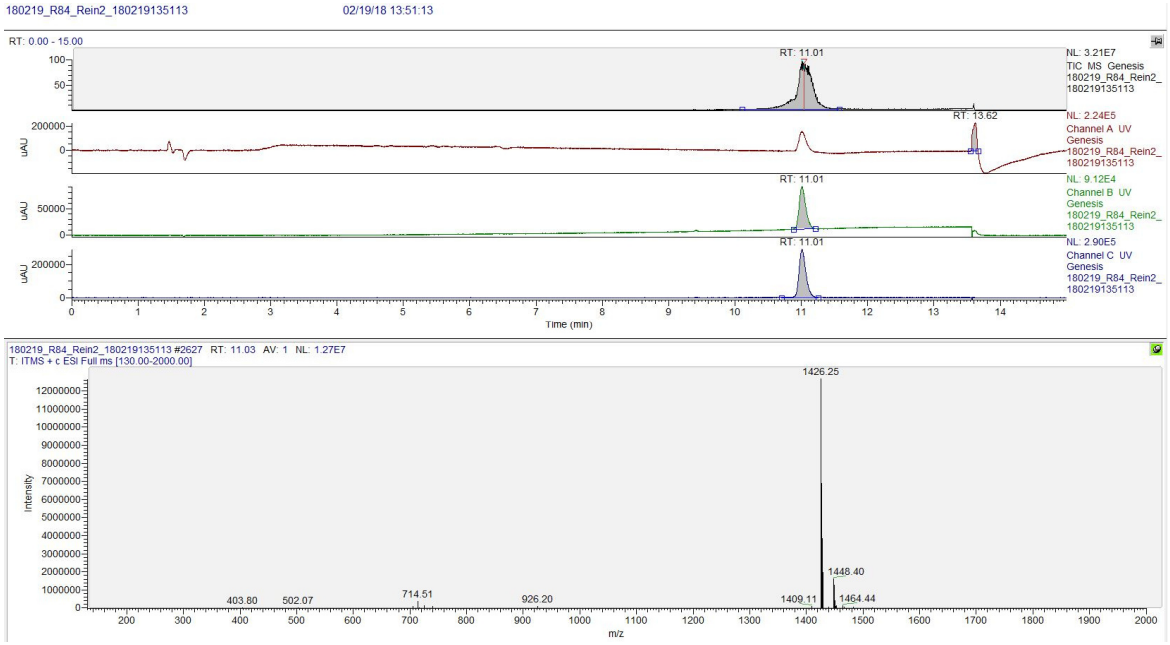

Figure 150: LC-MS spectrum of synthetic Callyaerin A derivative *CalA_C4Aha*. From top to bottom: TIC (ESI+), UV channel A (λ = 210 nm), UV channel B (λ = 254 nm), UV channel C (λ = 280 nm), mass spectrum of highest peak from chromatogram.

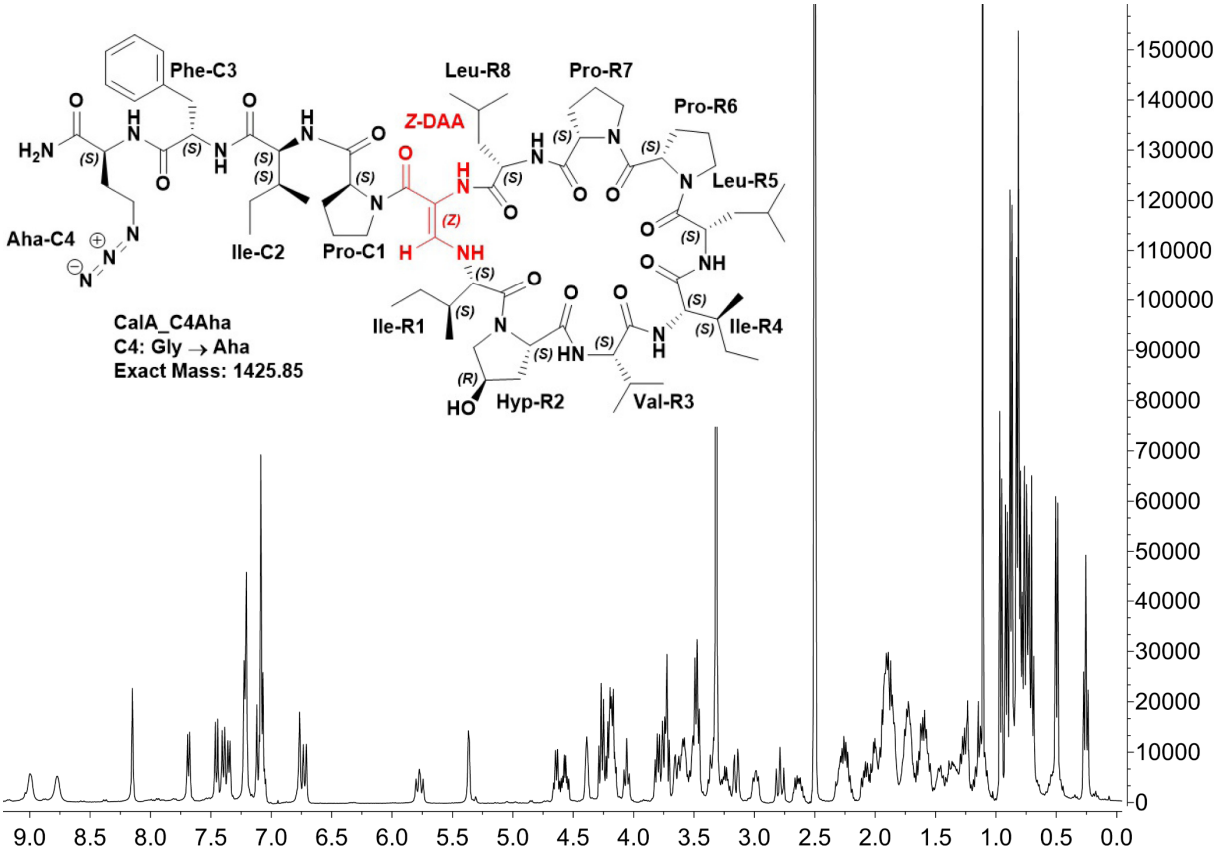

Figure 151: ^{1}H NMR spectrum (400 MHz, DMSO-d_6) of derivative *CalA_C4Aha*.

6.1.1.39 CalA_C5A

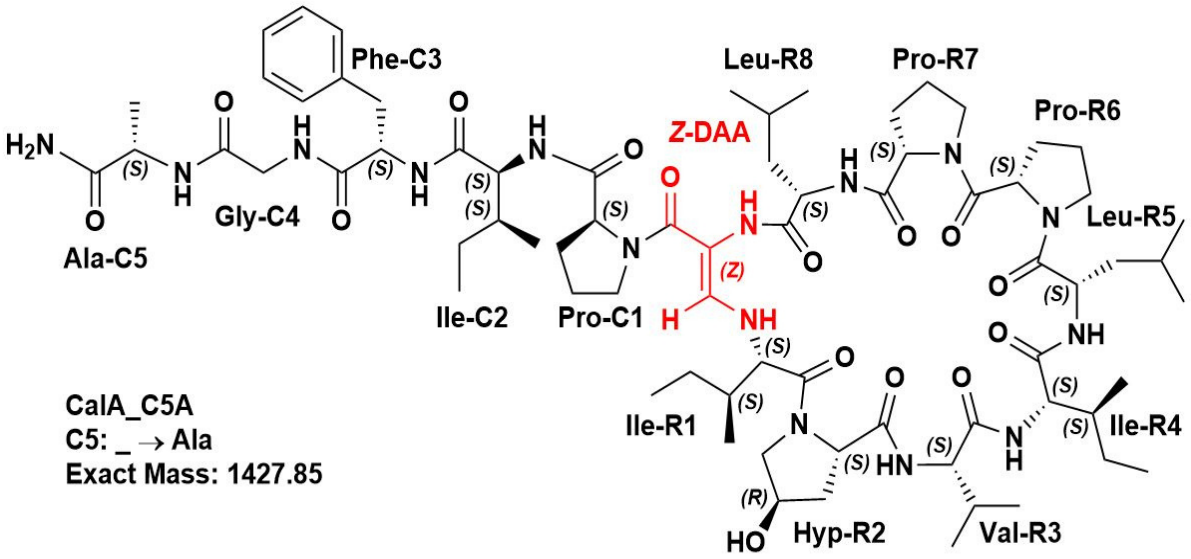

Figure 152: Chemical structure of derivative *CalA_C5A*

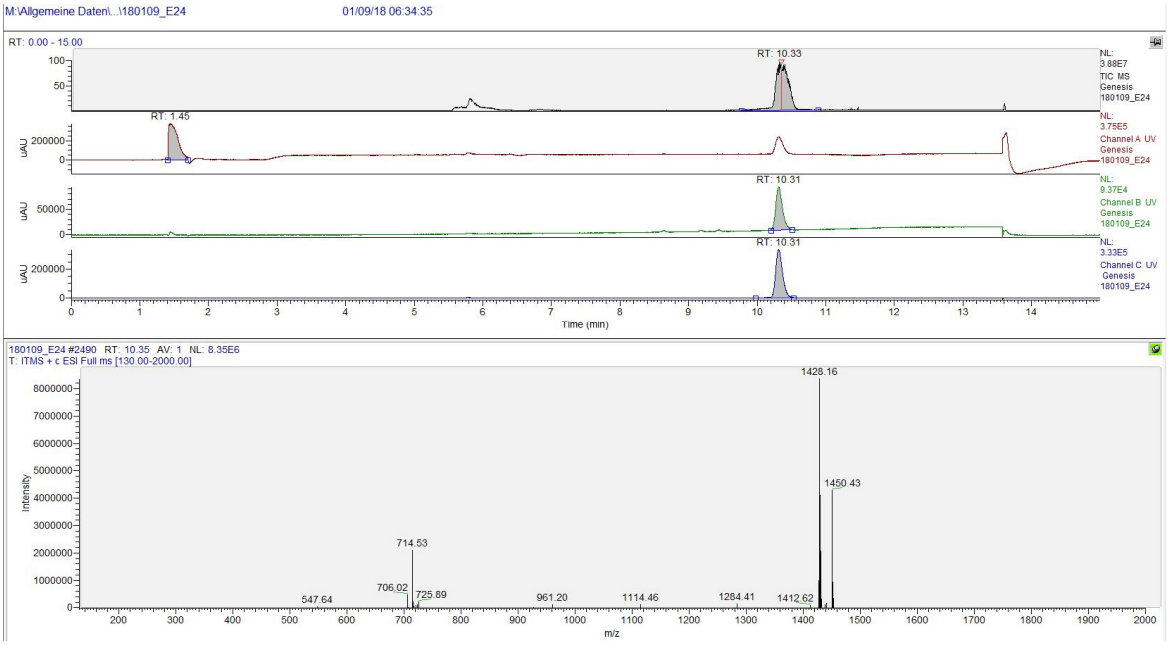

Figure 153: LC-MS spectrum of synthetic Callyaerin A derivative *CalA_C5A*. From top to bottom: TIC (ESI+), UV channel A (λ = 210 nm), UV channel B (λ = 254 nm), UV channel C (λ = 280 nm), mass spectrum of highest peak from chromatogram.

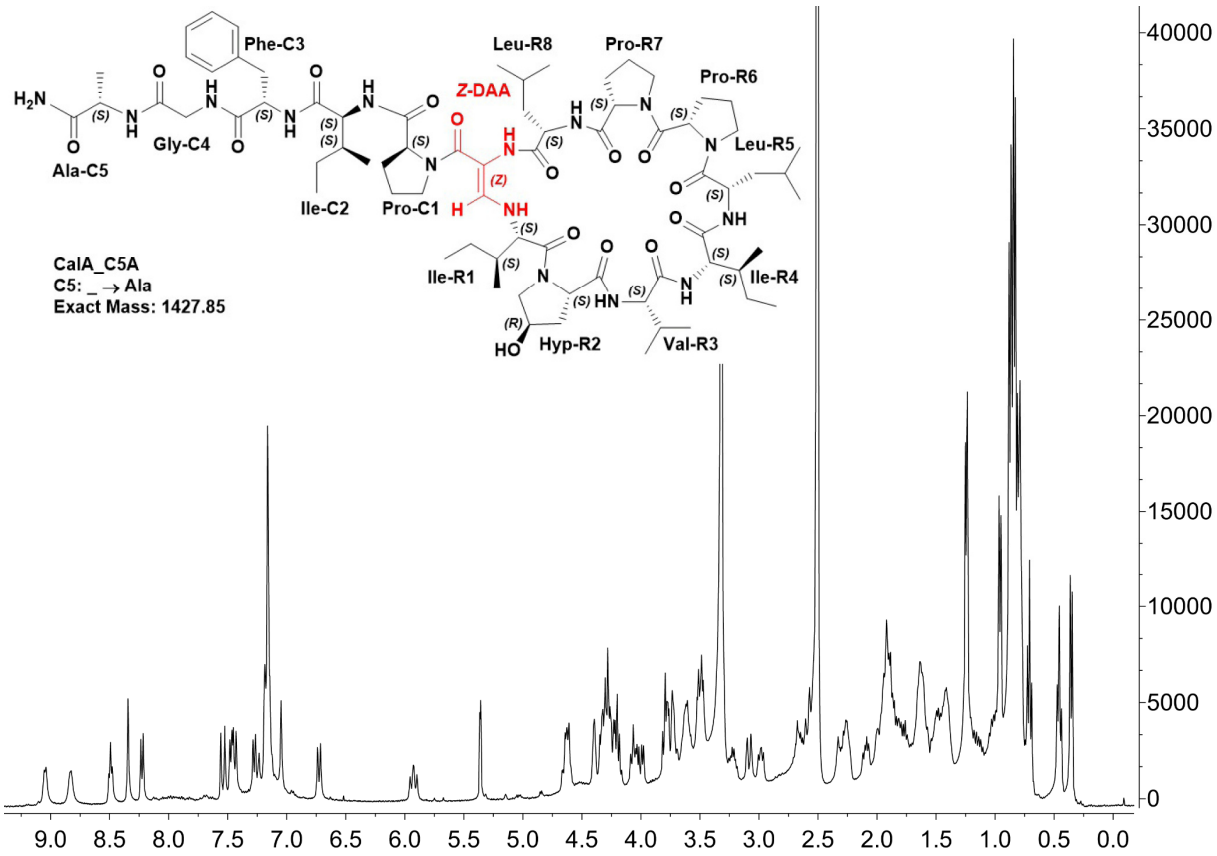

Figure 154: ^{1}H NMR spectrum (400 MHz, DMSO-d_6) of derivative *CalA_C5A*.

6.1.1.40 CalA_C3X+C4X

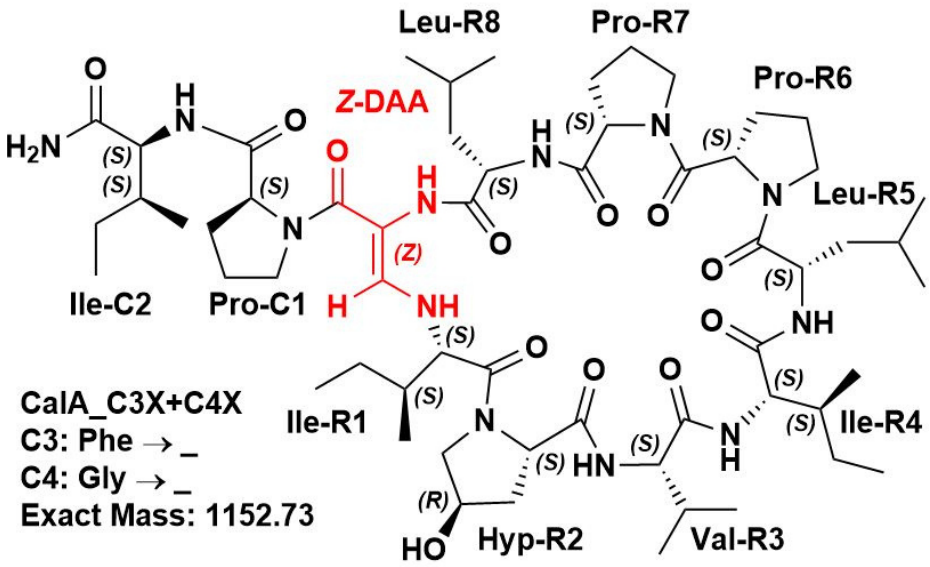

Figure 155: Chemical structure of derivative *CalA_C3X+C4X*

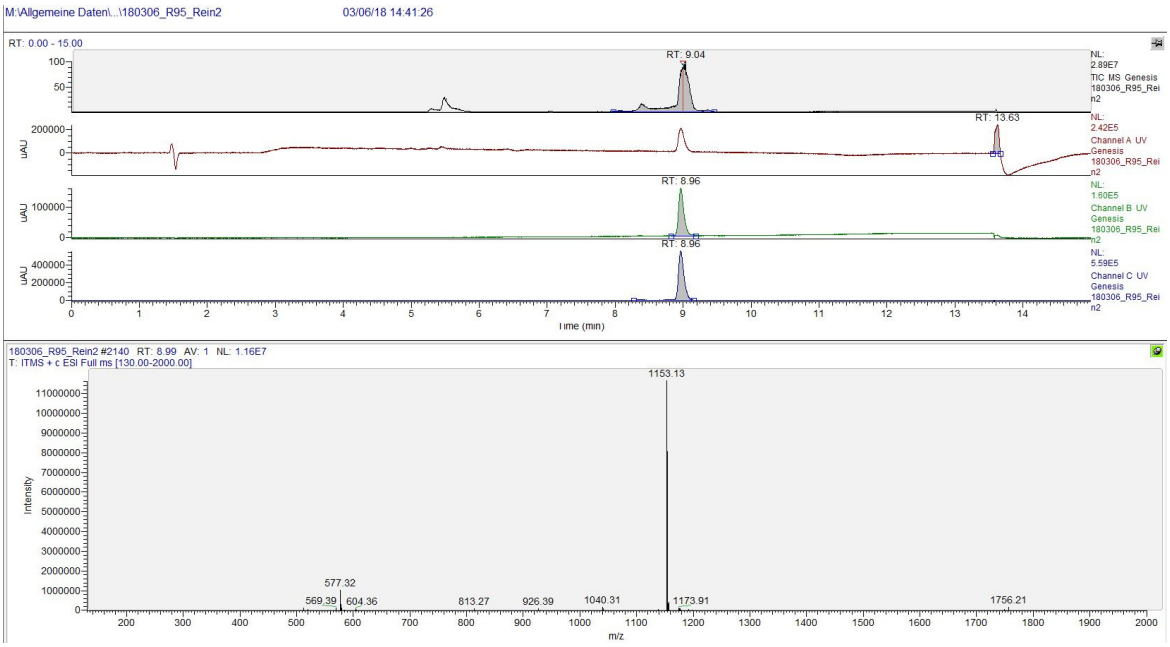

Figure 156: LC-MS spectrum of synthetic Callyaerin A derivative *CalA_ C3X+C4X*. From top to bottom: TIC (ESI+), UV channel A (λ = 210 nm), UV channel B (λ = 254 nm), UV channel C (λ = 280 nm), mass spectrum of highest peak from chromatogram.

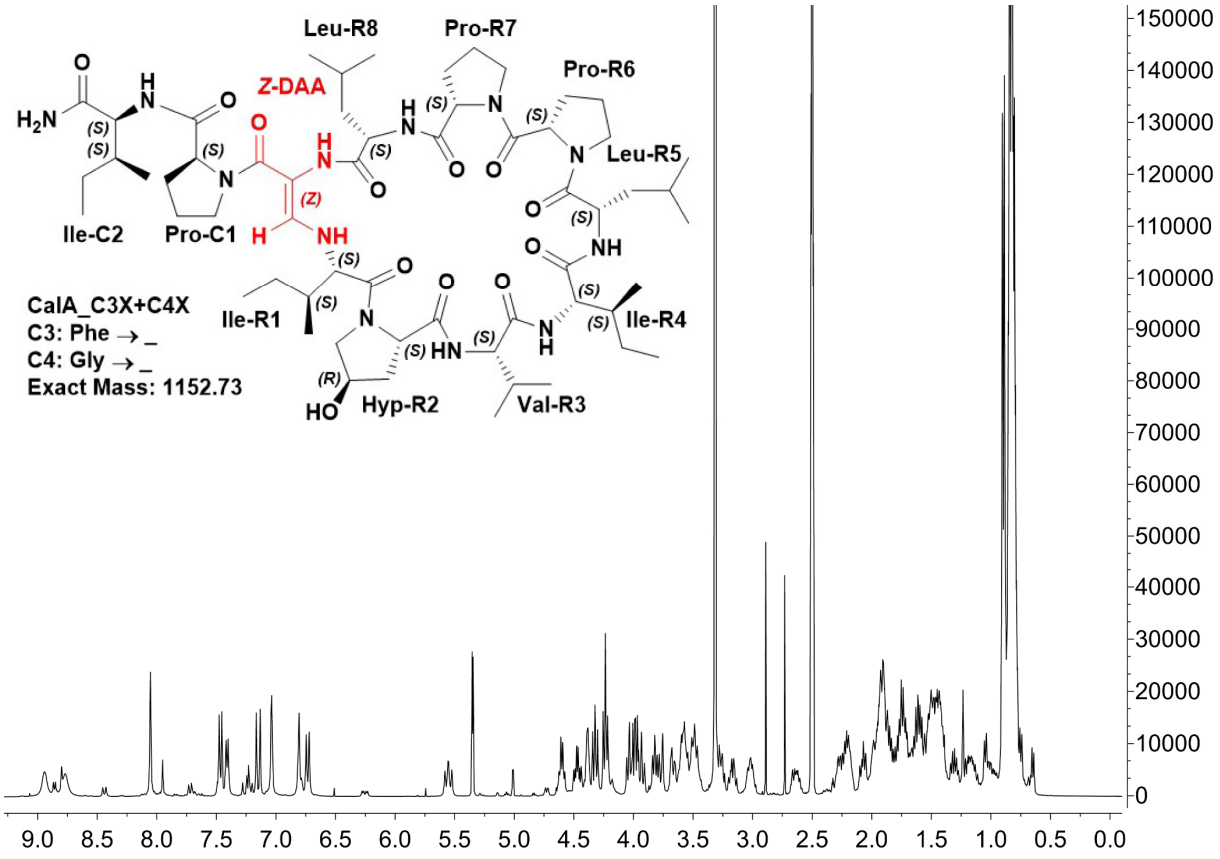

Figure 157: ^{1}H NMR spectrum (400 MHz, DMSO-d_6) of derivative *CalA_C3X+C4X*.

6.1.1.41 CalA_C3I+C4X

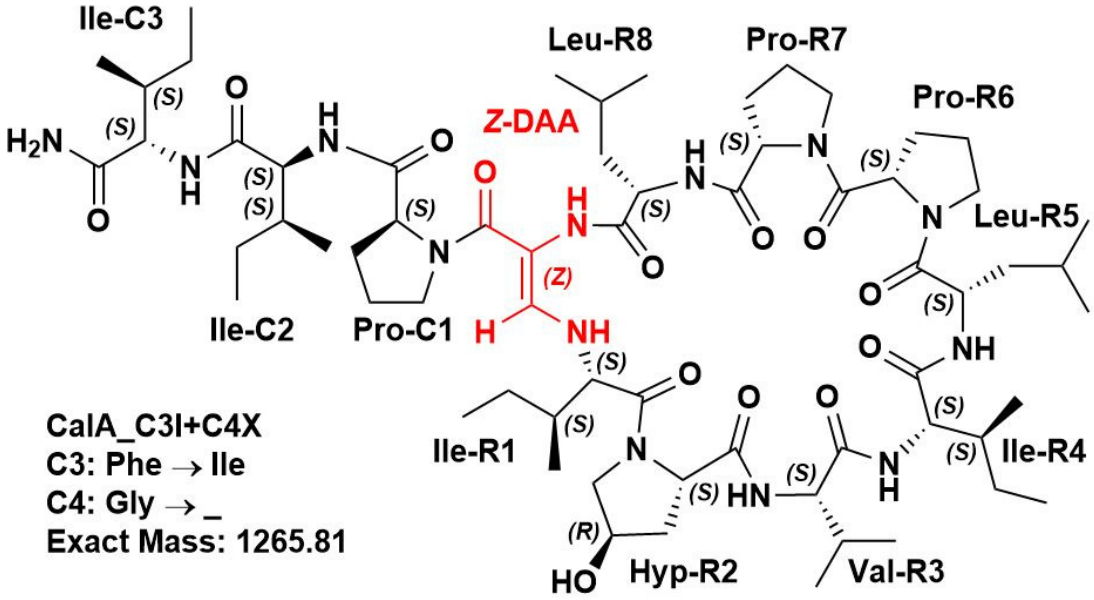

Figure 158: Chemical structure of derivative *CalA_C3I+C4X*

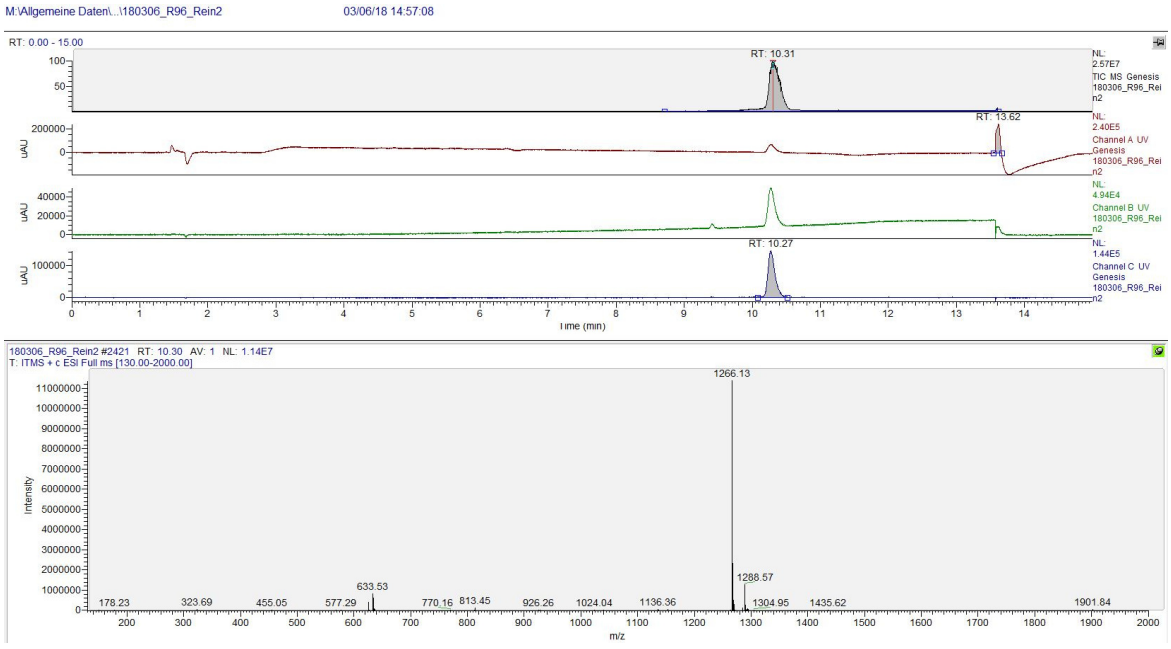

Figure 159: LC-MS spectrum of synthetic Callyaerin A derivative *CalA_C3I+C4X*. From top to bottom: TIC (ESI+), UV channel A (λ = 210 nm), UV channel B (λ = 254 nm), UV channel C (λ = 280 nm), mass spectrum of highest peak from chromatogram.

6.1.1.42 CalA_R2P+C3I+C4X

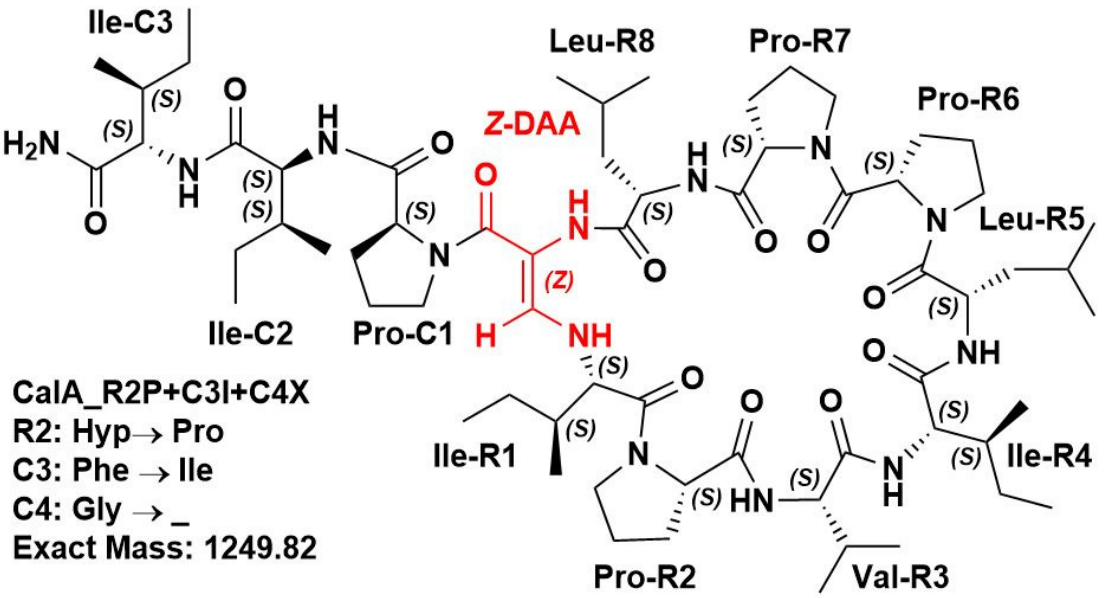

Figure 160: Chemical structure of derivative *CalA_R2P+C3I+C4X*

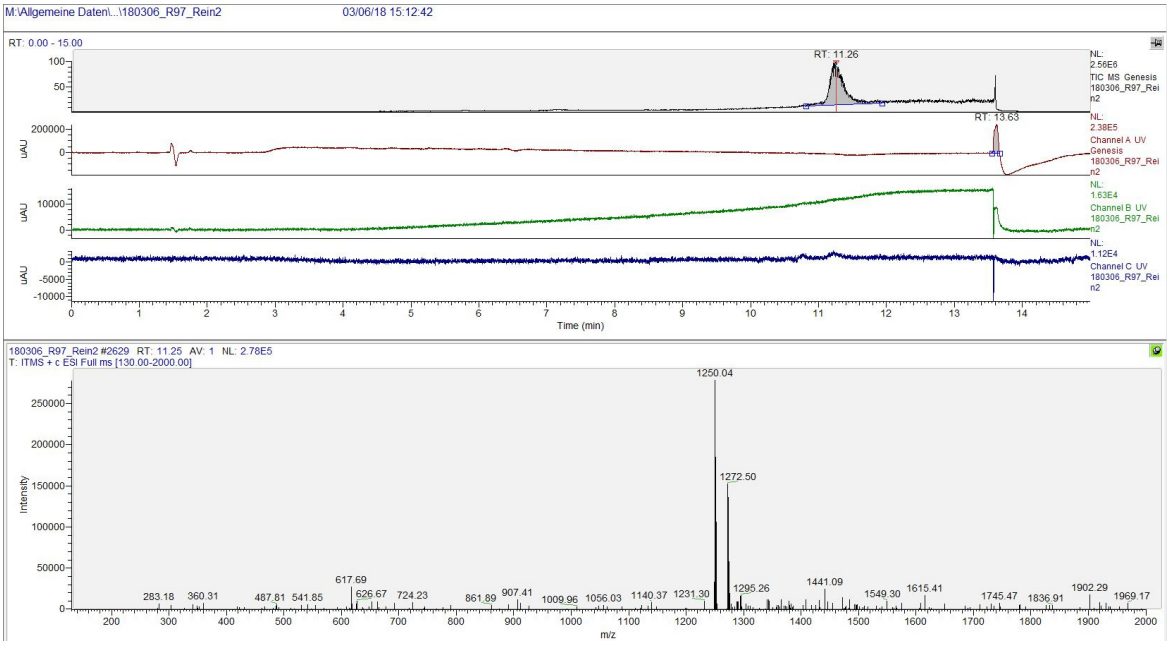

Figure 161: LC-MS spectrum of synthetic Callyaerin A derivative *CalA_R2P+C3I+C4X*. From top to bottom: TIC (ESI+), UV channel A (λ = 210 nm), UV channel B (λ = 254 nm), UV channel C (λ = 280 nm), mass spectrum of highest peak from chromatogram.

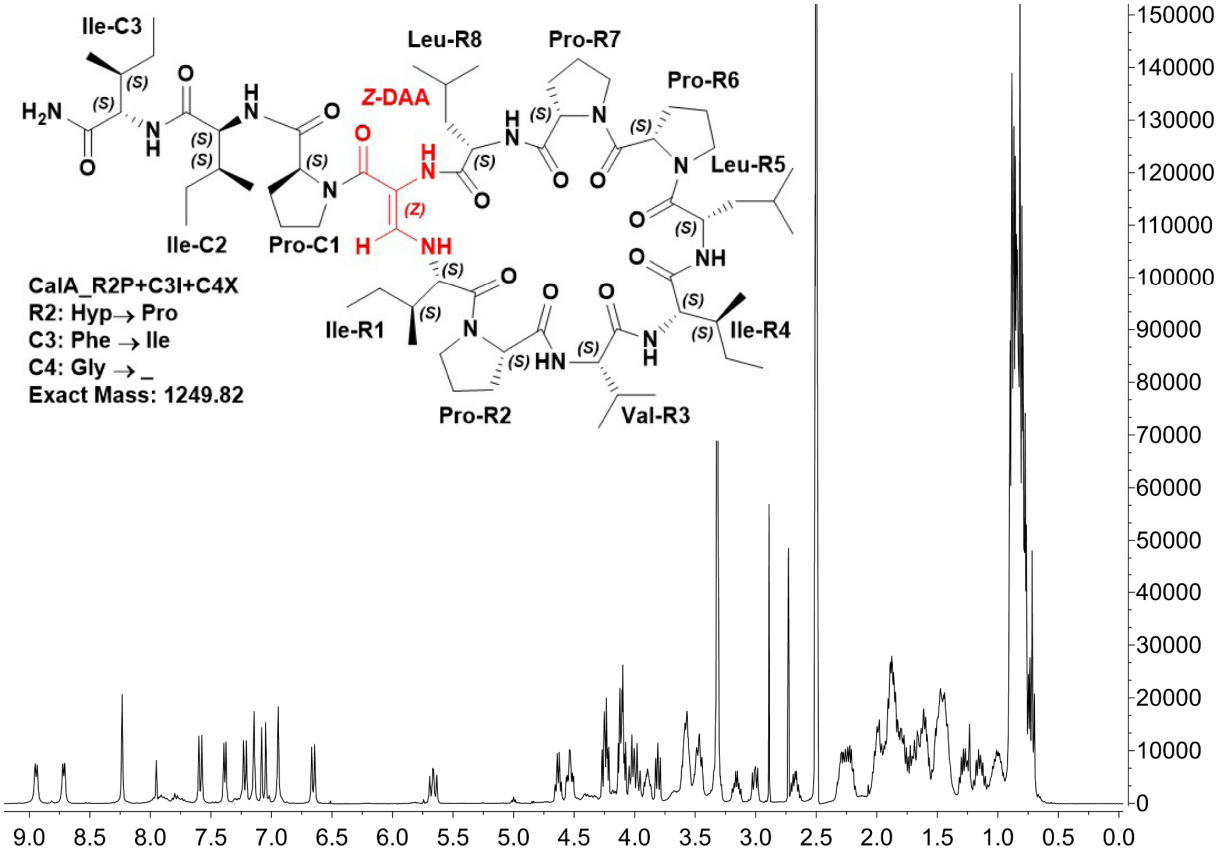

Figure 162: ^{1}H NMR spectrum (400 MHz, DMSO-d_6) of derivative *CalA_R2P+C3I+C4X*.

6.1.1.43 CalA_R3I+R2P

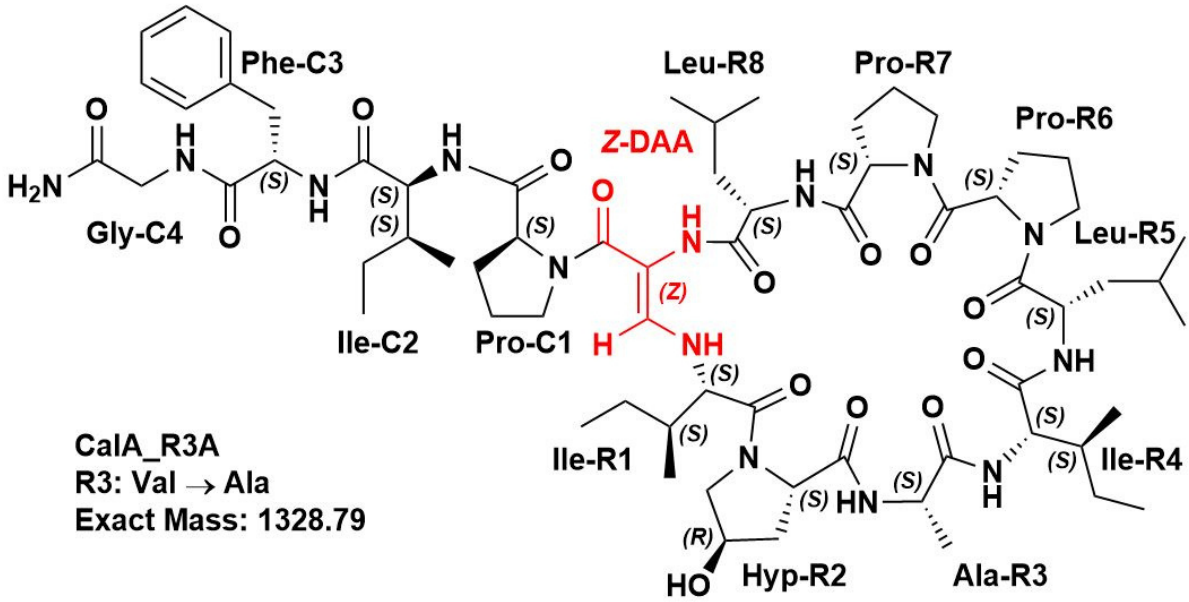

Figure 163: Chemical structure of derivative *CalA_R3I+R2P*

CalB_C4Pra

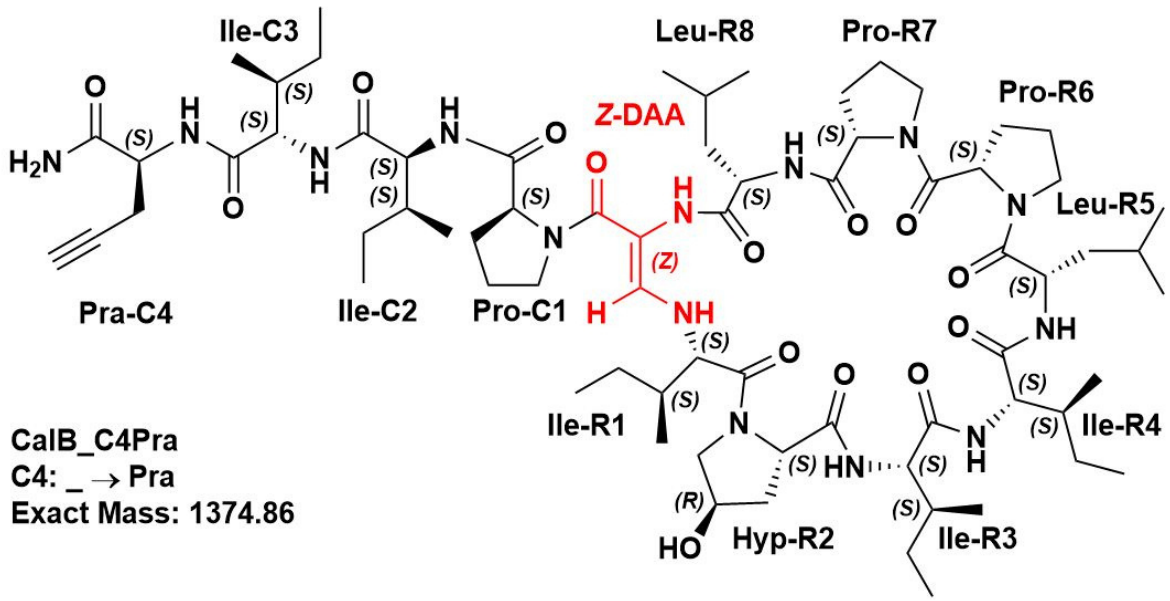

Figure 165: Chemical structure of derivative *CalB_C4Pra*

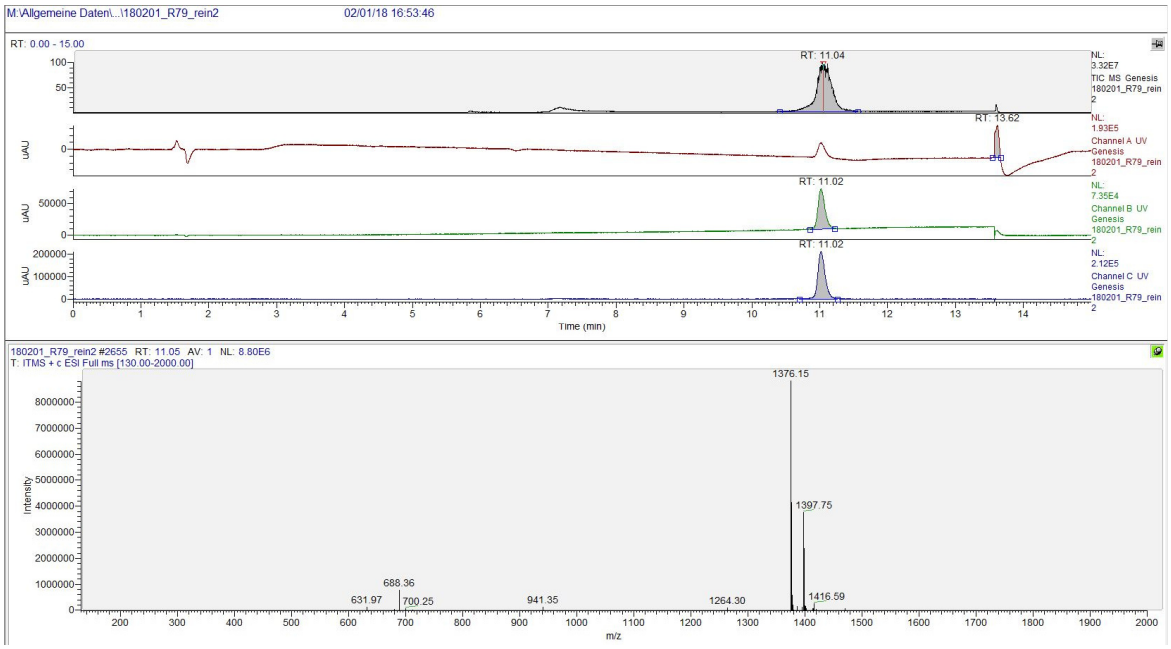

Figure 166: LC-MS spectrum of synthetic derivative *CalB_C4Pra*. From top to bottom: TIC (ESI+), UV channel A (λ = 210 nm), UV channel B (λ = 254 nm), UV channel C (λ = 280 nm), mass spectrum of highest peak from chromatogram.

6.1.1.44 Biotin-CalA probe

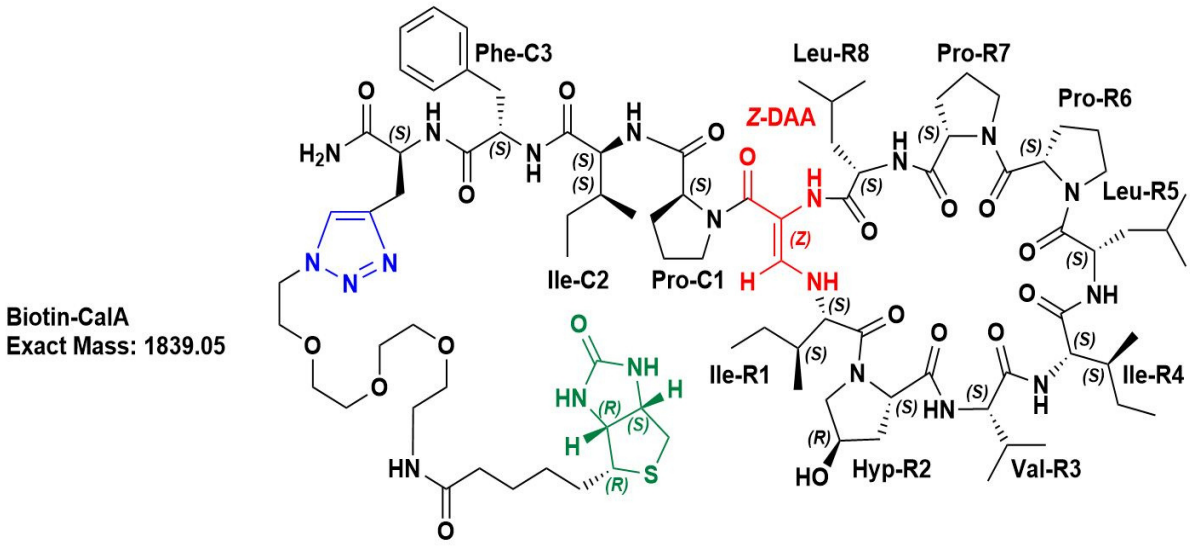

Figure 167: Chemical structure of *Biotin-CalA probe*

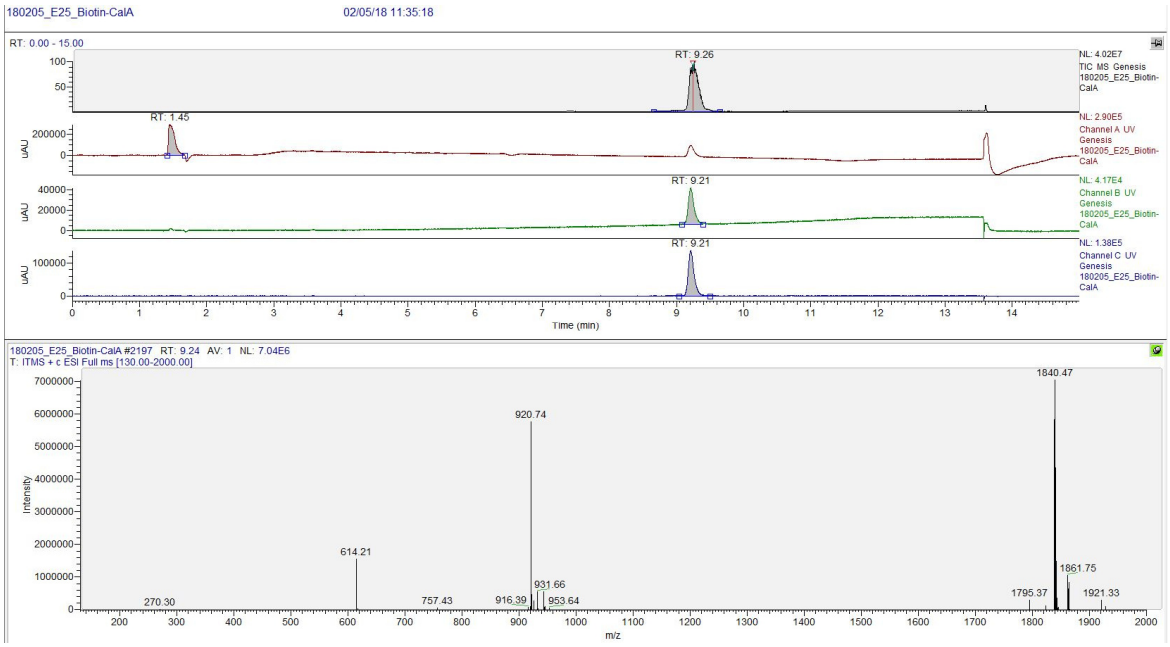

Figure 168: LC-MS spectrum of Biotin-CalA probe. From top to bottom: TIC (ESI+), UV channel A (λ = 210 nm), UV channel B (λ = 254 nm), UV channel C (λ = 280 nm), mass spectrum of highest peak from chromatogram.

6.1.1.45 Biotin-CalB probe

Biotin-CalB
Exact Mass: 1819.08

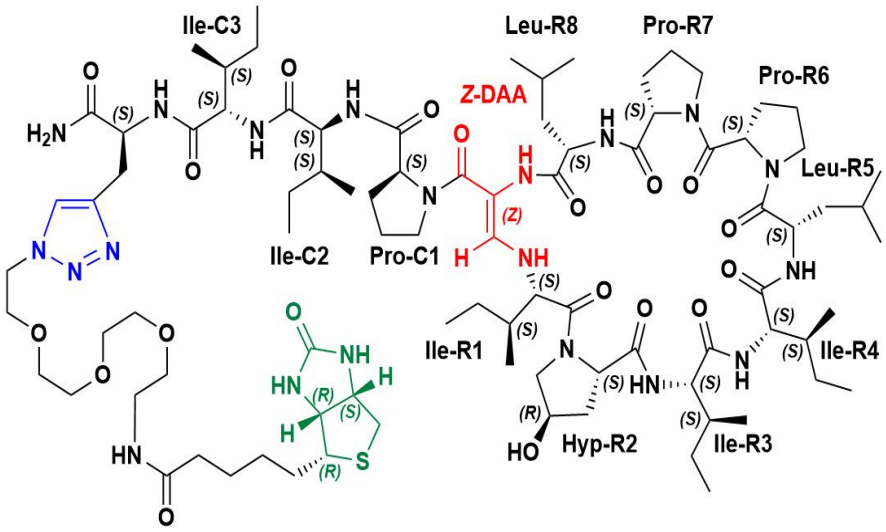

Figure 169: Chemical structure of *Biotin-CalB probe*

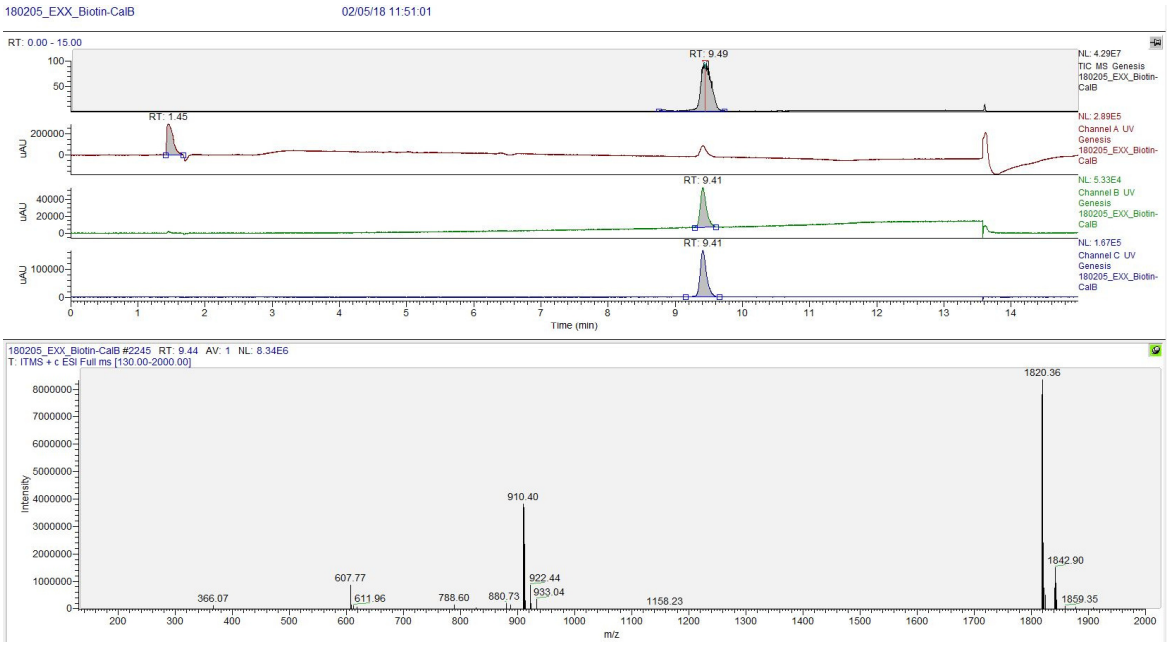

Figure 170: LC-MS spectrum of Biotin-CalB probe. From top to bottom: TIC (ESI+), UV channel A (λ = 210 nm), UV channel B (λ = 254 nm), UV channel C (λ = 280 nm), mass spectrum of highest peak from chromatogram.

6.1.1.46 Cy3-CalA probe

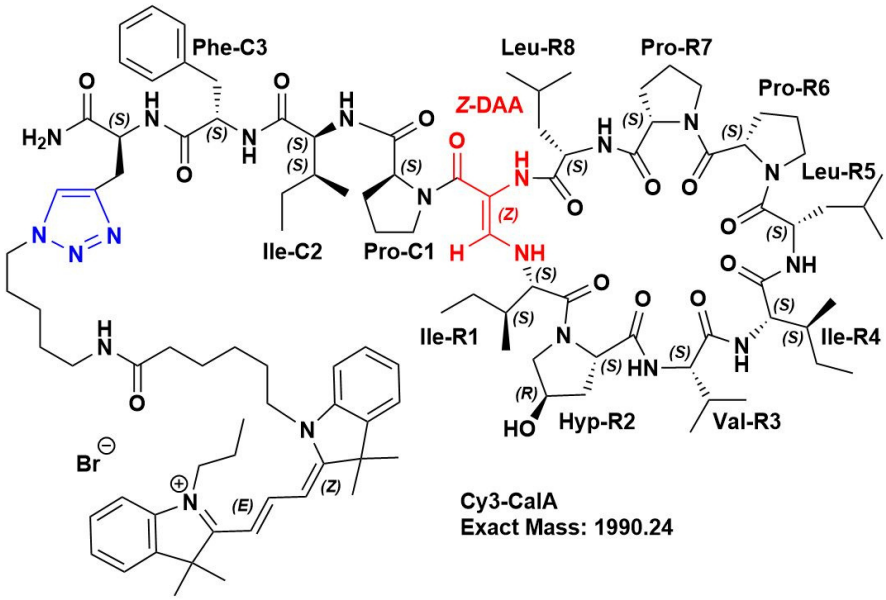

Figure 171: Chemical structure of *Cy3-CalA probe*

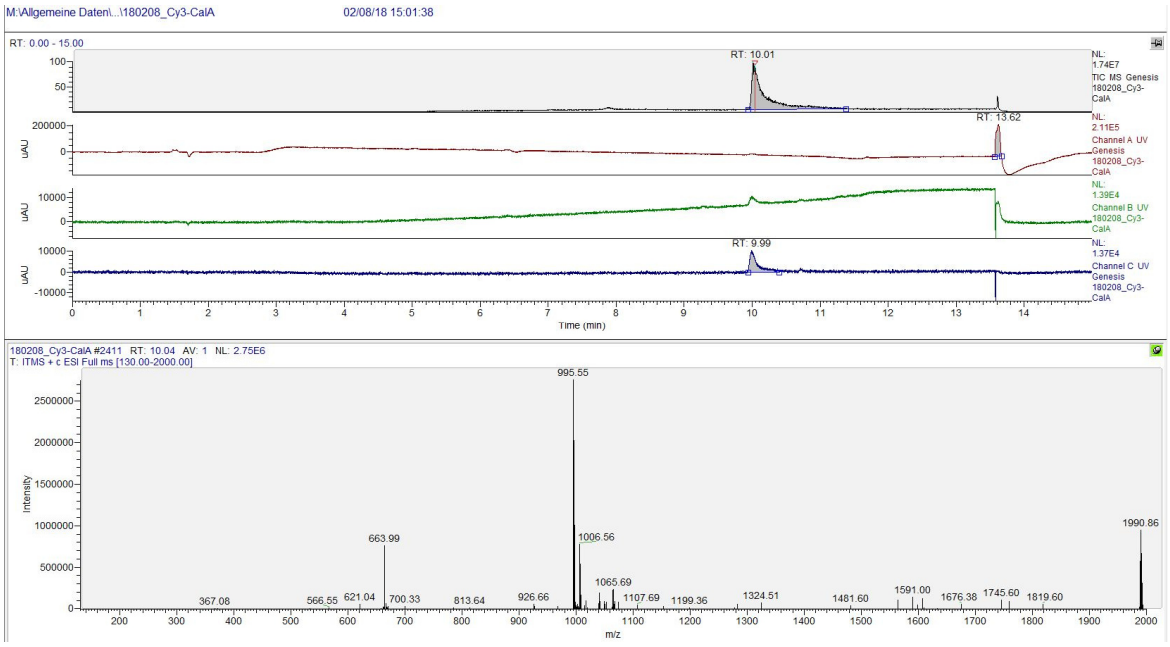

Figure 172: LC-MS spectrum of Cy3-CalA probe. From top to bottom: TIC (ESI+), UV channel A (λ = 210 nm), UV channel B (λ = 254 nm), UV channel C (λ = 280 nm), mass spectrum of highest peak from chromatogram.

6.2 List of abbreviations

ABC	Ammonium bicarbonate
ACN	Acetonitrile
AMOIPA	2-amino-3-(5-methoxy-2-oxoimidazolidin4-ylidene)propanoic acid
CalA	Callyaerin A
CalB	Callyaerin B
CID	Collision-induced dissociation
DAA	(*Z*)-2,3-diaminoacrylamide
DIC	*N*,*N*'-Diisopropylcarbodiimide
DIPEA	*N*,*N*-Diisopropylethylamine
DMF	Dimethylformamide)
DMSO	Dimethylsulfoxide
DTT	Dithiothreitol
FA	Formic acid
FTMS	Fourier transform-based mass spectrometer
HBTU	Hexafluorophosphate Benzotriazole Tetramethyl Uronium
HOBt	Hydroxybenzotriazole
IAM	Iodoacetamide
ITMS	Ion trap mass spectrometer
LC	Liquid chromatography
MDR-TB	Multi-drug-resistant tuberculosis
MeOH	Methanol
MIC	Minimal Inhibitory Concentration
MOI	Multiplicity of infection
MS	Mass spectrometry
Mtb	Mycobacterium tuberculosis
PBS	Phosphate buffered saline
PMA	Phorbol 12-myristate 13-acetate
RR-TB	Rifampicin resistant tuberculosis
RT	Room temperature
SNP	Single-nucleotide polymorphism
STSA	Stage tipping solution A
STSB	Stage tipping solution B
TFA	Trifluoroacetic acid
TIPS	Triisopropyl silane
Tri-FP	Trifunctional fluorophosphonate (with biotin and fluorophore tags)
XDR-TB	Extensively drug-resistant tuberculosis

6.3 List of literature

1. World Health Organization. *GLOBAL TUBERCULOSIS REPORT 2018* (WORLD HEALTH ORGANIZATION, [S.l.], 2018).
2. Millard, J., Ugarte-Gil, C. & Moore, D. A. J. Multidrug resistant tuberculosis. *BMJ (Clinical research ed.)* **350,** h882; 10.1136/bmj.h882 (2015).
3. Acosta, C. D., Dadu, A., Ramsay, A. & Dara, M. Drug-resistant tuberculosis in Eastern Europe: challenges and ways forward. *Public Health Action* **4,** S3-S12; 10.5588/pha.14.0087 (2014).
4. Lienhardt, C. *et al.* New drugs for the treatment of tuberculosis: needs, challenges, promise, and prospects for the future. *The Journal of infectious diseases* **205 Suppl 2,** S241-9; 10.1093/infdis/jis034 (2012).
5. Blanchard, J. S. Molecular mechanisms of drug resistance in Mycobacterium tuberculosis. *Annual review of biochemistry* **65,** 215–239; 10.1146/annurev.bi.65.070196.001243 (1996).
6. Ramaswamy, S. & Musser, J. M. Molecular genetic basis of antimicrobial agent resistance in Mycobacterium tuberculosis: 1998 update. *Tubercle and lung disease : the official journal of the International Union against Tuberculosis and Lung Disease* **79,** 3–29; 10.1054/tuld.1998.0002 (1998).
7. Somoskovi, A., Parsons, L. M. & Salfinger, M. The molecular basis of resistance to isoniazid, rifampin, and pyrazinamide in Mycobacterium tuberculosis. *Respir Res* **2,** 164–168; 10.1186/rr54 (2001).
8. Traore, H., Fissette, K., Bastian, I., Devleeschouwer, M. & Portaels, F. Detection of rifampicin resistance in Mycobacterium tuberculosis isolates from diverse countries by a commercial line probe assay as an initial indicator of multidrug resistance. *The international journal of tuberculosis and lung disease : the official journal of the International Union against Tuberculosis and Lung Disease* **4,** 481–484 (2000).
9. Zhang, Y., Heym, B., Allen, B., Young, D. & Cole, S. The catalase-peroxidase gene and isoniazid resistance of Mycobacterium tuberculosis. *Nature* **358,** 591–593; 10.1038/358591a0 (1992).
10. Rawat, R., Whitty, A. & Tonge, P. J. The isoniazid-NAD adduct is a slow, tight-binding inhibitor of InhA, the Mycobacterium tuberculosis enoyl reductase: adduct affinity and drug resistance. *Proceedings of the National Academy of Sciences of the United States of America* **100,** 13881–13886; 10.1073/pnas.2235848100 (2003).
11. Ramaswamy, S. V. *et al.* Single Nucleotide Polymorphisms in Genes Associated with Isoniazid Resistance in Mycobacterium tuberculosis. *Antimicrobial agents and chemotherapy* **47,** 1241–1250; 10.1128/AAC.47.4.1241-1250.2003 (2003).
12. Hazbón, M. H. *et al.* Population genetics study of isoniazid resistance mutations and evolution of multidrug-resistant Mycobacterium tuberculosis. *Antimicrobial agents and chemotherapy* **50,** 2640–2649; 10.1128/AAC.00112-06 (2006).
13. Takayama, K. & Kilburn, J. O. Inhibition of synthesis of arabinogalactan by ethambutol in Mycobacterium smegmatis. *Antimicrobial agents and chemotherapy* **33,** 1493–1499; 10.1128/AAC.33.9.1493 (1989).

14. Telenti, A. *et al.* The emb operon, a gene cluster of Mycobacterium tuberculosis involved in resistance to ethambutol. *Nature medicine* **3,** 567–570; 10.1038/nm0597-567 (1997).
15. Ramaswamy, S. V. *et al.* Molecular genetic analysis of nucleotide polymorphisms associated with ethambutol resistance in human isolates of Mycobacterium tuberculosis. *Antimicrobial agents and chemotherapy* **44,** 326–336 (2000).
16. Moazed, D. & Noller, H. F. Interaction of antibiotics with functional sites in 16S ribosomal RNA. *Nature* **327,** 389–394; 10.1038/327389a0 (1987).
17. Finken, M., Kirschner, P., Meier, A., Wrede, A. & Böttger, E. C. Molecular basis of streptomycin resistance in Mycobacterium tuberculosis: alterations of the ribosomal protein S12 gene and point mutations within a functional 16S ribosomal RNA pseudoknot. *Molecular microbiology* **9,** 1239–1246 (1993).
18. Scorpio, A. & Zhang, Y. Mutations in pncA, a gene encoding pyrazinamidase/nicotinamidase, cause resistance to the antituberculous drug pyrazinamide in tubercle bacillus. *Nature medicine* **2,** 662–667 (1996).
19. Shi, W. *et al.* Pyrazinamide inhibits trans-translation in Mycobacterium tuberculosis. *Science (New York, N.Y.)* **333,** 1630–1632; 10.1126/science.1208813 (2011).
20. Palomino, J. C. & Martin, A. Drug Resistance Mechanisms in Mycobacterium tuberculosis. *Antibiotics* **3,** 317–340; 10.3390/antibiotics3030317 (2014).
21. Caws, M. *et al.* Mutations prevalent among rifampin- and isoniazid-resistant Mycobacterium tuberculosis isolates from a hospital in Vietnam. *Journal of clinical microbiology* **44,** 2333–2337; 10.1128/JCM.00330-06 (2006).
22. Scorpio, A. *et al.* Characterization of pncA mutations in pyrazinamide-resistant Mycobacterium tuberculosis. *Antimicrobial agents and chemotherapy* **41,** 540–543 (1997).
23. Juréen, P., Werngren, J., Toro, J.-C. & Hoffner, S. Pyrazinamide resistance and pncA gene mutations in Mycobacterium tuberculosis. *Antimicrobial agents and chemotherapy* **52,** 1852–1854; 10.1128/AAC.00110-08 (2008).
24. Tan, Y. *et al.* Role of pncA and rpsA gene sequencing in detection of pyrazinamide resistance in Mycobacterium tuberculosis isolates from southern China. *Journal of clinical microbiology* **52,** 291–297; 10.1128/JCM.01903-13 (2014).
25. Okamoto, S. *et al.* Loss of a conserved 7-methylguanosine modification in 16S rRNA confers low-level streptomycin resistance in bacteria. *Molecular microbiology* **63,** 1096–1106; 10.1111/j.1365-2958.2006.05585.x (2007).
26. Fàbrega, A., Madurga, S., Giralt, E. & Vila, J. Mechanism of action of and resistance to quinolones. *Microbial biotechnology* **2,** 40–61; 10.1111/j.1751-7915.2008.00063.x (2009).
27. Aubry, A., Pan, X.-S., Fisher, L. M., Jarlier, V. & Cambau, E. Mycobacterium tuberculosis DNA gyrase: interaction with quinolones and correlation with antimycobacterial drug activity. *Antimicrobial agents and chemotherapy* **48,** 1281–1288 (2004).
28. Stanley, R. E., Blaha, G., Grodzicki, R. L., Strickler, M. D. & Steitz, T. A. The structures of the anti-tuberculosis antibiotics viomycin and capreomycin bound to the 70S ribosome. *Nature structural & molecular biology* **17,** 289–293; 10.1038/nsmb.1755 (2010).

29. Johansen, S. K., Maus, C. E., Plikaytis, B. B. & Douthwaite, S. Capreomycin binds across the ribosomal subunit interface using tlyA-encoded 2'-O-methylations in 16S and 23S rRNAs. *Molecular cell* **23,** 173–182; 10.1016/j.molcel.2006.05.044 (2006).
30. Georghiou, S. B. *et al.* Evaluation of genetic mutations associated with Mycobacterium tuberculosis resistance to amikacin, kanamycin and capreomycin: a systematic review. *PloS one* **7,** e33275; 10.1371/journal.pone.0033275 (2012).
31. DeBarber, A. E., Mdluli, K., Bosman, M., Bekker, L.-G. & Barry, C. E. Ethionamide activation and sensitivity in multidrug-resistant Mycobacterium tuberculosis. *Proceedings of the National Academy of Sciences* **97,** 9677–9682; 10.1073/pnas.97.17.9677 (2000).
32. Brossier, F., Veziris, N., Truffot-Pernot, C., Jarlier, V. & Sougakoff, W. Molecular investigation of resistance to the antituberculous drug ethionamide in multidrug-resistant clinical isolates of Mycobacterium tuberculosis. *Antimicrobial agents and chemotherapy* **55,** 355–360; 10.1128/AAC.01030-10 (2011).
33. Rengarajan, J. *et al.* The folate pathway is a target for resistance to the drug para-aminosalicylic acid (PAS) in mycobacteria. *Molecular microbiology* **53,** 275–282; 10.1111/j.1365-2958.2004.04120.x (2004).
34. Zhao, F. *et al.* Binding pocket alterations in dihydrofolate synthase confer resistance to para-aminosalicylic acid in clinical isolates of Mycobacterium tuberculosis. *Antimicrobial agents and chemotherapy* **58,** 1479–1487; 10.1128/AAC.01775-13 (2014).
35. Mathys, V. *et al.* Molecular genetics of para-aminosalicylic acid resistance in clinical isolates and spontaneous mutants of Mycobacterium tuberculosis. *Antimicrobial agents and chemotherapy* **53,** 2100–2109; 10.1128/AAC.01197-08 (2009).
36. Lakshmanan, M. & Xavier, A. S. Bedaquiline - The first ATP synthase inhibitor against multi drug resistant tuberculosis. *Journal of young pharmacists : JYP* **5,** 112–115; 10.1016/j.jyp.2013.12.002 (2013).
37. Bloemberg, G. V. *et al.* Acquired Resistance to Bedaquiline and Delamanid in Therapy for Tuberculosis. *The New England journal of medicine* **373,** 1986–1988; 10.1056/NEJMc1505196 (2015).
38. Worley, M. V. & Estrada, S. J. Bedaquiline: a novel antitubercular agent for the treatment of multidrug-resistant tuberculosis. *Pharmacotherapy* **34,** 1187–1197; 10.1002/phar.1482 (2014).
39. Ryan, N. J. & Lo, J. H. Delamanid: first global approval. *Drugs* **74,** 1041–1045; 10.1007/s40265-014-0241-5 (2014).
40. Matsumoto, M. *et al.* OPC-67683, a nitro-dihydro-imidazooxazole derivative with promising action against tuberculosis in vitro and in mice. *PLoS medicine* **3,** e466; 10.1371/journal.pmed.0030466 (2006).
41. Wallis, R. S. *et al.* Rapid evaluation in whole blood culture of regimens for XDR-TB containing PNU-100480 (sutezolid), TMC207, PA-824, SQ109, and pyrazinamide. *PloS one* **7,** e30479; 10.1371/journal.pone.0030479 (2012).

42. Williams, K. N. *et al.* Promising antituberculosis activity of the oxazolidinone PNU-100480 relative to that of linezolid in a murine model. *Antimicrobial agents and chemotherapy* **53,** 1314–1319; 10.1128/AAC.01182-08 (2009).
43. Tahlan, K. *et al.* SQ109 targets MmpL3, a membrane transporter of trehalose monomycolate involved in mycolic acid donation to the cell wall core of Mycobacterium tuberculosis. *Antimicrobial agents and chemotherapy* **56,** 1797–1809; 10.1128/AAC.05708-11 (2012).
44. Stover, C. K. *et al.* A small-molecule nitroimidazopyran drug candidate for the treatment of tuberculosis. *Nature* **405,** 962–966; 10.1038/35016103 (2000).
45. Baptista, R., Fazakerley, D. M., Beckmann, M., Baillie, L. & Mur, L. A. J. Untargeted metabolomics reveals a new mode of action of pretomanid (PA-824). *Scientific Reports* **8,** 5084; 10.1038/s41598-018-23110-1.
46. Li, X. *et al.* Discovery of a Potent and Specific M. tuberculosis Leucyl-tRNA Synthetase Inhibitor: (S)-3-(Aminomethyl)-4-chloro-7-(2-hydroxyethoxy)benzoc1,2oxaborol-1(3H)-ol (GSK656). *Journal of medicinal chemistry* **60,** 8011–8026; 10.1021/acs.jmedchem.7b00631 (2017).
47. Lee, R. E., Mikusova, K., Brennan, P. J. & Besra, G. S. Synthesis of the Arabinose Donor .beta.-D-Arabinofuranosyl-1-monophosphoryldecaprenol, Development of a Basic Arabinosyl-Transferase Assay, and Identification of Ethambutol as an Arabinosyl Transferase Inhibitor. *Journal of the American Chemical Society* **117,** 11829–11832; 10.1021/ja00153a002 (1995).
48. Wolucka, B. A. Biosynthesis of D-arabinose in mycobacteria - a novel bacterial pathway with implications for antimycobacterial therapy. *The FEBS journal* **275,** 2691–2711; 10.1111/j.1742-4658.2008.06395.x (2008).
49. Pethe, K. *et al.* Discovery of Q203, a potent clinical candidate for the treatment of tuberculosis. *Nature medicine* **19,** 1157–1160; 10.1038/nm.3262 (2013).
50. Cleghorn, L. A. T. *et al.* Identification of Morpholino Thiophenes as Novel Mycobacterium tuberculosis Inhibitors, Targeting QcrB. *Journal of medicinal chemistry* **61,** 6592–6608; 10.1021/acs.jmedchem.8b00172 (2018).
51. Padhi, A., Sengupta, M., Sengupta, S., Roehm, K. H. & Sonawane, A. Antimicrobial peptides and proteins in mycobacterial therapy: current status and future prospects. *Tuberculosis (Edinburgh, Scotland)* **94,** 363–373; 10.1016/j.tube.2014.03.011 (2014).
52. Yamasaki, K. & Gallo, R. L. Antimicrobial peptides in human skin disease. *European journal of dermatology : EJD* **18,** 11–21; 10.1684/ejd.2008.0304 (2008).
53. Khara, J. S. *et al.* Anti-mycobacterial activities of synthetic cationic α-helical peptides and their synergism with rifampicin. *Biomaterials* **35,** 2032–2038; 10.1016/j.biomaterials.2013.11.035 (2014).
54. Teng, T., Liu, J. & Wei, H. Anti-mycobacterial peptides: from human to phage. *Cellular physiology and biochemistry : international journal of experimental cellular physiology, biochemistry, and pharmacology* **35,** 452–466; 10.1159/000369711 (2015).
55. Thayil, S. M. & Kesavan, A. K. in *Bioresources and Bioprocess in Biotechnology. Volume 2 : Exploring Potential Biomolecules,* edited by S. Sugathan, N. S. Pradeep & S. Abdulhameed (Springer Singapore, Singapore, 2017), pp. 365–379.

56. Barkei, J. J., Kevany, B. M., Felnagle, E. A. & Thomas, M. G. Investigations into viomycin biosynthesis by using heterologous production in Streptomyces lividans. *Chembiochem : a European journal of chemical biology* **10,** 366–376; 10.1002/cbic.200800646 (2009).
57. Marrero, P., Cabañas, M. J. & Modolell, J. Induction of translational errors (misreading) by tuberactinomycins and capreomycins. *Biochemical and biophysical research communications* **97,** 1047-42 (1980).
58. Lin, Y. *et al.* The Antituberculosis Antibiotic Capreomycin Inhibits Protein Synthesis by Disrupting Interaction between Ribosomal Proteins L12 and L10. *Antimicrobial agents and chemotherapy* **58,** 2038–2044; 10.1128/AAC.02394-13 (2014).
59. Ling, L. L. *et al.* A new antibiotic kills pathogens without detectable resistance. *Nature* **517,** 455; 10.1038/nature14098 (2015).
60. Giltrap, A. M. *et al.* Total Synthesis of Teixobactin. *Organic letters* **18,** 2788–2791; 10.1021/acs.orglett.6b01324 (2016).
61. Khalil, Z. G., Salim, A. A., Lacey, E., Blumenthal, A. & Capon, R. J. Wollamides: antimycobacterial cyclic hexapeptides from an Australian soil Streptomyces. *Organic letters* **16,** 5120–5123; 10.1021/ol502472c (2014).
62. Asfaw, H., Wetzlar, T., Martinez-Martinez, M. S. & Imming, P. An efficient synthetic route for preparation of antimycobacterial wollamides and evaluation of their in vitro and in vivo efficacy. *Bioorganic & medicinal chemistry letters* **28,** 2899–2905; 10.1016/j.bmcl.2018.07.021 (2018).
63. Tsutsumi, L. S. *et al.* Solid-Phase Synthesis and Antibacterial Activity of Cyclohexapeptide Wollamide B Analogs. *ACS combinatorial science* **20,** 172–185; 10.1021/acscombsci.7b00189 (2018).
64. Asfaw, H. *et al.* Design, synthesis and structure-activity relationship study of wollamide B; a new potential anti TB agent. *PloS one* **12,** e0176088; 10.1371/journal.pone.0176088 (2017).
65. Renner, M. K. *et al.* Cyclomarins A−C, New Antiinflammatory Cyclic Peptides Produced by a Marine Bacterium (Streptomyces sp.). *Journal of the American Chemical Society* **121,** 11273–11276; 10.1021/ja992482o (1999).
66. Schmitt, E. K. *et al.* The natural product cyclomarin kills Mycobacterium tuberculosis by targeting the ClpC1 subunit of the caseinolytic protease. *Angewandte Chemie (International ed. in English)* **50,** 5889–5891; 10.1002/anie.201101740 (2011).
67. Barbie, P. & Kazmaier, U. Total Synthesis of Cyclomarin A, a Marine Cycloheptapeptide with Anti-Tuberculosis and Anti-Malaria Activity. *Organic letters* **18,** 204–207; 10.1021/acs.orglett.5b03292 (2016).
68. Iwatsuki, M. *et al.* Lariatins, antimycobacterial peptides produced by Rhodococcus sp. K01-B0171, have a lasso structure. *Journal of the American Chemical Society* **128,** 7486–7491; 10.1021/ja056780z (2006).
69. Inokoshi, J., Miyake, M., Shimizu, Y. & Tomoda, H. Analysis of essential amino acids in lasso peptide lariatins for anti-mycobacterial activity by single amino acid substitution. *Planta Med* **78**; 10.1055/s-0032-1320382 (2012).

70. Shibasaki, M., Iino, M., Osada, H., Koyama, N. & Tomoda, H. eds. *Mechanism of Action of New Antiinfectious Agents from Microorganisms. Chembiomolecular Science* (Springer Japan, 2013).
71. Gavrish, E. *et al.* Lassomycin, a ribosomally synthesized cyclic peptide, kills mycobacterium tuberculosis by targeting the ATP-dependent protease ClpC1P1P2. *Chemistry & biology* **21,** 509–518; 10.1016/j.chembiol.2014.01.014 (2014).
72. Harris, P. W. R., Cook, G. M., Leung, I. K. H. & Brimble, M. A. An Efficient Chemical Synthesis of Lassomycin Enabled by an On-Resin Lactamisation–Off-Resin Methanolysis Strategy and Preparation of Chemical Variants. *Aust. J. Chem.* **70,** 172; 10.1071/CH16499 (2017).
73. Lear, S. *et al.* Total chemical synthesis of lassomycin and lassomycin-amide. *Organic & biomolecular chemistry* **14,** 4534–4541; 10.1039/c6ob00631k (2016).
74. Gao, W. *et al.* Discovery and characterization of the tuberculosis drug lead ecumicin. *Organic letters* **16,** 6044–6047; 10.1021/ol5026603 (2014).
75. Gao, W. *et al.* The cyclic peptide ecumicin targeting ClpC1 is active against Mycobacterium tuberculosis in vivo. *Antimicrobial agents and chemotherapy* **59,** 880–889; 10.1128/AAC.04054-14 (2015).
76. Hawkins, P. M. E., Giltrap, A. M., Nagalingam, G., Britton, W. J. & Payne, R. J. Total Synthesis of Ecumicin. *Organic letters* **20,** 1019–1022; 10.1021/acs.orglett.7b03967 (2018).
77. Kling, A. *et al.* Antibiotics. Targeting DnaN for tuberculosis therapy using novel griselimycins. *Science (New York, N.Y.)* **348,** 1106–1112; 10.1126/science.aaa4690 (2015).
78. Pruksakorn, P. *et al.* Trichoderins, novel aminolipopeptides from a marine sponge-derived Trichoderma sp., are active against dormant mycobacteria. *Bioorganic & medicinal chemistry letters* **20,** 3658–3663; 10.1016/j.bmcl.2010.04.100 (2010).
79. Pruksakorn, P. *et al.* Action-mechanism of trichoderin A, an anti-dormant mycobacterial aminolipopeptide from marine sponge-derived Trichoderma sp. *Biological & pharmaceutical bulletin* **34,** 1287–1290 (2011).
80. Kavianinia, I., Kunalingam, L., Harris, P. W. R., Cook, G. M. & Brimble, M. A. Total Synthesis and Stereochemical Revision of the Anti-Tuberculosis Peptaibol Trichoderin A. *Organic letters* **18,** 3878–3881; 10.1021/acs.orglett.6b01886 (2016).
81. Xie, Y., Chen, R., Si, S., Sun, C. & Xu, H. A new nucleosidyl-peptide antibiotic, sansanmycin. *The Journal of antibiotics* **60,** 158–161; 10.1038/ja.2007.16 (2007).
82. Li, Y.-B. *et al.* Synthesis and in vitro antitubercular evaluation of novel sansanmycin derivatives. *Bioorganic & medicinal chemistry letters* **21,** 6804–6807; 10.1016/j.bmcl.2011.09.031 (2011).
83. Tran, A. T. *et al.* Sansanmycin natural product analogues as potent and selective anti-mycobacterials that inhibit lipid I biosynthesis. *Nature communications* **8,** 14414; 10.1038/ncomms14414 (2017).
84. Xie, Y., Xu, H., Si, S., Sun, C. & Chen, R. Sansanmycins B and C, New Components of Sansanmycins. *The Journal of antibiotics* **61,** 237; 10.1038/ja.2008.34 (2008).
85. Winn, M., Goss, R. J. M., Kimura, K.-i. & Bugg, T. D. H. Antimicrobial nucleoside antibiotics targeting cell wall assembly: recent advances in structure-function studies and nucleoside biosynthesis. *Natural product reports* **27,** 279–304; 10.1039/b816215h (2010).

86. Proksch, P., Putz, A., Ortlepp, S., Kjer, J. & Bayer, M. Bioactive natural products from marine sponges and fungal endophytes. *Phytochemistry Reviews* **9,** 475–489; 10.1007/s11101-010-9178-9 (2010).
87. Sagar, S., Kaur, M. & Minneman, K. P. Antiviral lead compounds from marine sponges. *Marine Drugs* **8,** 2619–2638; 10.3390/md8102619 (2010).
88. van Soest, R.W.M. *et al.* World Porifera database. Accessed at http://www.marinespecies.org/porifera on 2018-04-16 (2018).
89. Leal, M. C., Puga, J., Serôdio, J., Gomes, N. C. M. & Calado, R. Trends in the discovery of new marine natural products from invertebrates over the last two decades--where and what are we bioprospecting? *PloS one* **7,** e30580; 10.1371/journal.pone.0030580 (2012).
90. Wang, G. Diversity and biotechnological potential of the sponge-associated microbial consortia. *Journal of industrial microbiology & biotechnology* **33,** 545–551; 10.1007/s10295-006-0123-2 (2006).
91. Anjum, K. *et al.* Marine Sponges as a Drug Treasure. *Biomolecules & therapeutics* **24,** 347–362; 10.4062/biomolther.2016.067 (2016).
92. Kusama, T. *et al.* Bromopyrrole alkaloids from a marine sponge Agelas sp. *Chemical & pharmaceutical bulletin* **62,** 499–503 (2014).
93. Viegelmann, C. *et al.* Isolation and identification of antitrypanosomal and antimycobacterial active steroids from the sponge Haliclona simulans. *Marine Drugs* **12,** 2937–2952; 10.3390/md12052937 (2014).
94. Hrckova, G. & Velebny, S. *Pharmacological Potential of Selected Natural Compounds in the Control of Parasitic Diseases* (Springer Vienna, 2012).
95. Ibrahim, S. R. M. *et al.* Callyaerins A-F and H, new cytotoxic cyclic peptides from the Indonesian marine sponge Callyspongia aerizusa. *Bioorganic & medicinal chemistry* **18,** 4947–4956; 10.1016/j.bmc.2010.06.012 (2010).
96. Desqueyroux-Faúndez, R. Description de la Faune des Haplosclerida (Porifera) de la Nouvelle-Calédonie. I. Niphatidae-Callyspongiidae. *Revue suisse de Zoologie* **91,** 765–827 (1984).
97. Daletos, G. *et al.* Callyaerins from the Marine Sponge Callyspongia aerizusa: Cyclic Peptides with Antitubercular Activity. *Journal of natural products* **78,** 1910–1925; 10.1021/acs.jnatprod.5b00266 (2015).
98. Berer, N., Rudi, A., Goldberg, I., Benayahu, Y. & Kashman, Y. Callynormine A, a new marine cyclic peptide of a novel class. *Organic letters* **6,** 2543–2545; 10.1021/ol0491787 (2004).
99. Kay, B. K., Williamson, M. P. & Sudol, M. The importance of being proline: the interaction of proline-rich motifs in signaling proteins with their cognate domains. *FASEB journal : official publication of the Federation of American Societies for Experimental Biology* **14,** 231–241 (2000).
100. Mechnich, O., Messier, G., Kessler, H., Bernd, M. & Kutscher, B. Cyclic Heptapeptides Axinastatin 2, 3, and 4: Conformational analysis and evaluation of the biological potential. *Helv. Chim. Acta* **80,** 1338–1354; 10.1002/hlca.19970800503 (1997).

101. Zhang, S. *et al.* Total Synthesis and Conformational Study of Callyaerin A: Anti-Tubercular Cyclic Peptide Bearing a Rare Rigidifying (Z)-2,3- Diaminoacrylamide Moiety. *Angewandte Chemie (International ed. in English)* **57,** 3631–3635; 10.1002/anie.201712792 (2018).

102. Dierks, T. *et al.* Posttranslational formation of formylglycine in prokaryotic sulfatases by modification of either cysteine or serine. *The Journal of biological chemistry* **273,** 25560–25564 (1998).

103. Chruszcz, M. *et al.* Crystal structure of a covalent intermediate of endogenous human arylsulfatase A. *Journal of inorganic biochemistry* **96,** 386–392 (2003).

104. Dierks, T., Lecca, M. R., Schmidt, B. & Figura, K. von. Conversion of cysteine to formylglycine in eukaryotic sulfatases occurs by a common mechanism in the endoplasmic reticulum. *FEBS letters* **423,** 61–65; 10.1016/S0014-5793(98)00065-9 (1998).

105. Rush, J. & Bertozzi, C. R. An alpha-formylglycine building block for fmoc-based solid-phase peptide synthesis. *Organic letters* **8,** 131–134; 10.1021/ol052623t (2006).

106. Pappo, D., Vartanian, M., Lang, S. & Kashman, Y. Synthesis of cyclic endiamino peptides. *Journal of the American Chemical Society* **127,** 7682–7683; 10.1021/ja050299r (2005).

107. Bhavaraju, S., McGregor, M. A. & Rosen, W. Nucleophilic reactivity of amines with an α-formylglycyl enol-tosylate fragment. *Tetrahedron Letters* **48,** 7751–7755; 10.1016/j.tetlet.2007.09.018 (2007).

108. Malins, L. R. *et al.* Peptide Macrocyclization Inspired by Non-Ribosomal Imine Natural Products. *Journal of the American Chemical Society*; 10.1021/jacs.7b01624 (2017).

109. Daletos, G. Dissertation. Universitäts- und Landesbibliothek der Heinrich-Heine-Universität Düsseldorf (2016).

110. Ordway, D. *et al.* The hypervirulent Mycobacterium tuberculosis strain HN878 induces a potent TH1 response followed by rapid down-regulation. *Journal of immunology (Baltimore, Md. : 1950)* **179,** 522–531 (2007).

111. Valway, S. E. *et al.* An outbreak involving extensive transmission of a virulent strain of Mycobacterium tuberculosis. *The New England journal of medicine* **338,** 633–639; 10.1056/NEJM199803053381001 (1998).

112. Sharpe, M. L., Gao, C., Kendall, S. L., Baker, E. N. & Lott, J. S. The structure and unusual protein chemistry of hypoxic response protein 1, a latency antigen and highly expressed member of the DosR regulon in Mycobacterium tuberculosis. *Journal of Molecular Biology* **383,** 822–836; 10.1016/j.jmb.2008.07.001 (2008).

113. Sun, C. *et al.* Mycobacterium tuberculosis hypoxic response protein 1 (Hrp1) augments the pro-inflammatory response and enhances the survival of Mycobacterium smegmatis in murine macrophages. *Journal of medical microbiology* **66,** 1033–1044; 10.1099/jmm.0.000511 (2017).

Acknowledgements

Acknowledgements are left out in the electronic version due to protection of privacy.

Declaration of academic integrity

With this statement I declare, that I have independently completed the above PhD thesis entitled

«A rational Synthesis and Anti-Tubercular Evaluation of the Callyaerins, a marine Cyclic Peptide Class bearing a (*Z*)-2,3-Diaminoacrylamide Moiety».

The thoughts taken directly or indirectly from external sources are properly marked as such. This thesis was not previously submitted to another academic institution and has also not yet been published.

Essen, _____ Florian Schulz